Soil variability and its consequences in geotechnical engineering

Von der Fakultät für Bau– und Umweltingenieurwissenschaften
der Universität Stuttgart
zur Erlangung der Würde eines Doktors der Ingenieurwissenschaften (Dr.-Ing.)
genehmigte Abhandlung,

vorgelegt von

DIPL.-ING. DIPL.-ING. MAXIMILIAN HUBER

aus Leonding (Österreich)

Hauptberichter:	Prof. Dr.-Ing. Pieter A. Vermeer
Mitberichter:	Prof. Dr.techn. Dr.-Ing. Andras Bardossy
	Prof. Dr. Michael A. Hicks
Tag der mündlichen Prüfung:	19. Juni 2013

Institut für Geotechnik der Universität Stuttgart

2013

Mitteilung 69
des Instituts für Geotechnik
Universität Stuttgart, Germany, 2013

Editor:
Univ.-Prof. Dr.-Ing. habil. Christian Moormann

Institut für Geotechnik
Universität Stuttgart
Pfaffenwaldring 35
70569 Stuttgart

Keywords: soil variability, spatial variability, correlation length, Random Finite Element Method, uncertainty quantification.

Printed by e.kurz + co, druck und medientechnik GmbH, Stuttgart, Germany, 2013

ISBN 978-3-921837-69-6
(D93 - Dissertation, Universität Stuttgart)

Preface of the editor

With issue no. 69 of the proceedings the Institute of Geotechnical Engineering at the University of Stuttgart (IGS) the dissertation study of Dr.-Ing. Maximilian Huber is published. Dr. Huber's thesis is related to soil and rock heterogeneity, to the mathematical approaches for describing soil variability and to its consequences in geotechnical engineering.

Soils and rocks as natural geological materials exhibit spatial variability of material properties. The spatial variability, frequently referred to as heterogeneity, is anisotropic, often depth-dependent and occurs at multiple scales: at the very small scale, also called grain scale, as seen in the arrangement of solid particles of sand or in the arrangement of pellets in clay, at the decimeter to meter scale, as observed in specimen testes in laboratory or in CPT/SPT-soundings in soil layers; and at larger scales too, like the geotechnical scale relevant for geotechnical structures like foundation, excavations or tunnels, or at the geological scale of several hundreds of meters, which is affected by the layering of soils of different types. Spatial variability of soils and rocks influences the material behaviour in mechanical and hydraulic sense, the flow of groundwater water and the performance of geotechnical structures. Traditional deterministic analyses based on single "representative" soil property values lead to partial or global factors of safety, which provide no information regarding probability of failure and which does not consider the uncertainty that arises through having incomplete information about the subsoil conditions. In contrast probabilistic approaches allow defining soil properties in statistical terms and simulating geotechnical performance probabilistically for example on terms of reliability. The reliability, defined as the complement of the failure probability, is a rational measure of safety.

The scientific work of Dr. Huber focuses on the evaluation of the effects of soil variability by using advanced mathematical models within the framework of probabilistic methods. The evaluation of stochastic soil properties including spatially correlated soil properties is investigated on a wide theoretical basis. These results are used in case studies on the evaluation of the spatial correlation of different measurement data sets. Considering these outcomes finally the effects of soil variability are evaluated in typical problems in tunnelling and foundation engineering demonstrating the effect of soil heterogeneity and spatial variability at different scales.

The thesis of Dr. Huber shows that probabilistic analyses are powerful and versatile tools for investigating the influence of uncertainties on a given geotechnical problem, but indicates the meaning of the given input data and limitations of probabilistic analyses also.

Safety, reliability and risk are key issues in situations with continuously increasing complexity especially in geotechnical engineering. In this regard the doctoral thesis of Dr. Huber proves as a valuable contribution.

Christian Moormann
Stuttgart, July 2013

Preface of the supervisor of the PhD thesis

As yet probabilistic analyses are not common in geotechnical engineering and will probably never be introduced for regular structures and foundations, but it is expected that it will become more and more used for major engineering projects in difficult ground. As usual in most branches of engineering, loads on structures are stochastic, but the natural variability of soil properties exceeds by far the variability of man-made engineering materials. As a consequence, a special need of probabilistic design exist in geotechnical engineering. For this reason, I have encouraged Maximilian Huber to do a doctoral study on the application of probabilistic methods in geotechnics, leaving the choice of a more precise topic entirely to him.

The first idea he came up with was to perform borehole jacking tests in a particular layer of mudstone to measure its stiffness and to assess the corresponding correlation length. I was very happy to learn that my colleague Prof. Andras Bardossy was willing to support these field measurements even financially. These experiments had to be done in the Fasanenhof tunnel, being at that time under construction at Stuttgart by the companies Weiss & Freitag and Max BÃűgl. I am not only indebted to the support from these companies, but also for the support of the owner of the tunnel, i.e. the Stuttgarter Strassenbahnen AG.

The candidate has chosen to focus this study on soil variability, being usually taken into account by distinguishing between different soil layers. In probabilistic studies soil properties within a layer are based on a probabilistic density function, as defined by a mean value, a standard deviation and possibly skewness. In such an approach the spatial variability within a soil layer may be disregarded on assuming homogeneity. On approaching reality more closely, spatial variability within soil layers may be modelled in combination with a correlation length, i.e. "a scale of fluctuation" for the soil property considered. I consider such developments as fascinating and would like to know to which extent such approaches are already applicable in engineering.

This dissertation study convinced me of the matureness of probabilistic design in geotechnical engineering. On the other, it made me realise that variability within soil layers is still a topic of research, as the assessment of correlation lengths is not straight forward. The assessment of this length is probably the most important scientific achievement of this dissertation study on soil variability. Many of the case studies may also serve as a manual for the application of probabilistic design in advanced geotechnical engineering. As a consequence, his research has already attracted good attention in the international research community.

I got to know Maximilian Huber not only as a young researcher and teacher before my retirement from Stuttgart University, but also later in Delft when he worked with his external advisor Prof. M. Hicks. These visits to Delft also provided the opportunity of additional social contacts, which I enjoyed very much. So I had the pleasure of learning to know him not only as a talented researcher with creative ideas, but also as gifted musician with a wide field of interests.

Pieter A. Vermeer
Nederhorst den Berg, Netherlands, July 2013

Acknowledgments

The research presented in this thesis is the result of the work carried out during the years 2007 - 2013 at the Institute of Geotechnical Engineering of Stuttgart University. Behind this work there are important contributions and the significant support of a certain number of persons, whom I would like to thank sincerely.

I wish to express first of all my deep gratitude to Prof. Pieter Vermeer for his extensive, invaluable and steadfast guidance, for his support and patience, sharing his knowledge and experience, throughout my PhD studies.

Likewise, I thank Prof. Andras Bardossy and Prof. Michael Hicks for their expert advise and feedback as my co-supervisor throughout the time of my studies.

Throughout the years, I benefited from the cooperative and friendly support, advise and guidance of many others. With this regard, I would like to express my gratitude to Patrick Arnold, Dr. Robby Caspeele, Ed Calle, Anneke Hommels, Dr. Jon Nuttall, Prof. Christian Moormann, Dr. Massimiliano Moscatelli, Dr. Thomas Most, Dr. Dirk Proske and to longtime colleagues at the University of Stuttgart. Amongst them are Prof. Thomas Benz, Dr. Lars Beuth, Fursan Hamad, Dr. Issam Jassim, Dr. Annette Lächler, Dr. Axel Möllmann, Dr. Marcus Schneider, Peter Ströhle, Prof. Bernhard Westrich and Bernd Zweschper.

Of those mentioned here and many others whom I met during the exciting years of my PhD studies I maintain invaluable good memories. I am very grateful to my parents, to my sister and to friends, who gave me indispensable support through their company and advise.

Maximilian Huber
Weimar, July 2013

Contents

List of Figures

List of Tables

Summary

The core competences of civil engineers are designing, building and maintaining structures and buildings to enable life and business for society. This includes the prevention against natural hazards such as climatological, hydrological, meteorological and geophysical disasters. Such complex hazards asks for sophisticated techniques to ensure appropriate safety standards for society. Too low safety standards can result in many casualties and much economic damage, whereas too high standards results in overly expansive systems. Therefore, these phenomena ask for sophisticated methods to consider their impacts on structures. Especially geotechnical engineers are asked for integrated concepts to design structures withstanding the above mentioned hazards.

This research is focusing on the evaluation of the effects of soil variability within the framework of probabilistic methods. The evaluation of stochastic soil properties including spatially correlated soil properties is deeply investigate on a theoretical basis. These results are used in case studies on the evaluation of the spatial correlation of different measurement data sets. These outcomes are also used in different case studies, which are focusing on the effects of soil variability for typical geotechnical problems.

This thesis is organized thematically in the following parts:

Chapter 2: The basics of probabilistic site characterization are described within this chapter including a comparison to the state-of-the-art. This involves the description of the basics of statistics and geostatistics in order to describe the variability and the spatial correlation of soil properties. Besides this, the main sources of error in geotechnical engineering are summarized, which influence probabilistic site characterization. Also an overview of sampling schemes is provided. Three main methods for the mathematical characterization of spatial variability are derived. These methods are used to analyse and quantify spatial variability of soil properties.

Chapter 3 The possibilities and limitations of the three different approaches on the evaluation of spatial variability can be deduced from the results of four different case studies. At first, an analytically defined random process is used to show the capabilities of the three different methods. On basis of this, three case studies are presented on the evaluation of spatial variability of equally spaced and irregular spaced data sets. These datasets are used to explain the concepts of probabilistic site characterization, which includes the identification of trends and layers as well as a novel scheme for the combination of different models for spatial variability by means of statistical approaches.

The results of these case studies are compared to a large literature study on the spatial correlation of soil properties, which is enriched by the results of an extensive study on cone penetration tests in different soil types. Finally, these different sources of information on the correlation length are combined via the Bayesian Model Averaging methodology.

Chapter 4: This chapter focuses on the basics of safety and reliability in engineering. It provides a description of common approaches for dealing with uncertainties and safety in geotechnical engineering. Global and partial safety factors as well as the basics of uncertainty quantification and reliability based design are described and compared with a special focus on the basics of the generation of random numbers and random fields as well as on the computation of failure probabilities.

Moreover, an introduction into local and global sensitivity analyses is given.

Chapter 5: Typical geotechnical design problems are investigated within the framework of uncertainty quantification.

At first, an analytical limit state equation (LSE) is used to investigate the effects of soil variability on the design of a tunnel lining.

In another case study the bearing capacity of a strip footing is investigated by means of probabilistic methods. Within this, semi-analytical LSEs are derived from 2D FEM simulations, which considers the Mohr-Coulomb, Matsuoka-Nakai, Lade-Duncan failure criteria to model the soil behaviour. These LSEs are used to investigate the effects of the soil variability, of the geometry of the problem and of the load uncertainty. Sensitivity analyses evaluate the contribution of the random properties to the probability of failure.

The tunnel face stability problem is investigated in a similar way. The semi-analytical LSEs are derived from parametric 3D FEM simulations using the Mohr-Coulomb, Matsuoka-Nakai, Lade-Duncan failure criteria. The effects of soil variability, geometry and construction processes on the probability of failure are quantified by means of uncertainty quantification and sensitivity analyses.

Chapter 6: The effects of spatial soil variability are evaluated in typical problems in tunnelling and foundation engineering by using the framework of uncertainty quantification.

In the first case study, the effects of spatially correlated soil properties on surface settlements, which are induced by the construction of a tunnel, are investigated. Starting from traditional approaches of a single-layered subsoil, a novel concept for considering the spatial variability at multiple scales is presented.

The effects of soil variability at different scales are also investigated within slope stability problems. These studies also include sensitivity analyses to investigate the contribution of spatial variability to the probability of failure.

Finally, the effects of large scale spatial variability is focused in the case study on the risk-based characterisation of an urban site. The macro-scale variability of the subsoil is simulated via the Pluri-Gaussian simulation approach. This approach captures the uncertainty of the boundaries of the spatially distributed soil types, incorporating expert

judgements, soil investigations and stochastic properties of the soil types. These simulation results analysed using fragility curves. Herein, fragility curves suggest admissible footing pressure due to differential settlements. These results are used for the generation of risk maps of the investigated urban site.

Chapter 7: This chapter comprises a summary of the objectives of this thesis and a summary of the conclusions. Further research topics are announced in the outlook.

Zusammenfassung

Die Kernkompetenzen des Bauingenieurwesens sind das Planen, Erstellen und Erhalten von Bauwerken, um die Existenz und Wirtschaftsleben einer Gesellschaft zu ermöglichen. Dies umfasst auch Maßnahmen gegen Naturkatastrophen wie z.B. Klimawandel, Hochwasser oder Massenbewegungen. Diese komplexen Gefahren erfordern hochentwickelte Technologien, um ein angemessenes Level an Sicherheit für die Gesellschaft zu sichern. Zu niedrige Sicherheiten können zu großen Verlusten und hohen ökonomischen Schäden führen, wohingegen zu hohe Sicherheitsanforderungen in einem teuren und einer nicht wirtschaftlichen Bemessung von Bauwerken enden. Daraus kann abge-leitet werden, dass hochentwickelte Methoden notwendig sind, um die Einwirkungen auf Bauwerke zu simulieren. Speziell in der Geotechnik ist es in Folge der hohen Variabilität des Untergrundes erforderlich, integrierte Konzepte für die Bemessung von Bauwerken gegen die zuvor genannten Einwirkungen anzuwenden.

Im Rahmen dieser Dissertation wird die mathematische Beschreibung von Bodenvariabilität und die Bestimmung der Konsequenzen dieser Variabilität in verschiedenen geotechnischen Fragestellungen untersucht. Hierbei werden probabilistische Methoden angewendet, um die Folgen von unsicheren und räumlich streuenden Bodenkenngrößen zu bestimmen. Neben der Zusammenstellung der theoretischen Grundlagen der Quantifizierung von räumlichen Varaibliät wird die Anwendung exemplarische in mehreren Fallbeispielen aufgezeigt. Diese Resultate werden in weiterführenden Untersuchungen verwendet, in welchen die Folgen von Bodenvariabilität in geotechnischen Problembestellungen beispielhaft analysiert werden.

Diese Dissertation ist thematisch in die folgenden Teile unterteilt:

Kapitel 2: In diesem Kapitel werden die Grundlagen für eine probabilistische Charakterisierung des Untergrundes zusammengestellt. Dies umfaßt die theoretischen Grundlagen der Statistik und Geostatistik, welche für die Beschreibung von Variabilität und räumlicher Korrelation von Bodeneigenschaften erforderlich sind. Drei gängige Methoden für die Analyse von räumlicher Variabilität in der Geotechnik werden hergeleitet und einander gegenübergestellt. Diese ist notwendig, um die Ergebnisse der Analyse von Messdaten in Hinblick auf die räumliche Variabilität zu verstehen und zu interpretieren.

Kapitel 3: In vier verschiedenen Fallstudien wird die Bestimmung der räumlichen Variabilität von Bodeneigenschaften erläutert.

In der ersten Fallstudie werden drei verschiedene Analysemethoden von räumlicher Variabilität an einem analytische definiertem Zufallsprozess angewandt, um so plakativ die Vor- und Nachteile der verschiedenen Methoden aufzuzeigen.

Auf Basis dieser Ergebnisse wird in der zweiten Fallstudie eine Datenbank von CPT Feldversuchen analysiert, welche im Rahmen einer Großbaustelle durchgeführt wurden. Exemplarisch wird hier das Erstellen eines stochastischen Modells des Baugrundes gezeigt. Hierbei wird mittels empirischer und statistischer Methoden die Variabilität des Untergrundes auf verschiedenen Skalen charakterisiert. Exemplarisch wird das Kombinieren verschiedener Analysemodelle von räumlicher Variabilität aufgezeigt. Dies Herangehensweise beruht auf dem Satz von Bayes.

In einer weiteren Fallstudie wird die räumliche Variabilität von Steifigkeiten in einer homogenen Bodenschicht untersucht. Anhand dieser Analyse wird eine Methodik zur Bestimmung der Unsicherheit von Modellen der räumlichen Variabilität abgeleitet.

In der vierten Fallstudie wird die räumliche Variabilität einer sehr großen Anzahl von Festigkeitsmessungen analysiert, welche auf verschiedenen Baustellen durchgeführt wurden. Die Ergebnisse werden mit den Daten einer umfangreichen Literaturstudie verglichen und verifiziert.

Abschließend wird eine Methodik für die Kombination von gemessener räumlicher Varaibität mit einer Expertenmeinung vorgestellte. Das Bayes'sche Prinzip wird verwendet, um verschiedene Vorinformationen, Expertenwissen, Literaturergebnisse und Messdaten miteinander zu kombinieren. Dieses Vorgehen wird exemplarisch an einem Datensatz aufgezeigt.

Kapitel 4: In diesem Kapitel sind die Grundlagen für Sicherheit und Zuverlässigkeit zusammengestellt. Ausgehend vom Stand der Technik, bei dem globale und partielle Sicherheiten verwendet werden, werden die Grundlagen der Zuverlässigkeitsanalyse von Bauwerken erklärt. Hierbei wird besonders auf die in der Geotechnik gängigen Näherungsverfahren zur Ermittelung der Versagenswahrscheinlichkeit eingegangen, wobei auch das Generieren von Zufallszahlen und -feldern beschrieben wird.

Die mathematischen Grundlagen für die Konzept zur lokalen und globalen Sensitivitätsanalyse werden am Ende dieses Kapitels erklärt.

Kapitel 5: In diesem Kapitel wird das Konzept der Quantifizierung von Unsicherheit anhand von verschiedenen Fallstudien in der Geotechnik erläutert. Hierbei wird die Bodenvariabilität durch Zufallszahlen simuliert.

In der ersten Fallstudie im Tunnelbau werden die Folgen von streuenden Bodenkenngrößen in der Bemessung einer Tunnelschale untersucht. Hierfür wird eine analytische Versagenszustandsgleichung für die Bestimmung der Änderung der Wahrscheinlichkeit eines Versagens in Folge von streuenden Bodenkenngrößen untersucht. Lokale bzw. globale Sensitivitäten quantifizieren den Einfluss der streuenden Eigenschaften mit Hilfe statistischer Methoden.

Die Folgen von Bodenvariabilität auf die Tragfähigkeit von vertikal belasteten Streifenfundaments mittels probabilistischen Methoden untersucht. Darüber hinaus werden neben der Variabilität der Festigkeitseigenschaften des Untergrundes auch die Geometrie und die Belastung des Streifenfundamentes analysiert. Dies wird mit verschiedenen Versagenszustandsgleichungen beschrieben, welche aus 2D FEM Untersuchungen mit verschiedenen stofflichen Versagenskriterien (Mohr-Coulomb, Matsuoka-Nakai, Lade-Duncan) abgeleitet werden. Für die Analyse dieser Fragestellung werden Fragilitätsgraphen verwendet. Fragilitätsgraphen beschreiben in diesem Zusammenhang zwischen aufgebrachter Last und Versagenswahrscheinlichkeit.

In einer weiteren Fallstudie wird Stabilität der Ortsbrust im Tunnelbau untersucht. Das Versagen der Ortsbrust wird mit verschiedenen stofflichen Versagenskriterien (Mohr-Coulomb, Matsuoka-Nakai, Lade-Duncan) in Kombination mit Methoden der Zuverlässigkeitsanalyse untersucht, wobei in diesem Zusammenhang neben der Untergrundvaribilität auch die Geometrie und der Herstellungsvorgang mittels Zufallsvariablen berücksichtigt werden. Der Vergleich der verschiedenen Ergebnisse wird mit einem Vergleich der Sensitivitäten der verwendeten Zufallsvariablen abgerundet.

Kapitel 6: In diesem Kapitel werden die Auswirkungen von räumlicher Variabilität in Fallbeispielen aus dem Tunnelbau und Grundbau dargestellt.

Der Auswirkungen von räumlich streuenden Bodenkenngrößen wird in einer Fallstudie zur Setzungen infolge Tunnelbau untersucht. Ausgehend von der konventionellen Herangehensweise von homogenen Zufallsfeldern wird eine Erweiterung für die Berücksichtigung von räumlich korrelierten Bodeneigenschaften auf mehreren Skalen präsentiert und die Auswirkungen exemplarisch aufgezeigt.

Auch in der Fallstudie zur Böschungsstabilität werden die Auswirkungen von räumlicher Variabilität auf mehreren Skalen untersucht. Im Rahmen dieser Untersuchungen wird ein Schema zur Bestimmung der Sensitivität der Eingangsparameter für räumliche Variabilität auf verschiedenen Skalen aufgezeigt.

In einer letzten Fallstudie werden die Folgen von makro-skaliger Bodenvariabilität untersucht. Hierfür werden die Ergebnisse einer gestatistischen Simulation verwendet, welche Expertenmeinung, Bodenaufschlüsse und stochastische Bodeneigenschaften verschiedener Bodentypen berücksichtigt. Diese Ergebnisse werdenfür die Erstellung von Risikokarten verwendet. Die erstellten Risikokarten geben eine zulässige Last an, welche für ein definiertes Gebäude und eine zulässige Verdrehung möglich ist.

Dieses Kapitel schließt mit einer Zusammenfassung der Erkenntnisse, welche aus den präsentierten Fallstudien abgeleitet werden.

Kapitel 7: Im abschließenden Kaptiel werden die Themen dieser Dissertation zusammengefasst und die Schlußfolgerung werden präsentiert.

Chapter 1

Introduction

1.1 Background and rationale

The core competence of civil engineers are designing, building and maintaining structures and buildings to enable life and business for society. This includes the prevention against natural hazards. Natural hazards can be subdivided into climatological, hydrological, meteorological and geophysical disasters. As defined in the INTERNATIONAL DISASTERS DATABASE, climatological disasters are (bush, forest, scrub and grassland) fires, meteorological disasters are local storms, extra-tropical and tropical cyclones. Hydrological disasters are general floods, flash floods, mudslides, storm surges and coastal floods. The complexity of natural hazards becomes more evident in figure 1.1. Herein, the annual frequency of floods, mass movements, seismic activities, storms, vulcanos, and wildfires is plotted with respect to the lost lives. These results from the INTERNATIONAL DISASTERS DATABASE [378] show good agreement with data from Christian & Baecher [23] on nuclear power plants, dam failures, explosions air crashes and man-caused fatalities. The Dutch Government Group Risk Criteria [395] indicate that these natural hazards are not acceptable risks and have to be mitigated with advanced concepts. This asks for sophisticated techniques to ensure appropriate safety standards for society.

Too low safety standards can result in many casualties and much economic damage, whereas too high standards results in overly expansive systems. Therefore, it is important to evaluate the safety of structures with appropriate approaches, which allow to consider variability and uncertainty in a proper way. These complex phenomena cause tremendous economical damage as shown in figure 1.2. One can deduce that sophisticated methods to consider their impacts on structures are urgently needed. Especially geotechnical engineers are asked for integrated concepts to design structures withstanding the above mentioned hazards.

In international conferences and workshops the state-of-the-art safety concepts are continuously improved. The global and partial safety factor concepts are mainly driven by experience and now enriched and extended by the results of probabilistic analyses. Theses new developments help to contribute to more economic and safe design approaches.

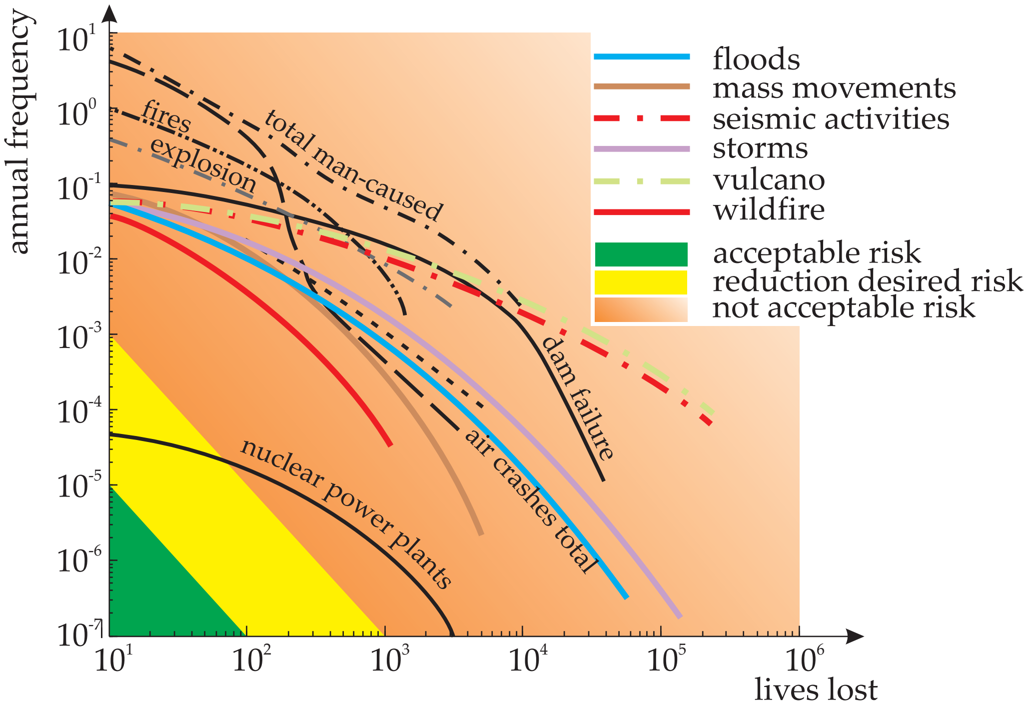

Figure 1.1: Data on the frequency of natural and industrial disasters against number of lost humans lives. In colour shading data from Dutch Government Group Risk Criteria [395] for floods, data on other natural disaster as reported by the NATURAL DISASTERS DATABASE NATURAL DISASTERS DATABASE and Christian & Baecher [23].

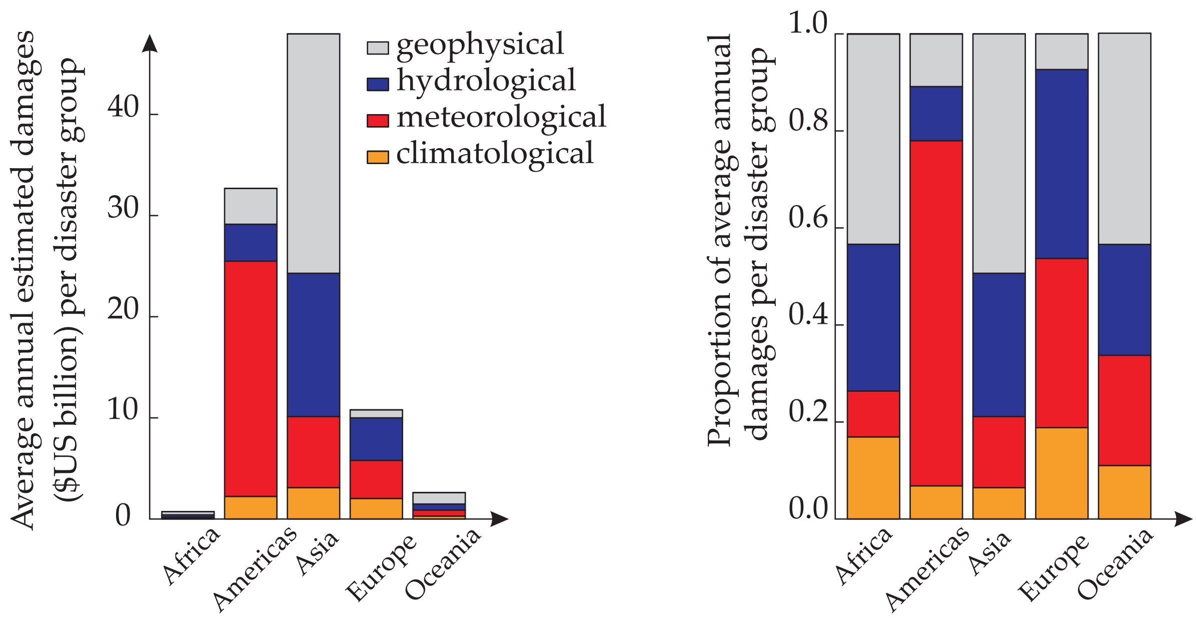

Figure 1.2: Average annual damages ($US billion) caused by reported natural disasters 1990 - 2011 by the INTERNATIONAL DISASTERS DATABASE [378].

1.2 Research aim

The research is focusing on the evaluation of the effects of soil variability within the framework of probabilistic methods. To achieve this aim, several topics are studied to quantify the effects of spatially correlated soil properties. Topics studied include evaluation of spatially correlated properties, geostatistical simulation methods, and probabilistic methods within geotechnical and civil engineering. In addition to this, case studies are elaborated to demonstrate the application of probabilistic methods in tunnelling and foundation engineering. These established calculation procedures for uncertainty quantification are seen as guidelines for reliability based design in geotechnics.

1.3 Thesis scope

In addition to this introduction, the thesis is arranged in six chapters as indicated below:

At first, an introduction into probabilistic site characterization is given in chapter **Chapter 2**. This includes the description of the mathematical framework to quantify spatial variability at different scales.

Subsequently, this framework is applied in four different case studies within **Chapter 3**, which shall help the reader to understand and apply these concepts of spatial variability in geotechnical engineering. The results of these case studies compared to the results of an extensive literature review of contributions on spatial variability of soil properties. On top of this, these findings are compared with the results of a CPT database analysis. The evaluation of spatial variability is improved by merging different sources of knowledge and information together with measurement data.

Chapter 4 focuses on the basics of safety and reliability and provided a description of common approaches for dealing with uncertainties and safety in geotechnical engineering. Global and partial safety factors as well as the basics of uncertainty quantification and reliability based design are described and compared to each other. This includes the basics of the generation of random numbers and random fields as well as the computation of failure probabilities. This chapter also provides an introduction to local and global sensitivity analysis of systems.

In **Chapter 5**, typical geotechnical case studies dealing with tunnelling and footing analyses are investigated within the framework of uncertainty quantification. Herein, soil variability is represented by random variables. Starting from semi-analytical limit state equations (LSE) for the design of tunnel-linings, the ultimate limit state of a footing is investigated in 2D. This investigation encloses the effects of soil variability by means of fragility curves and probabilistic methods. Moreover, the effects of the Mohr-Coulomb, Masuoka-Nakai and Lade-Duncan failure criteria are investigated by means of probabilistic methods and compared to each other. In addition to this, the ultimate limit state of the tunnel face is investigated by using three different constitutive failure criteria. The results of these 3D FEM studies are used for the formulation of the LSE, which is used for the uncertainty quantification of the tunnel face stability.

Chapter 6 presents three different case studies in tunnelling and foundation engineering focusing on the effects of spatial soil variability. The effects of spatial variability on the estimation of tunnelling induced settlements are investigated for a single- and two layered subsoil using probabilistic methods. In addition to this, the effects of multi-scale soil variability are also investigated for soil slopes. The quantification of these effects by means of global sensitivity measures offers insight into the contribution of uncertain properties of single- and two-layered soil slopes. In the case study on the risk-based site characterisation the effects of macro-scale soil variability are investigated by means of the Pluri-Gaussian simulation method, expert judgement and the framework of uncertainty quantification.

Chapter 7 is a summary of the most relevant findings of this research, drawing conclusions and including recommendations for further research.

Chapter 2

Characterizing soil variability at different scales

2.1 Introduction

Interpretation of site exploration data is illustrated in figure 2.1 [22]. The presented geological maps were drawn 30 years apart and are quite different from each other, although the sample data are the same. According to Baecher [22], the theory of geology was reevaluated in the profession and this led to a different reinterpretation of the data.

One can conclude from [22] that for site characterization only parts of exploration can be statistically modelled. Statistical analysis of data can at most indicate how to logically modify what was thought before to what should be thought after.

For this reason, it is useful to use different statistical approaches and schemes to describe various phenomena in detail. Within this chapter, the basics of probabilistic site characterization are described, which involves a summary of uncertainties and main sources of error in geotechnical engineering. The focus of the author is to enlighten the mathematical framework to describe spatial variability at different scales. Herein, a basic description of the uncertainty of the spatial correlation is offered together with a summary of the anisotropy ratios of the spatial correlation.

2.2 Probabilisitic site characterization

According to Baecher & Christian [23], site characterization can be defined as a set of activities (e.g. processes), which will lead to information about site geology. In this way one can get estimates of parameters about site geology and finally one can get estimates of parameters to be used in modelling engineering processes. This has been previously

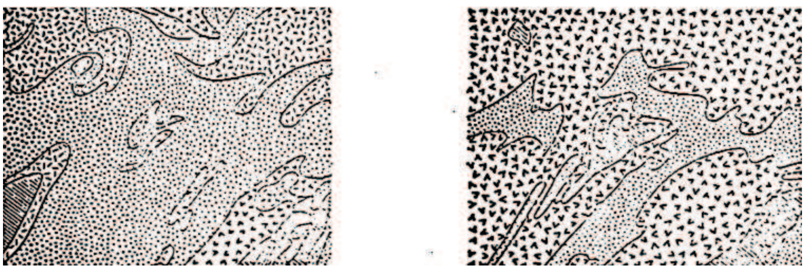

Figure 2.1: Mapping of the same area of Canada in 1958 (left) and in 1923 (right) using the same data [22].

thought of as an entirely intuitive process based on engineering judgement and without any analytical or mathematical consideration, but meanwhile approaches in site characterization have been developed in the oil, gas and mining industries. In these industries the importance of accurate estimates of oil reservoirs or mineral deposits are of greater economic consideration than, e.g., finding weak soil layers beneath a dam.

Baecher & Christian [23] developed a site characterization program including three stages: reconnaissance, preliminarily investigation and detailed investigation. In the *reconnaissance*, which is also called desk study, the engineer tries to find information on site geology from different sources. During the *preliminarily investigation*, the quantitative estimates of properties are used to verify the assumptions from the first stage. In [23], the authors stress that not too many tests are to be performed. After this, a *detailed investigation* is carried out to verify and refine the model of the site geology. One can easily conclude that for this reason a broad test program is required for accurate estimation of geometry and material properties.

For the description of the minimum requirements, for the extent and content of ground investigation, design analysis and site supervision, and the risks to property and life, three different geotechnical categories are described in the EN 1997-1 [119]:

- Small and relative simple structures, for which basic stability and performance requirements can be fulfilled by experience and qualitative ground investigation and for which risks are negligible. For this category, it is assumed that ground conditions are known by experience.

- Conventional structures and foundations that can be designed by routine geotechnical procedures. For this category, quantitative site investigation is required and should normally include quantitative analyses; it is to be verified that the design requirements are satisfied.

- This category refers to major civil engineering projects in difficult ground where both large sampling and large modelling is justified.

Within the concept of probabilistic site characterization the knowledge of standards like EN 1997-1 [119] is extended by using statistical and probabilistic methods to combine expert knowledge with the uncertainties of geology and the soil properties recommended [23, 286]. After setting up a conceptual model of the geology, one has to refine this model using a strategic programme of works to progressively reduce uncertainty and to provide the information necessary to assess the risk of the site as proposed by Chaplow [72].

According to Jaksa et al. [187], various factors influence the effectiveness of a site investigation program. Within the geological and geotechnical characterisation of a site one can use different techniques to describe soil layering and soil variability. The *geological and geotechnical characteristics of a site* (number of layers, stratigraphy of the layers and variability of the geotechnical properties) and the expected *response to external loads* (structure and foundation type) can also be used to judge the effectiveness of additional site investigations. A consequence of a first probabilistic characterization can also be the definition of uncertain regions of a site and to optimize any additional characterization efforts with the objective of reducing the amount of uncertainty. Journel and Alabert [189] report that the amount of material that is sampled in site characterization boreholes is typically only 10^{-6} to 10^{-9} of the total site volume, which creates a need for statistical techniques for characterizing uncertainty.

Several authors [320, 337, 341] used methods of artificial intelligence, e.g. artificial neural networks or support vector machines to characterize soil properties within a statistically homogeneous soil layer. Also geostatistical interpolation simulation techniques can be used to evaluate the uncertainty of a conceptual geological-geotechnical model [79, 250].

2.3 Sources of soil variability

Soils are geological materials formed by weathering, erosion and sedimentation processes and, save for residual soils, transported by physical means to their present locations [23]. They have been subjected to various stresses, pore fluids, and physical and chemical changes. Thus, it is hardly surprising that the physical properties of soils vary from place to place within resulting deposits. The scatter observed in soil data comes both from this spatial variability and from errors in testing as shown in table 2.1. Different coefficients of variation of soil parameters are summarized in this table to provide an overview of the variability of design soil parameters presented in literature [183, 282, 283].

Uncertainty in geotechnical engineering can be categorized into aleatoric, epistemic and decision model uncertainty [23, 286, 382]. *Aleatoric uncertainty* consists of physical uncertainty. Physical uncertainty is also known as inherent uncertainty and intrinsic uncertainty and is a natural randomness of a quantity such as the variability in the soil strength from point to point within a soil volume. Such physical uncertainty or natural variability is a type of uncertainty, which cannot be reduced on increasing site investigation according to guidelines presented in [106]. *Epistemic uncertainty* consists of model uncertainty and measurement uncertainty, which can be related to incomplete knowledge. This implies that epistemic uncertainty can be reduced by more data as a type of uncertainty associated with limited, insufficient or imprecise knowledge, as described in [23, 106]; model uncertainty involves imperfections and idealizations made in applied engineering models. Epistemic uncertainty also includes the uncertainty of the chosen distribution as well as the parameter uncertainty, as enlightened in [382], to represent a phenomenon as well as the choice of statistical distribution. In addition to this, Honjo [166] adds the decision model uncertainty. This type of uncertainty includes objectives, values and time preferences, which are related within a project management process within the design of structures. Other types of uncertainties exist such as workmanship, human errors and gross errors, but they are seldomly taken into account, as described in [23, 106, 286].

The different kinds of uncertainty and errors in geotechnical engineering are summarized in figure 2.2. Epistemic and aleatoric uncertainty arise, while setting up a conceptual model for the real ground. The probabilistic characterization of the subsoil model

Table 2.1: Approximate guidelines for coefficients of variation of some design soil parameters taken from [183, 282, 283].

design property [a]	test [b]	soil type	point COV [%]	spatial avg. COV [%] [c]	correlation equation [e]
s_u(UC)	direct (lab)	clay	$20-55$	$10-40$	-
s_u(UU)	direct (lab)	clay	$10-35$	$7-25$	-
s_u(CIUC)	direct (lab)	clay	$20-45$	$10-30$	-
s_u(field)	VST	clay	$15-50$	$15-50$	14
s_u(UU)	q_T	clay	$30-40$ [d]	$30-35$ [d]	18
s_u(CIUC)	q_T	clay	$35-50$ [d]	$35-40$ [d]	18
s_u(UU)	N	clay	$40-60$	$40-55$	23
s_u [e]	KD	clay	$30-55$	$30-55$	29
s_u(field)	PI	clay	$30-55$ [d]	-	32
φ	direct (lab)	clay, sand	$7-20$	$6-20$	-
φ (TC)	q_T	sand	$10-15$ [d]	10 [d]	38
φ (CV)	PI	clay	$15-20$ [d]	$15-20$ [d]	43
K_0	direct (SBPMT)	clay	$20-45$	$15-45$	-
K_0	direct (SBPMT)	sand	$25-55$	$20-55$	-
K_0	KD	clay	$35-50$ [d]	$35-50$ [d]	49
K_0	N	clay	$40-75$ [d]	-	54
E_{PMT}	direct (PMT)	sand	$20-70$	$15-70$	-
E_D	direct (DMT)	sand	$15-70$	$10-70$	-
E_{PMT}	N	clay	$85-95$	$85-95$	61
E_D	N	silt	$40-60$	$35-55$	64

[a] s_u = undrained shear strength
UU = unconsolidated-undrained triaxial compression test
UC = unconfined compression test
CIUC = consolidated isotropic undrained triaxial compression test
s_u(field) = corrected s_u from vane shear test
φ = effective stress friction angle
TC = triaxial compression
φ (CV) = constant volume φ at critical state
K_0 = in-situ horizontal stress coefficient
E_{PMT} = pressure-meter modulus
E_D = dilatometer modulus
[b] VST = vane shear test
q_T = corrected cone tip resistance
N = blow counts in the standard penetration test
KD = dilatometer horizontal stress index
PI = plasticity index
[c] averaging over 5 m
[d] COV is a function of the mean; refer to COV equations in [283] for details
[e] equation numbering in Phoon & Kulhawy [283]

shall take this into account; the transformation error is introduced through the design processes [166]. Uncertainties of the load, of the (mechanical) model and of the decision model are finally 'hidden' in the design result, as described in detail in Honjo & Kuroda [166]. As stated in the introduction, the focus of this chapter is in the description of the uncertainty estimation, which is introduced through the setting up of the conceptual geological ground model.

After doing site investigations, the engineer's aim is to estimate the values at unsampled locations. One would intuitively choose a procedure like interpolation in order to take the sampled properties in the neighbourhood of an unsampled location. A vast variety of methods for interpolation can be found in different textbooks, which are very present in fields like hydrology, statistics or geostatistics. These interpolation methods are based on the concept of spatial correlation. In contrast to the interpolation approach, there are the geostatistical simulation approaches, which are described in chapter 4.

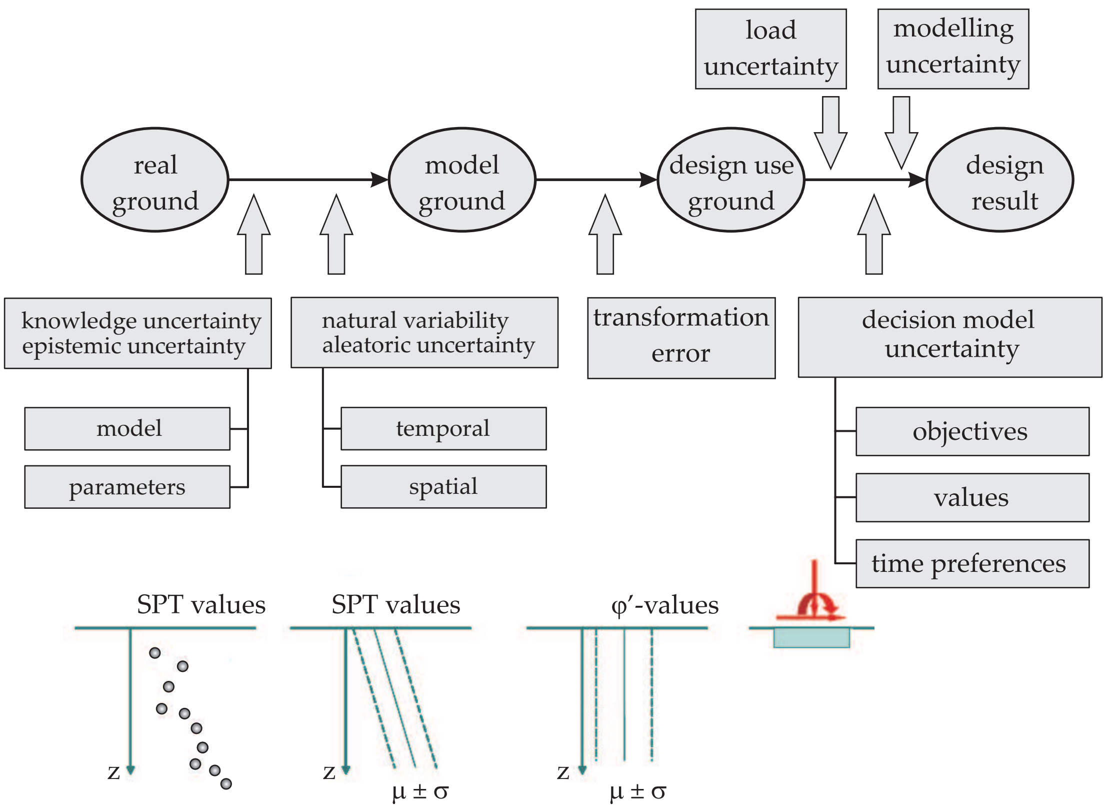

Figure 2.2: Uncertainties in Reliability Based Design modified from Baecher & Christian [23], Honjo [166], Phoon[286] and Phoon & Kulhawy [282, 283].

2.4 Describing spatial variability

2.4.1 Scales of variability in soil science

Many scientists have investigated the spatial variability of soil properties in different fields ranging from hydrology, soil sciences, reservoir engineering up to geotechnical engineering. Some of these findings have been collected and assembled in a database, as described in detail in section 3.5.

Among these authors, Koltermann & Gorelick [204] point out that the spatial variability of soil, and especially in subsurface flow, has to be treated at different scales (table 2.2). Depending on the scale of the study, several direct and/or indirect field investigation methods are thus applied in order to define the main characteristics of the variability of the site. Considering subsurface flow, Koltermann & Gorelick [204] and Matti [246] write that this includes geophysics, bore hole surveys, hydro-chemical analysis, hydraulic well and infiltrations tests, displacement measure, geotechnical laboratory testing. These methods allow a qualitative as well as quantitative description of the heterogeneity in the field of subsurface flow and reservoir engineering. Some may delineate large scale features such as permeable channels, whereas others may detect finer scale transitions. According to the author's knowledge, a comprehensive summary of similar techniques is not available in geotechnical engineering .

It can be clearly seen that there are different scales of variability, ranging from the micro level at the grain size scale to the geological scale of several tens and hundreds of meters as shown in figure 2.3. In this context, heterogeneity can be defined as the opposite of homogeneity and is further used as a synonym of spatial variability at large scales variability.

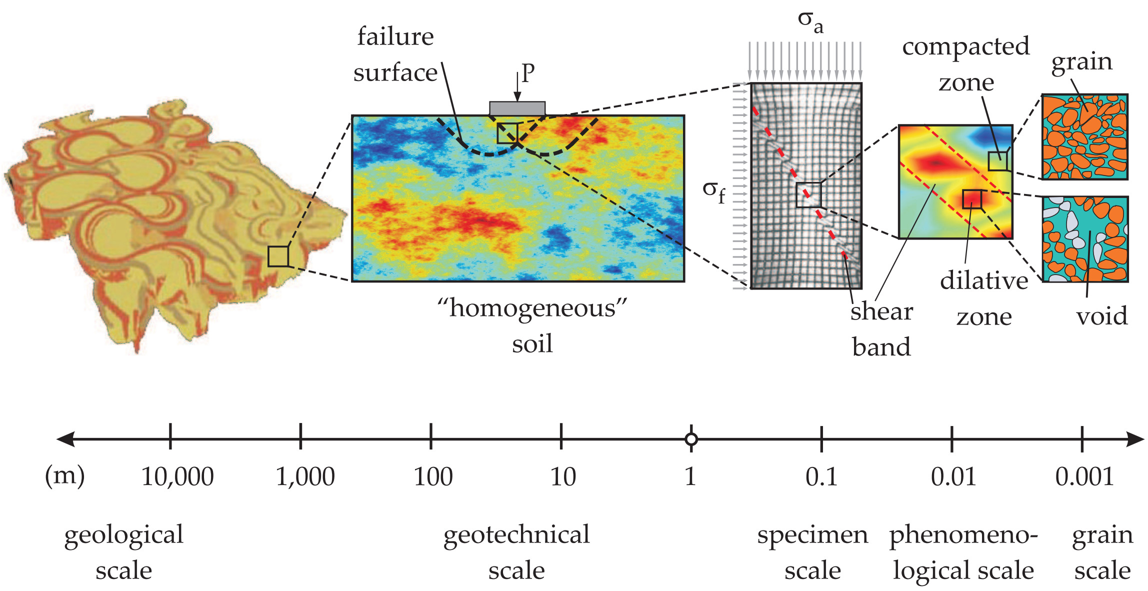

Figure 2.3: Illustration of the multi-scale nature of soil after Borja [48], Chen et al. [73], Christakos [82] and Wackernagel [401].

The geotechnical level is between the specimen scale and the geological scale; therefore, it is important to keep in mind that there is not a single spatial scale, but multiple spatial scales contributing to soil variability. Of course, this plays a role in the evaluation of spatial variability of soil properties as well in the evaluation of the effects of soil variability.

2.4.2 Mathematical description of spatial correlation

As pointed out above, soils are geological materials formed by weathering processes and, save for residual soils, transported by physical means to their present locations [23]. They have been subjected to various stresses, pore fluids, and physical and chemical changes. Thus, it is hardly surprising that the physical properties of soils vary from place to place within resulting deposits. Scatter observed in soil data comes both from this spatial variability and from errors in testing.

This can be mathematically described in a smooth way by using random variables and random functions. In comparison to this, a deterministic variable can just model one outcome; this outcome is either known or unknown leaving no flexibility for uncertainty [304]. Conversely, a *random variable* is an independent variable that can take a series of possible outcomes, each with a certain probability or frequency of occurrence. A random variable is typically denoted with the capital letter Z and its possible outcomes are denoted with the corresponding small case letter $z_i, i = 1, ..., n$. Most applications of geostatistics involve mapping, which is the joint consideration of variables at several locations in space and/or time. For this reason, random functions can be used to describe the joint spatial distribution of variables. A *random function* $Z(\mathbf{X})$ is a set of dependent random variables, each marked with a coordinate vector $\mathbf{x}$. The variable $\mathbf{X} = (x, y, z)$ can involve space coordinates, but also both space and time as e.g. atmospheric pressure, in which case $\mathbf{X} = (x, y, z, t)$, which is rather unusual in geotechnical engineering in comparison to other sciences like earth sciences or meteorology [79, 82].

Using well known means of univariate statistics, one can describe theses measurements using a mean value μ and the standard deviation σ, a coefficient of variation $COV = \sigma/\mu$ and a probability distribution function, as described in Appendix C. Univariate statistics is not able to describe the spatial structure of the data.

As stated by several authors [31, 79, 143, 144, 189], the simplest way of describing spatial variability is to choose the *multi-Gaussian* way. Within the multi-Gaussian approach, a random process or random field can be described by a mean value μ, a standard deviation σ and a covariance function C. For n pairs of a random variable Z of two different locations $\mathbf{X_i}$ and $\mathbf{X_j}$, the covariance $C(\mathbf{X_i}, \mathbf{X_j})$ of the random function $Z(\mathbf{X_i})$ and $Z(\mathbf{X_j})$ is given by equation 2.1. Herein, E denotes the expectation, as described in detail by equation C.1 in the Appendix C.

$$C(\mathbf{X_i}, \mathbf{X_j}) = \mathrm{E}\left[\, (\, Z(\mathbf{X}_i) - \mathrm{E}(Z(\mathbf{X}_i)\,)\,(\, Z(\mathbf{X}_j) - \mathrm{E}(Z(\mathbf{X}_j))\,)\,\right] \tag{2.1}$$

It has to be pointed out that the means of univariate statistics are not influenced by the covariance function. The probability density function can follow e.g. a normal distribution or a lognormal distribution whether or not the investigated data have a spatial

Table 2.2: Different scales of spatial variability of soil properties of sedimentary deposits by Koltermann & Gorelick [204].

Scale name:	Basin	Depositional environments	Channels	Stratigraphical features	Flow regime features	Pores
Approximate length scale	**3 km– 100 km**	**80 m–3 km**	**5 m–80 m**	**0.1 m–5 m**	**2 mm–0.1 m**	**< 2 mm**
Geologic features	Basin geometry, strata geometries, structural features, lithofacies, regional facies trends	Multiple facies, facies relations, morphologic features	Channel geometry, bedding type and extent, lithology, fossil content	Abundance of sedimentary structures, stratification type, upward fning/ or coarsening	Primary sedimentary structures: ripples, cross-bedding, parting lineation, lamination, soft sediment deformation	Grain size, shape, sorting, packing, orientation, composition, cements, interstitial clays
Heterogeneity affected by	Faults (sealing) folding, external controls (tectonic, sea level, climatic history), thickness trends, unconformities	Fractures (open or tight), intrabasinal controls (on fuid dynamics and depositional mechanism)	Frequency of shale beds, sand and shale body geometries, sediment load composition	Bed boundaries, minor channels, bars, dunes	Uneven diagenetic processes, sediment transport mechanisms, bioturbation	Provenance, diagenesis, sediment transport mechanisms
Observations/ measurement techniques	Maps, seismic profles, cross-sections	Maps, cross-sections, lithologic and geophysical logs, seismic profles	Outcrop, cross-well tomography, lithologic and geophysical logs	Outcrop, lithologic and geophysical logs	Core plug, hand sample, outcrop	Thin section, hand lens, individual clast, aggregate analysis
Support volume of hydraulic measurements	Shallow crustal properties	Regional (long term pumping or tracer tests)	Local (short term pumping or tracer tests)	Near-well (non-pumping tests-height of screened interval)	Core plug analysis (permeameter)	Several pores (mini-permeameter)

correlation. In the case of a multivariate distribution, all random variables are linked through a covariance matrix, as defined in equation C.1 in appendix C.

The basic assumptions for the description of spatial variability are as follows:

- STATIONARITY is defined as when the mean value μ and the standard deviation σ are constant over the whole domain. Moreover, the covariance $C(\boldsymbol{\tau})$ is only dependent on the separation $\boldsymbol{\tau}$ and not on the absolute position [403].

- HOMOGENEITY is defined as stationarity of the variance statistically spoken [284], which is closely linked to the definition of the stationarity.

- ERGODICITY is also closely related to stationarity. A random process is said to be ergodic, when the moments of the single observable realization in space approach those of the ensemble as the regional bounds expand towards infinity. According to Webster & Oliver [403], it is of mainly theoretical interest rather than of practical value because the regions studied in geotechnical engineering are finite.

2.5 Quantifying spatial dependence

Different researchers have focused on the description and estimation of spatial variability. Probably the most well known among them are Chiles & Delfiner [79], Journel & Huijbregts [190] and Deutsch & Journel [97] from the field of geostatistics; in the field of geotechnical engineering Vanmarcke [385], Fenton & Griffiths [127] and Phoon [286] have published important contributions. The effects of spatially variable soil properties are still topics of ongoing research in soil sciences [403] or hydrology [82] amongst other disciplines.

Generally speaking, there are two broad approaches in estimating the spatial correlation: the method of moments (MoM) and the maximum likelihood (ML) approaches.

2.5.1 Method of Moments

According to Phoon [286] and Baecher & Christian [23], the most common method of estimating spatial variability is the Method of Moments (MoM). Herein, the statistical moments of the observations (e.g. sample means, variances and covariances) are used as estimators of the corresponding moments of the population being sampled.

The Method of Moments is a non-parametric approach, which means that no assumptions are needed about the mathematical shape of the autocovariance function; there is only a need to assume that the second moments exists. The moment estimator is consistent and asymptotically unbiased. Therefore, it is a desirable method as stated in [23, 27, 79, 182].

The Method of Moments can be subdivided into the variogram technique (MoM_{var}), the autocorrelation function approach and the local average (MoM_{LA}) approach.

2.5.1.1 Variogram approach

The semivariance $\widehat{\gamma}(\boldsymbol{\tau})$ of a random function $Z(\mathbf{X})$ can be computed using equation 2.2, which is also called the empirical variogram or semivariogram (figure 2.7). The lag vector $\boldsymbol{\tau}$ is generally a vector describing the mutual distance between the points. The lag vector $\boldsymbol{\tau}$ becomes a scalar $\tau = |\boldsymbol{\tau}|$ in case of an isotropic variogram. The isotropic variogram describes the spatial correlations as being the same in all directions, for which $\widehat{\gamma}$ can be computed only at integral multiples of the sampling interval.

$$\widehat{\gamma}(\boldsymbol{\tau}) \equiv \frac{1}{2} E\left[(Z(\mathbf{X}) - Z(\mathbf{X}+\boldsymbol{\tau}))^2\right] \approx \frac{1}{2\, m(\boldsymbol{\tau})} \sum_{i=1}^{m(\boldsymbol{\tau})} (Z(\mathbf{X_i}) - Z(\mathbf{X_i}+\boldsymbol{\tau}))^2 \qquad (2.2)$$

The variogram does not require the knowledge of the mean of the random function $Z(\mathbf{X})$ because the squared difference in equation 2.2 eliminates the mean value. Moreover, small variations are filtered out [79].

It has to be pointed out that the variogram approach describes the spatial dependence as an integral of the whole distribution of parameter values. The spatial correlation of the extreme values of the random function $Z(\mathbf{X})$ cannot be investigated separately. In contrast to this is the indicator approach. In equation 2.3 a threshold cut_k is used for truncating the random function $Z(\mathbf{X})$, which is investigated by the variogram approach. The truncation of the random function introduces difficulties in the estimation of the spatial correlation because the truncated random function suffers from a sometimes very skewed distribution. As shown in the following case studies in chapter 3, this causes additional difficulties in the estimation of the spatial correlation.

Choosing different percentile values (appendix C) of the cumulative distribution function of $Z(\mathbf{X})$, one can analyse the different spatial correlation of extreme values. In fact, it has long been recognized [29, 189] that different percentile values for example extremes can have a different spatial dependence structure from the central values. Indicator variograms can be used to express the difference in dependence as a function of the observed values. This requires the specification of the random function $Z(\mathbf{X})$ and threshold cut_k to create the indicator transform $I(\mathbf{X}; cut_k)$ as defined in equation 2.3. Different authors [29, 176, 189] noted that with the help of indicator variograms in many cases the dependence between variables departs considerably from the variogram approach.

$$I(Z(\mathbf{X}; cut_k) = \begin{cases} 1 & \text{if } Z(\mathbf{X}) \leq cut_k \\ 0 & \text{otherwise} \end{cases} \qquad (2.3)$$

The expected value of the indicator random function $I(\mathbf{X}; cut_k)$ identifies the cumulative probability, i.e. the proportion of the property no greater than cut_k [29]:

$$\begin{aligned} \mathrm{E}\,(\, I(\,\mathbf{X}; cut_k)\,) &= 1 \times \mathrm{Prob}\,\{\, Z(\mathbf{X}\,) \leq cut_k\} + 0 \times \mathrm{Prob}\,\{\, Z(\mathbf{X}) > cut_k \,\} \\ &= \mathrm{Prob}\,\{\, Z(\mathbf{X}) \leq cut_k \,\} = F(cut_k) \end{aligned} \qquad (2.4)$$

Similarly, the indicator cross-covariances for two thresholds cut_k and cut'_k and for a separation distance $\boldsymbol{\tau}$ identifies the bivariate (two-point) cumulative distribution function

$F(\cdot)$ [144].

$$\begin{aligned} \mathrm{E}\,(\,I(\,\mathbf{X}; cut_k); I(\,\mathbf{X}+\tau; cut'_k)\,) &\equiv \text{Prob}\,\{\,Z(\mathbf{X}) \leq cut_k, Z(\mathbf{X}+\boldsymbol{\tau}) \leq cut'_k\} \\ &\equiv K_I\,(\boldsymbol{\tau}; cut_k, cut'_k) \end{aligned} \tag{2.5}$$

The indicator cross-covariance describes the covariance between cut_k and cut'_k and is written as:

$$\begin{aligned} C_I\,(\boldsymbol{\tau}; cut_k, cut'_k) &\equiv E\,(\,[I(\mathbf{X}; cut_k) - F(cut_k)]\,[I(\mathbf{X}; cut'_k) - F(cut'_k)]\,) \\ &\equiv K_I\,(\tau; cut_k, cut'_k) - F(cut_k)\,F(cut'_k) \end{aligned} \tag{2.6}$$

For $cut_k = cut'_k$ the indicator cross-covariance becomes the indicator covariance, which can be interpreted as a two point connectivity function [144].

$$C_I\,(\boldsymbol{\tau}; cut_k) \equiv K_i\,(\boldsymbol{\tau}; cut_k) - F^2(cut_k) \tag{2.7}$$

It has to be stressed that connectivity is here used in a probabilistic sense; a high value of the indicator covariance indicates that there is a high probability that any two locations separated by the vector $\boldsymbol{\tau}$ be jointly below the threshold cut_k, but this is not enough to ensure the existences of a continuous path between two points. The indicator covariances are symmetric with respect to the median threshold as derived in [144].

Illustrative results of an indicator analysis of an analytically generated random function can be found in chapter 3.1. The indicator varigoram analysis of measurement data and the involved difficulties are also shown in the case studies in chapter 3.

2.5.1.2 Autocorrelation function approach

The autocorrelation function approach is coming originally from mathematicians and is also applied by engineers to describe spatial variations in soil properties [23]. The formula to compute the (empirical) autocorrelation function $\widehat{\rho}(\boldsymbol{\tau})$ at lag $\boldsymbol{\tau}$ is shown in equation 2.8.

$$\widehat{\rho}(\boldsymbol{\tau}) \equiv \frac{\mathrm{E}\,(Z(\mathbf{X}), Z(\mathbf{X_i}+\boldsymbol{\tau}))}{\mathrm{var}\,(Z\,(\mathbf{X}))} \tag{2.8}$$

Herein, $\boldsymbol{\tau}$ stands for the lag separating the pairs of the random function $Z(\mathbf{X})$. Linking the semivariogram approach shown in figure 2.7 with the autocorrelation function one has to follow equation 2.9.

$$\widehat{\gamma}(\boldsymbol{\tau}) = \mathrm{var}\,(Z\,(\mathbf{X}))\,(1 - \widehat{\rho}\,(\boldsymbol{\tau})) \tag{2.9}$$

2.5.1.3 Local average theory

Central to the development of robust random field models is the concept of the "local average" of a random field. It is seldom useful or necessary to describe in detail the local "point-to-point" variation occuring on a micro-scale in time or space [385]. Even if such information were desired, it may be impossible to obtain. Vanmarcke [385] states that

Heisenberg's principle of uncertainty asserts that true patterns of point–to–point variation cannot be known: there is a basic trade-off between the accuracy of a measurement and the time or distance interval within which the measurement is made. Strain-gauges, stress cells, heat sensors or anemometers (owing to size, inertia, etc.) all measure some kind of local average over space and time. Moreover, through information processing, so called raw data are often transformed into average or aggregate quantities (e.g. one-minute averages, daily or annual totals).

The spatial correlation can be derived from the variance function Γ, which adequately explains the effects of spatial averaging as pointed out by Vanmarcke [385] as well as Wickremesinghe & Campanella [404] among others. Within this thesis this local average approach will be abbreviated with $\mathrm{MoM_{LA}}$.

In general, measurement data are skewed and follow a non-symmetric probability density function. This implies difficult estimation of the variance function. Therefore, these data are transformed to a normal distribution $\mathcal{N}(\mu = 0, \sigma = 1)$ by using a quantile-quantile transformation [79] as shown in figure 3.2.

These data are first considered in pairs ($n = 2$); a moving average series for the data is obtained, where the length of averaging will be equal to the spacing of the data points $Z_2(\mathbf{X})$. The standard deviation σ_2 of this series is also calculated, which will be lower than the standard deviation of the original data set σ due to the cancelling out of fluctuation due to spatial averaging. The above procedure is then extended to $n = 3$, and the corresponding standard deviation σ_3 is calculated with the spacing Z_3 being equal to twice the spacing of the original data points. This procedure is continued until n approaches the total number of data N. The effect of spatial averaging will be more significant with increasing n which $\widehat{\sigma}_1 > \widehat{\sigma}_2 > \widehat{\sigma}_3 > \widehat{\sigma}_4 > \ldots \sigma_n$ as described by [385, 404]. For each n the variance function can be calculated from:

$$\Gamma^2(\mathbf{Z_n}) = \frac{\widehat{\sigma}^{\mathbf{2}}_{\mathbf{n}}}{\widehat{\sigma}^{\mathbf{2}}} \tag{2.10}$$

Herein, $\widehat{\sigma}_n^2$ is the variance of the derived moving average series of degree n, and $\widehat{\sigma}^2$ is the variance of the original data. If the spacing of the data is d, $\mathbf{Z_n}$ in equation 2.10 will be equal to $(n-1)d$. The variance function $\Gamma^2(\mathbf{Z_n})$ in equation 2.10 can be determined for different sizes of the averaging window, which is used for the caluculation of $\widehat{\sigma}_n$. Wickremesinghe & Campanella [404] derive the scale of fluctuation for large values of $\mathbf{Z}$ and very large values of n.

$$\theta = \max(\,\Gamma^2(\mathbf{Z_n}\,)\;\mathbf{Z}\,) \tag{2.11}$$

Wickremesinghe & Campanella [404] recommend to pick the value of $\Gamma^2(\mathbf{Z})$ from the curve of $\Gamma^2(\mathbf{Z_n})\;\mathbf{Z}$ vs. n at a reasonably high value of $\mathbf{Z}$, where there is a distinct change in the curve. $\mathrm{MoM_{LA}}$ offers nearly the same results like other methods of the state-of-the-art for equally spaced and normally distributed data. It can be deduced from the case studies B, C and D in chapter 3 that the $\mathrm{MoM_{LA}}$ approach does not offer reliable results in the case of non equally spaced measurement data. This can be related to the different number of measurement data, which have been used to calculate the variance of different distance classes. This results in a not clearly detectable maximum of equation 2.11.

2.5.2 Maximum likelihood method

The Maximum Likelihood (ML) method of estimating the the unknown parameters $\widehat{\boldsymbol{\Theta}}$ is a parametric method assuming that the distribution of the data is known. ML takes the value of $\boldsymbol{\Theta}$ as an estimate of the unknown parameters $\widehat{\boldsymbol{\Theta}}$ that provides the greatest probability of having measurements $\mathbf{Z}$, as calculated from the joint probability distribution of the observations conditioned on $\boldsymbol{\Theta}$.

The possible outcomes $z(\mathbf{X})$ of the random function $Z(\mathbf{X})$ with mean value $\bar{Z}$ and covariance matrix $\mathbf{C_{ZZ}}$ are assumed to be described by a n-dimensional multivariate normal distribution in equation 2.12.

$$f_{\mathbf{z}}(\mathbf{z}) = \frac{1}{\sqrt{(2\pi)^n\,|\mathbf{C_{ZZ}}|}} \exp\left[-\frac{1}{2}\,(\mathbf{z}-\bar{Z})^T\,\mathbf{C}_{\mathbf{ZZ}}^{-1}\,(\mathbf{z}-\bar{Z})\right] \tag{2.12}$$

The covariance matrix $\mathbf{C_{ZZ}}$ contains the values of the auto-covariance function $C(\mathbf{Z}_i, \mathbf{Z}_j)$ of each possible pair of measurements. Selecting the unknown parameters in a vector $\boldsymbol{\Theta} = [\bar{Z}, \sigma_r, \theta_h, \theta_v]^T$ the log-likelihood for $\boldsymbol{\Theta}$ is given in equation 2.13.

$$L(\boldsymbol{\Theta}|\mathbf{z}) = -\frac{n}{2}\ln(2\pi)\;-\;\frac{1}{2}\ln|\mathbf{C_{ZZ}}|\;-\;\frac{1}{2}(\mathbf{z}-\bar{Z})^T\,\mathbf{C}_{\mathbf{ZZ}}^{-1}\,(\mathbf{z}-\bar{Z}) \tag{2.13}$$

By maximizing the likelihood, the optimal parameter set $\boldsymbol{\Theta}$ can be obtained by standard optimization strategies, for example the simplex method. The advantage of the simplex algorithm is that the results are independent of the initial parameters, hence only depending on data.

De Groot & Baecher [90] state that the maximum likelihood estimators $\widehat{\boldsymbol{\Theta}}$ are asymptotically jointly normally distributed:

$$\widehat{\boldsymbol{\Theta}} \sim \mathcal{N}(\boldsymbol{\Theta}, \mathbf{B}^{-1}) \tag{2.14}$$

where the information matrix $\mathbf{B}$ can be obtained as

$$\mathbf{B} = \mathrm{diag}(B_{\bar{Z}}, \mathbf{B}_{\boldsymbol{\Theta}}) \tag{2.15}$$

where $\boldsymbol{\Theta} = [\sigma_r, \theta_h, \theta_v]^T$ is a vector containing the parameters of the theoretical variogram model. The entries of the information matrix are given in [90] as follows:

$$\begin{aligned} B_{\bar{Z}} &= \mathbf{1}^T\,\mathbf{C}_{\mathbf{ZZ}}^{-1}\,\mathbf{1} \\ B_{\boldsymbol{\Theta}ij} &= \frac{1}{2}\,\mathrm{tr}\left(\mathbf{C}_{\mathbf{ZZ}}^{-1}\,\frac{\partial\mathbf{C_{ZZ}}}{\partial\Theta_i}\,\mathbf{C}_{\mathbf{ZZ}}^{-1}\,\frac{\partial\mathbf{C_{ZZ}}}{\partial\Theta_j}\right) \end{aligned} \tag{2.16}$$

where $\mathbf{1}$ is a unit vector of length n. Using the information matrix $\mathbf{B}$, the accuracy of the obtained parameters is estimated.

2.5.2.1 Consideration of a trend within the ML approach

Assuming a linear regression model to remove a certain trend from the data, the random function $z(\mathbf{x})$ is represented as

$$z(\mathbf{x}) = \mathbf{p}^T(\mathbf{x})\, \boldsymbol{\beta} + \varepsilon(\mathbf{x}) \tag{2.17}$$

where $\mathbf{p}(\mathbf{x})$ is the basis vector of the regression model and $\boldsymbol{\beta}$ contains the regression coefficients. If the correlation structure of the measurements is known in advance, the regression coefficients could be estimated.

$$\hat{\boldsymbol{\beta}} = (\mathbf{P}^T\, \mathbf{R}_{\mathbf{ZZ}}^{-1}\, \mathbf{P})^{-1}\, \mathbf{P}^T\, \mathbf{R}_{\mathbf{ZZ}}^{-1}\, \mathbf{z} \tag{2.18}$$

where $\mathbf{P}$ is the so-called level matrix in the regression model containing the basis vector terms for the measurement positions, and $\mathbf{R}_{\mathbf{ZZ}}$ is the correlation matrix, which is related to the covariance matrix by the residual variance $\mathbf{C}_{\mathbf{ZZ}} = \sigma_r^2\, \mathbf{R}_{\mathbf{ZZ}}$.

The correlation matrix, which can be directly calculated from the correlation lengths and the measurement positions, is generally not known in advance. Thus, the regression can be done only by assuming an initial guess and updating the required parameters iteratively by using either the moment estimator or the maximum likelihood formulation from equation (2.13). Another possibility is to incorporate the regression coefficients directly in the maximum likelihood approach as proposed in [90].

$$L(\boldsymbol{\Theta}|\mathbf{z}) = -\frac{n}{2}\, \ln(2\pi) - \frac{1}{2}\, \ln|\mathbf{C}_{\mathbf{ZZ}}| - \frac{1}{2}(\mathbf{z} - \mathbf{P}\, \boldsymbol{\beta})^T\, \mathbf{C}_{\mathbf{ZZ}}^{-1}\, (\mathbf{z} - \mathbf{P}\, \boldsymbol{\beta}). \tag{2.19}$$

The accuracy of the estimated parameters can be estimated again using the inverse of the information matrix $\mathbf{B}$ where only a slight modification of equation (2.16) is necessary:

$$\begin{aligned} \mathbf{B} &= \mathrm{diag}(B_{\boldsymbol{\beta}}, \mathbf{B}_{\boldsymbol{\Theta}}) \\ B_{\boldsymbol{\beta}} &= \mathbf{P}^T\, \mathbf{C}_{\mathbf{ZZ}}^{-1}\, \mathbf{P} \\ \mathbf{B}_{\boldsymbol{\Theta} ij} &= \frac{1}{2}\, \mathrm{tr}\left(\mathbf{C}_{\mathbf{ZZ}}^{-1}\, \frac{\partial \mathbf{C}_{\mathbf{ZZ}}}{\partial \Theta_i}\, \mathbf{C}_{\mathbf{ZZ}}^{-1}\, \frac{\partial \mathbf{C}_{\mathbf{ZZ}}}{\partial \Theta_j} \right) \end{aligned} \tag{2.20}$$

2.5.2.2 Residual maximum likelihood approach

It has been established [100, 199, 200, 239] that the simultaneous estimation of drift and covariance parameters produces biased estimates of the covariance. The Residual Maximum Likelihood avoids this problem by using special linear combinations of the data (called generalized increments) instead of the original observations. These generalized increments filter the drift and only the covariance parameters are estimated. The generalized increments can be represented as

$$\bar{\mathbf{z}} \equiv \boldsymbol{\Lambda}\, \mathbf{z} \tag{2.21}$$

where the matrix $\boldsymbol{\Lambda}$ is constructed from the projection matrix $\hat{\mathbf{P}}$

$$\hat{\mathbf{P}} \equiv \mathbf{I} - \mathbf{P}\, (\mathbf{P}\, \mathbf{P}^{\mathbf{T}})^{-\mathbf{1}}\, \mathbf{P}^{\mathbf{T}} \tag{2.22}$$

dropping out p rows, because among the generalized increments

$$\bar{\mathbf{z}} = \hat{\mathbf{P}}\ \mathbf{z} \tag{2.23}$$

p increments are linearly dependent on the others [197]. The matrix $\hat{\mathbf{P}}$ has the property that:

$$\hat{\mathbf{P}}\ \mathbf{P} = \mathbf{0} \tag{2.24}$$

then

$$\bar{\mathbf{P}}\ \bar{\mathbf{z}} = \hat{\mathbf{P}}\ \mathbf{P}\ \boldsymbol{\beta} + \hat{\mathbf{P}}\mathbf{e} = \hat{\mathbf{P}}\ \boldsymbol{\varepsilon} \tag{2.25}$$

and the drift is filtered out, whatever the coefficients $\boldsymbol{\beta}$ are. Here, the increments $\mathbf{z}$ are assumed to be normally distributed $\mathcal{N}(\mu = 0, \sigma = 1)$ and the covariance parameters are estimated by the minimization of the negative log-likelihood function similar to equation 2.19. Herein, $\mathbf{z}$ is substituted by $\bar{\mathbf{z}}$, $\mathbf{C_{ZZ}}$ by $\boldsymbol{\Lambda}\ \mathbf{C_{ZZ}}\ \boldsymbol{\Lambda}^{\mathbf{T}}$ and $\mathbf{P}\ \boldsymbol{\beta}$ is dropped [270].

$$\begin{aligned} L(\widehat{\sigma}^2, \theta|\bar{\mathbf{z}}) \;&=\; \frac{m}{2}\ \ln(2\ \pi) + \frac{m}{2} - \frac{m}{2}\ \ln(m)\ + \\ &+\frac{1}{2}\ \ln(\boldsymbol{\Lambda}\ \mathbf{C_{ZZ}}\ \boldsymbol{\Lambda}^{\mathbf{T}}) + \frac{\mathbf{1}}{\mathbf{2}}\ \ln\left(\bar{\mathbf{z}}^{\mathbf{T}}(\boldsymbol{\Lambda}\ \mathbf{C_{ZZ}}\ \boldsymbol{\Lambda}^{\mathbf{T}})^{\mathbf{-1}}\ \bar{\mathbf{z}}\right) \end{aligned} \tag{2.26}$$

where $m = n - p$. The same method of minimization can be used to obtain the Residual Maximum Likelihood estimates of $\boldsymbol{\Theta}$.

The accuracy of the estimated parameters can be estimated by using equation 2.27 as shown in [403].

$$\sigma = \frac{1}{n-p}\ \mathbf{z}^T \left(\boldsymbol{\Lambda}\ \mathbf{C_{ZZ}}\ \boldsymbol{\Lambda}^{\mathbf{T}}\right)^{-1} \mathbf{z} \tag{2.27}$$

2.5.3 Additional approaches

Hybrid approaches: The Akaike Information Criterion, which is described in detail in section 2.6.4, was merged with the ML-approach by Honjo [165]. Due to efficiency, this was extended with a Bayesian approach to the Extended Bayesian Method.

Bayesian inference has not been widely used in geotechnical or geostatistical applications [42, 110, 198, 400] for the evaluation of the correlation length. It is less well developed than the MoM or ML approach.

Transition probability & Markov chain: Especially in capturing the uncertainty in subsurface flow simulation as well in soil pattern simulation, the concept of Markov chains is used to describe heterogeneity as pointed out in Elfeki [115] and Carle & Fogg [69]. A Markov chain is a probabilistic model that exhibits a special type of dependence [79, 115]. In formulae, let $Z_0, Z_1, \ldots, Z_m$ be a sequence of random variables taking values in the state space $S_1, S_2, \ldots, Z_n$. The sequence is a Markov chain model, if

$$\text{Prob}(Z_i = S_k|Z_{i-1} = S_l|Z_{i-2} = S_n|Z_{i-3} = S_r, \ldots Z_0 = S_p) \equiv p_{lk} \tag{2.28}$$

where the symbol "|" is the symbol for conditional probability. In one dimensional problems a Markov chain is described by a single transition probability matrix. Transition probabilities correspond to relative frequencies of transitions from a certain state to another state. Theses transition probabilities can be arranged in a square matrix form.

$$\mathbf{p} = \begin{bmatrix} p_{11} & p_{12} & \dots & \dots & p_{1n} \\ p_{11} & \ddots & \dots & \dots & \vdots \\ \vdots & \dots & p_{lk} & \dots & \vdots \\ p_{n1} & \dots & \dots & \ddots & p_{nn} \end{bmatrix} \tag{2.29}$$

where p_{lk} denotes the probability of transition from state S_l to state S_k; n is the number of states in the system. Thus the probability of a transition from S_1 to $S_1, S_2, \dots S_n$ is given by p_{1l} , $l = 1, 2, \dots n$ in the first row and so on. The matrix $\mathbf{p}$ has to fulfil specific properties. Its elements are non-negative, $p_{lk} \geq 0$ and the elements of each row sum up to one. For a more detailed explanation and extension of this approach (e.g. to more dimensions, to multiple steps or to conditioning to measurements) and application of this concept the reader is referred to Elfeki [115] and Caers [64].

Copula approach: Geostatistical literature [4, 29, 31, 151] offers via the copulas statistics another means to describe spatial dependence. Copula describe the dependence structure between random variables in a more general but also complex way than the variogram. Therefore, copulas are useful tools to describe the spatial dependence. A detailed explanation of copulas and their relationship to indicator variograms is presented by Bardossy [29].

2.5.4 Sampling strategies

It is stated by various authors like Webster & Oliver [403] or Brus & de Gruijter [56] amongst others [90, 142] that the classical statistical theory of independent, identically distributed samples is not applicable in geosciences because in this case data are spatially correlated. For this purpose, new methods have been developed taking into account two sources of randomness: the location of the samples and the measurement error as shown in table 2.3.

Brus & de Gruijter [56] define the fully deterministic, design based and model based as well as fully random strategies via the fixed or random locations as well as values.

Table 2.3: Types of sampling strategies defined by two sources of randomness according to Brus & de Gruijter [56].

		VALUES AT GIVEN LOCATIONS	
		fixed	random
SAMPLE LOCATIONS	fixed	fully deterministic strategies	model base stategies
	random	design based strategies	fully random strategies

In the *design based approach*, stochasticity is introduced at the stage of sampling [56]; the sample locations are selected by predefined procedures such as pure random sampling. Stratified sampling, clustered sampling or nested sampling offer a smooth way of describing a heterogeneous population [21, 23, 56, 84]. Basically spoken, homogeneous groups are set up inside the heterogeneous population, in which properties can be linked to the variance of the population. This approach is widely used in geostatistics and will be described in detail later.

In the *model-based approach* the soil forming process, which has led to the field of values of a property in the study area, is modelled as a stochastic process. The difference of these two approaches is how the sample data are weighted. In the design-based approach the weights are derived from the sampling design; in the model-based approach the weights are derived from the chosen model and the actual configuration of the sample locations. According to [56], the model based approach is used in the field of geo-environmental engineering in the context of contaminated soils.

Chiles & Delfiner [79] state that the choice of the sampling concept depends on the objective of the sampling (e.g. exploration or placement of a new well in petroleum exploration). Of course, one has also to take practical constraints such as accessibility and costs into account. They emphasize that the randomness as introduced by sampling on a regular grid is smaller compared to stratified random sampling and pure random sampling.

In geotechnical literature, Baecher [21] provides an overview of search theory and its implications in probabilistic site description. Later, Tang [370] and Halim & Tang [150] worked on geometric models of anomalies using the Bayesian principle. Herein, single stage search and grid search concepts are used in a Bayesian context leading finally to a sequential search approach.

Recently, Schweckendiek & Calle [331] used the Bayesian approach in a risk based concept. Li et al. [220] proposed an alternative approach using copula statistics in this context. In the field of geography [146] an alternative approach based on the fuzzy method is presented. Sampling schemes, which are optimized by adaptive sampling [237] procedures or simulated annealing [359] are presented in the soil sciences as promising new developments.

2.5.5 Estimation of the different scales of spatial variability

As pointed out in chapter 2.4.1, spatial variability of soil properties occurs at different scales depending on the type of problem. Among others [61, 82, 125, 184, 401], Vanmarcke [384] recognizes the multiple scales of soil variability. He suggests that geotechnical properties may exhibit two or more superimposed scales of fluctuation, depending on the modelling scale. In the one dimensional case, Vanmarcke [384] suggests to combine different correlation functions by simply summing them up. Jacksa [184] uses this concept in an illustrative case study to combine two scales, as shown in figure 2.4.

In geostatistics [79, 190, 401], a nested models refers to a model of spatial variation, which may be described by the simple addition of spatial variograms with different parameters and possibly by different forms. A nested variogram $\gamma(\boldsymbol{\tau})$ is set up by adding

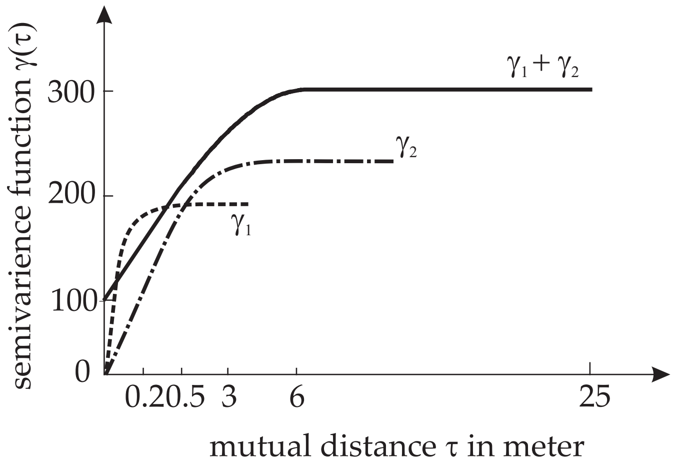

Figure 2.4: Nested variogram from Jaksa [184].

n elementary variograms (figure 2.4). This approach is not very common in geotechnical literature [184, 384].

$$\gamma(\boldsymbol{\tau}) = \sum_{i=1}^{n} \gamma_i(\boldsymbol{\tau}) \tag{2.30}$$

An alternative way is offered by the so called fractal approach. Herein, fractals are used to model the self-similarity of natural phenomena. This offers the opportunity to describe the phenomena at different scales and fractals can portray an exact self-similarity. Fenton [126] suggested that such fractal or long memory behaviour is likely to be present due to the large scale mixing processes (e.g. erosion, transportations, deposition and weathering) that are involved in the formation of soils.

According to Webster & Oliver [403], Bellehumeur & Legendre [33], Cheng [74] and Burrough [59–61], the fractal dimension of transects and surfaces can be related to the variogram. One big advantage of this approach is the modelling of irregular spaced data, but a vast amount of data are needed for this method.

In environmental and agricultural sciences, the nested sampling approach is used to characterize multi-scale phenomena. Nested sampling refers to a form of multi-stage sampling, because the higher stage units are "nested" within the lower stage units [281, 403].

Apart from these nested structures and the nested sampling approach, various authors offer hybrid approaches combining the different approaches mentioned above or adding new promising schemes like adaptive schemes [237], sequential schemes [187], Bayesian approaches [150] or copula statistics [220].

2.6 Variogram calculation

The simplest case for calculating the variogram is an equally spaced dataset as shown in figure 2.5 (a). First, the squared differences between neighbouring pairs of values z_1 and

z_2, z_2 and z_3 are determined for each position and averaged.

If there are missing values at some locations, then there will be fewer neighbouring pairs as indicated in figure 2.5 (b).

If data are irregularly scattered then the average semivariance of a particular lag can be derived only by grouping the individual lag distances between pairs of points, as depicted in figure 2.6 and as shown in equation 2.31. In typical geostatistical literature [30, 97], the classical equation of determination of the semi-variogram is

$$\hat{\gamma}(\boldsymbol{\tau}) = \frac{1}{2N(\boldsymbol{\tau})} \sum_{(ij)\in R(\boldsymbol{\tau})} [Z(\mathbf{X}_i) - Z(\mathbf{X}_j)]^2 \tag{2.31}$$

where

$$R(\boldsymbol{\tau}) = \{\boldsymbol{\tau} - w/2 \ \leq \ d_s(u_i, u_j) \ \leq \ \boldsymbol{\tau} + w/2\} \tag{2.32}$$

$d_S(\mathbf{X}_i, \mathbf{X}_j)$ is the spatial distance between the spatial point sets $\mathbf{X}_i, \mathbf{X}_j$, $N(\boldsymbol{\tau})$ is the number of pairs in $R(\boldsymbol{\tau})$ and w is the width of the spatial distance class as shown in figure 2.6. The bigger the w becomes, the smoother is the semi-variogram because the ε filters out the very high and low values.

The variograms of second-order stationary processes reach upper bounds, at which they remain constant after their initial increases as shown in figure 2.7. A variogram may reach its sill at a finite lag distance, in which case it has a range, also known as the correlation length; since this is the range at which the autocorrelation becomes 0 (figure 2.7). This separation marks the limit of spatial dependence. Places further apart than this are spatially independent. For practical purposes their effective ranges are usually taken as the lag distances at which they reach 95% of their sills [79, 97, 190, 401].

Some semi-variograms may approach their sills asymptotically, and so they have no strict ranges. This can indicate a trend in the data. In some instances the variogram decreases from its maximum to a local minimum and then increases again, figure 2.7. This maximum is equivalent to a minimum in the covariance function, which appears as a hole. This form arises from fairly regular repetition in the process. A variogram

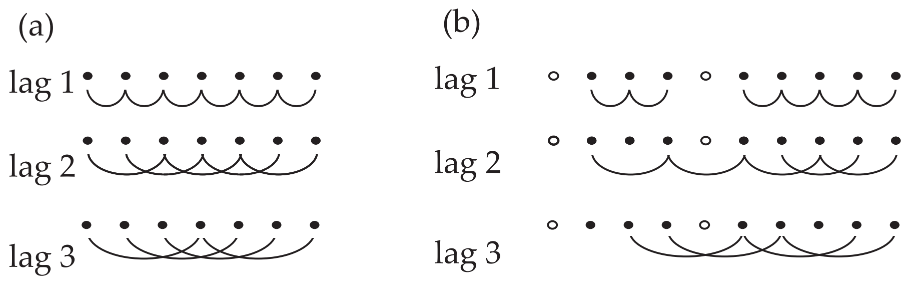

Figure 2.5: Comparison for computing a variogram from regular sampling on a transect: (a) with a complete set of data, indicated with $\bullet$ and (b) with missing values indicated by $\circ$ from [403].

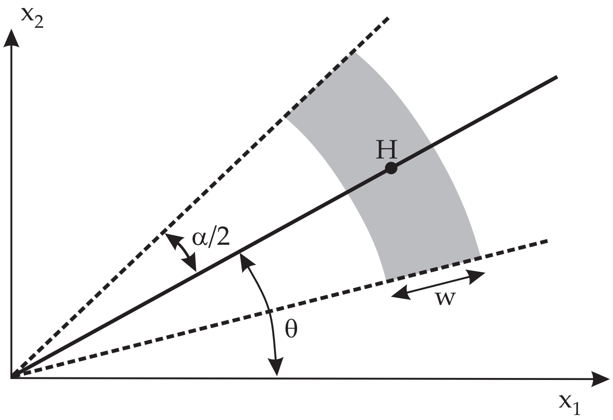

Figure 2.6: The geometry for discretizing the lag into bins by distance and direction in two dimensions from [403].

that continues to fluctuate with a wave-like form with increasing lag distance signifies greater regularity.

If there is only a neglectable or just a little range in the semivariogram, this is called a *nugget effect*. This discontinuity at the origin of the semivariogram is used to characterize the residual influence of all variabilities, which have a range much smaller than the available distances of observation [190]. The nugget effect is equivalent to the well known phenomenon of white noise in physics.

A semivariogram is said to display a *hole effect* when its growth is not monotonic and shows bumps, which reflects the tendency for high values to be systematically surrounded by low values and vice versa [79]. Journel & Huijbregts [190] attribute the hole effect to different reasons. They recommend in case of periodic sampling distances that the hole effect may result in a refined investigation scheme.

2.6.1 Theoretical variogram models

It is necessary to know the variogram $\gamma(\boldsymbol{\tau})$ at any value of $\boldsymbol{\tau}$, if one wants to use the variogram in terms of geostatistical simulation or interpolation. For this reason it is necessary to fulfil the continuity, the differentiability condition and the conditional positiveness as shown in detail in Chiles & Delfiner [79]. Amongst others, Gascuel-Odoux & Boivin [134] specify several sources of error: firstly only one realization is generally available in nature and it is considered as representative; also errors in the experimental variogram due to sampling and measurement must be considered; secondly, errors may result from the choice of the model and estimation of the theoretical variogram [134].

The semivariogram has to be approximated to be able to simplify further work like e.g. performing a stochastic simulation or interpolation between measurements. For this reason, the behaviour of the variogram model has to be defined at the origin and over the entire range. Different theoretical variogram models can be classified, according to [190], into *models with a sill* (bilinear model equation 2.33), *spherical variogram* (linear

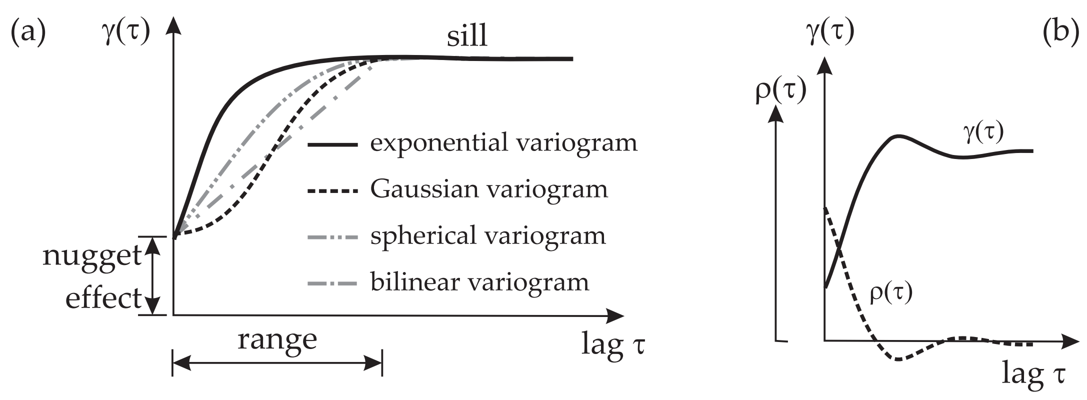

Figure 2.7: Theoretical variogram functions (a) and comparison of semivariance function and autocorrelation function (b).

behaviour at the origin, equation 2.34), *exponential variogram* (linear behaviour at the origin, 2.35), *Gaussian variogram* (parabolic behaviour at the origin, equation 2.36), *models without a sill* (power functions, fractal model, logarithmic variogram). Other models like the cubic model, generalized Cauchy models, K-Bessel model, power-law model, pentaspherical model, Matern model or logarithmic model can be found in standard geostatistical textbooks [79, 190, 401, 403].

$$\gamma(\boldsymbol{\tau}) = \begin{cases} \boldsymbol{\tau}/a & \text{for } \boldsymbol{\tau} \leq a, \\ a & \text{for } \boldsymbol{\tau} > a \end{cases} \tag{2.33}$$

$$\gamma(\boldsymbol{\tau}) = \begin{cases} c\{\frac{3\boldsymbol{\tau}}{2\,b} - \frac{1}{2}\left(\frac{\boldsymbol{\tau}}{b}\right)^3\} & \text{for } \boldsymbol{\tau} \leq b\,, \\ c & \text{for } \boldsymbol{\tau} > b \end{cases} \tag{2.34}$$

$$\gamma(\boldsymbol{\tau}) = 1 - \exp\left(-\frac{\boldsymbol{\tau}}{c}\right) \tag{2.35}$$

$$\gamma(\boldsymbol{\tau}) = 1 - \exp\left(-\frac{\boldsymbol{\tau}^2}{d^2}\right) \tag{2.36}$$

2.6.2 Estimation of the theoretical variogram function

To compare different theoretical variogram models, it is necessary to fit theoretical variogram models in a standard way and automatically to the sample variogram in order to avoid judgement errors. In the course of a detailed geostatistical analysis, an automatic fit rarely provides definitive results [79]. Chiles & Delfiner [79] as well as Deutsch & Journel [97] point out that this can be only the first step of a manual fit.

Generally, we look for a variogram $\gamma(\boldsymbol{\tau}; \mathbf{b})$ where $\mathbf{b}$ represents a vector of the parameters of the variogram (e.g. range, sill, nugget effect,...) of n available pairs of data. This vector $\mathbf{b}$ can be evaluated by minimizing the following equations:

- ORDINARY LEAST SQUARES:

$$Q(\mathbf{b}) = \sum_{\mathbf{j=1}}^{\mathbf{n}} \left[\widehat{\gamma}(\boldsymbol{\tau}_{\mathbf{j}}) - \gamma(\boldsymbol{\tau}_{\mathbf{j}}; \mathbf{b})\right]^{\mathbf{2}} \tag{2.37}$$

- GENERALIZED LEAST SQUARES:
  By minimizing equation 2.38, one can take into account the different correlations between the different values of the sample variogram.

$$Q(\mathbf{b}) = \left[\widehat{\gamma}(\boldsymbol{\tau}_{\mathbf{j}}) - \gamma(\boldsymbol{\tau}_{\mathbf{j}}; \mathbf{b})\right]^{\mathbf{T}} \ \mathbf{V}^{\mathbf{-1}} \ \left[\widehat{\gamma}(\boldsymbol{\tau}_{\mathbf{j}}) - \gamma(\boldsymbol{\tau}_{\mathbf{j}}; \mathbf{b})\right] \tag{2.38}$$

  Herein, $\widehat{\gamma}(\boldsymbol{\tau}_j)$ is the vector of the empirical variogram, $\mathbf{V}$ is the variance-covariance matrix of $\widehat{\gamma}(\boldsymbol{\tau})$. The calculation of the variance covariance matrix is rather complicated as highlighted by Ortiz & Deutsch [268].

$$\mathbf{V}(\boldsymbol{\tau}) = \mathrm{E}\left\{ \left[Z(\mathbf{X}_i) - Z(\mathbf{X}_i + \boldsymbol{\tau}) \right]^2 \cdot \left[Z(\mathbf{x}_\mathbf{j}) - \mathbf{Z}(\mathbf{X}_\mathbf{j} + \boldsymbol{\tau}) \right]^2 \right\} - \left[2\,\widehat{\gamma}(\boldsymbol{\tau}) \right]^2 \tag{2.39}$$

- WEIGHTED LEAST SQUARES:
  A compromise between efficiency and simplicity is the weighted least squares, namely the minimization of $Q(\mathbf{b})$:

$$Q(\mathbf{b}) = \sum_{\mathbf{j=1}}^{\mathbf{n}} \mathbf{w}_{\mathbf{j}}^{\mathbf{2}} \ \left[\widehat{\gamma}(\boldsymbol{\tau}) - \gamma(\boldsymbol{\tau}_{\mathbf{j}}; \mathbf{b}))\right]^{\mathbf{2}} \tag{2.40}$$

  Herein, $\mathbf{w}$ is the weight, which can be the reciprocal of the number of pairs at each lag, as proposed by Matheron [240] or also the variance at each point [79, 268]. The variance-covariance matrix in equation 2.39 can be used to calculate the variance of the variogram. The expression 2.41 tells us that the uncertainty in the variogram at a distance $\boldsymbol{\tau}$ is the average covariance between the pairs of the pairs used to calculate the variogram for that particular lag assuming a multivariate Gaussian distribution of the variables.

$$\mathbf{w} = \frac{1}{\sigma^2_{2\gamma(\boldsymbol{\tau})}} = n(\boldsymbol{\tau}) / \sum_{i=1}^{n(\boldsymbol{\tau})} \sum_{j=1}^{n(\boldsymbol{\tau})} V_{ij}(\boldsymbol{\tau}) \tag{2.41}$$

  There are different approaches for choosing the weights $\mathbf{w}$. Cressie [87] shows that for equally spaced Gaussian variables, the variance of the estimates can be approximated by equation 2.42:

$$\mathbf{w} \approx \frac{N(\boldsymbol{\tau})}{2\left[\,\widehat{\gamma}(\boldsymbol{\tau})\,\right]^2} \tag{2.42}$$

  where $\hat{\gamma}^2(\boldsymbol{\tau})$ is the value of the theoretical variogram and $N(\boldsymbol{\tau})$ is the number of pairs at a mutual distance of $\boldsymbol{\tau}$. It is argued by several authors [79, 87, 272] that this estimation is too crude to construct confidence intervals.

McBratney & Webster [247] redefined this further:

$$\mathbf{w} \approx \widehat{\gamma}^3(\boldsymbol{\tau})/m(\boldsymbol{\tau})\,\widehat{\gamma}(\boldsymbol{\tau})^2 \tag{2.43}$$

where $\widehat{\gamma}(\boldsymbol{\tau})$ is the observed value of the semivariance at $\boldsymbol{\tau}$. This is usually desirable for kriging , though it might be less desirable if the aim is to estimate the spatial scale of variation. The process of fitting must iterate even where all the parameters are linear because the weights in the two schemes depend on the values expected from the model.

2.6.3 Alternative approaches

The theoretical variogram can also be fitted to the experimental variogram by using different techniques. This can be done by maximizing the likelihood function of the residual between the theoretical variogram function and the semivariogram values, as explained in Chiles & Delfiner [79] in detail. Another possibility is offered by Ecker & Gelfand [110], offering a Bayesian approach to conduct the fitting of the theoretical variogram. Using the ML approach, the theoretical variogram function is fitted to the available data as pointed out above.

2.6.4 Model selection using the AKAIKE Information criterium

The selection of the most appropriate model is done via the AKAIKE INFORMATION CRITERITUM (AIC) [6], which is defined for a finite sample set n:

$$\text{AIC} \;=\; 2\,k \;-\; 2\;\ln(L) \tag{2.44}$$

where k is the number of parameters in the statistical model, and L is the maximum value of the likelihood function for the estimated model. The first term is a measure of the quality of fit of a model and the second is a penalty factor for the introduction of additional parameters into the model. AIC is a measure of the loss of information incurred by fitting an incorrect model to the data. Therefore, given a set of different models for the data, the preferred model is the one with the minimum AIC value. Hence AIC not only rewards goodness of fit, but also includes a penalty that is an increasing function of the number of estimated parameters. This penalty discourages overfitting. The preferred model is the one with the lowest AIC value. Assuming that the model errors are normally and independently distributed, the AIC can be rewritten for a fitting by least squares. Herein, the residual sum of the squares (RSS) are defined:

$$\text{AIC} \;=\; 2\,k \;-\; n\,[\,\ln(\,2\pi\,\text{RSS}/n\,) \;+\; 1\,] \tag{2.45}$$

$$\text{RSS} = \sum_{i=1}^{n} \widehat{\varepsilon}_i \tag{2.46}$$

One can clearly see by looking at equations 2.45 and 2.44 that for a big sample size n the AIC is independent of n.

Alternatively, different information criteria amongst others like BIC or KIT can be used for small sample sizes or other boundaries, which is described in detail in literature [7, 52, 403].

Table 2.4: Relationship between the scale of fluctuation δ and the correlation distance θ for various autocorrelation functions from Vanmarcke [384].

Autocorrelation function		δ	$\frac{\theta}{\delta}$
$\rho(\boldsymbol{\tau}) = \begin{cases} 1 - \lvert\boldsymbol{\tau}\rvert / a & \text{for } \lvert\boldsymbol{\tau}\rvert < a \\ 0 & \text{for } \lvert\boldsymbol{\tau}\rvert \geq a \end{cases}$	bilinear model	a	1
$\rho(\boldsymbol{\tau}) = e^{-\lvert\boldsymbol{\tau}\rvert/b}$	Markov model	$2b$	$1/2$
$\rho(\boldsymbol{\tau}) = e^{-(\lvert\boldsymbol{\tau}\rvert/c)^2}$	Gaussian model	$\sqrt{\pi}c$	$1/\sqrt{\pi}$

2.7 On the correlation length

Within the description of spatial variability one has to distinguish between the correlation length and its related model parameters. The definition of the correlation length was introduced by Vanmarcke [385], which is refereed to by other authors [27, 68, 127, 156, 184, 288, 408]. They often call it scale of fluctuation.

Vanmarcke [385] defines the correlation length in equation 2.47. The correlation length θ is the distance within which points are significantly correlated (i.e. by more than about 10 %), as described by Fenton [127]. Conversely, two points separated by a distance more than θ will be largely uncorrelated.

$$\theta = \int_{-\infty}^{\infty} \rho(\boldsymbol{\tau})\, d\tau = 2 \int_{0}^{\infty} \rho(\boldsymbol{\tau})\, d\boldsymbol{\tau} \tag{2.47}$$

The correlation length is defined without the factor of 2 shown to the right-hand side of equation 2.47 especially in the geostatistical literature e.g. Journel & Huijbregts [190]. Equation 2.47 implies that θ has to be finite; otherwise, alternative concepts like fractal processes have to be used [127]. Another consequence for the application in engineering sciences as well as in earth sciences is that the correlation function is only meaningful for strictly non-negative correlation functions.

The correlation length can also be defined in terms of the variance function in the local averaging context as a limit [127, 385], whereas the correlation length θ is assumed to be finite.

$$\theta = \lim_{T \to \infty} T\, \gamma(T) \tag{2.48}$$

DeGroot & Baecher [90] state that the Method-of-Moments (MoM) is unbiased in the case of infinite samples. Otherwise, the correlation length is dependent on the sample size. It can be clearly seen in figure 2.8 that for a finite record length L of the data, which are sampled with a mutual separation distance $\boldsymbol{\tau}$, the estimation of the correlation length is strongly biased. These findings coincide with the suggestions of Journel & Huijbregts [190] or Chiles & Delfiner [79]. They recommend to sample with a distance between the measurement points that is at least smaller than $1/5$ to $1/4$ of the correlation length.

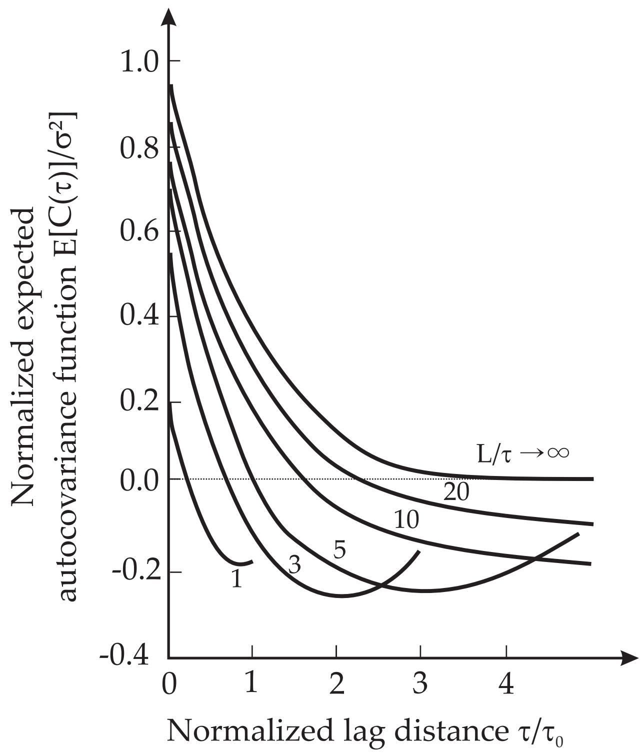

Figure 2.8: Dependency of the correlation length on the sample size, taken from DeGroot & Baecher [90].

2.7.1 Uncertainty of the correlation length

In [79, 403], the uncertainty of the correlation length is connected with the application e.g. spatial interpolation or (geostatistical) simulation. Within the concept of interpolation, cross-validation is used to investigate the influence of the correlation length, as described in detail in Webster & Oliver [403].

As mentioned above, different sources like measurement and modelling errors (statistical model, nested structures,... etc.) cause an uncertainty of the evaluated correlation length. Focusing on the Method of Moments, the main source of uncertainty is the definition of the distance and direction classes (figure 2.6). In the case of too wide classes, the resulting variogram will be smoothed too much, whereas in the other case the variogram will be too *noisy*. As pointed out in section 2.6.2, several authors express the uncertainty of the correlation length via the experimental variogram $\widehat{\gamma}(\boldsymbol{\tau})$ to calculate the variance and the correlations of the values of the experimental variogram $\widehat{\gamma}(\boldsymbol{\tau})$. Herein, they use an approximation of the variance-covariance matrix of the experimental variogram by assuming a normal distribution for the variance-covariance matrix, which is difficult to verify in any application. The variances of $\widehat{\gamma}(\boldsymbol{\tau})$ can be used as weights for fitting the theoretical variogram to the values of the experimental variogram. This offers also a link to the uncertainty of the correlation length.

In the Maximum Likelihood approach, the assumption of normal distributed variables

Table 2.5: Typical ratios of the horizontal θ_{hor} and vertical correlation lengths θ_{ver} collected from literature [27, 79, 96, 97, 190, 204, 401, 408].

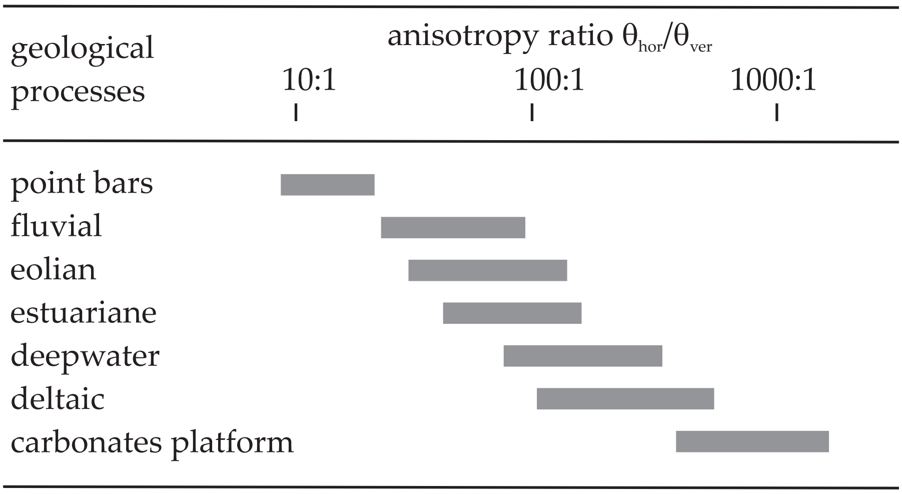

is governing the whole evaluation of the correlation length. The estimation of the uncertainty of the evaluated spatial correlation is a by-product of the ML procedure as shown in equation 2.16 and for data with a linear trend equation 2.19. Via these equations it is possible to estimate the error of the estimated variogram model-parameters and consequently also of the correlation length.

2.7.2 Anisotropy with respect ot the correlation length

Following the introduction to geostatistics presented in Chiles & Delfiner [79], Deutsch & Journel [97] and Wackernagel [401], one will encounter the anisotropy in the spatial correlation of measurement data. Anisotropy, being defined as the ratio of horizontal θ_{hor} and vertical correlation length θ_{ver}, can be classified in zonal and horizontal-to-vertical anisotropy.

Zonal anisotropy is related to stratification. This implies that the sill value of the horizontal and vertical variogram are different, which can attributed to different sample distributions. Deutsch [96] points out the importance of the conceptual geological model to describe this in detail (e.g. figure 2.7).

Horizontal-to-vertical anisotropy can be related to the geological processes which formed the investigated statistically homogeneous layer.

Different anisotropy ratios from literature [27, 79, 96, 97, 190, 204, 401, 408] are summarized in table 2.5. Most of these sources are from geostatistics as well as from petroleum engineering. Therefore, the names of the different categories in table 2.5 come from engineering geology and petroleum engineering. It can be deduced from table 2.5 that the bigger the geological process is the bigger will be the anisotropy ratio $\theta_{hor}/\theta_{ver}$. The anisotropy ratios range from from $10:1$ up to $1,000:1$. Therefore, it can be concluded that it is of major importance to set up a conceptual geological model before working on the spatial variability.

2.8 Synopsis

Within this chapter different approaches to quantify spatial variability are presented, which are used to quantify the different scales of soil variability. The literature review on this showed that the most used approaches are the variogram approach, the local average approach and the Maximum Likelihood approach. Therefore, the author is concentrating on these methods to evaluate purely the spatial variability of soil properties without considering a trend.

Chapter 3

Case studies on the evaluation of spatial variability

This chapter provides a comparison of the Method-of-Moments (MoM) and the Maximum Likelihood (ML) approaches by applying them to four different case studies. The Method-of-Moments methods include the variogram (MoM_{var}) in chapter 2.5.1.1 and the local average approach (MoM_{LA}) in chapter 2.5.1.3. These approaches are used to analyse data fulfilling the basic assumptions of stationarity, homogeneity and ergodicity. Via this, the possibilities and limitations of these approaches are discussed while applying them to analytically generated random sequence as well as to equally and non equally spaced data.

Moreover, the indicator approach is used to analyse the correlation structures of measurement data to compare theses results to the indicator correlation lengths of an analytically defined random process.

The results of these case studies are compared to the literature database, which is covering the author's knowledge of publications on the spatial variability of soil properties.

On top of this, the results of a study on the spatial correlation of different soil types is presented, which is based on the analysis of CPT databases. Finally, these different sources of information on spatial variability are merged via the Bayesian Model Averaging approach.

3.1 Case study A – Random function

The aim of this case study is the investigation of the possibilities and limitations of MoM_{var}, MoM_{LA} and ML through the analysis of a random process with a predefined correlation length. All three approaches offer the same correlation length for a symmetrical probability density function (pdf) of the random process. It is shown that the more skewed the lognormal pdf becomes, the more differ the correlation lengths evaluated by the MoM_{var}, MoM_{LA} and ML approach. In addition to this, different levels of random noise are added to the random process. This adds additional difficulty to the calculation of the correlation length using MoM_{var}, MoM_{LA} and ML, which offers additional insights into the strengths of each approach.

Besides this, the indicator approach is used to investigate the spatial correlation of the quantiles of the lognormal random process with a low coefficient of variation, which implies a nearly symmetric probability density function. This investigation of the indicator correlation lengths of very low and high values allows a more detailed picture of analytically defined, multivariate-Gaussian random processes, which can be extended to random fields.

3.1.1 Generation of the random process

The simplest model to describe spatially correlated numbers is the multivariate Gaussian distribution. A multivariate Gaussian distribution can be described only by its mean value and its covariance function. If the data are one dimensional, then it is called a random process and otherwise random field. Due to the simple definition of the spatial covariance by only one correlation function, the entropy or spatial disorder of the random process or random field is assumed maximal [144]. As described by Bucher [57], the joint probability density function of a multidimensional Gaussian distribution function is defined in equation 2.12.

Different sources of error discussed in section 2.3 are considered by adding a normal distributed measurement noise ε. Theses sources of error are used to compare the robustness of $\mathrm{MoM}_{\mathrm{var}}$, $\mathrm{MoM}_{\mathrm{LA}}$ and ML approaches.

The covariance matrix $\mathbf{C_{ZZ}}$ is symmetric and non-negative definite (e.g. it does not have any negative eigenvalues). Therefore, the covariance matrix can be factored by a Cholesky decomposition [57].

$$\mathbf{C_{ZZ}} = \mathbf{L}\mathbf{L}^{\mathbf{T}} \tag{3.1}$$

In equation (3.1), $\mathbf{L}$ is a non-singular lower triangular matrix. The Cholesky factor $\mathbf{L}$ can be utilized for a representation of the random function $\mathbf{Z}$ in terms of zero-mean uncorrelated random variables $\mathbf{Y}$ by applying a linear transformation in equation (3.2).

$$\mathbf{Z} = \mathbf{L}^{-1}\,\mathbf{Y} + \bar{\mathbf{Y}} \tag{3.2}$$

In this case study, artificially generated data are investigated, which are represented by a random function. This artificially generated data represent measurement data. This random function with a mean value of $\bar{\mathbf{Y}} = 1$, a standard deviation of $\hat{\sigma} = 1$, a spatial correlation of $\theta = 10$ m, a length of 300 m and a spacing of the data every 1 m is transformed by a q-q transformation into a lognormal distribution, as shown in figure 3.2. This lognormal distribution has a mean value of $\bar{\mathbf{X}} = 1.5$ m and has different values of the coefficient of variation COV $= \sigma/\mu = 1 - 100\%$. It can be clearly seen in figure 3.1 that the higher COV the more skewed and asymmetric is the probability density function. In order to show the possibilities of the different approaches to quantify spatial variability, different intensities of noise are added to the lognormal distributed random sequence. The noise ε is following a normally distributed standard normal distribution $\mathcal{N}(\mu = 0, \sigma = 0.01 - 1.0)$.

$$\hat{\mathbf{Z}} = F\left(F^{-1}(\mathbf{X})\right) + \varepsilon \tag{3.3}$$

3.1.2 Analysis

The $\mathrm{MoM}_{\mathrm{var}}$ and the $\mathrm{MoM}_{\mathrm{LA}}$ approach as well as the ML approach are used to analyse a set of 300 independent, identically distributed (iid) random functions $\hat{\mathbf{Z}}$. $\mathrm{MoM}_{\mathrm{var}}$

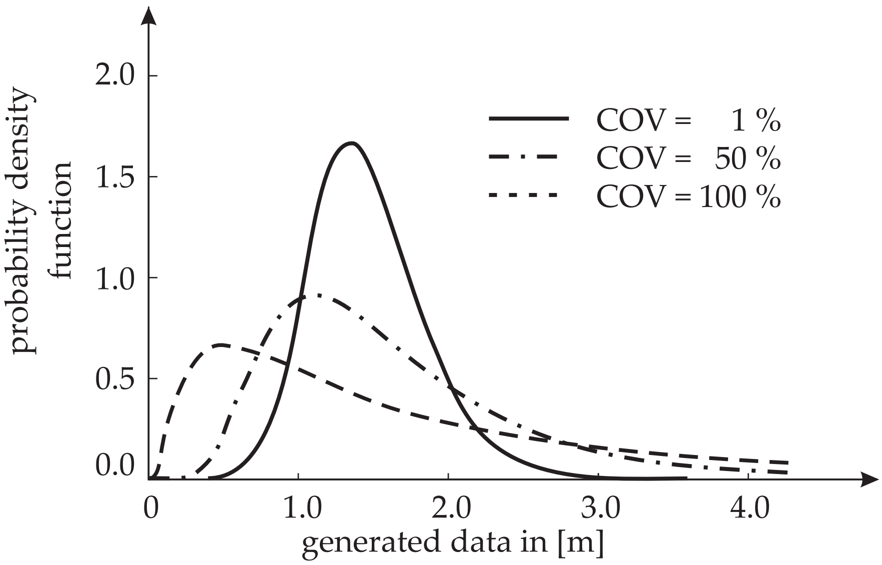

Figure 3.1: Lognormal distribution with a mean value of $\bar{Y} = 1$ and different coefficients of variation.

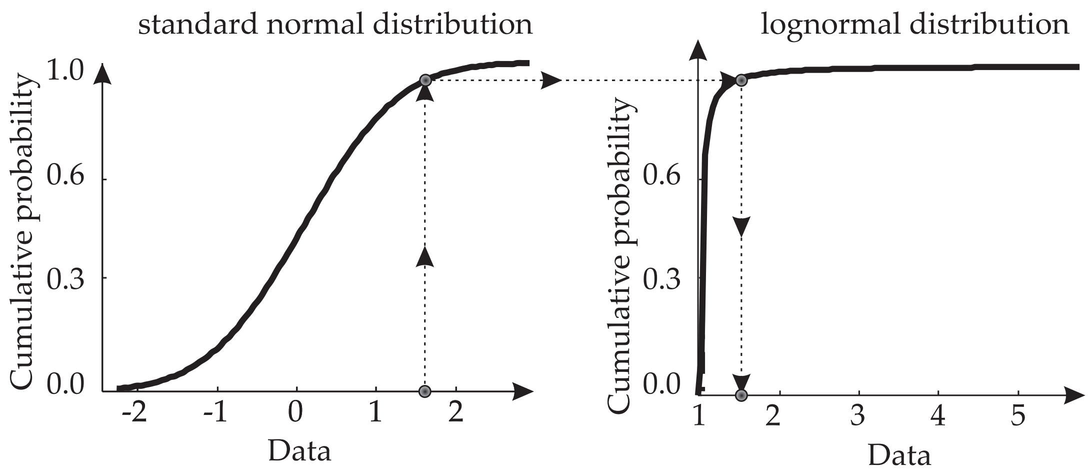

Figure 3.2: Quantile-quantile transformation of normally $\mathcal{N}(\mu = 0, \sigma = 1)$ into lognormally distributed data log-$\mathcal{N}(\mu = 1.5, \sigma = 10)$.

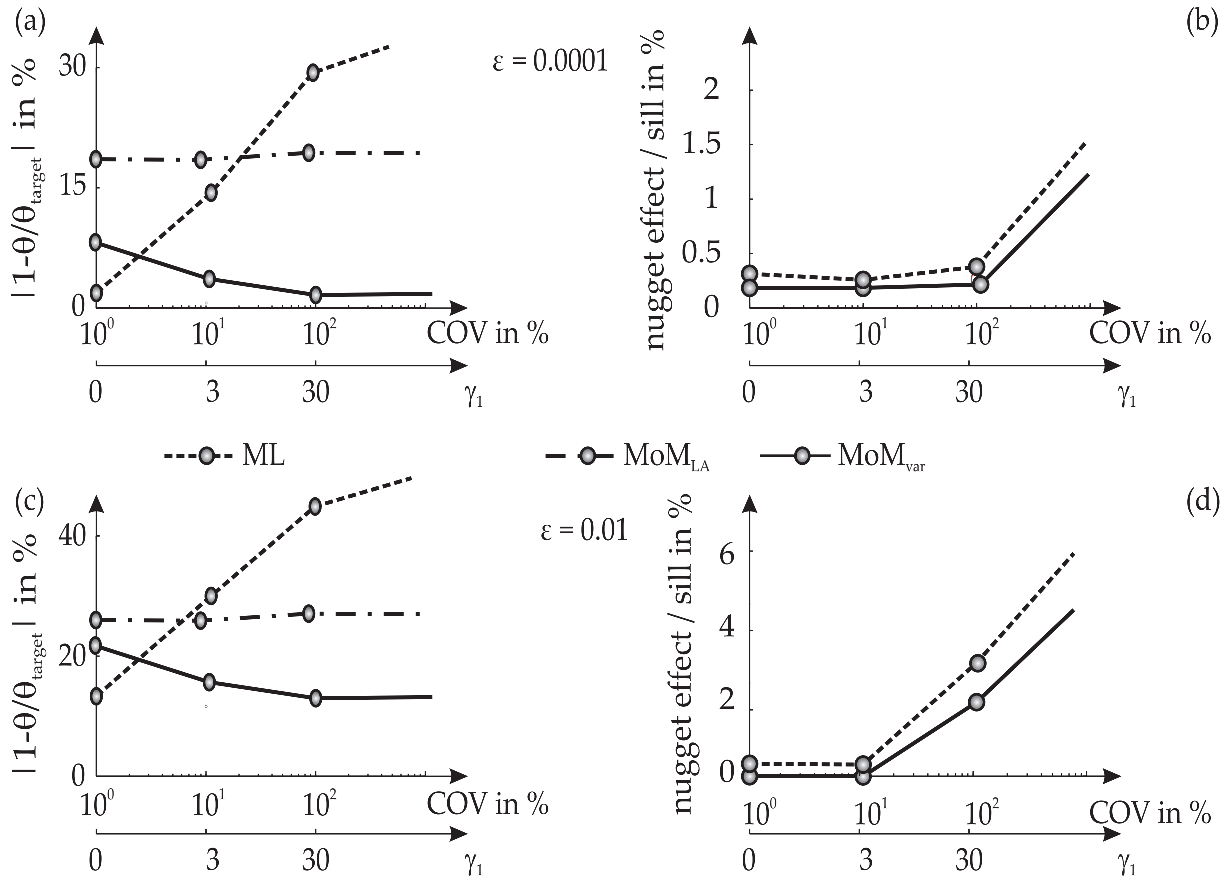

Figure 3.3: Evaluated correlation lengths using $\mathrm{MoM_{var}}$, $\mathrm{MoM_{LA}}$ and ML approach (a,c) and resulting nugget/sill ratios (b,d) using $\mathrm{MoM_{var}}$ and ML approach for different error levels $\varepsilon = 0.01$ (a,b) and $\varepsilon = 0.0001$ (c,d).

and $\mathrm{MoM_{LA}}$ have been implemented into a MATLAB program to analyse the data in an efficient way for all case studies in this thesis. The program of Pardo-Iguzquiza [270] has been modified and applied for the ML approach. The ML approach was chosen for calculating the correlation length of data without a trend in all following case studies; otherwise, the Residual Maximum Likelihood method (chapter 2.5.2.2) would be more difficult to compare because the trend of data is eliminated also. The bilinear, spherical, exponential and Gaussian variogram functions have been fitted to the experimental variogram values using the weighted least squares method using the weight defined by McBratney & Webster [247]. The same theoretical variograms have been used within the ML approach to evaluate the range of noisy random sequences. After this, the Akaike Information Criterion approach has been applied to select the best fitting correlation length of the variogram and the ML approach.

The evaluated correlation lengths of the iid random functions $\hat{\mathbf{z}}$ are fitted to a lognormal distribution function using the maximum likelihood method. In figure 3.3 one can see the influence of the skewness of the distribution as well as consequences of the noise. The deviation $|1 - \theta/\theta_{target}|$ of the evaluated correlation length from the target correla-

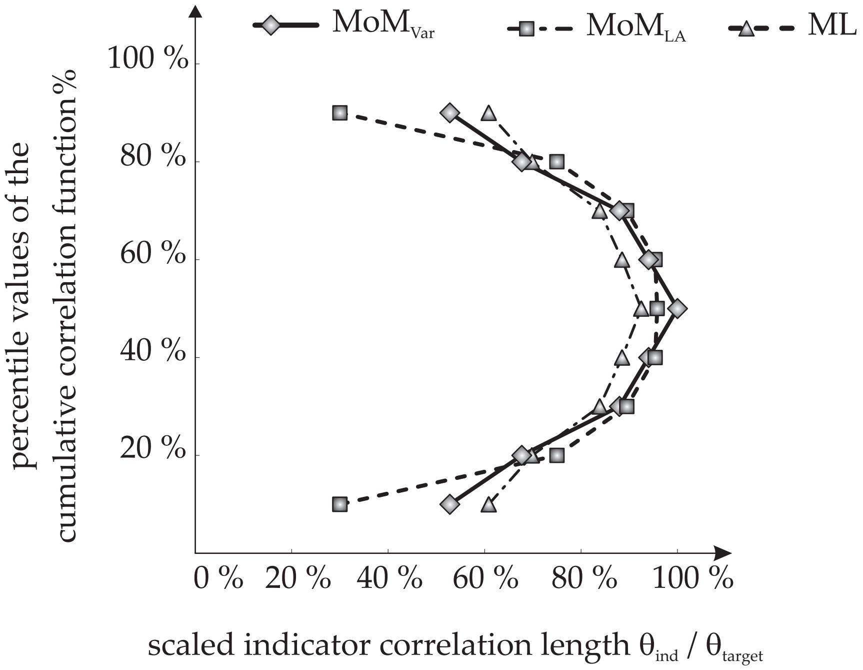

Figure 3.4: Case study A: Analysis of the indicator correlation lengths for the different quantiles of the CDF (log-$\mathcal{N}\left(\mu = 1.5, \sigma = 10\right)$) and a measurement noise of $\mathcal{N}\left(\mu = 0, \sigma = 0.01\right)$.

tion length $\theta_{target} = 10$ m is shown as a function of the skewness and asymmetry of the underlying distribution of $\widehat{Z}(\mathbf{X})$. Moreover, the ratio of the nugget effect and the sill is shown as a function of the COV in figure 3.3.

The bigger the skewness of the underlying distribution and the bigger the measurement noises, the worse is the evaluated spatial correlation. It was also observed by Kerry & Oliver [193, 194] that the variogram approach becomes unreliable when the data are strongly asymmetric or skewed as well as in presence of outliers or extreme values. Similar to the findings of Webster & Oliver [403], it can be seen in figure 3.3 that as COV and the skewness increase the nugget and the sill variances also increase. It is also shown that the ratios of the nugget to sill increase as the skewness increases even though this is not considered in the generation of the random process. Webster & Oliver [403] also observed this and point out that the ratio of nugget to sill is a combination of the degree of asymmetry and the spatial distribution of data points of the tail of the distribution.

By comparing the three approaches in figure 3.3, MoM_{var} and MoM_{LA} show more stable results in comparison to the ML approach, which can be traced back to the basic assumptions of normally distributed data. All three approaches become more unreliable the more noisy the data are.

The indicator approach is employed to evaluate the correlation lengths of 300 iid random processes $\hat{\mathbf{z}}$. The different percentiles of the cumulative distribution function of $Z(\hat{\mathbf{X}})$ are used as thresholds cut_k, as described in section 2.5.1.1. The random process

$Z(\mathbf{X})$ is truncated by the thresholds cut_k. $\mathrm{MoM_{var}}$, $\mathrm{MoM_{LA}}$ and ML approaches are used to calculate the indicator correlation lengths θ_{ind}. One would expect that theses indicator correlation lengths would be the same, but this is not the case as shown in figure 3.4. This becomes clear, if one recalls the generation of the random process: only one correlation length is used to define the spatial correlation. The indicator correlation lengths of the different thresholds are symmetric towards the median value, as reported in [143]. Moreover, the extreme values have significantly lower correlation lengths than the median value, as shown in in figure 3.4.

3.1.3 Remarks

The non-parametric $\mathrm{MoM_{var}}$ technique has proven its strengths in comparison to the $\mathrm{MoM_{LA}}$ and ML approach. It can be seen in figure 3.3 that the variogram technique is more robust than the $\mathrm{MoM_{LA}}$ and ML approaches in the presence of a high noise as well as when the underlying distribution is highly skewed and asymmetric, which coincides with the findings in [193, 194]. The $\mathrm{MoM_{LA}}$ and ML approaches use the q-q transformation to convert the underlying distribution into standard normal distributed variables $\mathcal{N}(\mu = 0, \sigma = 1)$. This transformation causes the inaccuracies shown in figure 3.3, especially in the presence of an asymmetric distribution.

It has to be pointed out that the variogram methodology is working in the best way for normally distributed values $\mathcal{N}(\mu = 0, \sigma = 1)$. If the underlying distribution becomes skewed the outcome is less reliable, which is also true for the $\mathrm{MoM_{LA}}$ and the ML approach. For this reason, robust techniques are offered in a geostatistical framework as described in detail amongst other by Chiles & Delfiner [79], Bardossy & Kundzewicz [30] and Marchant & Lark [236]. Following publications summarized in [403], different estimators like the Cressie & Hawkins estimator, median variogram estimators or Genton's estimator can overcome this problem in a complicated way. The form of these estimators does not allow explicit computing of their correlation structure as stated by Genton [137].

There are differences in the evaluated correlation length using the non-parametric $\mathrm{MoM_{var}}$ and $\mathrm{MoM_{LA}}$ approaches as well as the parametric ML approach. Moreover, one has to keep in mind that there has been performed a q-q transformation for the $\mathrm{MoM_{LA}}$ and the ML. The difference for the ML approach can be related to the smoothing due to the definition of lag classes in the variogram approach. In this context Webster & Oliver [403] stress the benefit of the ML approach not to smooth the spatial structure because there is no ad hoc definition of lag classes; the model parameters are calculated directly from the variance-covariance matrix of the full data. The ML and $\mathrm{MoM_{var}}$ approach assume that the data follow a multivariate Gaussian distribution, which is a simplification of the data and very difficult to verify in practice [403].

The relative error $\varepsilon_{\mathrm{target}}$ is shown for the $\mathrm{MoM_{var}}$, $\mathrm{MoM_{LA}}$ and ML approaches for a lognormally distributed random function with a COV$=1$ % in figure 3.5 (a) and COV$=100$ % in figure 3.5 (b). A measurement noise of $\mathcal{N}(\mu = 0, \sigma = 0.01)$ was added to show the influence of the asymmetry of the underlying lognormal distribution function on the evaluated correlation length. The shifted, lognormal distribution functions show in the case of a nearly symmetric distribution with COV = 1 % comparable results. The $\mathrm{MoM}_{\mathrm{var}}$ and ML approaches offer more or less the same result for the correlation length. The mean value of the distribution function is below $\varepsilon_{\mathrm{target}} < 10$ %; the results of the $\mathrm{MoM}_{\mathrm{LA}}$ approach offer a slightly higher relative error $\varepsilon_{\mathrm{target}}$. In the case of a COV$= 100$ % of the underlying distribution, the robustness of the $\mathrm{MoM}_{\mathrm{var}}$ approach is strengthened again in comparison to the ML and $\mathrm{MoM}_{\mathrm{LA}}$ methods, which are very sensitive to asymmetric and skewed distributions.

For the correlation lengths in general, it can be concluded for that one has to pay attention to the univariate distribution of the data: the higher the skewness and asymmetry, the more attention has to be paid in evaluating the correlation length. One has to pay more attention when analysing skewed data because then the results of the three methods scatter significantly.

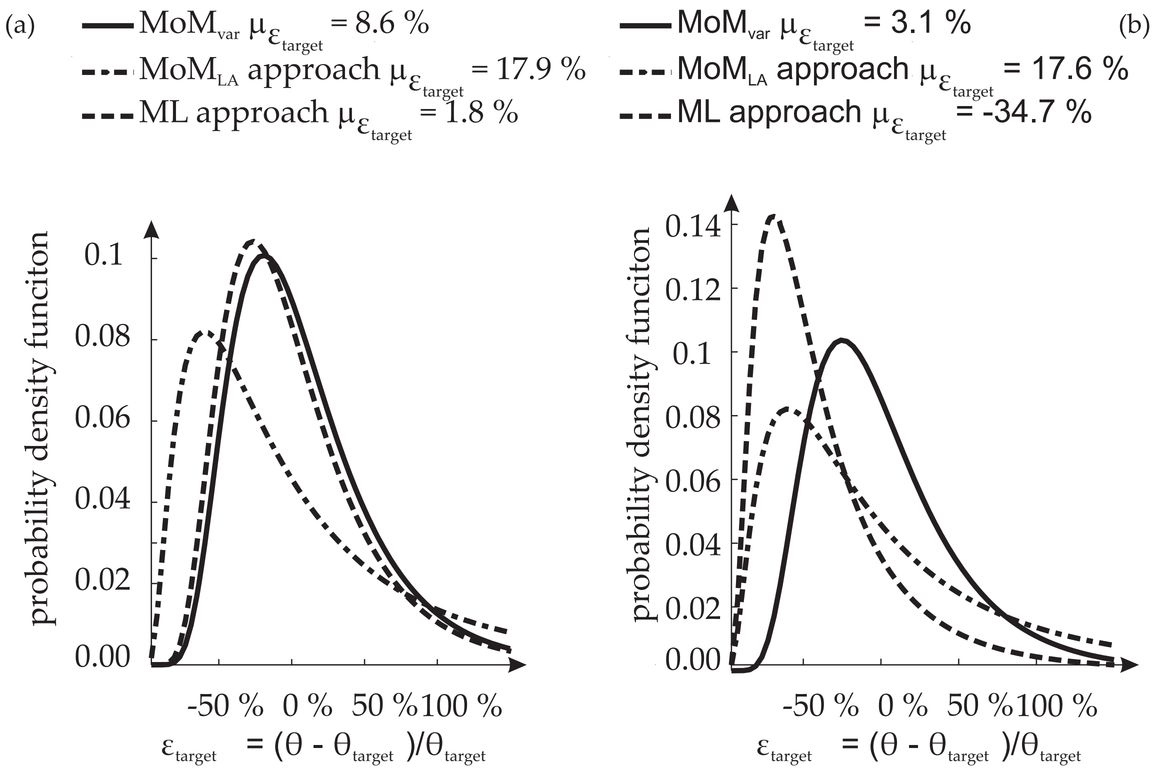

Figure 3.5: Case study A: distributions of the relative errors $\varepsilon_{\mathrm{target}}$ of the $\mathrm{MoM}_{\mathrm{var}}$, $\mathrm{MoM}_{\mathrm{LA}}$ and ML- approaches for COV = 1 % (a) and COV = 100 % (b).

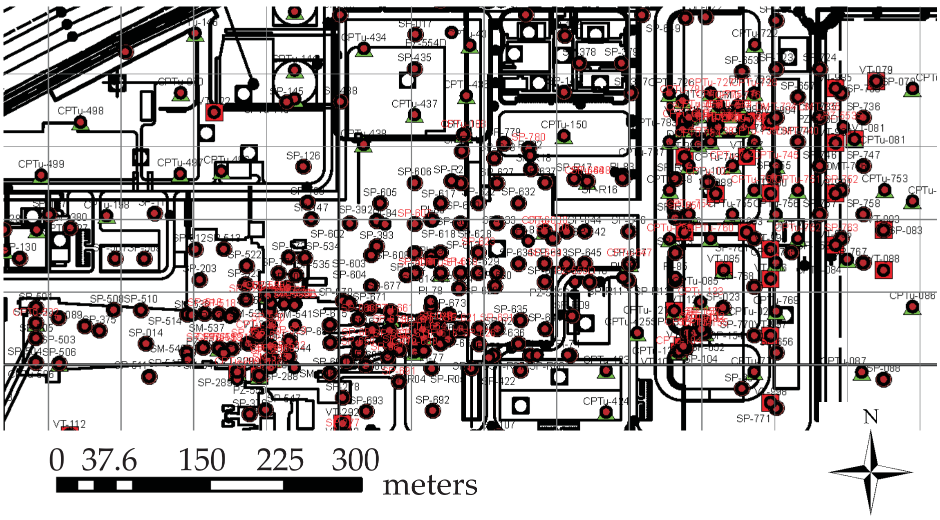

Figure 3.6: Case study B: plan view of the 138 CPT measurement locations.

3.2 Case study B – CPT data evaluation

This case study deals with a stochastic site description, involving the identification of soil layering and the detection of trends in the measurement database, in which the engineering judgement is enriched by using mathematical and statistical methods. The variogram approach ($\mathrm{MoM_{var}}$), the local average approach ($\mathrm{MoM_{LA}}$) and Maximum Likelihood (ML) approach are combined to analyse a big CPT dataset with the focus on the vertical spatial variability. The evaluation of the vertical spatial variability within each layer is conducted within the developed scheme of probabilistic site description.

The results of the $\mathrm{MoM_{var}}$, the $\mathrm{MoM_{LA}}$ and ML approach are combined on the basis of BAYES principle, which allows the statistical combination of different models of spatial variability.

3.2.1 Site description & measurement technique

An extensive field investigation has been carried out for a big industrial construction project in South America. Within an extensive exploration campaign, 67 standard penetration tests and 138 cone penetration tests with measurement of pore pressure according to the DIN $4094-1$ [103] have been carried out [139], as shown in figure 3.6. For this case study 138 closely spaced CPT measurements have been selected for evaluation.

Under a crust with a thickness of a few decimetres up to one meter a very soft soil layer exists down to a depth of about 2.2 to 5.9 m, generally in depth of 3.6 to 4.7 m under ground level. The soft layer consists mainly of silty clay. The crust at the groundlevel is more solid due to roots, consolidation and other influences. Beneath the first layer of 1.8 m, there is layer of clayey sand with a mean value of 2.4 m. At the base of this first sand layer a second clay layer is found down to a depth of about 12 to 15 m below ground-level. The layer is largely similar to the clay layer above. Up to the total

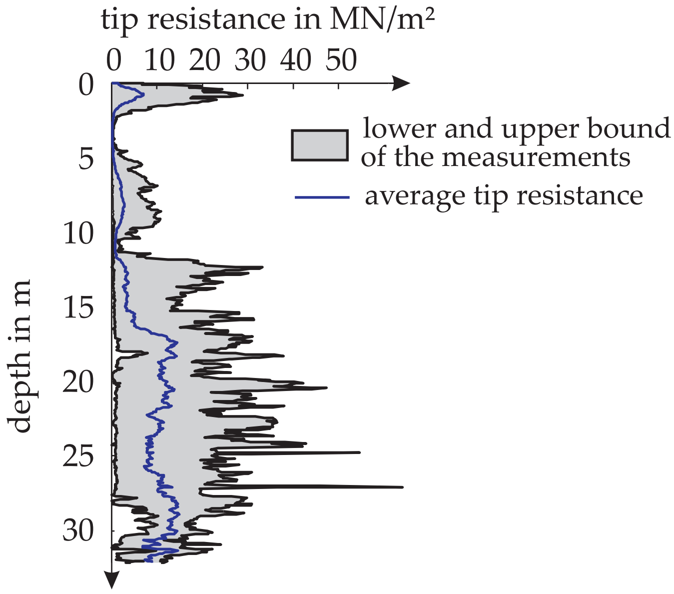

Figure 3.7: Case study B: Average, minimum and maximum measurement values of the CPT data.

depth of the field investigations sand can be found again with different properties: fine to coarse sand, sometimes even sand with a silty part. The density has been detected over a range from loose to dense. The groundwater level has been measured at a depth of 0.6 to 1.4 m below ground level. Due to the high precipitation, the groundwater level is expected to be at the surface of the area.

The summary of the measurement results is shown in figure 3.7. The upper and lower bounds of the measurement data are shown together with the mean value of the CPT measurements.

3.2.2 Analysis of the data

By looking at the upper and lower bounds of the measurements in figure 3.7, one can easily see the need for a concept in the probabilistic site characterization as described in chapter 2.

The basic steps of the probabilistic site characterization are summarized in figure 3.8. The first step is the engineering judgement on soil layering and setting up of preliminary boundaries. After this, the measurement data have to fulfil the homogeneity and stationarity criteria. Therefore, the measurement data have to undergo statistical tests. In the presence of a significant trend of the data, one has to detrend the measurements inside each layer. Now each layer is analysed by the MoM_{var}, MoM_{LA} and ML approaches to evaluate the correlation lengths.

Of course, one has to check now the sensitivity of the correlation length inside each layer to the small changes of the layer boundaries. This is important because the subdivision of a soil profile into layers and the detrending inside each layer has a significant impact on the correlation length.

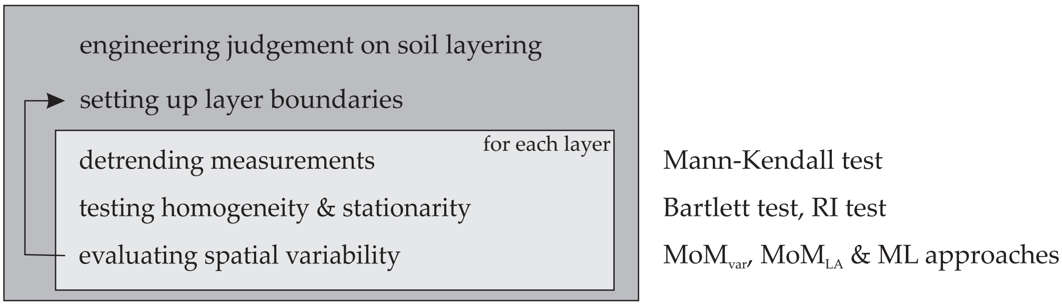

Figure 3.8: Steps of the stochastic site characterisation and involved methods.

Using this scheme, one can separate different scales of spatial variability (figure 2.3): the large geologically based spatial variability are separated from the meso-scale phenomena, which can be investigated without injuring the basic assumptions of the theory pointed out in section 2.4.2. Via this separation of the different scales of spatial variability, it is possible to reduce the noise significantly, which was simulated in section 3.1 via a normally distributed random noise ε because the homogeneity and stationarity criteria are fulfilled.

By looking at the measurement data CPT(z) in figure 3.7, one can clearly indicate a trend of the measurements with depth, which can be described by equation 3.4 where $m(z)$ is a deterministic function giving the mean measurement value at a depth z below the surface level; and $\varepsilon(z)$ are the random residuals.

$$\text{CPT}(z) = m(z) + \varepsilon(z) \tag{3.4}$$

To apply the theory to evaluate the spatial variability, one has to check the basic assumptions of this theory in order to use the MoM$_{var}$ MoM$_{LA}$ and ML approaches. If a trend is not removed from the measurement data, the evaluation of the correlation lengths is more difficult or even impossible as shown in figure 3.10 (b). Therefore, a selection of techniques to identify and test measurement data on stationarity and homogeneity are presented in this section.

STATIONARITY can be defined by a constant mean value and variance within the test data. Various authors have proposed techniques for detecting the stationarity of the data. Only some are enlightened in this section. Amongst others, Jacksa [184] as well as Bennett [36] propose different methods to detect a trend.

- VISUAL INSPECTION: Mere inspection of the raw data is often sufficient to detect non-stationarity. Visual inspection, however, is not sufficient to detect the form of the trend, nor most cases of non-stationary variance.

- HISTOGRAM PLOTS: A simple, though crude technique, is to split the random field into a number of subsections and to plot each of their histograms. Comparison of these histograms enables shifts in the means and variances to be detected.

- INSPECTION OF THE EMPIRICAL VARIOGRAM: Box and Jenkins [51] as well as Bennett [36] investigated this approach amongst others. It can be deduced from looking at equation (2.2) that non-stationary data will impose also a trend in the empirical variogram. The range cannot be determined. This feature can be used to indicate a trend of measurement data as shown in figure 3.10.

- SIGNIFICANCE TESTS ON TRENDS: Another smooth way to detect stationarity of measurements is offered by the non-parametric method of Mann-Kendall's τ [234]. Alternatively, Sachs [316] offers a different test for testing the significance of trends, namely the Cox-Stuart test or Neumann test. The Mann-Kendall test is based on the statistics S. Each pair of observed values $y_i, y_j (i > j)$ is inspected to find out whether $y_i > y_j$ or $y_i < y_j$. Let the number of the former type of pairs be P, and the number of the latter type of pairs be M. Then S is defined as

$$S = P - M \tag{3.5}$$

For $n > 10$, the sampling distribution of S is as follows. Z follows the standard normal distribution, where

$$Z = \begin{cases} (S-1)\sigma_s & \text{if } S > 0 \\ 0 & \text{if } S = 0 \\ (S+1)\sigma_s & \text{if } S < 0 \end{cases} \tag{3.6}$$

$$\sigma_s = \sqrt{\frac{n(n-1)(2n+5)}{18}}$$

The null hypothesis that there is no trend is rejected if the computed Z value is greater than $Z_{\alpha/2}$ in absolute value. Herein, the significance $\alpha = 1\%$ is chosen according to [287].

After identifying the trend via the described approaches, the least squares method [34] is used to fit a linear trend to the data as recommended by [23, 286]. Alternatively, one could also use different approaches based on the Bayesian principle or on a Maximum Likelihood method [23, 286].

After removing the trend of the measurement data by fitting a linear function by least squares, Maximum-Likelihood or Bayesian approach to the measurement data, one has to check the data on homogeneity. This can be done be engineering judgement; but also statistical can support this judgement on a mathematical basis.

Homogeneity can be defined as stationarity of the variance as presented in [284, 316]. The intra-class correlation coefficient and the Bartlett statistics are used herein for checking the homogeneity of the measurements.

Intra-class correlation coefficient: The intra-class correlation coefficient RI is reported as a useful statistical method for detecting layer boundaries using CPT soundings, Wickremesinghe [404]. The RI profile is generated by moving two continuous windows containing m data points each over a measurement profile and computing the following index at the centre of the double window.

$$RI = 1/\left(1 + \frac{1}{(m-1)/m + (\hat{\mu}_1 - \hat{\mu}_2)^2/2/(\hat{s}_1^2 + \hat{s}_1^2)}\right) \tag{3.7}$$

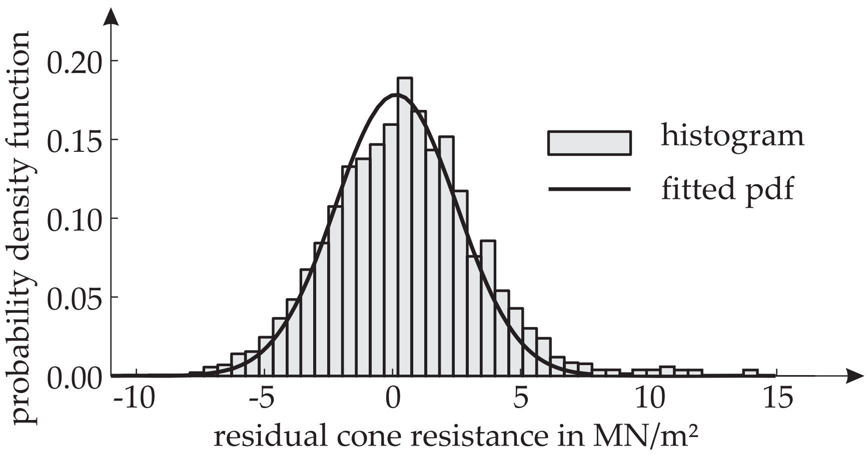

Figure 3.9: Histogram and fitted normal distribution function of the detrended cone resistances in sand of CPT 4 $\mathcal{N}(\mu = 0.10$ kN/m$^2|\sigma = 2.51$ kN/m$)$ with a skewness $\gamma_1 = 0.40($ kN/m$^2)^3$ and an excess kurtosis $\gamma_{2,excess} = -0.51($ kN/m$^2)^4$.

Basically, ergodicity of the mean value and the variance within the moving window is assumed. This is only valid for symmetric distributions according to various authors [154, 417]. The critical RI value RI_{crit} is estimated according to Hegazy et al. [154]. The boundaries are identified quantitatively at locations where RI exceeds the empirical relationship of the mean μ_{RI} and standard deviation σ_{RI} of the RI profile: $RI_{crit} = \mu_{RI} + 1.65\sigma_{RI}$; it is recommended to check the computed results visually and to judge the evaluated soil layer. The critical RI according to Hegazy et al. [154] is slightly higher than the recommendation of Zhang & Tumay [417] $RI_{crit} = 0.7$, which is also an empirical rule. Others [154, 417] also point out that the choice of RI_{crit} does not seem to depend on the underlying correlation structures of the profile, which is also discussed by Phoon et al. [284].

Bartlett statistics: This classical test is used to test the equality of multiple sample variances for independent data sets. This has not to be taken into account in this case study because a normal distribution function can be fitted to the residuals of the CPT measurements as depicted in figure 3.9.

For the case of two sample variances, s_1^2 and s_2^2, the Bartlett test statistic reduces to:

$$B_{stat} = \frac{2.30295(m-1)}{1 + 2/(1(m-1))}[2\log s^2 - (\log s_1^2 + \log s_2^2)] \tag{3.8}$$

where m is the number of data points used to evaluate s_1^2 or s_2^2. The total variance s_2^2 is defined as:

$$s = \frac{s_1^2 + s_2^2}{2}$$

While using the Bartlett statistics, one has to keep in mind that this procedure is very sensitive to non-normally distributed and skewed variables. According to Sachs [316], he implies that in the case of a small deviation from the symmetric normal distribution, the procedure will not offer reliable results. Especially in the presence of a skewness $\gamma_1 \neq 0(\text{ kN/m}^2)^3$ and an excess kurtosis $\gamma_{2,excess} \neq 0(\text{ kN/m}^2)^4$, which can be observed very often in the case of measurement data.

A continuous Bartlett statistic profile can be easily generated by moving a sampling window over the simulated soil profile. Campanella et al. [68] as well as Wickremesinghe [405] recommend a window width of approximately the scale of fluctuation in the layer. This is also pointed out by Phoon et al. [284]. This implies an iterative approach. The sampling window is divided into two equal segments and the sample variance s_1^2 and s_2^2 is calculated from data points lying within each segment. The Bartlett statistic basically indicates the difference between the sample variances in these two adjacent segments. As shown in equation 3.8, the Bartlett statistic is zero if s_1^2 and s_2^2 are equal. Phoon et al. [284] offer a critical value B_{crit} under the framework of the MODIFIED BARTLETT STATISTICS taking into account the spatial correlation using an exponential model. Herein, $I_1 = n/k$ ranges between 5 and 50 and $I_2 = m/k$ where k is the number of points in one scale of fluctuation; n is the total number of points in the entire soil record and m is the number of points in one sampling window.

$$B_{stat,crit} = (0.23k + 0.71)\ \log(I_1)\ +\ 0.91k\ +\ 0.23 \tag{3.9}$$

This critical value B_{crit} is calculated for every layer to take the different correlation lengths into account. The lowest critical value B_{crit} is used for the whole CPT profile. In figure 3.10 the detrended measurement data are used to evaluate the RI as well as the Bartlett statistics. The width of the sampling window is chosen as big as the correlation length. The critical values RI_{crit} and B_{crit} indicate the boundary between both soil layers.

Application of the Intra-class correlation coefficient and the Bartlett statistics: RI and B_{stat} offer help in the soil layer identification using statistical methods, but these approaches can just support the engineering judgement, due to the above mentioned assumptions and simplifications as stated by Phoon et al. [284]. The above mentioned methods are well suited to normally distributed data. Therefore, it is has to be stressed that these methods support the engineer in detecting different soil layers from CPT measurements. This statement becomes more clear when looking at figure 3.10 (a). By looking at the geological profile, which is derived by an engineer [139], one can clearly see the correlation between the soil layering and the cone resistance. The changes in the cone resistance offer a reasonable basis for the soil layering. These soil layer boundaries are detected by the BARTLETT STATISTICS, whereas the RI-profile does not show all boundaries in a reliable way. Therefore, it can be deduced that the BARTLETT STATISTICS offers a more detailed insight and is more suitable to detect layer boundaries by means of statistics. The RI concept shows poor results in this study and is not suitable for a clear detection soil layers from CPT measurement data.

Data processing: The CPT measurement data are detrended by the a least square fitting of a linear function within one layer.

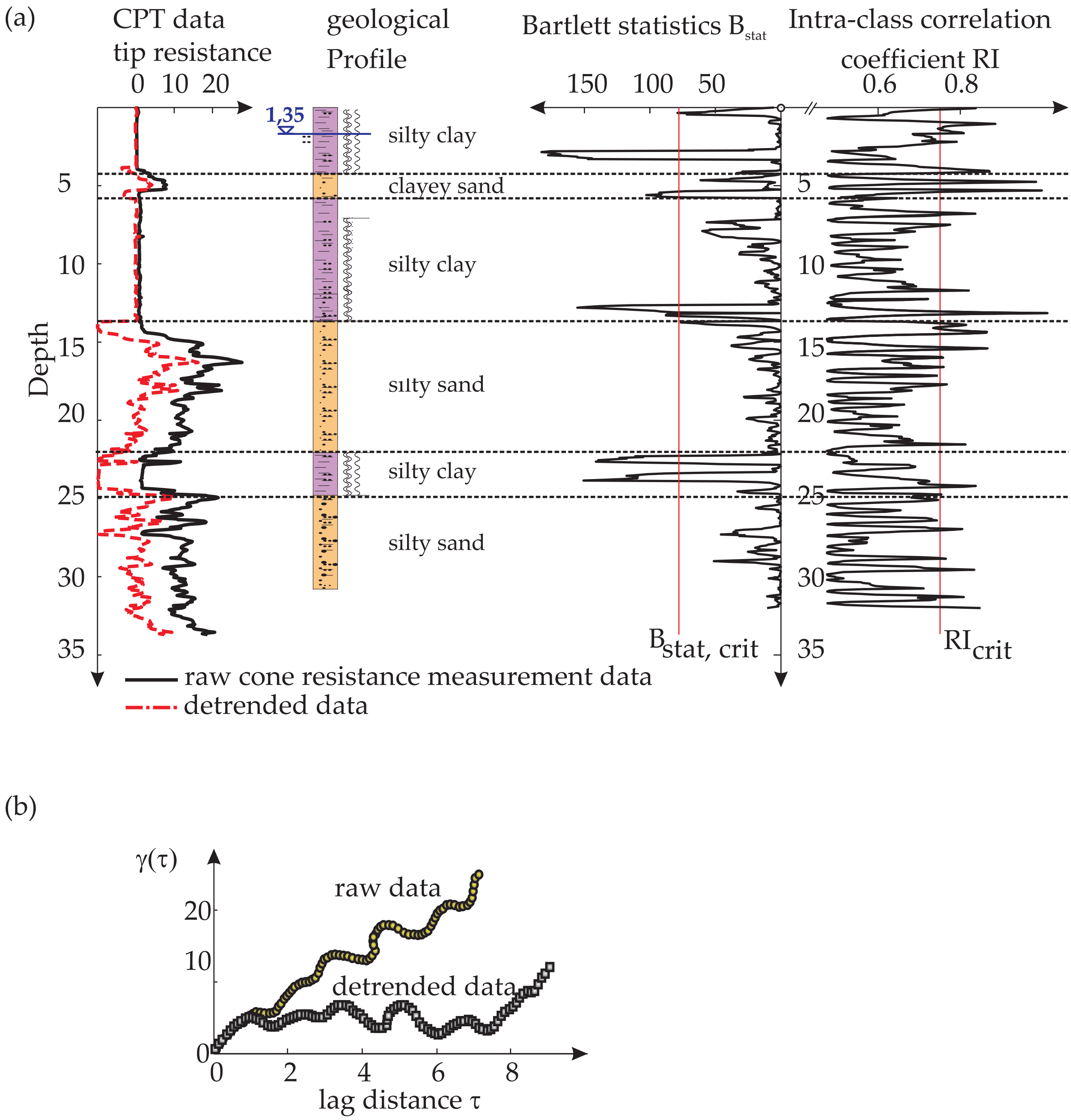

Figure 3.10: (a) Cone resistance $q_c(z)$ measured with depth z and soil layer identification of CPT 4 data using RI and Bartlett statistics and (b) semivariogram on the raw and detrended data of the silty clay layer at 10 m depth.

After identifying the homogeneous section of the CPTs and the detrending by least square fitting of a linear function to these homogeneous sections, the $\mathrm{MoM_{var}}$, $\mathrm{MoM_{LAS}}$ and ML approaches are used to evaluate the spatial variability of the site for each layer. Different theoretical variogram functions (namely spherical, exponential bilinear and Gaussian functions) are fitted to the experimental variogram values using the weighted least squares and Akaike Information criterion to identify the best fitted theoretical variogram function. Also within the ML approach the Akaike Information criterion was used to identify the best suitable theoretical variogram model.

The analysis of the correlation lengths and of the indicator correlation lengths is carried out for the different soil types. For this reason, the charts of Robertson [308] were used to evaluate the the soil types from the normalized cone resistance and the friction ratio of a CPT test as shown in figure 3.23. For theses soil layers the the cumulative distribution function was used for the evaluation of the different thresholds $cut_{k,i}$. This has been used for each of the 138 CPT measurements to evaluate the indicator correlation length of each threshold $cut_{k,i}$. It is found that these indicator correlation lengths follow a lognormal distribution function. The mean values θ_{ind} of each threshold $cut_{k,i}$ are shown in figure 3.12, which is scaled by the correlation length evaluated by the variogram approach θ.

3.2.3 Remarks

Combination of different models: One can clearly see in figure 3.11 that the $\mathrm{MoM_{var}}$, the $\mathrm{MoM_{LAS}}$ and the ML approaches offer comparable results. This can be deduced from the nearly symmetric distribution of the residual values shown in figure 3.9, because there is only a very small skewness of the measurement data. These three probability density functions of the MoM and ML approaches are equally probable and can be merged by using the so called BAYESIAN MODEL AVERAGING (BMA) scheme [162, 300], which is based on the Bayes' theorem.

The Bayes' theorem updates a subjective, prior probability distribution $f(\theta)$ with a likelihood function $\mathrm{L}(\theta|z_1, z_2, ..., z_n)$, which is the conditional probability function of $z_1, z_2, ..., z_n$ e.g. measurement values.

$$f(\theta|z_1, z_2, ..., z_n) \;\propto\; f(\theta) \cdot \mathrm{L}(\theta|z_1, z_2, ..., z_n) \tag{3.10}$$

The resulting posterior pdf $f(\theta|z_1, z_2, ..., z_n)$ of the variable of interest θ is conditioned on the prior probability $f(\theta)$ and on the Likelihood function $L(\theta|z_1, z_2, ..., z_n)$, [70, 136, 382].

If θ is the quantity of interest, then its posterior distribution given data D is

$$\mathrm{Prob}(\theta|D) = \sum_{k=1}^{K} \mathrm{Prob}(\theta|M_k, D) \cdot \mathrm{Prob}(M_k|D) \tag{3.11}$$

This is an average of the posterior distributions under each of the models considered, weighted by their posterior model probability. In equation 3.11 $M_1, M_2, ..., M_k$ are the models considered. The posterior probability for the model M_k is given by

$$\mathrm{Prob}(M_k|D) = \frac{\mathrm{Prob}(D|M_k) \cdot \mathrm{Prob}(M_k)}{\sum_{l=1}^{K} \mathrm{Prob}(D|M_l)\,\mathrm{Prob}(M_l)} \tag{3.12}$$

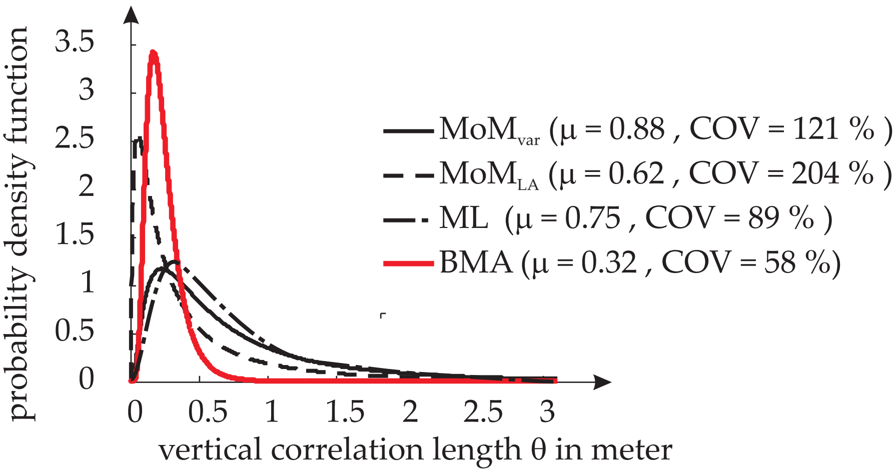

Figure 3.11: Case study B: probability density function of the $\mathrm{MoM_{var}}$, $\mathrm{MoM_{LA}}$ and ML approach and the combined probability density functions using Bayesian Model Averaging of the silty clay layer.

where

$$\mathrm{Prob}(D|M_l) = \int \mathrm{Prob}(D|\theta_k, M_k)\,\mathrm{Prob}(\theta_k|M_k)\,\mathrm{d}\theta_k \tag{3.13}$$

is the integrated likelihood of model M_k, θ_k is the vector of parameters of model M_k, $\mathrm{Prob}(\theta_k|M_k)$ is the prior density of θ_k under model M_k, $\mathrm{Prob}(D|\theta_k, M_k)$ is the likelihood and Prob(M_k) is the prior probability that M_k is the true model under the assumption that one of the models considered is true. All probabilities are implicitly conditional on the set of all models being considered.

Hoeting et al. [162] report that BMA presents several difficulties: the specification of the prior distribution over competing models has to be carried out with attention. Another fundamental task is to choose the models over which the averaging can be performed; one of the most challenging tasks is the evaluation of the integral in equation 3.13. Within [70, 162, 300, 382], it is recommended to use Markov Chain Monte Carlo methods to evaluate this integral for the very general combination of different functions. In the simple case of the combination of two (log)normal distribution functions equation 3.13 can be solved by numerical integration [382].

The combination of the three distribution functions using BMA is shown in figure 3.11. The resulting distribution function has a lower variance as well as a lower mean value of the correlation length. Via BMA all information from the three different models ($\mathrm{MoM_{var}}$, $\mathrm{MoM_{LA}}$ and ML) have been incorporated and this higher level of information is leading to a significant reduction of the coefficient of variation of the combined pdf. This pdf of the correlation lengths is an extension of the state of the art. It is stated in standard geostatistical textbooks [79, 401] that a correlation length is needed for interpolation or simulation of spatial variability. The correlation length is assumed as one single value without uncertainty. This case study shows that the analysed correlation lengths of CPT measurement data follow lognormal distributions. These results extend the state of the art presented in literature [23, 79, 184, 286]. Herein, one single correlation length is

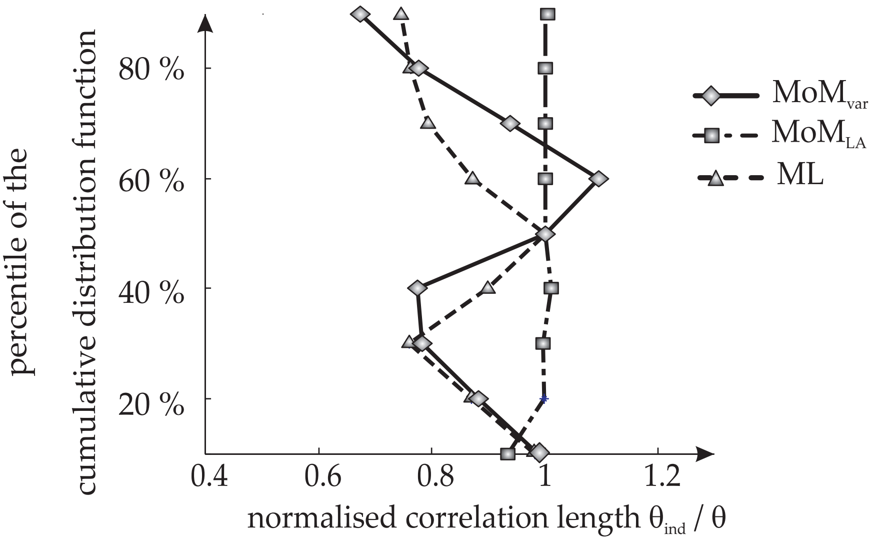

Figure 3.12: Casestudy B: Analysis of the correlation lengths for indicators of the CDF using MoM_{var}, MoM_{LA} and ML with fitted lognormal distribution functions for silty clay layer.

used to interpolate or simulate spatial variable data under the assumption of one single, known correlation length. On basis of the presented results, the author recommends to take the most probable value e.g. the mean value from the distribution in figure 3.11 for this issues. Moreover, the effects of a distributed correlation lengths is investigated in chapter 6.2.

Indicator correlation lengths analysis: The results of the indicator correlation length analyses are shown in figure 3.12. Around the median value the indicator correlation lengths are slightly higher in comparison to the other thresholds, but have nearly the same indicator correlation lengths for all quantiles of the CDF. Comparing these results to figures 3.4 and 3.12, one can conclude that the correlation structure of these CPT measurements cannot be fully characterized by the mean value, standard deviation and covariance function; it can be concluded that this measured structure of spatial variability cannot be described by only one correlation function as it is done in the well known multi-Gaussian model ,[143]. This was also found out by other researchers [143, 144, 189]. The extreme low and high values have indicator correlation lengths. The results of the MoM_{var}, MoM_{LA} and ML approaches show a comparable behaviour: the indicator correlation lengths are nearly the same for all thresholds. The scattering of the indicator correlation lengths can be related to the indicator approach: The symmetrically distributed data shown in figure 3.9 are transformed through the indicator approach in equation 2.3 into skewed and asymmetric datasets. As shown before, this asymmetric distribution causes less reliable results for the correlation length analysis. The MoM_{var}, MoM_{LA} and ML methods are very sensitive to deviations from the normal distribution (e.g. skewness $\gamma_1 > 1$, excess kurtosis $\gamma_{2,excess} \neq 0$). Finally, it has to be emphasised that the indicator correlation length analyses clearly show a non-multi-Gaussian behaviour, which cannot be fully captured by standard geostatistical simulation approaches (e.g. LU-decomposition or Sequential Gaussian Simulation algorithm) as used section 3.1. According to the author's knowledge, this has not been observed by others in geotechnical engineering, but mentioned in geostatistics [79, 144].

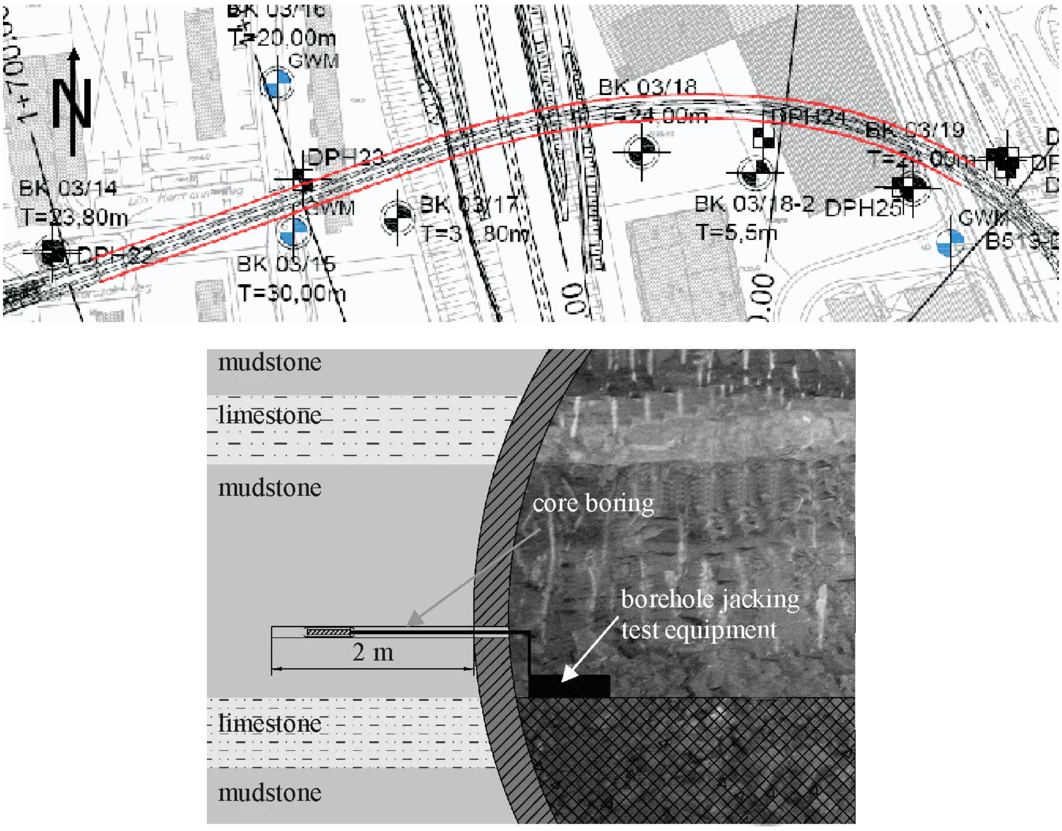

Figure 3.13: Plan view and cross section of the experiments in the Fasanenhof tunneling project.

3.3 Case study C – Fasanenhof-tunnel

This case study on the evaluation of spatial variability describes the evaluation of the spatial variability of equally spaced measured data within a homogeneous soil layer. The variogram approach ($\mathrm{MoM_{var}}$), the local average approach ($\mathrm{MoM_{LA}}$) and the Maximum Likelihood (ML) approach are used for this. The evaluation of the uncertainty of the correlation length from a relatively small number of measurement data is shown focusing on the uncertainty of the spatial correlation.

In addition ot this, the indicator correlation lengths are investigated using the $\mathrm{MoM_{var}}$, $\mathrm{MoM_{LA}}$ and ML approaches.

3.3.1 Site description & measurement technique

During the tunnelling construction process of the Fasanenhoftunnel in Stuttgart (Germany) 45 horizontal core borings have been carried out as shown in figure 3.13. These horizontal core-borings were grouped within a geologically homogeneous layer of mudstone with a separation distance of 2.5 m. The elevation of the boreholes was varied according to the gradient of the tunnel. Therefore, the first and the last borehole have a difference in the elevation of approximately 2.5 m. 45 borehole jacking tests have been carried out at an approximate depth of 1.35 m as shown in figure 3.13.

Figure 3.14 shows the equipment of the borehole jacking test according to the German standard DIN $4094-5$ [104]. Two half-shells are pressed diametrically against the walls of each borehole. Three different loading cycles are executed. The pressure is raised up to three different levels of 1 MN/m^2, 2 MN/m^2 and 3 MN/m^2. During this loading process the deformation of the pressure plates is measured as illustrated by the schematic curve in figure 3.15. The stiffnesses E_1, E_2 and E_3 for loading and reloading are evaluated using equation 3.14.

Herein, d is the initial borehole diameter, p the pressure of the plates into the soil and $f(\nu)$ is a constant, which depends on the Poisson's ratio (e.g. $f(\nu = 0.30) = 0.972$).

$$E = f(\nu)\,\frac{\Delta p}{\Delta d}\,d \tag{3.14}$$

3.3.2 Analysis of the data

Correlation length analyses: The measurement data have been analysed in terms of homogeneity and stationarity as described in chapter 3.2. Fulfilling these basic assumptions, the univariate statistics of the measurement data have been analysed. The results are summarized in table 3.1. A χ^2–goodness-of-fit-test showed that the results of the loading as well as the reloading experiments can be described by a lognormal distribution as shown by Huber et al. [172]. The mean values of the initial loading stiffness $E_{L,i}$ are lower than the mean value of the reloading stiffness $E_{R,i}$, whereas the COV is just slightly higher in the case of reloading.

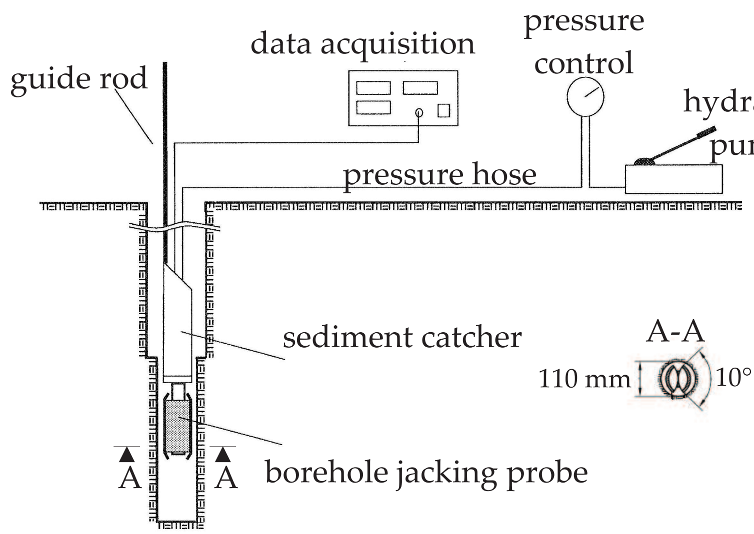

Figure 3.14: Experimental equipment of the borehole jacking probe according to the DIN 4094-5 [104].

The MoM_{var}, MoM_{LA} and ML approach have been used to analyse the spatial variability of the measurements. The Akaike-Information-Criterion has been used to identify the best–fit in the variogram and ML approaches. The results are summarized in table 3.2. The different approaches offer different results: the correlation lengths for loading and reloading are different for the loading and reloading data within the variogram method, which is not present in the other approaches; for the initial loading measurements, the MoM_{var} and the MoM_{LA} approach have more or less the same results, whereas the ML method has longer correlation lengths.

The ML approach offers in contrast to MoM_{var} and MoM_{LA} methods a possibility to make a statement on the accuracy of the estimated correlation lengths as described in equation 2.16. To overcome this drawback of the MoM_{var} and MoM_{LA} methods, the non-parametric JACKKNIFE method is introduced to evaluate the reliability of the correlation length. The basic idea of the JACKKNIFE approach lies in systematically recomputing the statistic estimate, leaving out one or more observations at a time from the sample set as

Table 3.1: Lognormally distributed results of the experiments in the Fasanenhof tunnel.

		mean value	$COV = \sigma/\mu$
$E_{L,1}$	loading	124 MN/m^2	54 %
$E_{R,1}$	reloading	660 MN/m^2	64 %
$E_{L,2}$	loading	229 MN/m^2	53 %
$E_{R,2}$	reloading	432 MN/m^2	57 %
$E_{L,3}$	loading	229 MN/m^2	59 %
$E_{R,3}$	reloading	397 MN/m^2	61 %

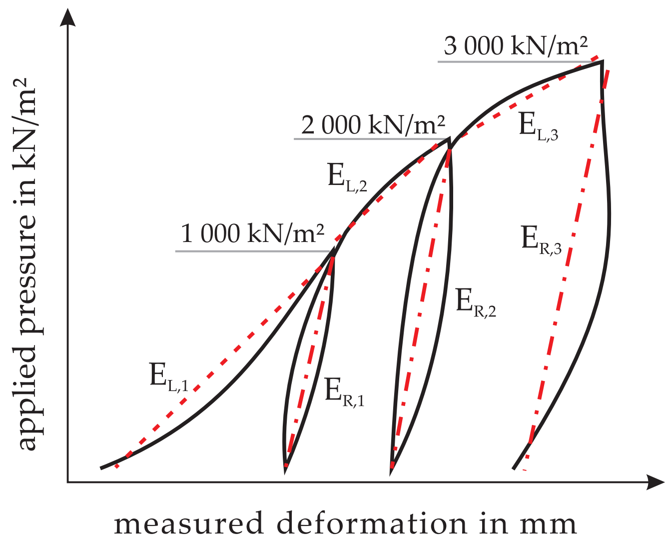

Figure 3.15: Loading, unloading and reloading cycles performed in the boreholejacking tests according to DIN $4094 - 5$ [104].

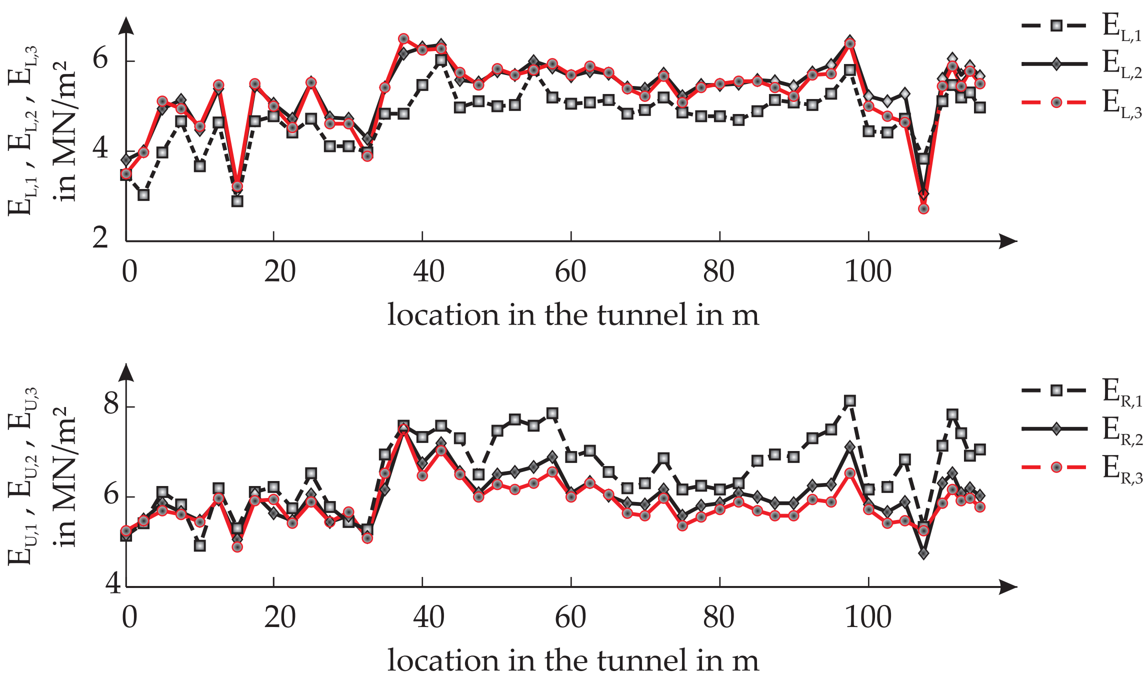

Figure 3.16: Measurement results within the Fasanenhoftunnel.

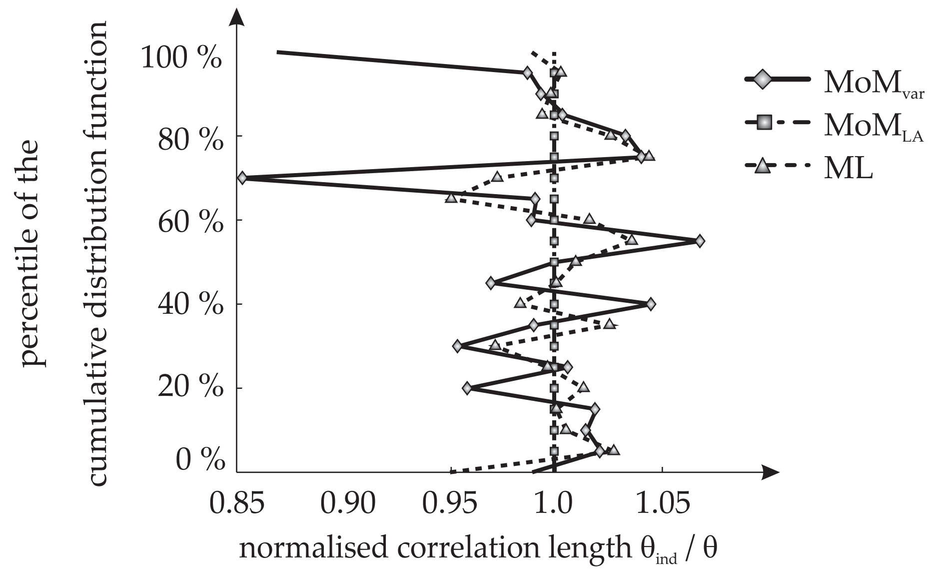

Figure 3.17: Casestudy C: Analysis of the indicator correlation lengths using MoM_{var}, MoM_{LA} and ML of the $E_{U,3}$.

Table 3.2: Case study C: Comparison of the evaluated correlation lengths θ.

		Method of Moments		Maximum likelihood approach	
		MoM_{var}	MoM_{LA}	ML	
	selected model	θ [m]	θ [m]	selected model	θ [m]
$E_{L,1}$	exponential	4.59	4.72	exponential	44.98
$E_{U,1}$	Gaussian	19.66	6.10	Gaussian	46.82
$E_{L,2}$	exponential	5.96	4.67	exponential	42.44
$E_{U,2}$	exponential	12.49	5.37	Gaussian	31.27
$E_{L,3}$	Gaussian	8.67	4.62	Gaussian	45.21
$E_{U,3}$	exponential	18.86	6.31	Gaussian	44.13

elaborated by Efron [111] and Journel [188].

An estimate for the bias and an estimate for the variance of the statistic can be calculated from these 300 new sets of replicates of the statistic. The benefit of this non-parametric approach is obvious: one can evaluate the consequences of the outliers in a non-parametric way; moreover, it is also possible to estimate the variability of the estimated correlation length using the MoM_{var} and MoM_{LA} approaches. Within the JACKKNIFE approach the selection of the theoretical variogram is carried out using the Akaike Information criterion. The results are shown in table 3.3. Comparing the mean values in table 3.3 with the correlation lengths in table 3.2, one encounters big differences, which can be explained by the influence of the extreme values. This influence is be detected by the JACKKNIFE approach in the results in table 3.3.

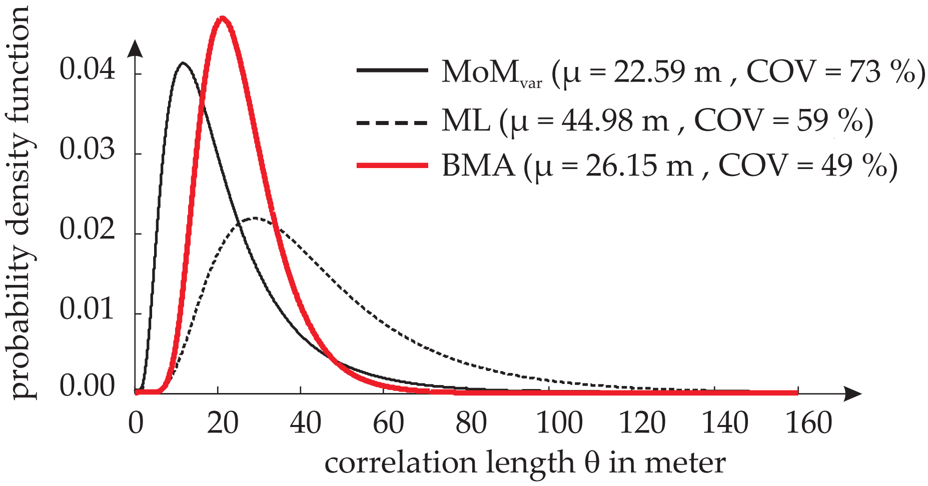

Figure 3.18: Case study C: combination of the results using BMA.

Indicator correlation length analyses: The JACKKNIFE method is used in a similar way for the analysis of the indicator correlation lengths. The thresholds are the percentile values of the measurement data. MoM_{var}, MoM_{LA} and ML methods offer comparable results in figure 3.17. The indicator correlation lengths are nearly the same for all thresholds; comparing theses results with the ones of case study A, one can clearly see that the extreme high and low values show indicator correlation lengths that are more or less the same as for the median value, as shown for $E_{U,3}$ in figure 3.17. Although there is a scattering, the distribution of the indicator correlation length at different thresholds does not show the same distribution as in the analytical case shown in figure 3.4. This can be attributed to a non Multi-Gaussianity of the measurement data, which cannot be described by knowing solely the mean valued, the standard deviation and the spatial correlation of measurements.

Table 3.3: Correlation lengths using the JACKKNIFE approach for the MoM_{var} approach in comparison to the mean value and the standard error of the ML approach.

	MoM_{var} $\mu \pm \sigma$ [MN/m^2]	ML $\mu \pm \sigma$ [MN/m^2]	BMA $\mu \pm \sigma$ [MN/m^2]
$E_{L.1}$	22.59 ± 16.60	44.98 ± 26.33	26.15 ± 12.81
$E_{U,1}$	25.30 ± 22.30	46.82 ± 27.42	28.28 ± 12.16
$E_{L,2}$	9.31 ± 23.24	42.44 ± 25.91	22.76 ± 12.44
$E_{U,2}$	29.27 ± 16.71	31.27 ± 16.71	24.83 ± 9.35
$E_{L,3}$	11.31 ± 22.38	45.21 ± 27.69	23.98 ± 12.86
$E_{U,3}$	37.29 ± 11.58	44.13 ± 27.96	34.73 ± 9.50

3.3.3 Remarks

A main concern in this measurement setting has been the different sources of error, which are summarized in chapter 2.3. To keep the measurement error as small and constant as possible, the same people carried out all the tests with the same equipment. The knowledge error and description error were kept minimal by interviewing different experts to judge the geological and geotechnical circumstances in order to identify the homogeneous layer as shown in figure 3.13. After this, the spatial variability inside a homogeneous layer was assumed to be the main source of uncertainty. But one has to be aware that the mutual distance between the samples itself is also a source of error.

In tables 3.2 and 3.3 the results of the correlation length are presented; the results for each loading and reloading cycle show an almost similar spatial correlation within the MoM_{var}, MoM_{LA} and ML approaches. The MoM_{var}, MoM_{LA} and ML approaches show different results. The differences between the three approaches can be related to the different evaluation schemes of the spatial correlation. By looking at the results, one can conclude that the results of the MoM_{LA} approach are not reliable. If one compares the results of the MoM_{LA} approach to the sampling scheme of the test results every 2 m, the results of the MoM_{LA} approach are not reliable because there are just 2 measurements within the correlation length. Therefore, MoM_{LA} is not considered for JACKKNIFE approach.

The JACKKNIFE approach is employed to evaluate the uncertainty of the spatial correlation, which is new to the reader's knowledge. Moreover, this offers the possibility to combine via the Bayesian Model Averaging Scheme the results of the MoM_{var} and the ML approach. Different assumptions and different approaches are merged in the Bayesian Model Averaging scheme, which enables a more precise characterization of the spatial correlation length with a lower COV $= 49\%$ in figure 3.18.

When looking at the results of the indicator correlation length analysis, one can clearly see that the normalised correlation lengths is nearly the same for all investigated thresholds. The normalised correlation lengths differ significantly from the analytically defined case in case study A (section 3.1) From these new findings, one can conclude that the simple methods for the simulation of spatial variability (by using a mean value, a standard deviation and only one single covariance function) do not fully acknowledge the measured spatial correlation structure.

3.4 Case study D – Sheikh Zayed road in Dubai

This case study deals with vertically, non equally spaced soil properties following a skewed lognormal distribution. The resulting problems and challenges are presented while using the variogram approach (MoM_{var}), the local average approach (MoM_{LA}) and the ML approaches.

3.4.1 Site description

Within this case study measurements from Wolff [406] are used to identify the spatial properties of the uniaxial compressive strength (UCS) in limestone. Lab tests have been carried out on 198 samples from different depths in 31 boreholes at four different construction sites at the Sheikh Zayed road in Dubai. To make a clear statement on the sources of error for these measurement data is not easy, as data have been collected from different sites and the UCS tests have been conducted by different persons using different measurement equipment.

The plan view of the four sites is given in figure 3.19. A χ^2 goodness-of-fit-test showed that the measured UCS in figure 3.20 (a) may be assumed to have a lognormal distribution with a mean value $\mu = 2.49$ MN/m^2 and a coefficient of variation of COV $= 44$ % as shown in figure 3.20 (b).

3.4.2 Analysis of the data

The measurement data have been tested for their homogeneity and stationarity. After this, the MoM_{var}, the MoM_{LA} and the ML approaches have been used to explore the spatial variability. As shown in figure 3.19, there are just four sites for the investigation of the vertical correlation length. The horizontal correlation length is not investigated, because one would need more data to get reliable results as pointed out in section 3.8.

The uncertainty of the vertical correlation length is investigated by using MoM_{var}, MoM_{LA} and ML approaches ntogether with the JACKKNIFE approach. The Akaike-

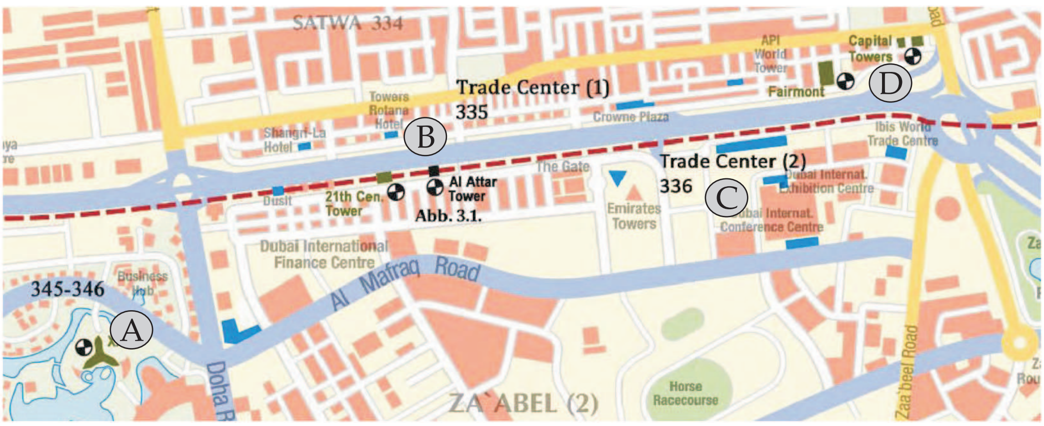

Figure 3.19: Case study D: Plan view of the four sites at the Sheikh Zayed road in Dubai.

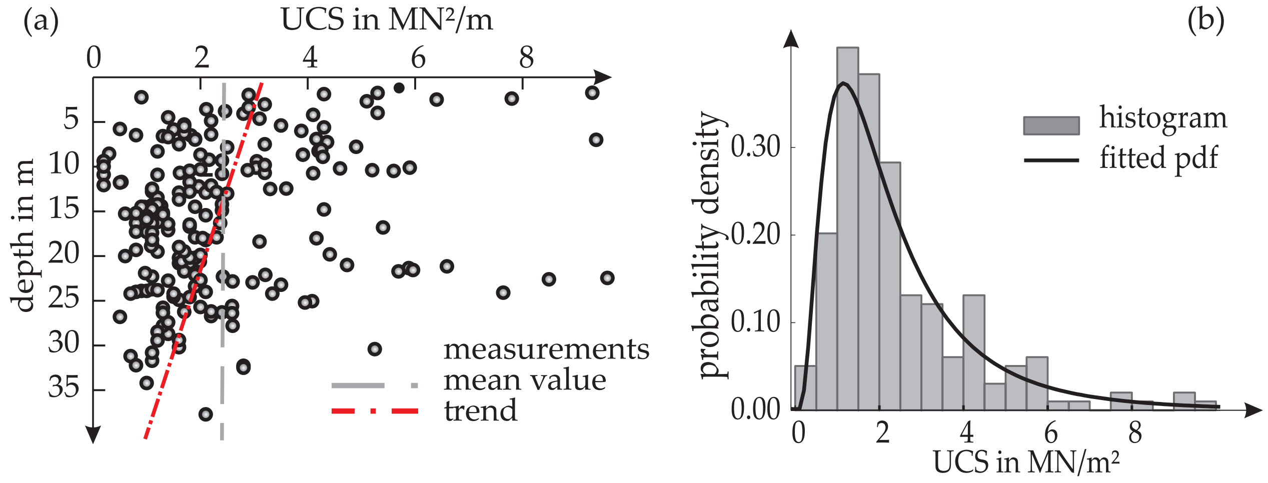

Figure 3.20: (a) Observations of the uniaxial compressive strength,
(b) histogram and fitted lognormal probability distribution function of the UCS at the Sheikh Zayed road in Dubai.

Information-Criterion is employed to select the best fitting theoretical variogram model within these approaches. The results of these investigations is shown in figure 3.21.

The data have been also analysed in terms of their indicator correlation lengths for different thresholds cut_k as shown in figure 3.22.

3.4.3 Remarks

The data, which have been evaluated in this section are non equally spaced, as shown in figure 3.20. Therefore, the evaluation of the variogram has to follow equation 2.31 and figure 2.6.

The strength of the $\mathrm{MoM}_{\mathrm{var}}$ approach can be clearly seen in figure 3.21. It has by far the lowest variations of the resulting correlation length, which is not the case for the ML and $\mathrm{MoM}_{\mathrm{LA}}$ approaches. This can related to the subdivision of the non-equidistant measurements into distance classes. If there are outliers in these distance classes, they can influence the correlation length significantly. The problem of outliers is also captured by the JACKKNIFE approach as a side effect; via this algorithm the influence of these outliers on the correlation length is evaluated through the variance of the correlation length as shown in figure 3.21. This challenge of non-equidistant data is not really present for the ML approach because all data and their mutual correlation are captured trough the correlation matrix. The ML approach is also just slightly influenced by the q-q transformation.

In comparison to the variogram approach, the ML and $\mathrm{MoM}_{\mathrm{LA}}$ approaches show a high COV of the correlation length. This can be related to the q-q transformation and to the relative high skewness of the distribution, which is influencing the reliability of these methods, as shown in case study A.

When looking at the results of the indicator correlation length analysis in figure 3.22, one has to keep in mind the high skewness and asymmetry introduced by the indica-

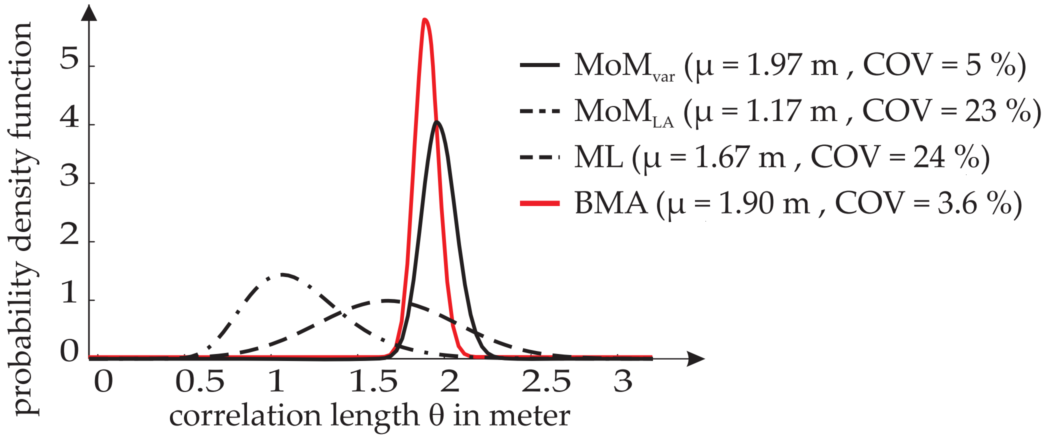

Figure 3.21: Case study D: Combination of the MoM_{var}, the MoM_{LA} and the ML approach using BMA.

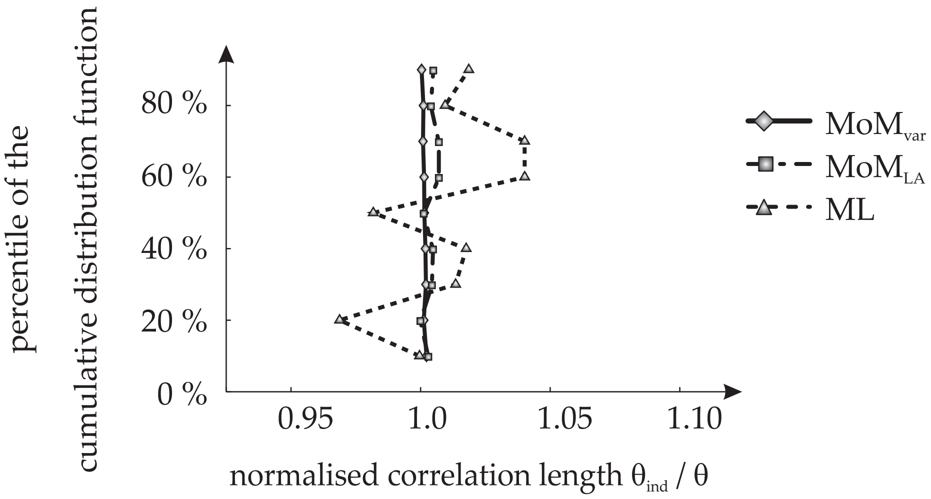

Figure 3.22: Case study D: Analysis of the indicator correlation lengths using using the MoM_{var}, the MoM_{LA} and the ML approach.

tor approach. As in case studies B and C, the results are different from the findings of the generated random process following a multi-variate Gaussian distribution in case study A. The lower extreme values show a significantly higher correlation length than the lower extreme values and the median value. Similar findings for permabaility measurement data are presented in literature [144]. In this context, the indicator correlation lengths are more or less the same for all thresholds [144].

3.5 Literature database on the spatial correlation of soil properties

Geostatistical textbooks [79, 97, 190, 401] always refer to expert knowledge, experience or expert intuition in the interpretation of measurement results. No doubt, which is even necessary in the presence of an automated fitting procedure as pointed out in section 2.6.2. But it is very difficult to develop this experience. For this reason, the author studied a vast number of publications (127 journal papers, technical reports, PhD theses and conference proceedings) to gain more knowledge in the spatial variability of soil properties. Afterwards the author set up three databases describing the spatial variability of rock as well as frictional and cohesive soils. The database in Appendix A has the following categories: property, soil type, vertical θ_{ver} and horizontal correlation length θ_{hor} and applied theoretical correlation function.

The main test types can be grouped into three classes; most of the investigations on spatial variability are base on CPT measurements; another source of information are observations of permeability among other measured properties. The uncertainties of different sources e.g. sampling, measurement or statistical models are not investigated within this database.

In Appendix A the different techniques can be seen in detail, which have been used for the investigation of rock, frictional soils and cohesive soils. Additional investigations have been carried out using the databases of frictional and cohesive soil as well as rock in order to describe the horizontal correlation length θ_{hor} and the vertical correlation lengths θ_{ver} by means of probability density functions. For this reason the entries in the database have been grouped into cohesive soils and frictional soils. For cohesive soils 99 entries for θ_{ver} and 64 entries for θ_{hor} and for frictional soils 63 for the θ_{ver} and 52 entries for θ_{hor} have been found. Several authors offered only a lower and upper bound instead of one single value for θ_{hor} and/or θ_{ver}. To perform a proper analysis of the collected data, these bounds have been used to generate variables, which follow a uniformly distributed random variable between the lower and upper bound. One could argue that the uniform distribution is quite a simple and conservative way to describe the probability distribution of the correlation length. This is true, but in the absence of more detailed information, it is possible to use it. The histograms of the θ_{ver} and θ_{hor} for frictional and cohesive soils are shown in figures A.3, A.4, A.5 and A.6.

Figures A.3 and A.4 show the empirical histogram of the correlation length for cohesive soils. In figures A.5 and A.6 the empirical histogram the correlation length for frictional soils are depicted. In all four figures it can be seen clearly that the correlation length can be described at different scales with different mean values and corresponding standard deviations of fitted lognormal distribution functions. Table 3.4 summarize the findings of the literature database. It offers mean values and standard deviations for vertical as well as horizontal correlation length. It was found that frictional soils have two different scales of correlation in the horizontal and vertical directions. Something similar was found for cohesive soils. These findings can be explained by the different scales of soil variability as mentioned in section 2.4.1.

The literature database on the spatial correlation of soil properties is offering an insight

Table 3.4: Properties of the lognormally distributed horizontal and vertical correlation lengths of CPT data for frictional and cohesive soils.

	frictional soils		cohesive soils		
scale	$0 \sim 10$ m	$10 \sim 30$ m	$0 \sim 15$	$15 \sim 40$	$40 \sim 60$
vertical	0.18 ± 0.78 m	30 m	0.29 ± 1.14 m	23.30 ± 1.6 m	50 m
scale	$0 \sim 50$ m	$50 \sim 100$ m	$0 \sim 100$ m	$100 \sim 500$ m	
horizontal	2.35 ± 0.43 m	90 m	2.27 ± 1.72 m	25.54 ± 0.30 m	

into correlation lengths of different soil. The presented database is used to derived upper and lower limits of vertical and horizontal correlation lengths of different soil types. This can be used to set up efficient sampling schemes because the spatial correlation length is essential to investigate the micro-, meso- or macro scale soil variability. Moreover, the presented database links soil types and spatial variability presented in literature.

3.6 Evaluation of the vertical correlation length using CPT databases of different soil types

One can clearly deduce from the literature database in Appendix A that there is need for more experimental investigations on the correlation lengths in different soils. But most experiments for the detection of the correlation length are cost intensive. Therefore, not many case studies are carried out. One way out of this is offered by the cone penetration test (CPT). This relatively cheap and simple technique allows one to measure nearly continuously soil properties, which can be evaluated for their correlation length; a big number of publications on this has been collected in the database in appendix A .

A database of the National Geotechnical Experimentation Sites (NGES) [50, 129, 380] and of the Pacific Earthquake Engineering Research Center (PEER) [275] offer a large number of vertical CPT measurements of different sites together with soil profiles. The key-points of the different CPT sites such as number of CPTs, minimum and maximum depth and sampling rate are summarized in table 3.5. In Appendix B a plan view of the CPTs together with a typical CPT profile is added.

Just like the CPT measurements presented in case study 3.2, all 671 CPT measurements are analysed by the stochastic site characterization scheme described in case study 3.2. The subdivision of each CPT profile into homogeneous soil layers combines expert judgement and statistical techniques; the vertical correlation length was investigated inside each layer.

After this, the charts of Robertson [308] in figure 3.23 are used to classify each layer into one of the 9 proposed soil types. Herein, q_t is the cone resistance, σ_{v0} is the initial, total vertical stress, σ'_{v0} is the initial, effective vertical stress, u_0 the pore water pressure and u_z the measured pore water pressure and f_s the sleeve friction. These quantities are used to calculate the normalized cone resistance Q_t, the friction ratio F_s and the normalized pore water pressure B_q.

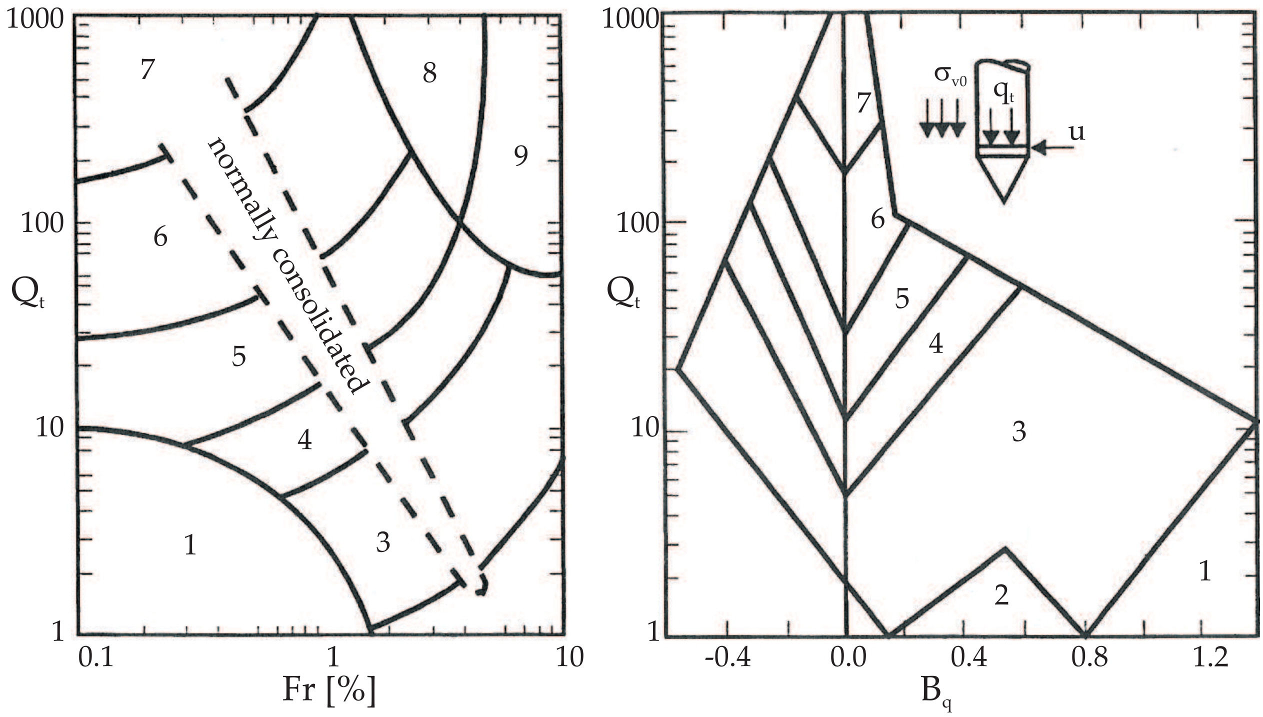

$$Q_t = \frac{q_t - \sigma_{v0}}{\sigma'_{v0}} \qquad B_q = \frac{u_z - u_0}{q_t - \sigma_{v0}} \qquad F_t = \frac{f_s}{q_t - \sigma_{v0}} \cdot 100\%$$

Figure 3.23: Soil classification into 9 soil behaviour types according to Robertson [308]:
zone 1: sensitive fine grained
zone 2: organic soil-peat
zone 3: clay-silty clay
zone 4: clayey silt - silty clay
zone 5: silty sand - sandy silt
zone 6: clean sand to silty sand
zone 7: gravelly sand to sand
zone 8: very stiff sand to clayey sand and
zone 9: very stiff to fine grained soil.

The vertical correlation lengths for the soil types are statistically analysed and the mean values and coefficients of variation of the fitted lognormal distribution functions are summarized in table 3.6. This table also contains the results of the BMA scheme, which were used to combine the results of the MoM_{var}, the MoM_{LA} and the ML approach. The above cited databases do not cover the investigated CPT measurements of the soil type 7 "gravelly sand to sand", soil type 8 "very stiff sands to clayey sand" and soil type 9 "very stiff, fine grained sand".

One can clearly see that the difference between "sensitive fine grained soils" and "clean sands to silty sands" is not that big. For the MoM_{var}, the MoM_{LA} and the ML approach, the mean values of the vertical correlation length ranges between $\theta_{\text{vert}} = 0.4$ m and $\theta_{\text{vert}} = 0.8$ m. Also the COV values do not show a big scatter. Maybe this can be linked

Table 3.5: Summary of the different CPT databases [50, 129, 275, 380].

site	number of CPTs	depth min	depth max	sampling rate
		m	m	#/m
NGES Alameda	195	9.65	50.75	0.025
NGES Evansville	40	12.00	33.25	0.025
NGES Lancaster	41	8.35	23.25	0.025
NGES San Bernardino County	88	10.00	27.00	0.050
NGES San Luis Obispo	37	13.50	30.00	0.050
NGES Santa Clara County	163	3.15	38.50	0.050
NGES Solano County	12	13.60	25.00	0.050
PEER Anssall	8	10.60	30.83	0.050
PEER Berkeley	87	2.40	10.20	0.050

Table 3.6: Mean value and COV of the vertical correlation lengths of the different CPT databases and the BMA combination results.

soil types	MoM_{LA}		MoM_{var}		ML		BMA	
	μ in m	COV in %	μ in m	COV in %	μ in m	COV in %	μ in m	COV in %
sensitive, fine grained	0.78	170	0.47	160	0.54	101	0.53	64
organic soil to peat	0.53	145	0.46	120	0.51	79	0.49	53
clay to silty clay	0.43	121	0.45	127	0.48	81	0.46	52
clayey silt to silty clay	0.53	126	0.50	135	0.56	80	0.54	53
silty sand to sandy silt	0.75	201	0.51	140	0.57	79	0.56	57
clean sand to silty sand	0.45	116	0.48	100	0.29	108	0.47	54

to the genesis of the tested soils because all of the tested soils can belong to sediment soils. It is very difficult to compare the presented results to other works because no comparable study is available to the author's knowledge.

The presented results are an extension of the literature database in section 3.5 using measurement data. On basis of CPT measurements, the vertical correlation lengths of various soil types are evaluated. These results offer a detailed insight into the spatial correlation of CPT measurements, which have been performed in 6 different soil types. These results are contributing to a general description of stochastic soil properties of 6 different soil types.

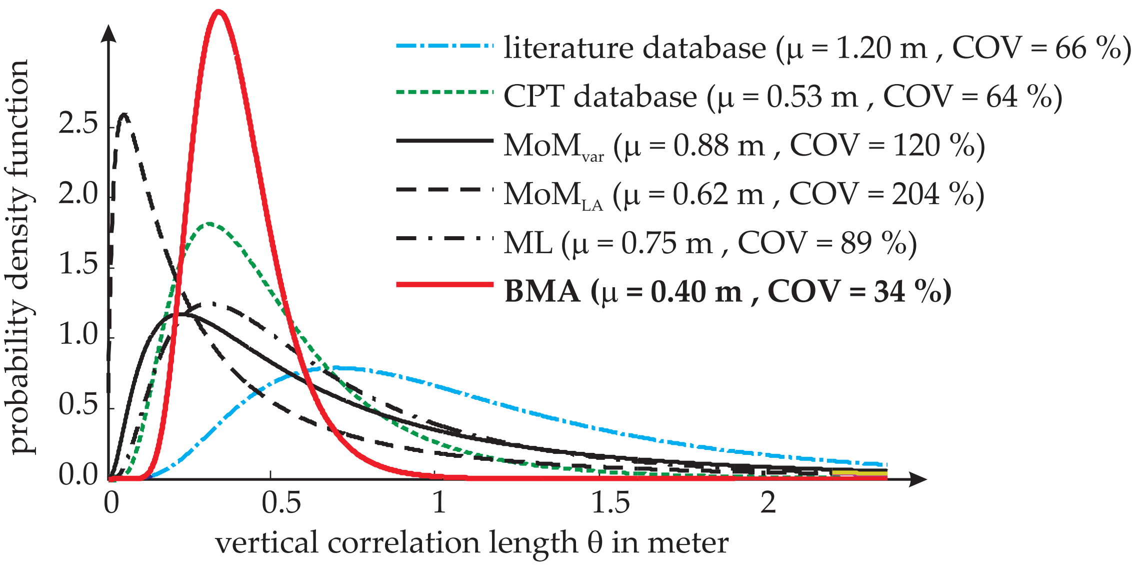

Figure 3.24: Combination of measurement data of silty clay, results of the literature database and results of the CPT databases using Bayesian Model Averaging.

3.7 Combining expert knowledge and measurements

Before making use of data collected at the site [369, 382], the engineer can express his information from a literature study or similar measurement or even his expert judgement concerning the set of uncertain parameters.

This combination of prior (subjective) information and "objective" data can be carried out via the BAYESIAN MODEL AVERAGING (BMA) scheme, which is already explained in case study B in section 3.2.3. The BMA scheme enables the combination of different models as well as different sources of information in a relativly simple manner, namely the BAYES theorem. Via this approach it is possible to derive a conditional probability distribution, which considers different sources of information.

This scheme is been applied to the results of the CPT data of a silty clay from CASE STUDY B. As shown in figure 3.11, the the MoM$_{var}$, the MoM$_{LA}$ and the ML approaches can be combined sequentially via the BMA scheme. This is proceeded by adding additional information to the results: the results from the literature database and CPT database offer additional expert knowledge of comparable soil types. By looking at figure 3.24, one can see that the combined model has a lower mean value as well as a lower COV. The results of the literature database have a relatively flat and wide pdf, which does not have a big influence on the combined model. Those pdfs have a high influence on the combined model, which have a low COV. This can be explained by the availability of information: the more information is available, the more precise is the description of the probability density function.

3.8 Summary and consequences of the case studies

The application of different methods for evaluating the correlation length to an analytical random process shows the strength and weaknesses of Mthods-of-Moment and ML approaches, which are even more highlighted by the evaluation of equally and non-equally spaced measurement data.

Case study A: The simplest boundary conditions are used in CASE STUDY A; artificially generated, homogeneous, stationary data with a known correlation length θ_{target} and an added error are analysed by the MoM_{var}, the MoM_{LA} and the Maximum Likelihood approaches. The data are quasi continuously defined in order to exclude a sampling induced errors. It is shown that all three approaches offer nearly the same results under ideal conditions of a symmetric probability density function.

In addition to this, the indicator approach is employed to analyse the spatial correlation of extreme low and high values. The indicator correlation length of the extreme low and high values of the random process show a significantly lower correlation than the median values. Via this, the indicator correlation length of a theoretical multivariate-Gaussian random process is analysed and shown, which help to understand the results of the case studies in the latter.

Case study B: A scheme for stochastic site characterization is used to describe the soil tested by 138 vertical CPT measurements in CASE STUDY B. This procedure combines engineering judgement and these statistical techniques to identify soil layering. Moreover, the spatial variability of each soil layer is identified and statistically described by a lognormal distribution function. The presented scheme enables the engineer to separate different scales of variability, e.g. the geological macro-scale and and smaller geotechnical meso-scale inside each layer. By separating the macro- and the meso-scale, the evaluation of the correlation lengths becomes more easy because measurement data from the observed layers do contain less erroneous parts of e.g. large scale fluctuations.

The results of the the MoM_{var}, the MoM_{LA} and the ML approaches offer independent interpretation of the measurement data. Due to the big number of CPT measurements it is possible to identify a lognormally distributed vertical correlation length, which is a novel insight into this context.

The results of the MoM_{var}, the MoM_{LA} and the ML approaches are combined using the BAYESIAN MODEL AVERAGING scheme, which combines the information of different models using the BAYES theorem. This procedure results in a probability density function of the correlation length, which contains different models and assumptions in one results. The resulting probability density function of the correlation length is a new insight into spatial variability.

The indicator correlation length analyses clearly show that the measurement data have a particular correlation of the extreme low and high values. This implies that these spatial correlations cannot be modelled by conventional simulation approaches using one single correlation function.

Case study C: Equi-distant in-situ measurement of stiffnesses are analysed within this case study. In order to analyse the uncertainty of the correlation length, the well known the $\mathrm{MoM}_{\mathrm{var}}$ and the $\mathrm{MoM}_{\mathrm{LA}}$ approach approach is extended by using the JACKKNIFE procedure. Via this novel approach, a comparison with the uncertainty measures of the ML approach is possible.

Furthermore, the results of the the $\mathrm{MoM}_{\mathrm{var}}$, the $\mathrm{MoM}_{\mathrm{LA}}$ and the ML approaches can be combined with the introduced Bayesian Model Averaging scheme.

In addition to this, the indicator correlation length analyses indicate a spatial structure of the measurement data, which cannot be fully described by standard approaches using one single correlation length used in case study A.

Case study D: In case study D the non-equidistant data are investigated. These measurement results of the soil strength follow a skewed, lognormal distribution. Apart from the challenges of analysing these data, the BAYESIAN MODEL AVERAGING approach offers an elegant tool to combine the results of the the $\mathrm{MoM}_{\mathrm{var}}$, the $\mathrm{MoM}_{\mathrm{LA}}$ and the ML methods.

The results of the presented case studies show that the presented methodologies can evaluate the correlation length of equally and irregularly spaced measurement data. The results in the case studies show different ratios of the nugget effects to sill values. This implies that different scales of variability are involved. But one has to keep in mind that the the $\mathrm{MoM}_{\mathrm{var}}$, the $\mathrm{MoM}_{\mathrm{LA}}$ and the ML approaches can only identify the spatial correlation of one scale. Therefore, the sampling concept of the measurement data is essential and has a major impact on the results. One has to know in advance the scale in order to measure it correctly. But there are no satisfying solutions offered in literature, as pointed out in section 2.5.4. The big drawback of the presented design-based sampling concepts of geostatistics is the high sampling effort, which implies high costs. Model based design approaches like nested-sampling design [403] or adaptive sampling approaches offer a promising alternative; but this is suffering from the assumption of normally distributed variables.

Due to the multi-scale nature of spatial soil variability no general answer for the minimum sampling effort to describe spatial variability can be given. Barnes [32] states that the upper bound of required sampling for spatially dependent samples has to be lower than for identically, independently distributed samples. Different authors focused on this but only some of them like Journel & Huijbregts [190] or Lark [214] offer rules of thumb for a one dimensional spatial correlation. Here, the number of pairs should be at least 30 to 50 pairs. In the field of ecology and environmental engineering, Marchant & Lark [236] recommend to have at least 100 to 150 samples for a two dimensional spatial analysis, whereas Webster & Oliver [402] recommend at least 200 samples. Other publications [90, 197–200, 270, 271] refer to a minimum sampling size of $100 - 150$ samples in a two dimensional analysis of the spatial correlation using the ML approach. DeGroot & Baecher [90] provide in figure 2.8 a relationship between the correlation length and the sample size, which also gives comparable suggestions for a minimum required sample size.

If the number of pairs is lower, the uncertainty of the correlation length becomes very dominant and complicated for the ML approach as well for the presented JACKKNIFE method.

Literature database and CPT databases: At the end of an evaluation of measurement data, one has to compare the resulting correlation lengths with knowledge, which reflects experience, the state-of-the-art or the state-of-science. This can be done by using the presented databases of literature, which presents data on spatial variability of different soil types in literature.

In addition to this, presented results of the CPT databases offer a more specific insight to this problems. The vertical correlation lengths of eight different soil types ranging from clay to sand are presented by indicating mean value and standard deviation of the lognormal distribution.

At the end of this chapter, the BAYESIAN MODEL AVERAGING procedure is used to fuse different model results. In a similar way, these results can be updated with additional knowledge coming form expert judgement, literature knowledge or results from comparable tests in similar soils. Via this, the probabilistic site characterisation can be enriched by expert knowledge or other sources of information within a mathematically defined framework.

Chapter 4

Safety and uncertainties

Within this chapter the basics of safety and reliability are highlighted. It provides a description of common approaches for dealing with uncertainties and safety in geotechnical engineering. Global and partial safety factors, as well as the basics of uncertainty quantification and reliability based design, are described and compared with a special focus on the basics of the generation of random numbers and random fields, as well as on the computation of failure probabilities. Moreover, an introduction to the local and global sensitivity analysis of systems is presented.

4.1 Safety in engineering

The goal of safety is the preservation of existence of an individual or a community. Since many general requirements of humans have found their way into laws, the preservation of psychological and physiological functioning of humans can be found in many constitutions and in the UN Charter of Human Rights as stated in Proske [295]. Although the term safety can be found in many laws, this does not necessarily mean that the content of the term is clearly defined. Many people have a different understanding of the term. Some common descriptions are presented in [163, 261, 295]:

- Safety is a state in which no disturbance of the mind exists, based on the assumption that no disasters or accidents are impending.
- Safety is a state without threat.
- Safety is a feeling based on the experience that one is not exposed to certain hazards or dangers.
- Safety is the certainty of individuals or communities that preventive actions will function reliably.

Safety requirements and safety concepts have a long history in some technical fields [295]. Nearly 4,000 years ago, this can be seen in the code of HAMMURABI, in which strong penalties in the case of collapsing structures were fixed. Probably the first application of a global safety factor in structural engineering dates back to PHILO from Byzantium [338] in 300 B.C., who introduced the global safety factor η in terms of:

$$\eta = \frac{\text{resistance}}{\text{load}} \tag{4.1}$$

Table 4.1: Factors of global safety in engineering according to Visodic [397].

Factor of safety	knowledge of load	knowledge of material	knowledge of environment
1.2 - 1.5	excellent	excellent	controlled
1.5 - 2.0	good	good	constant
2.0 - 2.5	good	good	normal
2.5 - 3.0	average	average	normal
3.0 - 4.0	average	average	normal
3.0 - 4.0	low	low	unknown

Table 4.2: Factors of global safety in geotechnical engineering after Terzaghi & Peck [373].

item	factor of safety
earthworks	1.3 – 1.5
earth retaining structures	1.5 – 2.0
excavations, offhore foundations	2.0 – 3.0
foundations on land	
uplift, heave	1.5 – 2.0
piping	2.0 – 3.0
load tests	1.5 – 2.0
dynamic formulas	3.0

Only in the last few centuries have the application of *global safety factors* become widespread. Over time many different values were developed for different materials [295]. In most cases, the values dropped significantly during the last century. Proske et al. [297] report that in 1880 in brick masonry, a factor of $\eta = 10$ was required, whereas 10 years later, a factor between $\eta = 7 - 8$ was required. In the 20^{th} century, the values have changed from a factor of $\eta = 5$, then to $\eta = 4$, and now for the recalculation of historical structures a factor of $\eta = 3$ is chosen [297].

Especially with the development of new materials, an increase in concern over the safe application of these materials has arisen. At the beginning of the 20^{th} century the development of safety factors for different materials led to initial efforts in developing material-independent factors, such as those shown in table 4.1. Visodic [397] shows that the knowledge of load, material and environment have an influence on the global safety factor depending on the state of knowledge: if there is more knowledge on the load, material and environment, the factor of global safety can be reduced to a certain limit [297]. A similar tendency can also be observed for other materials like steel. In geotechnical engineering, Meyerhof [251] reports that the factor of global safety for the stability of a retaining wall remained the same, since being introduced in the 18^{th} century by Belidor and Coulomb. The global factors of safety for different geotechnical problems are summarized in table 4.2. These values by Terzaghi & Peck [373] do not take into account the variability of the soil properties or additional knowledge on the soil.

More advanced changes might be considered to meet the demanding requirements of economic and safe structures in order to include the different levels of knowledge. Such developments include special safety factors for the different column heads in table 4.1, for example a safety factor for load and a safety factor for material. Indeed, this is the basic idea of the *partial safety factor* concept. A more precise consideration of the different uncertainties in loads and resistances yields a more homogeneous level of safety of a structure [297]. The proof of safety is carried out by the simple comparison of the load event E_d with the resistance of the structure R_d .

$$E_d \leq R_d \tag{4.2}$$

Subsequently, the load event can be built from several single elements, such as the characteristic dead load $G_{k,j}$ connected with a special safety factor $\gamma_{G,i}$ only for dead load, and the characteristic life load $Q_{k,j}$ connected with a special safety factor $\gamma_{Q,i}$ and $\psi_{0,i}$ for the combination of different life loads:

$$E_d = \sum \gamma_{G,i}\, G_{k,i} + \gamma_{Q,i}\, Q_{k,i} \sum \gamma_{Q,i}\, \psi_{0,i}\, Q_{k,i} \leq R_d \tag{4.3}$$

According to Proske [297], although the partial safety factor concept was first introduced in structural engineering after World War II, it took quite some time to become practically applicable. In geotechnical engineering Talyor [372] was one of the first amongst others to introduce separate factors of safety on the components of shear strength in slope stability estimation. It is reported in [251] that Brinch-Hansen generalized this approach and initiated partial safety factors in geotechnical engineering. In civil engineering, these partial factors were chosen to give about the same design estimate as conventional total factors of safety as stated by Schuppener [325, 330]. These factors have been refined subsequently by semi-probabilistic methods on the basis of the variability of the loads, soil strength parameters and other design data in practice [251]. Therefore, the development of partial safety factors is strongly connected to the development of the probabilistic safety concept in structural engineering [297].

The calibration of partial safety factors is described in EUROCODE [71] as shown in figure 4.1. The deterministic as well as the probabilistic approach can be used for calibration of the partial safety factors. The deterministic approach includes historical as well as empirical methods in civil engineering, which have shown their strengths over several years or even decades [297], for the calibration of partial safety factors. The probabilistic approach can use reliability methods and fully probabilistic methods (e.g. Monte Carlo approach) for the calibration of the partial safety factors. The probabilistic methods offer the basis for the calibration of the partial safety factors, which are used in the semi-probabilistic approach. In the semi-probabilistic approach, partial safety factors are used to consider the uncertainties in load, resistances and model uncertainties, [297].

The first proposals about probabilistic-based safety concepts were found in the 1930s in Germany and in the Soviet Union. The development of *probabilistic safety concepts*, in general, experienced a strong impulse during and after World War II, not only in the field of structures but also in the field of aeronautics. The Joint Committee of Structural

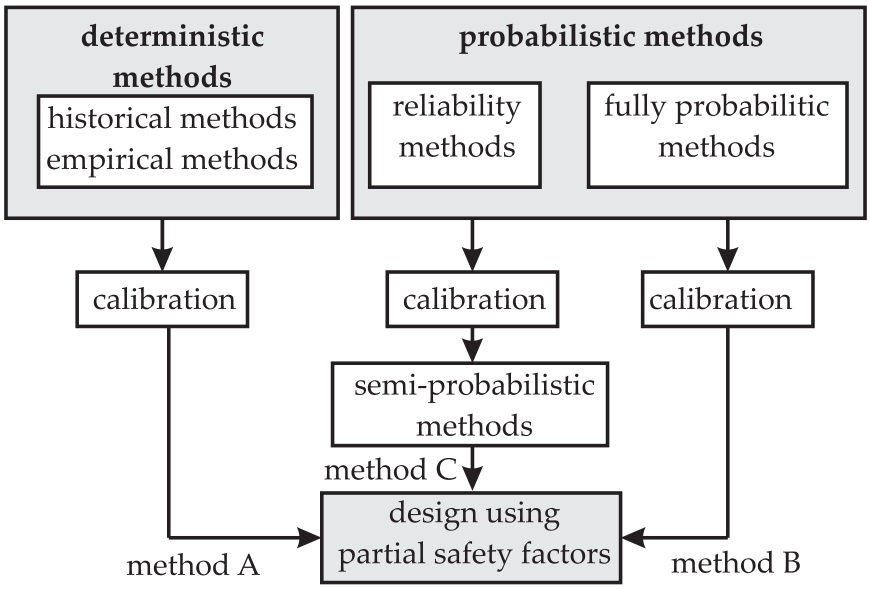

Figure 4.1: Calibration of the partial safety factors according to EUROCODE [71].

Safety (JCSS) introduced the probabilistic model code [121] on the basis of the probabilistic safety concept of structures. The probabilistic model code includes a detailed introduction to model the load and resistance parameters as random variables in order to calculate the probability of failure of structures.

In EUROCODE [71] the safety of structures is defined as the capability of structures to resist loads. Due to the fact that no building can resist all theoretically possible loads, the resistance has to reach only a sufficient level [71]. Only by using a quantitative measure can one offer a basis on decision on whether a structure is reliably or not. The reliability is interpreted as a probability of failure not occurring, which is explained in detail later in this chapter.

The design process including reliability is called reliability based design (RBD) [286]. Herein, the uncertain components of a system are simulated as random variables within the reliability framework to evaluate the probability of failure. The EUROCODE, as well other design codes [121, 127], probabilistic methods are used with the reliability based design concept calibration of partial safety factors.

Proske [297] offers in figure 4.2 an overview of most of the safety concepts in structural engineering. Starting from basic empirical rules, Proske [297] adds concepts with increasing complexity: As pointed out above, the global and semi-probabilistic safety concepts are less complex than simplified and exact probability safety concepts. As a next step, the reliability index and the probability of failure of a system are compared to the a target reliability and probability of failure. Probabilistic methods like First Order Reliability Method or Monte Carlo Method can be used for this, as described in the EUROCODE [71]. Relatively new concepts like fuzzy-probabilistic procedures [252] and risk based design concepts are also included in figure 4.2. One can deduce form this figure that different safety concepts can cover different aspects. Proske [297] states that only complex safety concepts fulfil the basic requirements indicated by basic human rights for safety and legal restrictions to save life.

Additional to the reliability-based safety concepts, there are the codes for structures known as risk performance based design and risk based design [168, 286, 295]. There exist several different viewpoints with respect to the term risk [295]. Generally spoken, risk is part of man's judgement, when negative impact of dangerous activities is balanced by their profits; such judgements are subject to bias and in many cases they contradict statistical facts, but they are the basis of acceptance or rejection of risks. Risk acceptance is often formulated in an FN criterion, as shown in figure 4.3. Within the framework of quantitative risk assessment, FN-curves show the frequency of occurrence (F) of an event in relation to the number of lost lives (N). FN-curves are mainly based on the discipline, in which the viewpoint was created and the requirements of that discipline. These viewpoints have been summarized by Renn [306] into insurance-statistic based view, toxicological-epidemiological view, engineering-technical view, economical view, psychological view, social-theoretical view and cultural-theoretical view. The first group is represented by the statistical-mathematical formulation and will be partly focused on in this chapter. This formulation is based on the general formula:

$$R = C \cdot P \tag{4.4}$$

where R is the risk, C is the negative consequence measure (damage or disadvantage) and P is the probability of the occurence of C. Proske [295] points out that all components can have different units, of course. For example, the negative consequences can be given in monetary units, in time required, loss of space, loss of humans, loss of creatures, loss of energy, loss of environment and so on.

The terms *safety* and *risk* have strong relations to the terms *hazard* and *danger*. The term hazard implies the occurrence of a condition or phenomenon, which threatens disasters to anthropogenic spheres of interest in a defined space and time [133]. In general, a *hazard* is a natural, technical or social process or event that is a potential damage source. There exist many further definitions of hazards; however, these will not be discussed here.

In general, a hazard might be completely independent from the activities of humans, for example an avalanche or a debris flow. However, if people are at the location of the process, then these people might be in danger. Within this definition, Proske [295] derives danger as a situation that yields without unhindered development to damage. On one hand, danger can be seen as the opposite of safety, where no resources have to be spent. Luhmann [225] stated that risks and hazards are opposites in terms of human contribution. According to Proske [295], risks require possible human actions, whereas hazards are independent from human actions. If that is true, however, then more technologies or more human resources simply means more risks due to the increased volume of human actions and decisions.

Vulnerability is a term that permits an extension of the classical risk definition by only two terms. Instead, further properties can be incorporated into the term vulnerability, which itself is then part of the risk definition:

$$R = f(p, A_0, \nu_0, p_0) \tag{4.5}$$

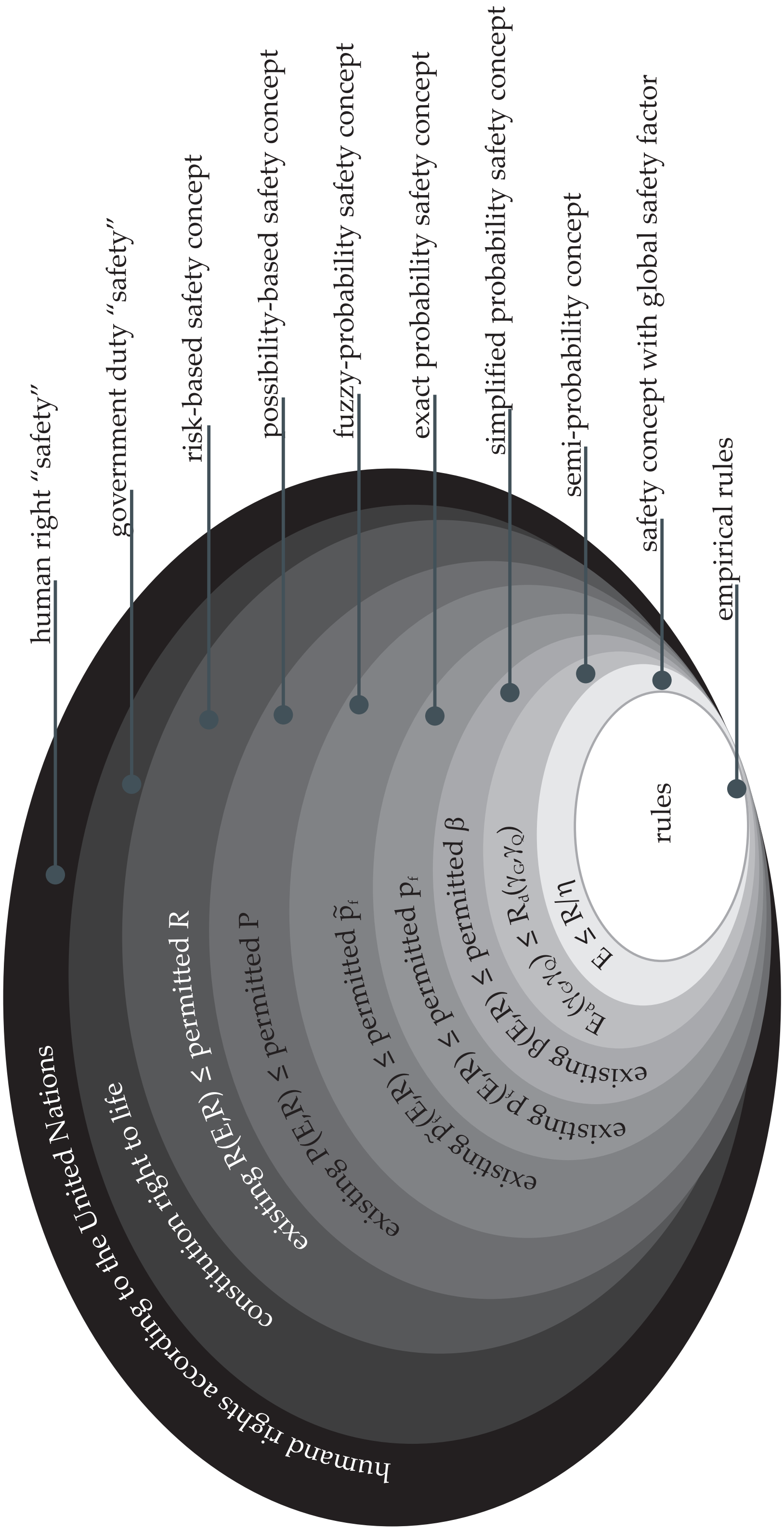

Figure 4.2: Safety concepts in the context of structural engineering from Proske [295].

Table 4.3: Target reliabilities according to EUROCODE [71].

Reliability classes	consequences for loss of human life, economic, social and environmental consequences	reliability index β_a	
		β_a for $T_a = 1$ year	β_a for $T_a = 50$ years
RC 3 - high	high	5.2	4.3
RC 2 - normal	medium	4.7	3.8
RC 1 - low	low	4.2	3.3

where R is the risk, p the probability of this event, A_0 the value of an object, ν_0 the vulnerability of the object during the event and p_0 the probability of exposure of the object during the event, e.g. flood or landslide amongst other natural hazards [133]. Equation 4.5 can be further extended to several event scenarios and objects. However, the term vulnerability remains to be defined. Again, as with many other terms, the variety of definitions of vulnerability is virtually unmanageable according to [133, 295]. Deeper discussion and examples can be found amongst others in [133, 295].

At the basis of *risk based design*, Baecher & Christian [23] summarized the annual failure probability and expected losses for a variety of common civil facilities and other large structures or projects in figure 4.3. Baecher & Christian [23] and Meyerhof [251] are the only two sources of FN-curves in geotechnical engineering according to the knowledge in geotechnical engineering. In figure 4.4 Meyerhof [251] shows the global safety factor in comparison to the lifetime probability of stability failure using different coefficients of variability (COV). On top of this, observed and theoretical probabilities of failure in soil engineering is compared to lifetime fatality risk per person. From figures 4.3 and 4.4 one can derive that there are different reliability levels for different structures.

Table 4.3 shows the classification of target reliability levels provided in the EUROCODE [71]. Reliability indices are given for two reference periods T (1 and 50 years) but without any explicit link to the design working life T_d. The reliability index β is a scalar measure of safety equivalent to the probability of failure p_f, but measured on another scale. A detailed description of the reliability index is given in section 4.3.1.

The values are based on calibration and optimization and reflect results from several studies. It is noted that similar β values as in table 4.3 are given in other national and international guidelines. Examples of buildings and civil engineering works for RC 3 are bridges and public buildings, for RC 2 residential and office buildings and for RC 1 agricultural buildings and greenhouses.

In addition to this, reliability indices with respect to consequences and to relative cost of safety measures are presented in JCSS [121] and ISO 2394 [183] offers more detail. The bigger the reliability index β becomes, the more unreliable is the occurrence of failure, which will be covered in section 4.3.1.

Calgaro [66] states that different criteria may be taken into account when choosing a target reliability index. He emphasis that the combination of economic, risk acceptance, psychological and legal criteria have to be taken into account.

The *Life Quality Index* (LQI) is a recently developed concept for determining acceptability of decisions involving life safety risks in engineering. It provides a rational basis

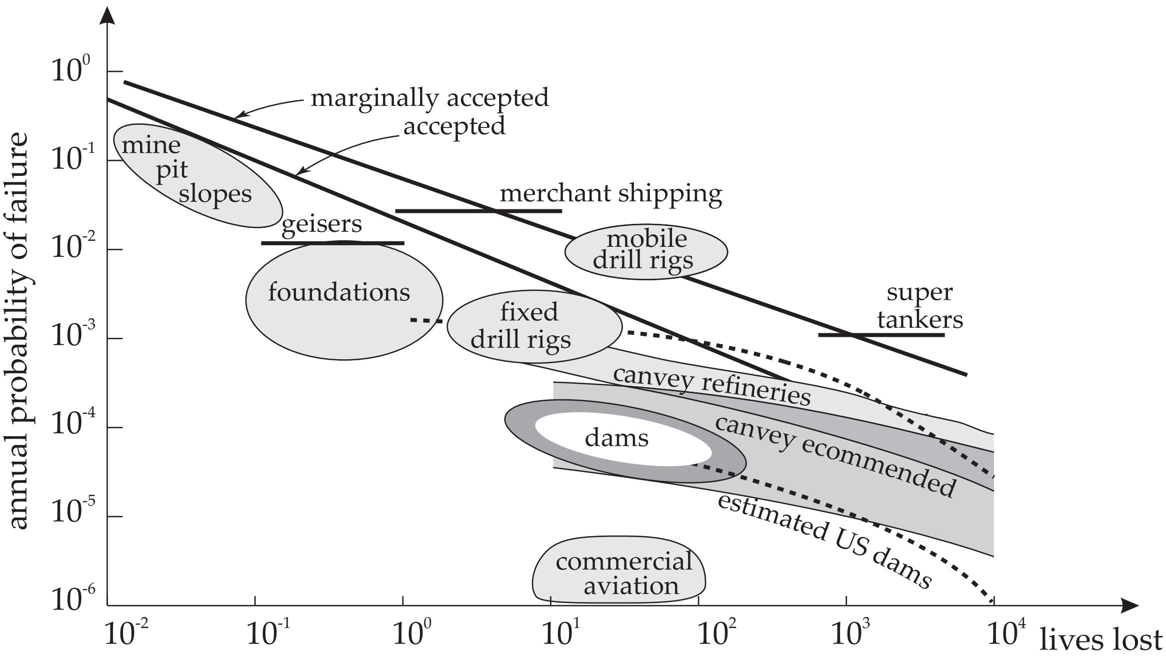

Figure 4.3: Chart showing average annual risks posed by a variety of traditional civil facilities and other large structures or projects proposed by Baecher & Christian [23].

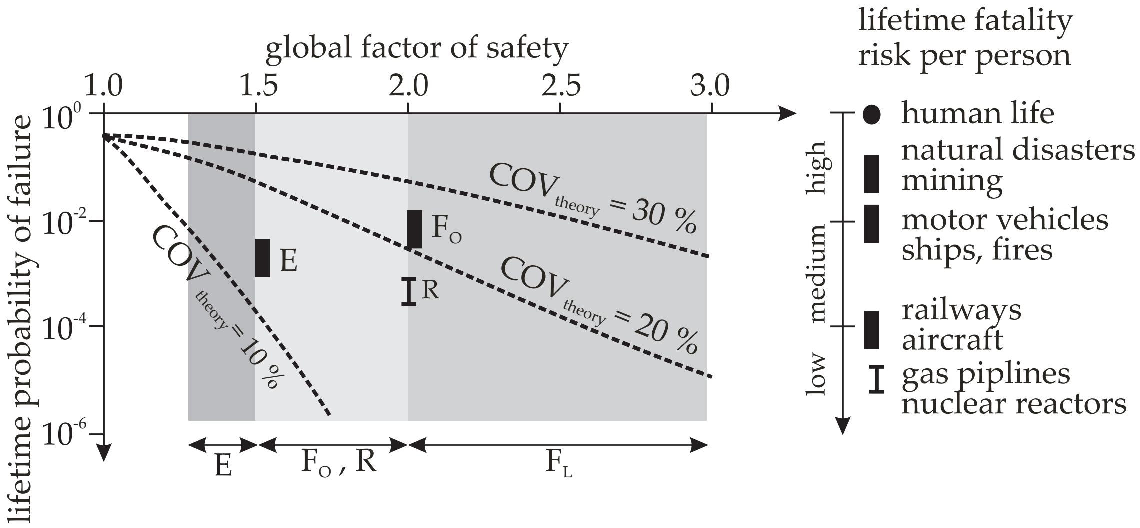

E = earthworks, F_L = foundations on land, F_O = offshore foundations,

R = earth retaining structures, COV_{theory} = theoretical COV in %

observed , theory ----------

Figure 4.4: Lifetime probabilities of stabilitiy failures and comparative human risks from Meyerhof [251].

Table 4.4: Reliability based design: different levels of accuracy from Honjo et al. [168].

level	basic variables	reliability
III	random variables & probability density function	probability of failure
II	random variables & mean & standard deviation	reliability index
I	deterministic variables	partial safety factors

for establishing target reliabilities for civil engineering systems [218, 299, 361]. The LQI is a socio-economic utility function that depends on the wealth and life expectancy of a society. Any decision that increases the value of the LQI is deemed acceptable. This increase can be due to an increase in life expectancy (reduction of fatalities) or an increase in societal wealth (reduced use of resources). In this way the LQI establishes a relation between the resources invested in improving the safety of an engineering facility and potential fatalities and injuries that are avoided by the investment. Hence it provides a means to quantify the optimal trade-off between safety and cost [299, 361].

4.2 Basics of uncertainty quantification

Uncertainty quantification is forming the framework to focus on the effects of variability within computational mechanics, as visualized in figure 4.5. In step A, a mechanical model is set up together with assessment criteria for the behaviour of the system. This step gathers all the ingredients used for a classical deterministic analysis of the physical system to be analysed. In the next step B, the quantification of sources of uncertainty is performed and random variables or random fields are used for the representation of the different sources of uncertainties of the system. Within the uncertainty propagation in step C, the response of the system is (with respect to the random input variables and fields) evaluated, enclosing the uncertainty of the system. Numerous methods exist to carry out this task as described in section 4.3.

Sudret [364] states that uncertainty propagation methods usually provide information on the respective impact of the random input parameters on the response randomness. A sensitivity analysis helps to identify the main sources of the response randomness. Moreover, Sudret [364] point out that this sensitivity analysis may sometimes be the unique goal of a probabilistic study.

Amongst others [57, 89], Sudret [364] reports that this representation can be done in several levels of accuracy. Honjo et al. [168] as well as Phoon [286] show different levels of accuracy summarized in table 4.4; different methods and approaches provide a more detailed insight into the reliability of the system and form the key requirement for reliability based design. In the basic case, one can use deterministic variables and partial safety factors to simulate random variables of a geotechnical problem. This can be improved by taking the mean value and the standard deviation of the random variables into account. A result of this analysis technique is the reliability index. On top of this is the simulation of random variables using the full probability density function. Via

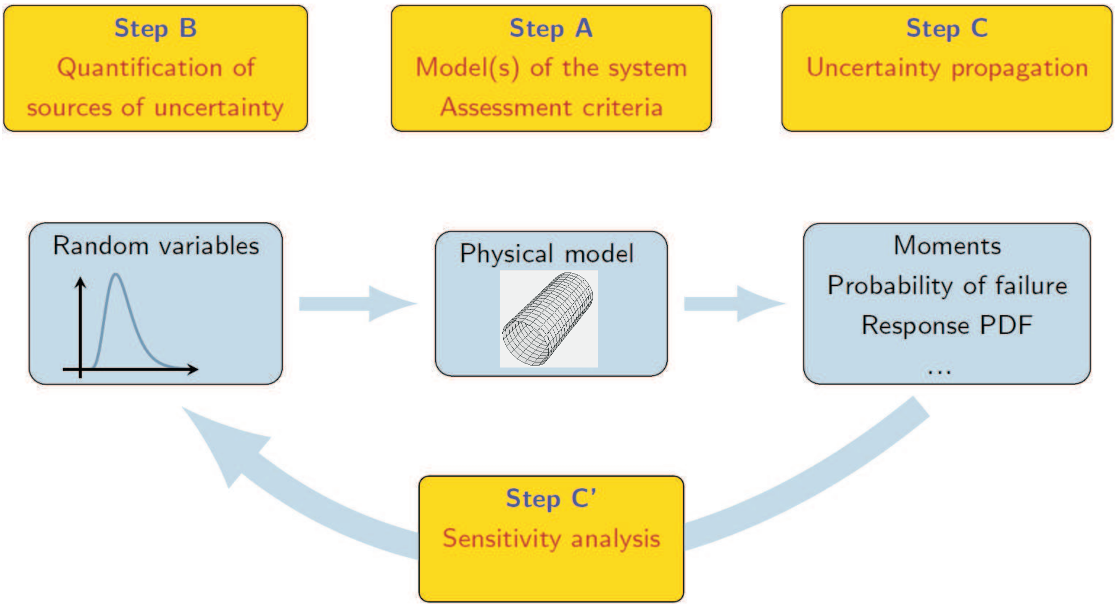

Figure 4.5: Steps in Uncertainty Quantification from Sudret [364].

this approach, it is possible to evaluate the probability of failure more precisely because more information is available in comparison to the other levels of RBD and uncertainty quantification.

4.2.1 Definition of the limit state function

When considering models of mechanical systems $\mathcal{M}$, random variables $\mathbf{X}$ usually describe the randomness in the geometry, material properties and loading. They can also represent model uncertainties [364]. This set also includes the variables used in the discretisation of random fields, if any. The model of the system yields a vector of response quantities $\mathbf{Y} = \mathcal{M}(\mathbf{X})$. In a mechanical context, these response quantities are e.g. displacements, strain or stress components, or quantities computed from the latter.

The mechanical system is supposed to fail when some requirements of safety or serviceability are not fulfilled. In the case of complex systems, one can set up different failure modes to capture the system behaviour in a precise way as described by Huber et al. [175]. For each failure mode, a failure criterion is set up. It is mathematically represented by a limit state function $g(\mathbf{X}, \mathcal{M}(\mathbf{X}), \mathbf{X}')$. The limit state function may depend on input parameters $\mathbf{X}$, response quantities $\mathcal{M}(\mathbf{X})$ that are obtained from the model and possibly additional random variables and parameters gathered in $\mathbf{X}'$. For the sake of simplicity, the sole notation $\mathbf{X}$ is used in the sequel to refer to all random variables involved in the analysis. Let $\mathcal{M}$ be the size of $\mathbf{X}$.

Conventionally, the limit state function g is formulated for the realisations $\mathbf{x}$ of the random variable $\mathbf{X}$ in such a way that:

$$\mathcal{D}_s = \{\mathbf{x} : g(\mathbf{x}) > 0\} \quad \text{is the safe domain in the space of parameters;} \tag{4.6}$$

$$\mathcal{D}_f = \{\mathbf{x} : g(\mathbf{x}) \leq 0\} \quad \text{is the failure domain.} \tag{4.7}$$

The set of points $\{\mathbf{x} : g(\mathbf{x}) = \mathbf{0}\}$ defines the limit state surface [364, 366]. Denoting by $f_{\mathbf{X}}(\mathbf{x})$ the joint probability density function of a random vector $\mathbf{X}$, the probability of failure p_f of the system is:

$$p_f = \text{Prob}\left[g\left(X_1, X_2, \ldots, X_n\right) \leq 0\right] = \int_{\mathcal{D}_f} f_{\mathbf{X}}(\mathbf{x}) d\mathbf{x} \tag{4.8}$$

Sudret [366] emphasis that in all but academic cases, this integral cannot be computed analytically. Indeed, the failure domain depends on response quantities (e.g. displacements, strains, stresses, etc.), which are usually computed by simplified equations [44, 57, 176, 286] or by means of numerical methods e.g. the finite element method [57, 176, 364, 366]. In other words, the failure domain is implicitly defined as a function of $\mathbf{X}$. Thus, numerical methods have to be employed to evaluate the probability of a failure.

4.2.2 Random number generation

The basis of the simulation of correlated random variables is the generation of random numbers following a uniform distribution in an interval from zero to one. According to Fenton & Griffiths [127], the most popular random number generators are the linear congruential generators (LCG). LCG generate independent, identically distributed numbers with a very long periodicity fast by not requiring too much memory. Moreover, LCG have the ability to reproduce a given stream of random numbers exactly, as emphasised by different researchers [85, 127, 266, 294].

The generation of non-uniform random numbers can be done via inverse transform, convolution and acceptance-rejection as described by Phoon [286] or Fenton & Griffiths [127] amongst others.

4.2.3 Generation of correlated random numbers

Widely used random number generators are optimized for producing sequences of numbers which appear to be uncorrelated. Hence the simulation of correlated random variables requires suitable transformations. The details of the transformation depend on the joint probability density function of these variables. If the joint density function is based on the Nataf model then the marginal density function $f_{Xi}(x_i), i = 1, \ldots n$ and the correlation coefficients $\rho_{ij}, i, j = 1, \ldots n$ have to be known. The simulation can then be performed in a loop for $k = 1, \ldots m$ using these steps:

- Generate one sample $u^{(k)}$ of a vector of n uncorrelated standardized Gaussian random variables.

- Transform the sample into correlated standard Gaussian space by means of

  $$\mathbf{v}^{(k)} = \mathbf{L}\ \mathbf{u}^{(k)} \tag{4.9}$$

  Here, $\mathbf{L}$ is the lower triangular matrix, which results from a Cholesky decomposition of the matrix of correlation coefficients ρ.

- Transform each variable separately into non-Gaussian space using

$$x_i^{(k)} = F_{X_i}^{-1}\left[\Phi\left(v_i^{(k)}\right)\right] \tag{4.10}$$

4.2.4 Generation of random fields

Unconditional random fields: Various random field generators exist, which fulfil the basic assumptions of homogeneity, stationarity, ergodicity and second order stationarity, [82]. Deutsch & Journel [97] categorize random field generators into three different categories: frequency domain simulation algorithms, random fractal simulation and marked point processes. Chiles & Delfiner [79] add here the Markov Chain algorithms. Deutsch & Journel [97] point out that frequency domain simulation algorithms are frequently used in mining, hydrogeology and petroleum applications. Examples of these algorithms are the Moving Average method (MA), Fast Fourier Transform (FFT), Turning band simulation (TB), Local Average Subdivision (LAS), Cholesky decomposition (LU) and Sequential Gaussian Simulation (SGSIM).

The Sequential Gaussian Simulation method (SGSIM) is the most straightforward algorithm for generating realizations of a multivariate Gaussian field in a sequential way according to [79, 97], which is explained in detail in appendix E.

Conditional random fields: All the above mentioned approaches simulate unconditional random fields, which are not taking data points into account from e.g. measurements, pre-knowledge, etc. Therefore, unconditional random fields are not spatially consistent in the presence of data points. By studying the explanation of the SGSIM in appendix E, one can derive the scheme of the *direct conditional simulation* within this sequential scheme. In figures E.4 and E.5 in appendix E an overview of the main characteristics of various random field simulators are shown.

In addition to this, there are also other approaches like the Kriging approach or simulated annealing, which can be used for conditioning random fields [79, 97].

Li & Der Kiureghian [219] state that many applications in civil engineering call for a combination of continuum mechanics and representation of uncertain media as random fields. Therefore, it is necessary to map a random field onto a grid of a Finite Element mesh. Several methods for *discretisation of random fields* have been proposed in the past amongst others by [219, 245, 364, 366] in the framework of stochastic Finite Elements (see section 4.3.3). These include the midpoint method (MP), the spatial averaging method (SA), weighted integral method, the shape function method (SF) and the series expansion method (SE), the Karhunen Loeve expansion (KL), the orthogonal series expansion and the expansion optimal linear exstimation method (EOLE).

The simplest method of discretisation of a random field within the domain Ω is the midpoint method. In this method, the field within the domain Ω_e of an element is described by a single random variable representing the value of the field at a central point of the element, e.g. the centroid $\mathbf{x}_c$, as shown in figure 4.6. The field value within the element is assumed to be a constant i.e.

$$\widehat{v}(\mathbf{x}) = v(\mathbf{x}_c) \quad ; \mathbf{x} \in \Omega_e \tag{4.11}$$

A realization of the field so defined is a stepwise function within discontinuities along the element boundaries.

The spatial averaging method proposed by Vanmarcke & Grigoriu [387] describes the field within each element in terms of the spatial average of the field over the element.

$$\widehat{v}(\mathbf{x}) = \frac{\int_{\Omega_e} v(\mathbf{x})\, d\Omega}{\int_{\Omega_e} d\Omega} = \widehat{v}_e \quad ; \mathbf{x} \in \Omega_e \tag{4.12}$$

The average values $\widehat{v}_e$ now form the vector $\mathbf{v}$. A realization of the field so defined is also a stepwise function with discontinuities along the element boundaries. Li & Kiureghian [219] state that the variance of the spatial average variable over an element is smaller than the local variance of the random field, in general. Moreover, this method can map a random field on structured as well as on non-structured finite element meshes.

The other above mentioned discretisation methods offer a continuous function of the discretized field, but ask for a more complicated mathematical background as explained in detail in literature [219, 245, 364, 366].

4.3 Computation of failure probabilities

Due to the vast amount of different methods available in this discipline existing probabilistic methods can be categorised in various ways from different point of views . A possible classification of probabilistic methods for uncertainty quantification is portrayed in figure 4.7, which includes the findings from different publications [57, 176, 191, 262]. Herein, it is differentiated between non-probabilistic and probabilistic methods. The *non-probabilistic approaches* include interval analysis [258, 298], fuzzy approaches [107,

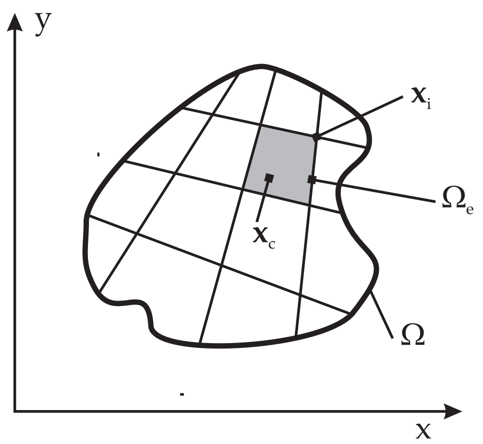

Figure 4.6: Random field discretisation after Li & Kiureghian [219].

278], grey number theory [296], imprecise probability method based on p-box representation [128, 415] and random set approaches [279, 290, 332], which are summarized briefly in [262]. The *probabilistic approaches* aim for a computation of the probability of failure, which is faster than the computationally time consuming Monte Carlo (MC) sampling approach. Here it should be realised that each alternative to the robust MC method implies some loss of accuracy. Therefore, the MC approach is used for verification and calibration of these approaches. The Bayesian approach in uncertainty quantification is described in various publications [23, 416] as well as the standard reliability methods (e.g. FOSM, FORM, SORM) in [57, 326] and iterative random point sampling methods in [57, 326, 327]. Prefixed point sampling methods like Taylor series, finite difference methods or the Point Estimate method can be found in recent publications [13, 374]. Fenton has worked in various publications [127] and different applications in geotechnical engineering on the simulation of spatial variability using random fields within the

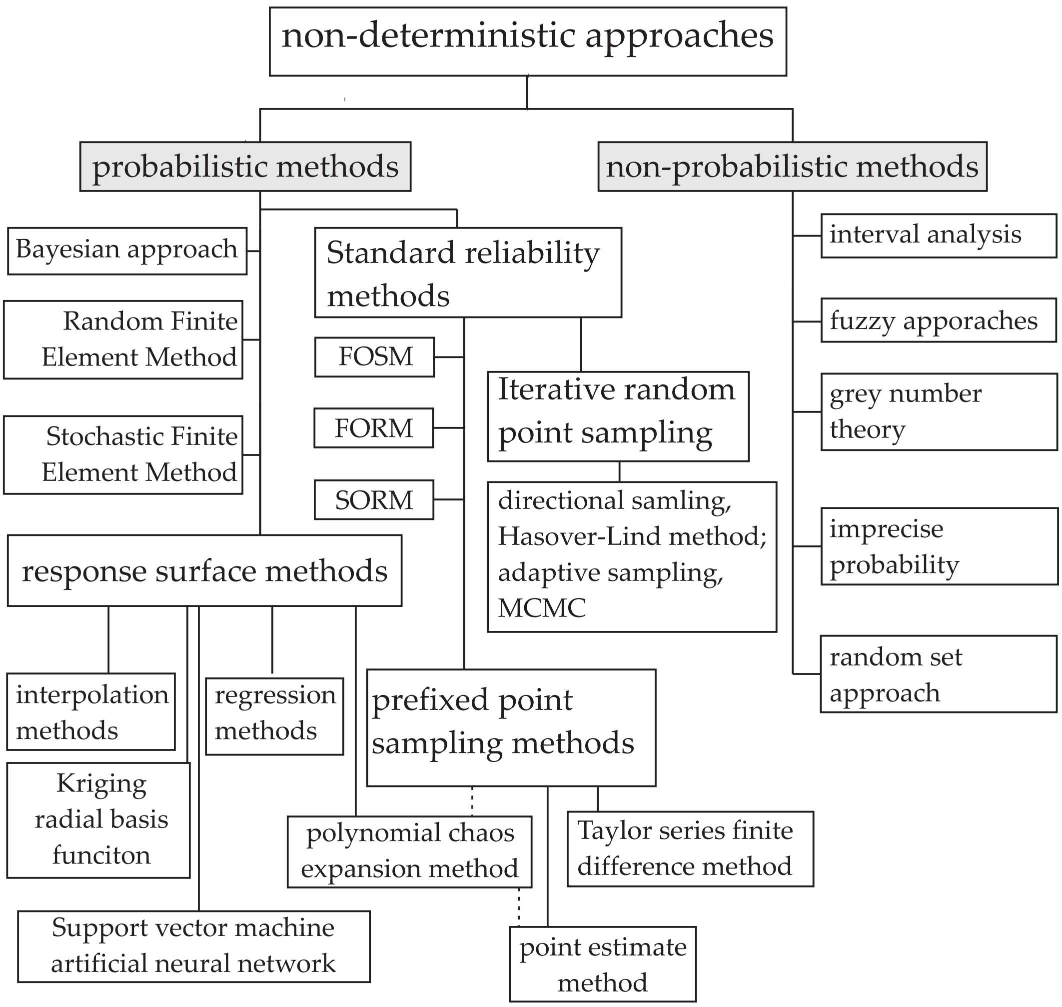

Figure 4.7: Non-deterministic approaches for uncertainty quantification modified from [57, 176, 191, 262].

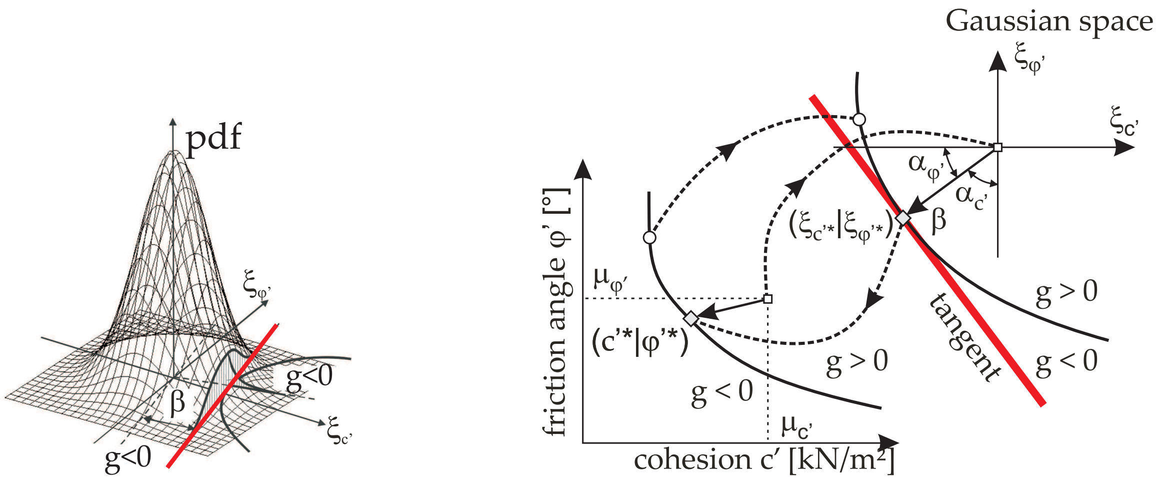

Figure 4.8: First order reliability method in Honjo [168] and Sudret [364].

the Random Finite Element Method.

Within this section, the principles of the First Order Reliability Method and Monte Carlo methods, together with the basics of the stochastic finite element method and the response surface method, are explained in order to help the reader to understand in depth the results of the next chapters.

4.3.1 First Order Reliability Method

The First Order Reliability Method (FORM) [152] is based on a description of the reliability problem in standard Gaussian space $\mathcal{N}(\mu = 0, \sigma = 1)$. In figure 4.8 the basics of FORM are visualized as presented in Huber et al. [177]. The two random variables $\mathbf{Z} = [c', \varphi']$ are transformed by the q-q transformation from the physical space into Gaussian variables $\xi_{c'}$ and $\xi_{\varphi'}$ with $\mathcal{N}(\mu = 0, \sigma = 1)$

$$Y_i = \Phi^{-1}[F_{Zi}(Z_i)]; i = 1 \cdots n \tag{4.13}$$

In the case of correlated variables $\mathbf{Y}$ the transformation from correlated Gaussian space to standard Gaussian space can be done by means of

$$\mathbf{\Xi} = \mathbf{L}^{-1}\,\mathbf{Y} \tag{4.14}$$

in which $\mathbf{L}$ is calculated from the Cholesky-decomposition of $\mathbf{C_{ZZ}}$.

$$\mathbf{C_{ZZ}} = \mathbf{L}\,\mathbf{L}^{\mathbf{T}} \tag{4.15}$$

Then a linearisation of the limit state function is performed in Gaussian space $(\xi_{c'}, \xi_{\varphi'})$. The expansion point $\boldsymbol{\xi}^*$ is chosen so as to maximize the pdf within the failure domain $\mathcal{D}_f$. Geometrically, this coincides with the point in the failure domain, having the minimum distance β from the origin. From a safety engineering point of view, the point $\boldsymbol{x}^* =$

$[c'^*, \varphi'^*]$ corresponding to $\boldsymbol{\xi}^* = [\xi_{c'^*}, \xi_{\varphi'^*}]$ is called the design point or most probable point (MPP).

From the geometrical interpretation of the expansion point $\boldsymbol{\xi}^*$ in standard Gaussian space it becomes quite clear that the calculation of the design point can be reduced to an optimization problem.

$$\boldsymbol{\xi}^* = \text{argmin}\left(\frac{1}{2}\boldsymbol{\xi}^T\boldsymbol{\xi}\right); \qquad \text{subjected to: } g\left[z(\boldsymbol{\xi})\right] = 0 \tag{4.16}$$

This leads to the Lagrange-function

$$L = \frac{1}{2}\boldsymbol{\xi}^T\boldsymbol{\xi} + \lambda\, g(\boldsymbol{\xi}) \;\rightarrow\; \text{Min.} \tag{4.17}$$

Standard optimization procedures can be utilized to solve for the location of $\boldsymbol{\xi}$ like e.g. Rackwitz-Fiessler algorithm, particle swarm algorithm amongst other methods described in e.g. [57].

The equation of this hyperplane may be cast as:

$$\beta - \boldsymbol{\alpha}\,\boldsymbol{\xi} = 0 \tag{4.18}$$

where the unit vector $\boldsymbol{\alpha} = \boldsymbol{\xi}/\beta$ is also normal to the limit state surface at the design point $\boldsymbol{\xi}^*$:

$$\boldsymbol{\alpha} = -\frac{\nabla g\left(\,T^{-1}\left(\boldsymbol{\xi}^*\right)\,\right)}{\|\nabla g\left(\,T^{-1}\left(\boldsymbol{\xi}^*\right)\,\right)\|} \tag{4.19}$$

Herein, T^{-1} is the q-q transformation from the Gaussian space into the physical space shown in figure 4.8. The vector $\boldsymbol{\alpha}$ describes the contributions of the random variables ξ_i to the probability of failure p_f.

A linear approximation of the failure surface at the design point will be accurate if the failure function is linear or weakly non-linear (relatively flat). For heavily non-linear failure functions, the FORM methods may not always be adequate to find a reasonably correct failure probability. In such cases, a better approximation of the failure surface at the design point is required. For this purpose, a second order (parabolic) failure surface is fitted to the non-linear failure function at the design point [53, 93, 131, 376] to give the Second Order Reliability Methods (SORM). It is a relatively complicated process and computationally more time consuming as well. A detailed description of this method can be found in Bucher [57] amongst others [53, 131, 191, 286, 366].

4.3.2 Monte Carlo simulation

The definition of the failure probability p_f as given in equation 4.8 can be written as an expected value, in which $I_g\left(x_1 \ldots x_n\right) = 1$ if $g(x_1 \ldots x_n) \leq 1$ and $I_g(\cdot)$ else.

$$p_f = \int_{-\infty}^{\infty}\int_{-\infty}^{\infty}\ldots\int_{-\infty}^{\infty} I_g\left(z_1 \ldots z_n\right)\; f_{z_1 \ldots z_n}\left(z_1 \ldots z_n\right)\; dz_1 \ldots dz_n \tag{4.20}$$

Monte Carlo Method: In order to determine p_f in principle all available statistical methods for estimation of expected values are applicable. If m independent samples $\mathbf{z}^{(k)}$ of the random vector $\mathbf{Z}$ are available then the estimator

$$\overline{p_f} = \frac{1}{m} \sum_{k=1}^{m} I_g \left(\mathbf{x}^{(k)} \right) \tag{4.21}$$

yields a consistent and unbiased estimate for p_f .

The problem associated with this approach is this: For small values of p_f and small values of m the confidence of the estimate is very low. The variance $\sigma^2_{\overline{p_f}}$ of the estimate $\overline{p_f}$ can be determined from

$$\sigma^2_{\overline{p_f}} = \frac{p_f}{m} - \frac{p_f^2}{m} \approx \frac{p_f}{m} \rightarrow \sigma_{\overline{p_f}} = \sqrt{\frac{p_f}{m}} \tag{4.22}$$

The required number m of simulations is independent of the dimension n of the problem.

Importance sampling: Bucher [57] states that in order to reduce the standard deviation $\sigma^2_{\overline{p_f}}$ of the estimator to the order of magnitude of the probability of failure itself m must be in the range of $m = 1/p_f$. For values of p_f in the range of 10^{-6} this cannot be achieved if each evaluation of the limit state function requires a complex analysis. Alternatively, strategies are employed, which increase the "hit-rate" by artificially producing more samples in the failure domain than should occur according to the distribution functions. One way to approach this solution is the introduction of a positive weighting function $h_{\mathbf{Y}}(\mathbf{z})$ which can be interpreted as a density function of a random vector $\mathbf{Y}$. Samples are taken according to $h_{\mathbf{Y}}(\mathbf{z})$. The probability of failure is then estimated from

$$\overline{p_f} = \frac{1}{m} \sum_{k=1}^{m} \frac{f_{\mathbf{Y}}(\mathbf{z})}{h_{\mathbf{Y}}(\mathbf{z})} I_g(\mathbf{z}) = \mathrm{E} \left[\frac{f_{\mathbf{Y}}(\mathbf{x})}{h_{\mathbf{Y}}(\mathbf{z})} I_g(\mathbf{z}) \right] \tag{4.23}$$

From the estimation procedure it can be seen that the variance of the estimator $\overline{p_f}$ becomes

$$\sigma^2_{\overline{p_f}} = \frac{1}{m} \mathrm{E} \left[\frac{f_{\mathbf{Y}}(\mathbf{x})^2}{h_{\mathbf{Y}}(\mathbf{x})^2} I_g(\mathbf{x}) \right] \tag{4.24}$$

A useful choice of $h_{\mathbf{Y}}$ should be based on minimizing $\sigma^2_{\overline{p_f}}$. Ideally, the weighting function should reduce the sampling error to zero. However, this cannot be achieved in reality since such a function must have the property

$$h_{\mathbf{Y}}(\mathbf{z}) = \begin{cases} \frac{1}{p_f} f_{\mathbf{Z}}(\mathbf{z}) & \text{for } g(\mathbf{z}) \leq 0, \\ 0 & \text{for } g(\mathbf{z}) > 0 \end{cases} \tag{4.25}$$

This property requires the knowledge of p_f, which - of course - is unknown. Special updating procedures such as adaptive sampling [57] can help to alleviate this problem.

Bucher [57] recommends to use the importance sampling concept in conjunction with the FORM approach. Based on the previous FORM analysis, it may be attempted to obtain a general importance sampling concept. The efficiency of this concept depends on the geometrical shape of the limit state function. In particular, limit state functions with high curvatures or almost circular shapes cannot be covered very well.

Apart form importance sampling there are several other techniques like line sampling, directional sampling, adaptive sampling, asymptotic sampling, line sampling or subset simulation, which are explained in detail in several sources [57, 326, 364].

4.3.3 Stochastic Finite Element Method

The Stochastic Finite Element Method (SFEM) was introduced by Ghanem & Spanos [138] and is an extension of the classical deterministic approach of the solution of stochastic (static and dynamic) problems [326, 358].

Basically spoken, SFEM involves finite elements whose properties and boundary conditions are random. From a mathematical point of view, SFEM is a powerful tool for the solution of stochastic partial differential equations (SPDEs) and it has been treated as such in numerous publications e.g. [57, 138, 286, 326, 358, 364, 366]. It has been successfully applied to a wide variety of problems (e.g. solid, structural and fluid mechanics, heat transfer, geotechnical engineering) as described in Stefanou [358], in which the stochastic medium is represented by random fields if appropriate. The result of the SFEM is a so called polynomial chaos expansion, which represents the stochastic system in a simplified way; in other disciplines this can be related with synonyms like surrogate, meta-models or response surfaces.

Intrusive SFEM: Within SFEM, different authors [286, 364, 366] distinguish between the so called intrusive and the non-intrusive approach.

Within the intrusive SFEM, named after the pioneering work of Ghanem & Spanos [138], the aim is to represent the complete response PDF in an intrinsic way. The implementation of the intrusive SFEM has to be carried out for each class of problem. Herein, the stiffness matrix as well as the boundary conditions consist of a mean (deterministic) part and of stochastic parts, which can be solved by using various methods such as the "weighted integral method", the "Neumann series expansion" method or the "Taylor series expansion" method, as described in detail in [245, 286, 366]. The response of the system (which, after proper discretisation of the problem, is a random vector of unknown joint probability density function) is expanded onto a particular basis of the space of random vectors of finite variance called "polynomial chaos".

There are two main variants of SFEM in the literature: i) the perturbation approach, which is based on a Taylor series expansion of the response vector [203] and ii) the spectral stochastic finite element method (SSFEM) [138], where each response quantity is represented using a series of random Hermite polynomials. A detailed description can be found in [336, 358, 366]. Amongst others, Sett & Jeremic [336] also applied the SSFEM framework to highly non-linear and dynamical geomechanical problems.

Sudret & Der Kiureghian [367] state as an overall conclusion that SSFEM has limited applicability to reliability problems involving small failure probabilities. The polynomial chaos expansion provides a global fit to each response quantity, which may be good in the central region of the respective distribution, but poor in the tail regions. Since small probability events are influenced by the tail regions of these probability distributions, accurate results from SSFEM cannot be expected for such problems. This limitation is more severe for problems involving random fields with short correlation lengths or large coefficients of variation.

Non-intrusive SFEM: In order to apply this approach in a similar way to a wider range of mechanical problems, the so called non-intrusive SFEM has been developed [286, 364].

Within the non-intrusive SFEM, the scalar response quantities $\mathbf{S}$ of the system e.g. nodal displacements, strain or stress components are directly expanded onto the polynomial chaos, which is truncated after the P term.

$$\mathbf{S} = h(\mathbf{X}) = \sum_{j=0}^{\infty} \mathbf{S}_j \Psi_j = \sum_{j=0}^{P-1} \mathbf{S}_j \Psi_j \tag{4.26}$$

The big advantage of this approach is the fact that - basically - it is just the post-processing of simulation results. Therefore, any FEM-code can be used to calculate the system response in contrast to the intrusive SFEM [286, 364].

Sudret [364] proposes two methods to compute the coefficients in this expansion from a series of deterministic finite element analyses, namely the projection method and the regression method.

The PROJECTION METHOD is based on the orthogonality of the polynomial chaos [3, 286]. By premulitplying equation 4.26 with Ψ_i and taking the expectation of both members, it becomes:

$$\mathrm{E}\left[\mathrm{S}\ \Psi\right] \approx \mathrm{E}\left[\sum_{j=0}^{\infty} \mathrm{S}_j \Psi_i \Psi_j\right] \tag{4.27}$$

Due to the orthogonality of the basis $E\left[\Psi_i \Psi_j\right]$ for any $i \neq j$, one can reformulate the following equation:

$$\mathbf{S} = \frac{\mathrm{E}\left[\mathbf{S}\ \Psi_j\right]}{\mathrm{E}\left[\Psi_j^2\right]} \tag{4.28}$$

In equation 4.28 the denominator is known analytically, as derived in Appendix D, and the numerator may be cast as a multi-dimensional integral:

$$\mathrm{E}\left[\mathbf{S}\Psi_j\right] = \int_{\mathbb{R}^M} h(\ \mathbf{X}(\boldsymbol{\xi})\ )\ \Psi_j(\boldsymbol{\xi})\ \varphi_m(\boldsymbol{\xi})\ \mathrm{d}\boldsymbol{\xi} \tag{4.29}$$

where φ_m is the M-dimensional mulit-normal PDF, and where the dependency of S in $\boldsymbol{\xi}$ through the iso-probabilistic transform of the input parameters $\mathbf{X}(\boldsymbol{\xi})$ has been given for the sake of clarity. This integral can be computed by crude Monte Carlo simulation [57, 286]. However, the number of samples required in this case should be large enough to obtain a sufficient accuracy. Sudret [364] states that in the case of using a computationally demanding model for the evaluation of the system response, this approach is practically not applicable. Alternatively, the Gaussian quadrature scheme can be used to evaluate the integral [43, 244] as a weighted summation of the integrand evaluated at selected points (the so-called integration points).

The Smolyak sparse grids are also quoted in literature [3, 286] as a promising approach for computing the integral of equation 4.29.

The REGRESSION METHOD is another approach for computing the response expansion coefficients. It is the regression of the exact solution S with respect to the polynomial chaos basis $\Psi_i(\boldsymbol{\xi})$. The scalar response quantity S consists of a residual ϵ (a zero mean random variable) and unknown coefficients $\widetilde{\mathrm{S}}$.

$$\mathbf{S} = h(\mathbf{X}) = \sum_{j=0}^{p-1} \mathbf{S}_j \Psi_j + \epsilon \tag{4.30}$$

The minimization of the variance of the residual with respect to the unknown coefficients leads to equation 4.31 by using a set of Q regression points in the standard normal space $\xi^{\mathbf{i}}$ and their isoprobabilistic transform $\mathbf{x}^i$

$$\widetilde{\mathrm{S}} = \mathrm{Argmin} \frac{1}{Q} \sum_{i=1}^{Q} \left\{ h(\mathbf{x}^i) - \sum_{j=0}^{p-1} \mathbf{S}_j \Psi_j(\xi^{\mathbf{i}}) \right\}^2 \tag{4.31}$$

Sudret [364] solves this minimization problem in the following way: Denoting by $\boldsymbol{\Psi}$ the matrix whose coefficients are given by $\Psi_{ij} = \Psi_j(\xi^{\mathbf{i}}), i = 1, \ldots, Q; j = 0, \ldots, p-1$ and by $\mathbf{S_{ex}}$ the vector containing the exact response valuse computed by the model $\mathbf{S_{ex}} = h(\mathbf{x^i}), i = 1, \ldots, Q$, the solution to equation 4.31 reads:

$$\mathbf{S} = \left(\boldsymbol{\Psi}^T\ \boldsymbol{\Psi}\right)^{-1}\ \boldsymbol{\Psi}^T\ \mathbf{S_{ex}} \tag{4.32}$$

This approach is comparable to the so called response surface method used in many domains of natural sciences and engineering. Within this context, the set of $\mathbf{x}^1, \ldots, \mathbf{x}^Q$ is the so called experimental design. In equation 4.32, $\boldsymbol{\Psi}^T \cdot \boldsymbol{\Psi}$ is the information matrix. Sudret [364] shows that an efficient design can be built from the roots of the Hermite polynomials as follows:

- If p denotes the maximal degree of the polynomials in the truncated PC expansion, then the $p+1$ roots of the Hermite polynomial of degree $p+1$ (denoted by He_{p+1}) are computed, say $r_1, ..., r_{p+1}$.
- From this set, M-tuplets are built using all possible combinations of the roots: $r^k = (r_{i1}, \ldots, r_{iM}), 1 \leq i_1 \leq \ldots \leq i_M \leq p+1, k = 1, \ldots, (p+1)^M$.
- The Q points in the experimental design $\boldsymbol{\xi}_1, \ldots, \boldsymbol{\xi}_Q$ are selected among the $\mathbf{r}^j$ by retaining those which are closest to the origin of the space, i.e. those with the smallest norm, or equivalently those leading to the largest values of the PDF $\varphi_M(\boldsymbol{\xi}^j)$.

To choose the size of Q of the experimental design, the following empirical rule was proposed by Berveiller et al. [44] based on a large number of numerical experiments.

$$Q = (M-1)\ P \tag{4.33}$$

Herein, P is the number of unknown coefficients defined by the following equation combining the PCE order M and the degree of the Hermite polynomial p.

$$P = \begin{pmatrix} M+p \\ p \end{pmatrix} = \frac{(M+p)!}{M!\,p!} \tag{4.34}$$

Representation of the response PDF: Once the coefficients S of the PC expansion of a response quantity are computed, the polynomial approximation can be simulated using Monte Carlo simulation as shown in [286]. A sample of standard normal random vectors $\boldsymbol{\xi}^{(1)}.\ldots,\boldsymbol{\xi}^{(n)}$ is generated.

Then the PDF can be plotted using a histogram representation [286, 366]. From equation 4.26 the mean and the variance σ_S^2, the skewness δ_S and kurtosis κ_S of the approximated response S are given by:

$$\mathrm{E}[S] = S_0 \tag{4.35}$$

$$\sigma_\mathrm{S}^2 \equiv \mathrm{Var}[S] = \sum_{j=1}^{P-1} S_j^2\ \mathrm{E}\left[\Psi_j^2\right] \tag{4.36}$$

$$\delta_S \equiv \frac{1}{\sigma_S^3}\mathrm{E}\left[(S-\mathrm{E}[S])^3\right] = \frac{1}{\sigma_S^3}\sum_{i=1}^{P-1}\sum_{j=1}^{P-1}\sum_{k=1}^{P-1}\mathrm{E}[\Psi_i\ \Psi_j\ \Psi_k]\ S_i\ S_j\ S_k \tag{4.37}$$

$$\kappa_S \equiv \frac{1}{\sigma_S^4}\mathrm{E}\left[(S-\mathrm{E}[S])^4\right] = \frac{1}{\sigma_S^3 4}\sum_{i=1}^{P-1}\sum_{j=1}^{P-1}\sum_{k=1}^{P-1}\sum_{l=1}^{P-1}\mathrm{E}[\Psi_i\ \Psi_j\ \Psi_k\ \Psi_l]\ S_i\ S_j\ S_k\ S_l \tag{4.38}$$

where the expectation of Ψ_j^2 is given in Appendix D. Various authors [286, 364, 366] describe that the moments of higher order are obtained in a similar manner.

Reliability analysis of the SFEM results: This metamodel can be used to construct the response PDF of the system as well as to compute the reliability of the observed system, which is approximated by a polynomial chaos expansion. Surprisingly, this link between structural reliability and the non-intrusive SFEM based on PC expansions is relatively new [43, 364, 366]. The PC expansion can be used as a meta-model within the framework of non deterministic approaches for uncertainty quantification, which offers the engineer a first insight into the reliability of a system. One has to keep in mind that the non-intrusive SFEM also has limited accuracy in evaluating small probabilities of failure due to the approximation via PC expansions.

Assessment of the polynomial chaos approximation: It has been shown in the previous section that polynomial chaos (PC) approximations of the mathematical model can be obtained using non-intrusive techniques, namely the projection approach or the regression approach. Both methods provide a stochastic response surface whose performance has to be assessed [47, 365]. Blatman & Sudret [47] point out that, in terms of statistical learning theory (see e.g. [388]), the discrepancy between the model response and the metamodel is measured by means of a risk functional, for instance the commonly used mean-square error. Such a quantity depends on the PDF of the response, which is unknown in our context.

The *generalized error* is defined in equation 4.39:

$$I\left[\mathcal{M}_{\widehat{\mathbf{X}},p}\right] = \mathrm{E}\left[(\mathcal{M}(\mathbf{x}) - \mathcal{M}_{\widehat{x},p})^2\right] = \int \left(\mathcal{M}(\mathbf{x}) - \mathcal{M}_{\widehat{X},p}\right)^2 f_{\mathbf{x}}(\mathbf{x})\, d\mathbf{x} \tag{4.39}$$

$\widehat{\mathbf{X}} = \left\{\mathbf{x}^{(1)}, \ldots, \mathbf{x}^{(N)}\right\}^T$ is the experimental design, the corresponding model evaluations are $\widehat{\mathbf{Y}} = \left\{y^{(1)} = \mathcal{M}\left(\mathbf{x}^{(1)}\right), \ldots, y^{(N)} = \mathcal{M}\left(\mathbf{x}^{(N)}\right)\right\}^T$ and $\mathcal{M}_{\widehat{X},p}$ are the resulting PC approximations. The notion of generalization error is a basic concept of statistical learning theory as presented in [388]. Computing $I[\mathcal{M}_{\widehat{X},p}]$ requires a perfect knowledge of the model function $\mathcal{M}$, which is not the case in the context of geotechnical engineering in general since the model is usually not analytical but numerical.

In literature [47, 388] it is proposed to compute the following *empirical error* or *training error* in order to estimate equation 4.39.

$$I_X\left[\mathcal{M}_{\widehat{X},p}\right] = \frac{1}{N}\sum_{i=1}^{N}\left(\mathcal{M}(\mathbf{x}^{(i)}) - \mathcal{M}_{\widehat{X},p}(\mathbf{x}^{(i)})\right)^2 \tag{4.40}$$

Of common use is the related *determination coefficient* R^2 which reads

$$R^2\left[\mathcal{M}_{\widehat{X},p}\right] = 1 - \frac{I_X\left[\mathcal{M}_{\widehat{X},p}\right]}{\widehat{Var}[Y]} \tag{4.41}$$

where

$$\widehat{Var}[Y] = \frac{1}{N-1}\sum_{i=1}^{N}\left(\mathcal{M}(\mathbf{x}^{(i)}) - \frac{1}{N}\sum_{i=1}^{N} y^{(i)}\right)^2$$

However, the use of R^2 statistics might be misleading for comparing two different regression base meta models since it automatically increases with the number of P basis polynomials; furthermore, it is highly biased since it tends to $R^2 = 1$ as P increases. Blatman & Sudret [47] report that R^2 generally underestimates the generalization error. Therefore, the *adjusted determination coefficient* R^2_{adj} is recommended.

$$R^2_{adj}\left[\mathcal{M}_{\widehat{X},p}\right] = 1 - \frac{N-1}{N-P-1}\left(1 - R^2\left[\mathcal{M}_{\widehat{X},p}\right]\right) \tag{4.42}$$

The R^2_{adj} statistic is penalized as P increases. Baltman & Sudret [47] report that R^2_{adj} still often overpredicts the true approximation accuracy.

The cross-validation technique consists of dividing the data sample into two subsamples. A metamodel is built from one subsample, i.e.the training set, and its performance is assessed by comparing its predictions to the other subset, i.e.the test set. Let $M_{X\setminus i}$ be the metamodel that has been built from the experimental design $X\setminus\left\{\mathbf{x}^{(i)}\right\}$, e.g when removing the i^{th} observation from the training set X. The predicted residual is defined as the difference between the model evaluation at $\mathbf{x}^{(i)}$ and its prediction based on $M_{X\backslash i}$

$$\Delta^{(i)} = \mathcal{M}\left(\mathbf{x}^{(i)}\right) - \mathcal{M}_{X\backslash i}\left(\mathbf{x}^{(i)}\right) \tag{4.43}$$

The generalization error is then estimated by the *mean predicted residual sum of squares (PRESS)*, i.e. the following empirical mean square predicted residual, [47].

$$I_X^*\left[\mathcal{M}_{\widehat{X},p}\right] = \frac{1}{N}\sum_{i=1}^{N}\left(\Delta^{(i)}\right)^2 \tag{4.44}$$

The corresponding *determination coefficient* with analogy to its empirical counterpart R^2 is denoted by Q^2, [47]:

$$Q^2\left[\mathcal{M}_{\widehat{X},p}\right] = 1 - \frac{I_X^*\left[\mathcal{M}_{\widehat{X},p}\right]}{\frac{1}{N-1}\sum_{=1} N\left(\mathcal{M}(\mathbf{x}^{(i)}) - \frac{1}{N}\sum_{i=1}^{N} y^{(i)}\right)^2} \tag{4.45}$$

Blatman & Sudret [47] derive I_X^* in equation 4.46 where h_i is the ith diagonal term of the matrix $\mathbf{\Psi}\left(\mathbf{\Psi}^T\mathbf{\Psi}\right)^{-1}\mathbf{\Psi}^T$:

$$I_x^*\left[\mathcal{M}_{\widehat{X},p}\right] = \frac{1}{N}\sum_{i=1}^{N}\left(\frac{\mathcal{M}\left(\mathbf{x}^{(i)}\right) - \mathcal{M}_{\widehat{x},p}\left(\mathbf{x}^{(i)}\right)}{1-h_i}\right)^2 \tag{4.46}$$

The above presented metrics for assessing the accuracy of the PC approximation are also quoted amongst other means by Field & Grigoriu [130].

4.3.4 Response surface methods

According to Bucher [57], response surface models are more or less simple mathematical models, which are designed to describe the possible experimental outcome (e.g., the structural response in terms of displacements, stresses, etc.) of a more or less complex structural system as a function of variable factors (e.g., loads or system conditions). Obviously, the chosen response surface model should give the best possible fit to any collected data. In general, we can distinguish two different types of response surface models:

- regression models (e.g. polynomials of varying degree or non-linear functions such as exponentials or Hermite polynomials) [57, 286],
- interpolation models (e.g. polyhedra, radial basis functions) [57],
- artificial neural networks, support vector machines [57, 58] and
- Kriging and radial basis functions [57, 339].

In most applications it is quite likely that the exact response function will not be known. Therefore, it has to be replaced by a sufficiently versatile function, which will express the relation between the response and the input variables satisfactorily.

Depending on the selected response surface model, support points have to be chosen to estimate the unknown parameters of the response surface in a sufficient way. A set of samples of the basic variables is generated for this purpose. In general, this is done by applying predefined schemes, so called DESIGN OF EXPERIMENTS. Bucher [57] recommends that it is most helpful to setup an experimental scheme in a dimensionless space. Within this, Bucher [57] describes saturated designs, which provide a number of support points that just suffice to represent a certain class of response functions exactly, and redundant designs, which provide more support points than required to define the response surface.

4.4 Sensitivity analysis

In chapter 5 and 6 the sensitivities analyses are used to quantify the relative importance of relative importance of each input parameter of system, as described in [286, 317, 364]. Methods of sensitivity analysis are usually classified into two categories:

- LOCAL SENSITIVITY ANALYSIS investigates the local impact of input parameters on the model. Sudret [364] points out that local SA is based on the computation of the gradient of the response with respect to its parameters around a nominal value.
- GLOBAL SENSITIVITY ANALYSIS aims for the quantification of the output uncertainty due to the uncertainty in the input parameters, which are taken singly or in combination with others, [364].

Saltelli et al. [317] group the different techniques in SA into regression-based methods and variance-based methods. Within the regression-based methods, the standardized regression coefficients, Pearson correlation coefficients, partial correlation coefficients, and standardized partial rank correlation coefficients are used to describe the correlation between inut and output. Sudret [364] points out that in the case of general non linear non monotonic models, these approaches fail to produce satisfactory sensitivity measures.

The variance-based methods aim at decomposing the variance of the output as a sum of the contributions of each input variables or combinations thereof. They are sometimes called ANOVA techniques for "ANalysis Of VAriance", [364]. The correlation ratios in McKay [249], the Fourier amplitude sensitivity test indices [319] and the Sobol indices [318, 347] enter this category.

For the sake of completeness, an extensive overview on additional methods of local and global sensitivity approaches can be found in Cacuci et al. [63] including screening methods, non-parametric methods, variance based methods and density based methods.

4.4.1 Local sensitivity

As shown in section 4.3.1, FORM leads to the computation of a linearised limit state function whose equation may be cast as:

$$g_{\text{FORM}}(\boldsymbol{\xi}) = \beta - \boldsymbol{\alpha} \cdot \boldsymbol{\xi} \tag{4.47}$$

Herein, β is the reliability index and $\boldsymbol{\alpha}$ is the unit vector to the design point. Sudret [364] considers this linearised limit state function to be a margin function, which quantifies the distance between a realization of the transformed input random vector and the failure surface. Its variance straightforwardly reads:

$$\text{Var}\left[g_{\text{FORM}}(\boldsymbol{\xi})\right] = \sum_{i=1}^{M} \alpha_i^2 = 1 \tag{4.48}$$

Thus, the coefficients $\{\alpha_i^2, i = 1 \ldots, M\}$, which are also called *FORM importance factors* by Ditlevsen & Madsen [105], correspond to the portion of the variance of the linearised margin, which is due to each ξ_i. When the input random variables $\mathbf{X}$ are independent, there is a one-to-one mapping between X_i and ξ_i , $i = 1 \cdots M$. Thus, α_i^2 is interpreted as the importance of the i-th input parameter in the failure event, [364]. When the input random variables are correlated, other measures of importance should be used as explained in Haukaas & der Kiureghian [153].

4.4.2 Global sensitivity

The computation of Sobol' indices is traditionally carried out by Monte Carlo simulation as reported by [317, 318], which may be computationally unaffordable in the case of time consuming models. In the context of non-intrusive SFEM, Sudret [364, 365] has shown that Sobol' indices can be derived analytically from the coefficients of the polynomial chaos expansion of the response S, once the lattes have been compute by the projection or regression approach. For instance, the first order Sobol' indices, which quantify what fraction of the response variance is due to each input variable :

$$\delta_i = \frac{\mathrm{Var}_{X_i}\left[\, \mathrm{E}\left[S|X_i\right]\,\right]}{\mathrm{Var}\left[S\right]} \tag{4.49}$$

can be evaluated form the coefficients of the PC expansions in equation 4.26 as follows:

$$\delta_i^{PC} = \sum_{\alpha \in I_i} S_\alpha^2 \, \mathrm{E}\left[\boldsymbol{\Psi}_\alpha\right] / \sigma_S^2 \tag{4.50}$$

Herein, σ_S^2 is the variance of the model response computed form the PC coefficients in equation 4.36 and the summation set

$$I_i = \{\alpha \ : \ \alpha_i > 0 \ , \ \alpha_{j \neq i} = 0\} \tag{4.51}$$

Higher order Sobol' indices, which correspond to interactions of the input parameters, can also be computed using this approach as described in Sudret [365] in detail.

By virtue of the knowledge of SA, engineers can rank the input variables by the amount of their contributions to the output, and thus take measures accordingly to improve the performance of the model, which is a core task in engineering.

4.5 Synopsis

This chapter summarises the concepts of safety and uncertainty. Besides this, the basics of uncertainty quantification are explained in detail: The mechanical system is represented via a limit state function and its variables are represented via random variables and/or random fields. Different methods to compute the failure probability of the mechanical system are discussed and followed up by the description of sensitivity analyses. Global and local sensitivity analyses quantify the importance of each input parameter within the scheme of uncertainty quantification.

Chapter 5

Selected case studies in uncertainty quantification using random properties

5.1 Introduction

Possibilities and limitations of probabilistic methods in civil engineering have been studied by Elishakoff [116]. Within a survey Elishakoff asked engineers and scientists on the applicability of probabilistic methods in their fields all over the world. He concluded that the engineering community can be divided into enthusiastic supporters of probabilistic approaches in engineering and sceptic opponents. The criticism of the opponents is mainly based on the complex mathematical and conceptual theory, which is necessary to apply probabilistic design in engineering .

On top of this, it is stated in various other publications [23, 168, 286] that the broader geotechnical engineering community is unfamiliar with reliability methods, particularly pertaining to computational details, practical usefulness, pitfalls, and probabilistic characterization of input parameters. In addition to this, the British Health and Safety Executive authority published the results of a survey on the application of reliability methods for offshore engineering in a technical report [410]. Many of the respondents thought that probabilistic techniques would be a welcome addition to their methods of analysis, but that the approach was yet to be widely applied. Besides this, it is pointed out that industry has concerns with the relatively small numbers of qualified and experienced companies and individuals who can carry out designs and, more importantly, audit and verify these designs.

Therefore, it is necessary to set up case studies to broaden and disseminate reliability applications beyond the researcher and enlighten the background of probabilistic design approaches as proposed by Phoon [286] amongst others. The key objectives of such case studies are education by examples, demonstration of usefulness of reliability based design in practical applications, development of user-friendly tools and evaluation of reliability methods as proposed by the Geotechnical Safety Network (GeoSNet) [360].

Within this chapter, typical geotechnical case studies dealing with tunnelling and footing analysis are investigated within the framework of uncertainty quantification. Starting from semi-analytical limit state equations (LSE), the reader is introduced to more complex LSE, which are derived from two and three dimensional FEM models.

5.2 Tunnel lining

According to prognoses of the European Commission, the growth in traffic between Member States is expected to double by 2020. To meet the challenges connected with the increased requirements for efficient traffic infrastructure the use of underground space often constitutes an efficient and environmentally friendly solution. But there can be also one essential disadvantage in building tunnels because, especially in an urban environment, large settlements due to tunnelling can cause tremendous consequences as reported in [174, 178]. In the last couple of years years innovative tender methods ask for the consideration of uncertainties in order to contribute usefully to risk management in tunnelling.

The use of global safety factors offers one way to face this problem of dealing with uncertainties, which is refined by partial safety factors later on. However, both approaches miss a mathematical framework, which precisely allocates safety margins to stress and resistance shares of the mechanical system.

This case study introduces the framework of uncertainty quantification by using analytical formulas of a typical two dimensional problem. This includes a description of the mechanical problem and of the stochastic variables, as well as a sensitivity study followed up by an interpretation of the results.

5.2.1 Mechanical description of the problem

A key point in tunnel design is the design of the lining as reported in well known and recent publications [108, 173, 177]. Möller [253] points out that the different phases of the tunnel construction, namely excavation and support phases, have to be taken into account to simulate the internal forces in the lining accurately. The earlier and simplified way of Ahrens et al. [5] and Erdmann [120] is used to estimate the internal forces in the tunnel lining. These analytical solutions of a two dimensional problem offer an insight into the complex interaction between the soil and tunnel. Moreover, these equations have been used to validate complex three dimensional numerical approaches by other authors e.g. [253, 278, 332–334, 374].

Figure 5.1 presents an analytical continuum model, which was solved by Ahrens et al. [5] and later adapted by Erdmann [120]. This analytical solution is based on the following simplifications and assumptions: The tunnel lining is circular with radius R. The tunnel longitudinal axis is parallel to the ground surface, inducing plane strain conditions. The thickness of the lining d is constant. The lining is deforming without any side contraction, i.e. Poisson's ratio $\nu_{concrete}$ is equal to zero. It is assumed that there is a uniform initial stress field, with $\sigma_h = K_0 \cdot \sigma_v$, where K_0 is the coefficient of lateral earth pressure and $\sigma_v = \gamma_{soil} \cdot H$. Here γ_{soil} is the soil unit weight and H is the tunnel depth as indicated in Figure 5.1.

The lining is installed before tunnel excavation and is assumed to be rough with full bonding. Both the lining and ground behave linear-elastically. Within this approach, second order theory is neglected. Erdmann [120] supplemented the findings of Ahrens et al. [5] to obtain equations (5.1) - (5.2) for a lining with full bonding, where ν is the Pois-

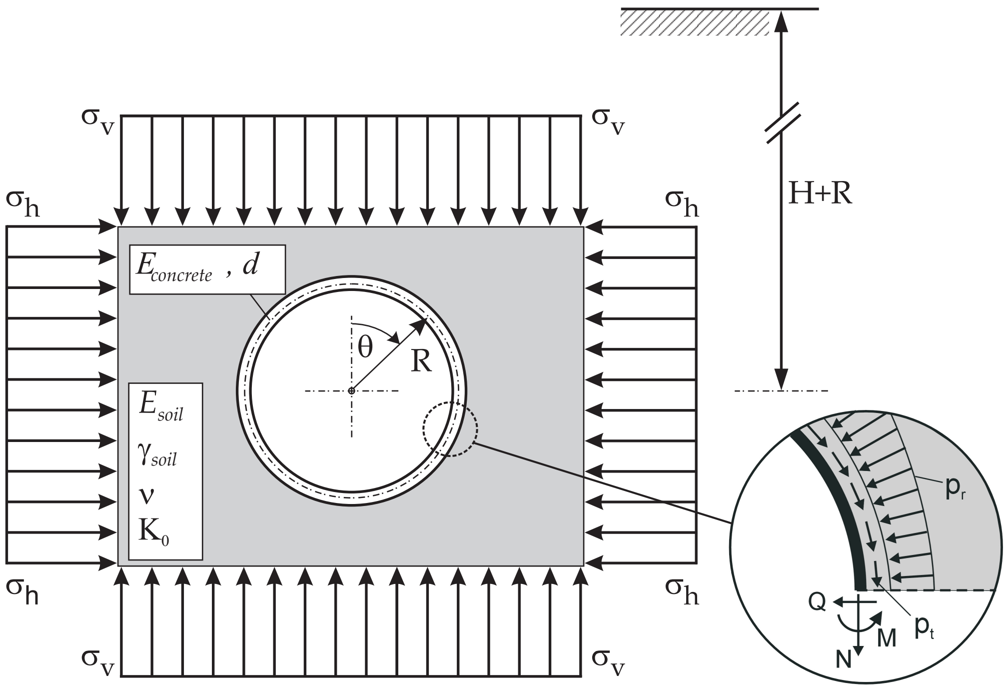

Figure 5.1: System of tunnel lining from Erdmann [120].

son's ratio of the soil, and $E_{concrete}F$ is the normal stiffness and $E_{concrete}I$ is the flexural rigidity of the lining respectively. E_{soil} is the elasticity modulus of the soil.

$$N = \gamma_{soil}\, H\, \frac{1+K_0}{2}\, R/\left(1+\frac{\beta}{1+\nu}+\frac{\beta}{\alpha}\right) + \gamma_{soil}\, H\, \frac{1-K_0}{2}\, R\, n_2 \cos(2\theta) \tag{5.1}$$

$$M = \gamma_{soil}\, H\, \frac{1-K_0}{2}\, R^2\, m_2 \cos(2\theta) \tag{5.2}$$

$$\alpha = \frac{E_{soil}R^3}{E_{concrete}I} \qquad \beta = \frac{E_{soil}R}{E_{concrete}F} \tag{5.3}$$

$$n_2 = \frac{1+\frac{\alpha}{12(1+\nu)}+\frac{\beta}{4(1+\nu)}}{1+\frac{\alpha(3-2\nu)}{12(3-4\nu)(1+\nu)}+\frac{\beta(5-6\nu)}{4(3-4\nu)(1+\nu)}+\frac{\alpha\beta}{12(3-4\nu)(1+\nu)^2}} \tag{5.4}$$

$$m_2 = \frac{1+\frac{\beta}{2(1+\nu)}}{2+\frac{\alpha(3-2\nu)}{6(3-4\nu)(1+\nu)}+\frac{\beta(5-6\nu)}{2(3-4\nu)(1+\nu)}+\frac{\alpha\beta}{6(3-4\nu)(1+\nu)^2}} \tag{5.5}$$

The system can be described with the limit state equation 5.6. This limit state equation combines the approaches of Erdmann [120] and Sudret [364]. Sudret [364] considers the interaction of the internal moment and normal force (see figure 5.1) via equation (5.6). Herein, ultimate internal forces are N_{ult} and M_{ult}, which are dependent on the compressive strength of the concrete $f_{concrete}$, as described by Sudret [364].

$$g(N, M) = \frac{(d \cdot N_{ult})^2 + M_{ult}^2}{(d \cdot N(\theta))^2 + M(\theta)^2} - 1 \tag{5.6}$$

Table 5.1: Properties of parametric studies on the tunnel lining.

	parametric study 1		parametric study 2	
property	COV	distribution	COV	distribution
$\nu = 0.30$	$15 - 40\%$	lognormal	$15 - 40\%$	lognormal
$K_0 = 2.5$	$1 - 10\%$	lognormal	$1 - 10\%$	lognormal
$\gamma_{soil} = 21$ kN/m^3	$15 - 45\%$	lognormal	$15 - 45\%$	lognormal
$E_{soil} = 27$ MN/m^2	$15 - 45\%$	lognormal	$15 - 45\%$	lognormal
$H = 30$ m	-	deterministic	5%	lognormal
$R = 5$ m	-	deterministic	1%	lognormal
$d = 0.35$ m	-	deterministic	1%	lognormal
$E_{concrete} = 1,500$ MN/m^2	-	deterministic	10%	lognormal
$f_{concrete} = 45$ MN/m^2	-	deterministic	6%	lognormal

5.2.2 Stochastic variables and parametric studies

On the basis of a literature study [23, 282, 283, 286], the stochastic variables are listed in table 5.1 for the following case studies.

Parametric study 1: At first, the influence of soil variability is investigated in parametric study 1. Therefore, the soil stiffness E_{soil}, Poisson's ratio ν, the soil unit weight γ_{soil} and the K_0 value are treated as random variables (table 5.1).

A combination of two reliability techniques is used for the uncertainty quantification of this system. The evaluation of the reliability index β and of the probability of failure p_f is done by the combination of First-Order-Reliability Method (FORM) and Importance sampling (IS). After the calculation of the design point using FORM, the IS algorithm is employed to investigate the probability of failure more accurately.

The expected influence of soil variability can be clearly seen in figure 5.2: A higher degree of soil variability leads to a lower degree of reliability of the system. In figure 5.2 (a), the reliability index β decreases with an increasing level of variability of the random variables and vice versa for the probability of failure in figure 5.2 (b).

However, on the basis of these results one cannot be sure if the uncertainty of the system is represented properly.

Parametric study 2: In order to quantify the effects of a fully random system, all variables are introduced with their random properties (table 5.1) in parametric study 2. Herein, the coefficients of variation are taken from literature [23, 217, 286, 364, 399]. Looking at the results shown in figure 5.2, one can clearly observe that the most influential parameters have been modelled by stochastic variables: the results of both parametric studies are almost similar, but one cannot quantify the influence of each random variable to the system behaviour.

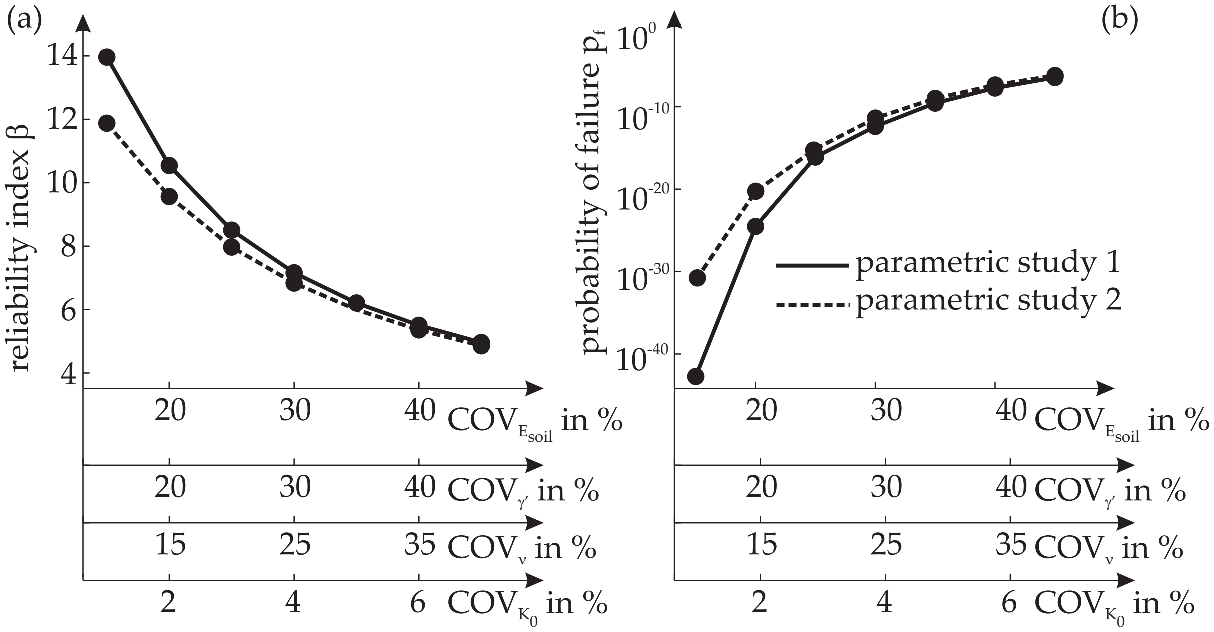

Figure 5.2: Influence of the variability in parametric studies 1 and 2 on the tunnel lining.

5.2.3 Sensitivity analysis

A local and global sensitivity analysis has been carried out to enlighten the influence of each random variable on the system response.

As mentioned in section 4.3.1, the *local sensitivity analysis* is a by-product of FORM. The values of the importance vectors is shown in figure 5.4 (left). The negative importance values α_i indicate resistance parameters and vice versa. One can clearly see that the thickness d and the soil stiffness E_{soil}, the soil weight γ', the Poisson's ratio ν, the overburden H and the compressive strength of concrete $f_{concrete}$ have the largest influence on the system behaviour.

The *global sensitivity analysis* is defined as the ratio between the variance of the investigated variable and variance of the system response as described in section 4.4.2. A Polynomial chaos expansion (PCE) is used to approximate the system response due to the uncertain random input parameters in table 5.1 (parametric study 2). The estimation of PCE-accuracy is shown in figure 5.3 using different approaches. Herein, the Sobol' indices δ_i^{PC} are analytically calculated from a PCE of the limit state equation as derived in section 4.4.2. The PCE approximations become impractical in the presence of a large number of variables ($n > 6$) as also reported by Phoon [286]. This is impractical due to the quite long computation time compared to the local sensitivity analysis. Figure 5.3 shows the accuracy of the approximated PCE, which is measured by different types of error (see section 4.3.3). It can be clearly seen in figure 5.3 evaluated accuracy of the PCE is increasing with the expansion order of the PCE. In addition to the *empirical error* also the *mean predicted residual sum of squares* (PRESS) in figure 5.3 (a) offers similar results for the increasing accuracy of the PCE with an increasing expansion order. It can be clearly seen in figure 5.3 (b) that the accuracy of the PCE fitting is expressed using the deter-

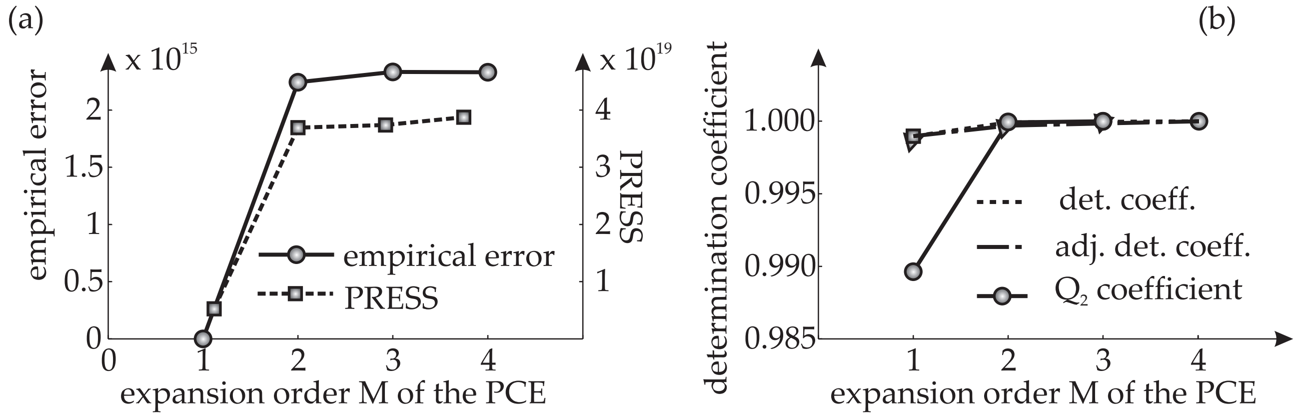

Figure 5.3: Accuracy estimation of the PCE in for the global sensitivity analysis.

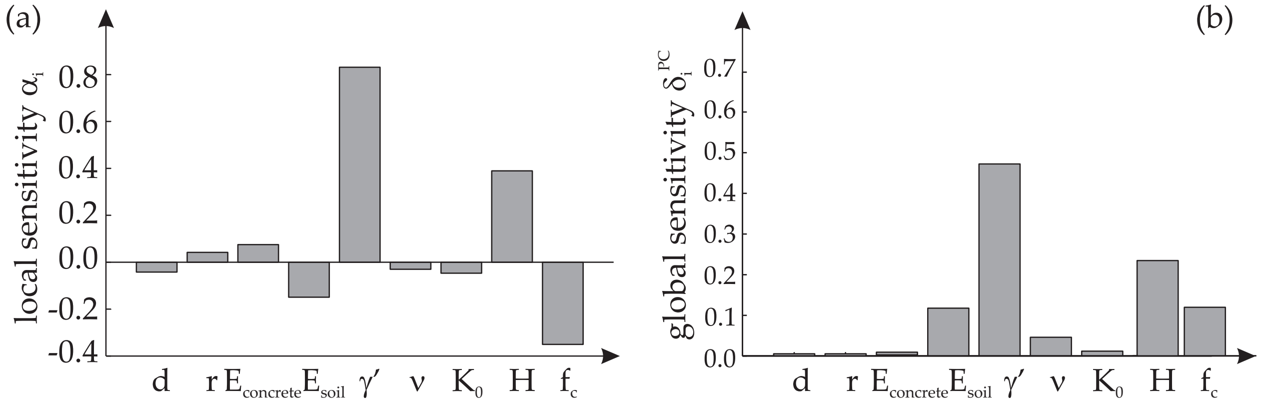

Figure 5.4: Results of the local (a) and global (b) sensitivity analysis in parametric study 2 of a tunnel lining in a soil with COV$_{\varphi'}$ = 20% and a COV$_{c'}$ = 10%.

mination coefficient, the adjusted determination coefficient and the Q_2 coefficient. One can derive from this that these measures quantify the PCE-fitting in a similar way: The expansion order M = 3 can be taken for the evaluation of the global sensitivity factors in figure 5.4.

By looking at the results of the global and local sensitivity analysis shown in figure 5.4 one can see comparable results for both techniques: E_{soil}, γ_{soil}, H and $f_{concrete}$ can be identified as most influential variables on the system behaviour from the results of both sensitivity measures. One would also expect the K_0 value to play a major role in this context, but both sensitivity measures are very small. This can be deduced to the low coefficient of variation in table 5.1. In case of a bigger COV, the sensitivity of the K_0 value is expected to increase.

The differences can be deduced to the afore mentioned definitions of these sensitivity measures. Besides this, it has to be pointed out that negative local sensitivity measures α_i indicate a resistance parameter of the investigated system and vice versa for load parameters.

5.2.4 Conclusions

This first case study is showing exemplarily the application of the uncertainty quantification framework in tunnelling. An analytical solution of a continuum problem in tunnelling is adapted to quantify the effects of soil variability as well as the performance of a local and global sensitivity study of the input parameters. The proposed concept allows one to investigate effects of soil variability precisely without using design approaches described in the EUROCODE 7 [329].

The soil behaviour is modelled on basis of a linear elastic, perfectly plastic soil model. Therefore, the results of this case study cannot be fully transferred into applied engineering. But the presented studies offer a probabilistic description of a soil structure interaction problem in tunnelling. It can be concluded that the reliability based design methodology can be applied to any geotechnical problem, which can be described via a limit state equation. This limit state equation can be a closed form solution or an equation, which is derived from FEM simulations.

On basis of these results, further investigations on the interaction between soil and tunnel using numerical methods in combination with advanced constitutive models would offer additional insights into this problem.

5.3 Bearing capacity of vertically loaded strip footings

One of the core competences in foundation engineering is the design of footings. Fenton & Griffiths [127] state that the design of a foundation involves the consideration of several limit states, which can be separated into two groups: serviceability, which generally translate into a maximum settlement or differential settlement, and ultimate limit states. The latter are concerned with the maximum load, which can be placed on the footing just prior to a bearing capacity failure.

This chapter contributes to the uncertainty quantification of strip footings. The effects of uncertain soil strength properties has been and is a topic of various publications e.g. Baecher & Christian [23], Breysse [54, 170], Cherubini [76], Phoon [285, 286], Russelli [312], Subra [351], and Peschl [279] amongst others. Also the effects of spatially correlated soil properties on the bearing capacity of footings has been investigated by Fenton & Griffiths [127], Popescu et al. [289] and Huber et al. [172] amongst others.

Within this case study, the effects of different constitutive failure criteria are investigated to contribute to the uncertainty of modelling soil behaviour. The presented case studies show the effects of different constitutive failure criteria and point out the importance for the bearing capacity problem of strip footings.

5.3.1 Mechanical description of the system

The German standard DIN 4017 [101] is formulating the state-of-the-art and provides equation 5.7 for the calculation of the bearing capacity of a vertically loaded strip footing.

$$q_f = N_c \cdot c' + q_0 \cdot N_q + \gamma_{soil} \cdot b \cdot N_b \tag{5.7}$$

$$N_c = \begin{cases} 2+\pi & \text{for} \quad \varphi' = 0 \\ (N_q - 1)/\tan\varphi' & \text{for} \quad \varphi' \neq 0 \end{cases} \tag{5.8}$$

$$N_q = e^{\pi \tan\varphi'} \left(\frac{1+\sin\varphi'}{1-\sin\varphi'} \right) \qquad\qquad N_b = 2\,(N_q - 1)\tan\varphi' \tag{5.9}$$

Herein, N_c is the cohesion stability number, c' the cohesion, N_q the depth stability number, q_0 the surface load, φ' is the effective friction angle, N_b the width stability number and γ_{soil} the soil unit weight.

The stability number N_c was derived analytically by Prandtl [293]. In 1920, Prandtl succeeded in finding a solution for the problem of a strip load on a half plane that is both statically and kinematically admissible. The material beneath the strip load can be subdivided into three zones, as pictures in figure 5.5: (I) a wedge shapes zone, in which the major principal stresses are vertical, called *active Rankine zone*, (II) a radial shear zone, called *Prandtl zone* and (III) a *passive Rankine zone*, [394]. Based on Mohr's stress theory and using Airy's stress function, Prandtl obtained an analytical expression for the ultimate bearing capacity of a weightless soil.

Veruijt [394] reports that Buisman extended Prandtl's theory by superimposing overburden pressure q_0 and the unit weight of soil γ_{soil}, which was further extended with experimental and theoretical investigations by Keverling, Caquot, Terzaghi and Brinch-Hansen amongst others. The theoretical investigations are focusing challenges: the analytical expression of Prandtl's ultimate bearing capacity is based on the assumption of a weightless soil, which simplifies the system of differential equations as reported by Perau [277]. Perau [277] collected different approaches on solving this issue numerically. The results from limit analysis approach [232], kinematic approaches [398] or the methods of characteristics [345, 348] are offering a scatter of stability number N_b, which are compared to the formula proposed in DIN 4017 [101] in figure 5.6.

Potts & Zdravkovic [292] derived the stability numbers from FEM calculations using a linear elastic, ideal plastic model. The findings of their numerical study shows good agreement with the results of equations 5.7 and 5.9.

On basis of this, parametric 2D-FEM studies are carried out to evaluate the stability numbers N_b and N_c for different constitutive failure criteria namely Mohr-Coulomb

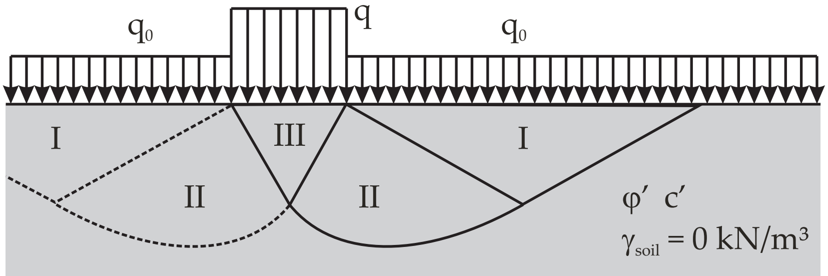

Figure 5.5: Failure mechanism of the classic bearing capacity theory from Prandtl [293].

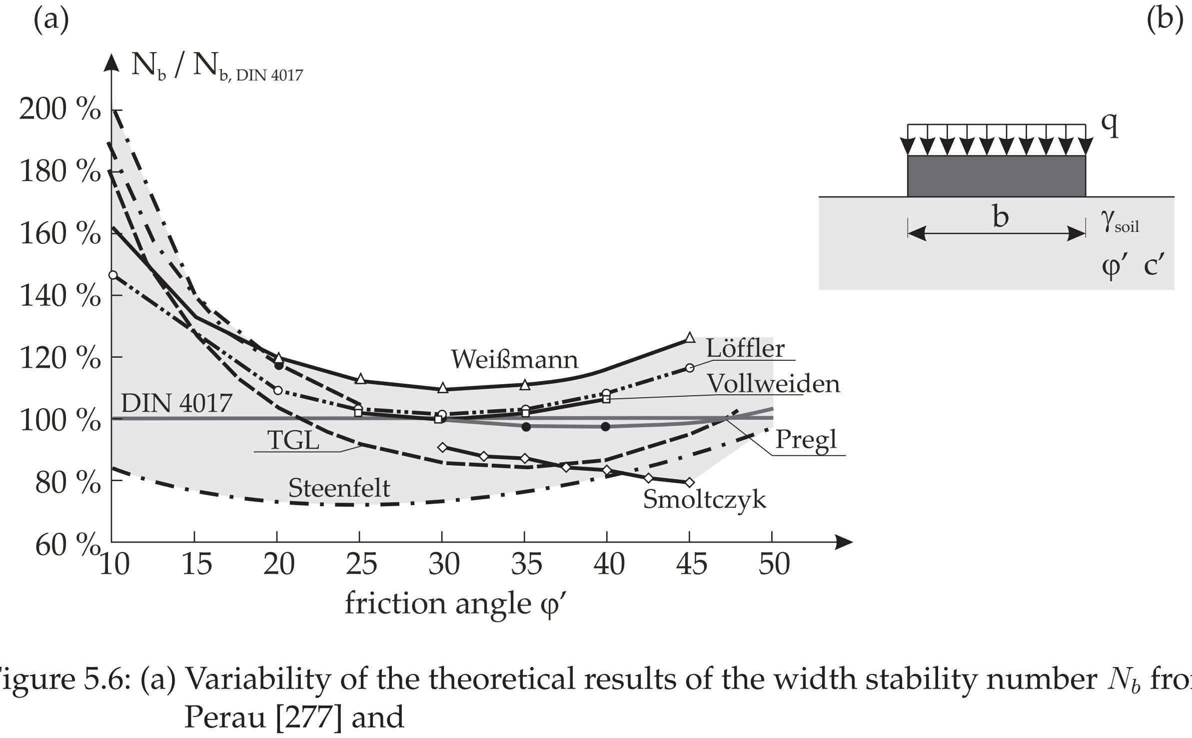

Figure 5.6: (a) Variability of the theoretical results of the width stability number N_b from Perau [277] and
(b) geometry of the rigid strip footing.

(MC) [243], Matsuoka-Nakai (MN) [243] and Lade-Duncan (LADE)[213]. Herein, the contact between the rigid footing and the contact with the soil is assumed as rough with full bounding. These three constitutive failure criteria are shown in figure 5.7. It can be seen that the MC, MN and LADE criteria are identical for triaxial compression, whereas MC and MN are identical for triaxial extension. It is clearly shown in the description in Appendix F that for the MN and LADE criteria no additional input variables are needed.

The results in figure 5.8 (a) show that the width stability number N_b is slightly influenced by the different constitutive failure criteria; the influence of MC, MN and LADE on the cohesion stability number N_c can be clearly seen in figure 5.8 (b). It can be concluded that the MC-criteria is a conservative lower bound for the estimation of the ultimate shear strength of soil, as reported by others e.g. Schad [321]. Moreover, it has to be pointed out that the advanced criteria MN and LADE have a larger friction angle under plane strain conditions.

The bearing capacity problem can be described with the limit state equation 5.10. This limit state equation compares the actual footing pressure q with the bearing capacity q_f.

$$g\left(c, \varphi'\right) = q - q_f \tag{5.10}$$

5.3.2 Stochastic variables and parametric study

Parametric study 1: In this parametric study the effects of three different levels of soil variability on the probability of failure are investigated. The variability of the friction angle and of the cohesion are summed up in table 5.2. The reliability of the strip footing is evaluated using the limit state equation 5.10 and the combination of the First-Order-Reliability-Method (FORM) and Importance sampling (IS) within the FERUM [49] libraries.

Fragility curves are used to study the effects of increasing the variability as shown in figure 5.9. Amongst others, Schultz et al. [328] describe that fragility curves show how the reliability of a structure changes over the range of loading conditions to which

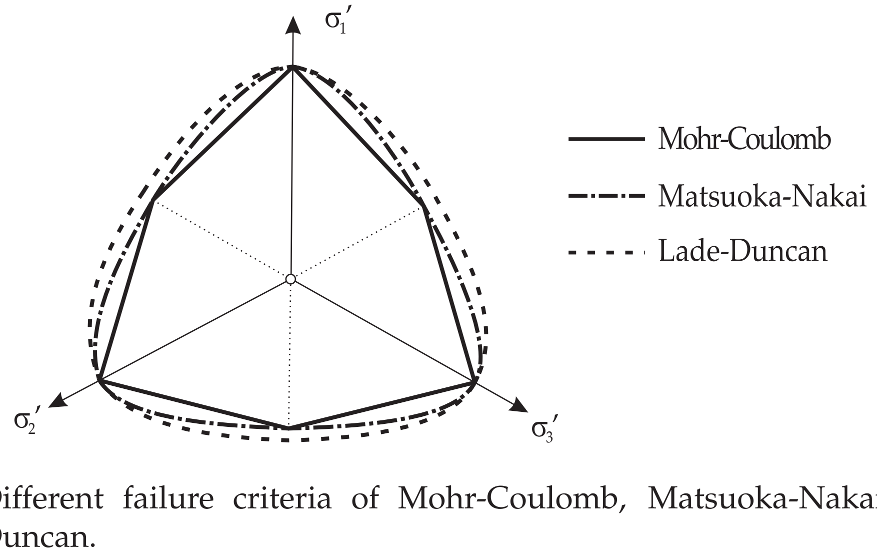

Figure 5.7: Different failure criteria of Mohr-Coulomb, Matsuoka-Nakai and Lade-Duncan.

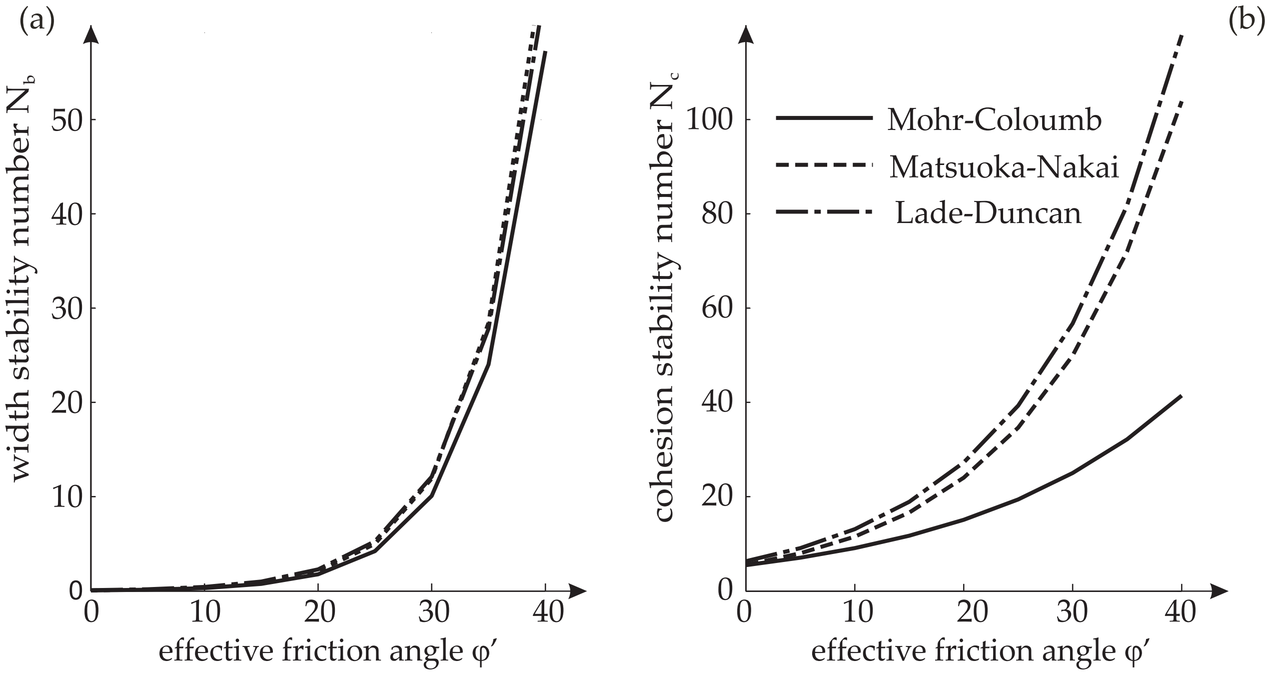

Figure 5.8: Stability numbers N_b (a) and N_c (b) for different constitutive failure criteria.

that structure might be exposed. This offers a more general approach for the probabilistic description of a system by incorporating deterministic input parameters into a probabilistic framework. The deterministic input in this parametric study is the footing pressure. Furthermore, Ellingwood et al. [117] show that the fragility curves of buildings follow a lognormal cumulative distribution function in general. This is a benefit because the fragility curve represented by a lognormal distribution function is continuously defined over the entire range of loads instead of discrete points, [117]. Therefore, lognormal cumulative distribution functions are fitted to the calculated failure probabilities as shown in figure 5.9. Furthermore, it can be clearly seen that the larger COV values of the cohesion and the friction angle cause a higher probability of failure.

In addition to this, the effects of different constitutive failure criteria are shown in

Table 5.2: Stochastic variables of the silty sand in two parametric studies.

	Parametric study 1		Parametric study 2	
	μ	COV	μ	COV
c'	10 kN/m^2	10 - 160 %	10 kN/m^2	10 - 160 %
φ'	25°	5 - 80 %	25°	5 - 80 %
ψ	0°	deterministic	0°	deterministic
γ_{soil}	20 kN/m^3	deterministic	20 kN/m^3	20 %
b	5 m	deterministic	5 m	10 %
d	0.8 m	deterministic	0.8 m	10 %
q	50 - 10,000 kN/m^2	deterministic	1,000 kN/m^2	20 - 80 %

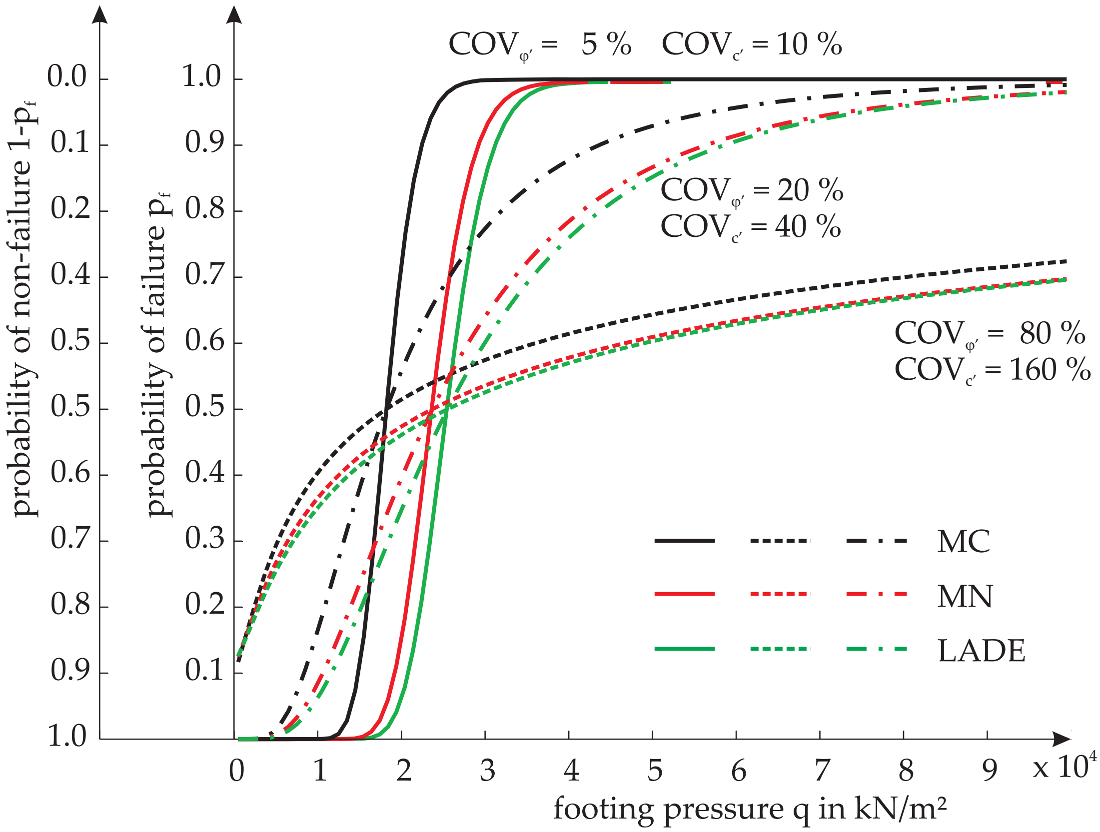

Figure 5.9: Fragility curves for different constitutive failure criteria and different COVs of the cohesion c' and of the friction angel φ'.

figure 5.9. The MC, MN and the LADE criteria have a significant influence on the probability of failure. For all investigated levels of soil variability, the MC criterion offers a higher probability of failure in comparison to the MN and LADE criteria. From these fragility curves it can be concluded that the MC criterion is the most conservative one in this context.

Parametric study 2: The concept of the fragility curves offers a good insight into the effects of soil variability. But this concept is based on a deterministic footing pressure. Therefore, this approach is extended in this second parametric study to a fully probabilistic analysis, which considers all input variables as random. Besides this, different levels of variability of the load q are investigated. The details of theses lognormal distributions are indicated in table 5.2.

It can be clearly deduced from figure 5.10 that the uncertainty and reliability of this system are related: the higher the degree of uncertainty is, the higher is the probability of failure. Again, the probability of failure for different levels of variability is evaluated by a combination of FORM and IS within the FERUM libraries [49]. In the same fashion is the influence of the variability of the load q. A high load variability is causing an higher probability of failure. This effect is more evident for low levels of soil strength properties

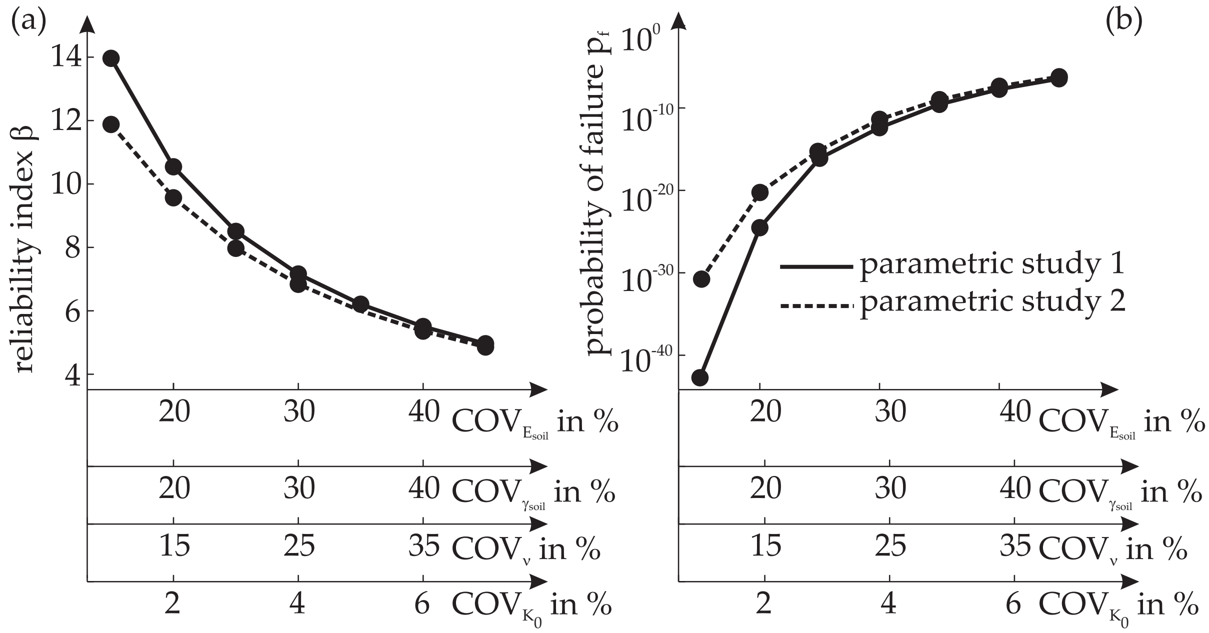

Figure 5.10: Influence of the COV of the cohesion c', of the friction angel φ' and of the footing pressure on the probability of the failure by using the MC-criterion in parametric study 2.

than for highly variable soils. One can conclude that the influence of the soil variability is higher than the variability of the load. The results in figure 5.10 are evaluated for the MC criterion.

5.3.3 Sensitivity analysis

Parametric study 1: Within parametric study 1, the local sensitivities are evaluated for the range of the footing pressure from $q = 500$ kN/m² to $q = 3,500$ kN/m² in figure 5.11. Within this, the coefficient of variation for the cohesion and the friction angle is kept constant.

It can be seen that influence of the cohesion is decreasing with increasing footing pressure and vice versa in the case of friction angle. Moreover, it is interesting to see that the local sensitivity measures of MC, MN and LADE are the same relative to each other. This can be related to the stress state and is explained in appendix F.

Parametric study 2: The local and global sensitivities are shown in figure 5.12 within parametric study 2. Both measures of sensitivity show the comparative importance of the investigated random input variables. In the left part of figure 5.12 the results of the local sensitivity analysis are shown. The negative local sensitivity indicates that the width of the footing B, the unit weight of soil γ_{soil} and the soil strength c' and φ' are resistance parameters, whereas the footing pressure q is a load parameter. From the measures of local and global sensitivity it can be concluded that the soil strength parameters have

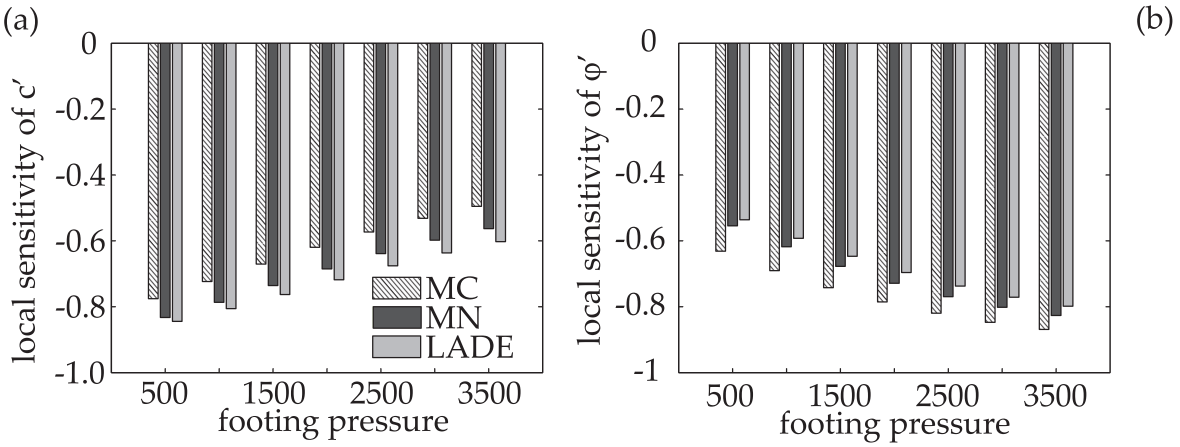

Figure 5.11: Local sensitivities of the cohesion c' and the friction angle φ' with respect to the deterministic footing pressure in parametric study 1.

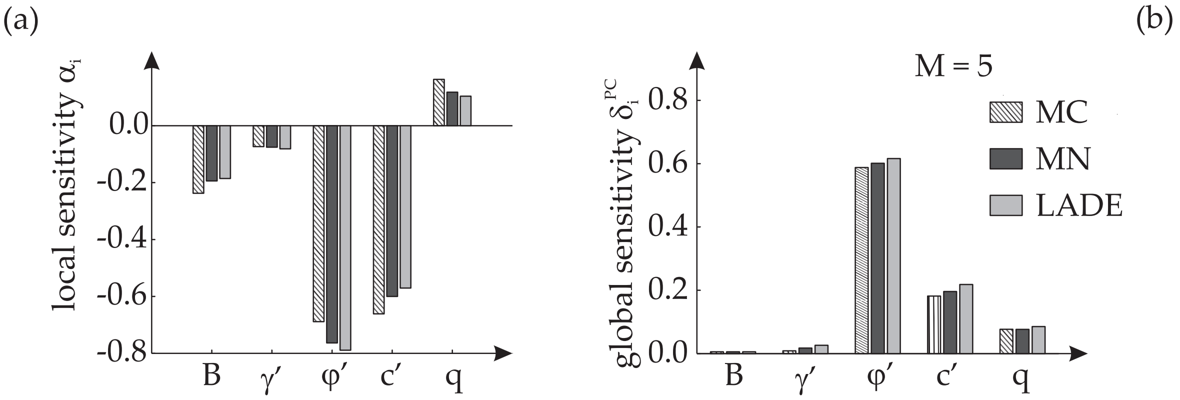

Figure 5.12: Local (a) and global (b) sensitivity factors of the full probabilistic analysis in parametric study 2 for COV$_{\varphi'} = 20\%$, COV$_{c'} = 40\%$ and COV$_{q} = 20\%$.

the biggest importance on the probability of failure. This implies that additional information on cohesion and friction angle have more impact than for other parameters e.g. the unit weight of soil γ_{soil}.

5.3.4 Conclusion

The bearing capacity problem is investigated by means of 2D FEM calculations and probabilistic methods within this case study. The results clearly indicate that the choice of the constitutive failure criterion within a linear elastic, perfectly plastic constitutive model has a significant impact on the deterministic bearing capacity as well as on the failure probability of strip footings. Therefore, this source of model uncertainty has to be considered within an uncertainty quantification. From a deterministic as well as from a probabilistic point of view, the Mohr-Coulomb criterion is the most conservative choice in comparison to Matsuoka-Nakai and the Lade-Duncan. This is investigated by means of fragility curves, which allow to visualize the influence of the different constitutive failure criteria over a wide range of vertical footing pressures.

The load and resistance parameters of the studied problem are clearly identified by a local sensitivity analysis and confirmed by the results of the global sensitivity analysis.

For sake of completeness, it has to be mentioned that the effects for a cross-correlation $\rho_{c',\varphi'}$ of the cohesion and the angle of friction are not investigated within the presented parametric studies. This has been already been investigated in various publications e.g. by Baecher & Christian [23] and Phoon [286] amongst others. Fenton [127] reports that the probability of failure decreases with an increase of the negative correlation coefficient $\rho_{c',\varphi'}$ and vice versa.

It can be concluded that the presented findings are extending the state of the art from a mechanical and a probabilistic point of view. The uncertainty of modelling the soil behaviour should be investigated in further studies to derive tools to quantify this model uncertainty in applied engineering.

5.4 Tunnel face stability

During the construction of shallow tunnels by means of earth pressure balance machines, the face stability is an important issue. To minimize settlements at the ground surface and to prevent an uncontrolled collapse of the soil in the tunnel, a support pressure must be maintained. The estimation of the required support pressures, e.g. for earth pressure balance (EPB) shields to ensure the stability of the face, has been the topic of research until the present day e.g. [12, 196, 216, 256, 311, 350, 392].

Within this case study the framework of uncertainty quantification is applied to the face stability problem. Due to the absence of an analytical model, the 3D mechanical system is modelled by the Finite Element Method (FEM) using different constitutive failure criteria. Formulae for the collapse pressure of the tunnel face are derived from these results, which offer the possibility to investigate the model uncertainty within the probabilistic framework.

5.4.1 Mechanical description of the problem

Different researchers have worked on this problem using various approaches. Horn [169] was the first using a wedge based model to calculate the minimum face pressure, which is necessary to guarantee the stability of the system as shown in figure 5.13. This approach was later improved by Anagnostou [12].

Leca & Dormieux [216] present an upper bound solution for the face stability of shallow tunnels by using a kinematic approach. This upper bound solution involves three solutions based on consideration of three mechanisms, which are derived form the motion of rigid conical blocks; specifically, two active and one passive collapse mechanism. According to Mollon et al. [256], the passive blow-out mode of failure does not occur for the cases currently encountered in practice. Therefore, this collapse mechanism is not investigated within this contribution.

Vermeer et al. [392] and Ruse [311] followed a different approach in evaluating the stability of a tunnel heading. In contrast to Leca & Dormieux [216], no assumptions on the shape of the collapse mechanism are made. By using the Finite Element Method (FEM) and the Mohr-Coulomb (MC) failure criterion, a formula was derived for the failure pressure of the tunnel face in equation 5.11. Herein c' is the effective cohesion,

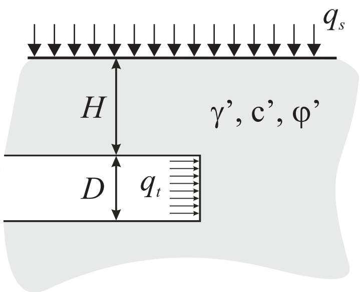

Figure 5.13: Geometry of the tunnel.

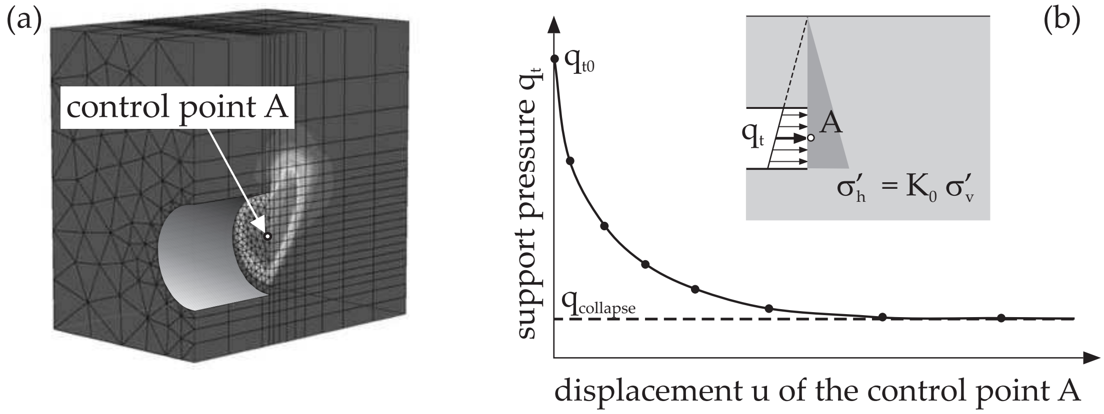

Figure 5.14: Flow area at collapse (a) and typical pressure displacement curve (b).

φ' the effective friction angle, γ' the unit weight of the soil and D the diameter of the circular tunnel (figure 5.13).

$$q_{collapse} \quad = \quad -c'\ N_c + \gamma'\ \mathrm{D}\ N_\gamma \tag{5.11}$$

$$N_{c',MC} = \frac{1}{\tan\varphi'} \qquad\qquad N_{\gamma',MC} = \frac{1}{9\ \tan\varphi'} - 0.05 \tag{5.12}$$

When the ratio of the overburden and the diameter of the tunnel D are bigger than H/D $= 1.5$, the overburden and the load q at the surface have no influence on the failure pressure $q_{collapse}$, nor on the stiffness, the dilatation angle or the Poisson's ratio of the soil, as reported by Vermeer et al. [392]. Additional 3D FEM studies on the influence of different constitutive failure criteria are conducted by the author.

As a symmetrical tunnel is considered, the collapse-load calculations are based on only half a circular tunnel, which is cut lengthwise along the tunnel axis. Figure 5.14 (a) shows a typical finite element mesh as used for the calculations. The ground is represented by 10-noded tetrahedral volume elements. The boundary conditions of the finite element calculations are as follows: the ground surface is free to displace, the side surfaces have roller boundaries and the base is fixed.

It is assumed that the initial stresses follow a geostatic stress distribution according to the rule $\sigma'_h = K_0 \cdot \sigma'_v$, where σ'_h is the horizontal effective stress and σ'_v is the vertical effective stress; K_0 is the coefficient of lateral earth pressure. Ruse [311] found that the K_0-value influences the magnitude of the displacements, but not the pressure at failure.

The first stage of the calculations is to remove the volume elements inside the tunnel and to activate the shell elements of the lining. This does not disturb the equilibrium as equivalent pressures are applied on the inside of the entire tunnel. To get full equivalence between the initial supporting pressure and the initial geostatic stress field, the pressure distribution is not constant but increases with depth. This is obviously significant for very shallow tunnels, but a nearly constant pressure occurs for deep tunnels. The minimum amount of pressure needed to support the tunnel is then determined by a stepwise reduction of the supporting pressure. A typical pressure-displacement curve is shown in Figure 5.14 (b) , where q_t is the support pressure at the level of the tunnel axis and u is the displacement of the corresponding control point A at the tunnel face. It has to be emphasised that this control point has to be chosen within the collapsing body; otherwise the load-displacement curve in Figure 5.14 (b) will come to an almost sudden end and the curve then cannot be used to conclude that failure has been reached.

The results of these parametric FEM studies using the Matsuoka-Nakai [243] (MN) and the Lade-Duncan [213] (LADE) criteria are shown in figure 5.15. It can be seen in figure 5.15 and derived from the equations below that the failure pressure $q_{collapse}$ is significantly reduced by introducing different constitutive failure criteria. One can conclude form the experimental results presented in literature e.g. Kirsch [196] that there is quite a wide range of possible values for N_c and N_γ in equation 5.11. The results of the MN and LADE criteria in equations below are derived from an ordinary least square fitting.

$$N_{c,MN} = \frac{1}{2\ \tan\varphi'} \qquad N_{\gamma,MN} = \frac{1}{67\ \tan\varphi'} - 0.01 \tag{5.13}$$

$$N_{c,LADE} = \frac{1}{3\ \tan\varphi'} \qquad N_{\gamma,LADE} = \frac{1}{79\ \tan\varphi'} - 0.012 \tag{5.14}$$

The system can be described with the limit state equation 5.15. This limit state equation compares the actual face pressure q_t with the failure pressure $q_{collapse}$, as proposed

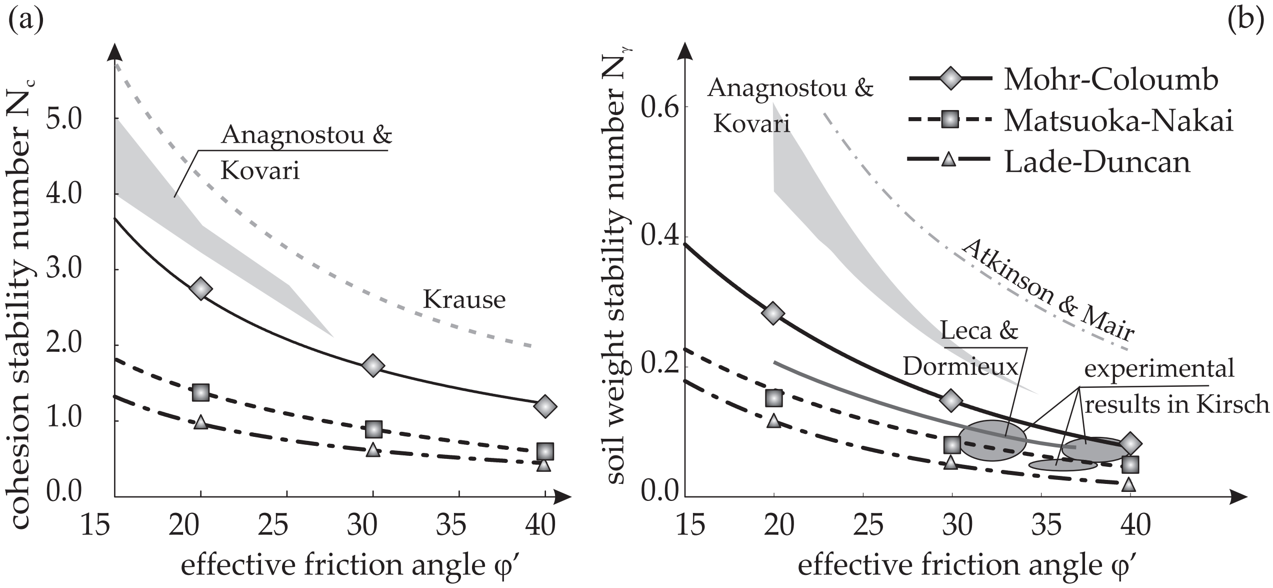

Figure 5.15: Variability of the stability numbers N_c (a) and N_γ (b) for different constitutive failure criteria (Mohr-Coulomb, Matsuoka-Nakai, Lade-Duncan) in comparison to experimental results from literature [196].

by Mollon et al. [255].

$$g\left(c',\varphi'\right) = q_t - q_{collapse} \tag{5.15}$$

For $g = 0$ one obtains a failure cure in the $c' - \varphi'$ plane. These failure curves are also refereed to as limit state surfaces. The limit state surfaces for different face pressures are shown in figure 5.17 (a) and emphasise the key message in figure 5.16: the higher the face pressure q_t, the more unlikely is the collapse of the system.

5.4.2 Stochastic variables

For the stochastic soil properties, Phoon & Kulhawy [282] stated that, from an exhaustive study of cone penetration test and triaxial test results, the coefficient of variation ($\text{COV} = \sigma_{c'}/\mu_{c'}$) of cohesion c' could vary from 10% to 55%; Cherubini [77] recommended $\text{COV}_{c'} = 12 - 45\%$ for stiff clays and a higher limit of 80% for very soft clays. For the $\text{COV}_{\varphi'}$ of the friction angle φ', Phoon & Kulhawy [282] proposed $\text{COV}_{\varphi'} = 5 - 15\%$.

On top of this, the correlation between cohesion and friction angle was found by Cherubini [75] to be $\rho_{c',\varphi'} = -60\%$, while Lumb [226], Phoon & Kulhawy [283], Wolff [407], Yucemen et al. [414] and Speedie [354], amongst others, reported correlations between $\rho_{c',\varphi'} = 0\%$ and $\rho_{c',\varphi'} = -70\%$.

The values used in this section for the statistical moments of the shear strength parameters belong to the intervals proposed by the above researchers. The stochastic variables used in this section are chosen on the basis of a literature and are shown in table 5.3 and 5.4.

5.4.3 Parametric studies

Parametric study 1: The aim of the presented parametric studies is to quantify the impact of soil variability for the tunnel heading problem using different constitutive failure criteria within a probabilistic framework. The limit state equations have been implemented into the FERUM libaries [49].

In accordance with section 5.3, figure 5.16 can also be interpreted like a quasi-fragility curve presented in section 5.3. It can be approximated by $1-\Phi$; Φ is the lognormal cumulative distribution function. The deterministic face pressure q_t is increased and plotted

Table 5.3: Properties of parametric study 1 on the tunnel heading using the Mohr-Coulomb failure criterion.

property	COV	distribution
$c' = 2.5$ kN/m ^{2}	$10 - 60$ %	lognormal
$\varphi' = 35°$	$5 - 30$ %	lognormal
$\gamma' = 18$ kN/m^3	-	deterministic
$D = 10$ m	-	deterministic
$q_t = 0 - 160$ kN/m ^{2}	-	deterministic

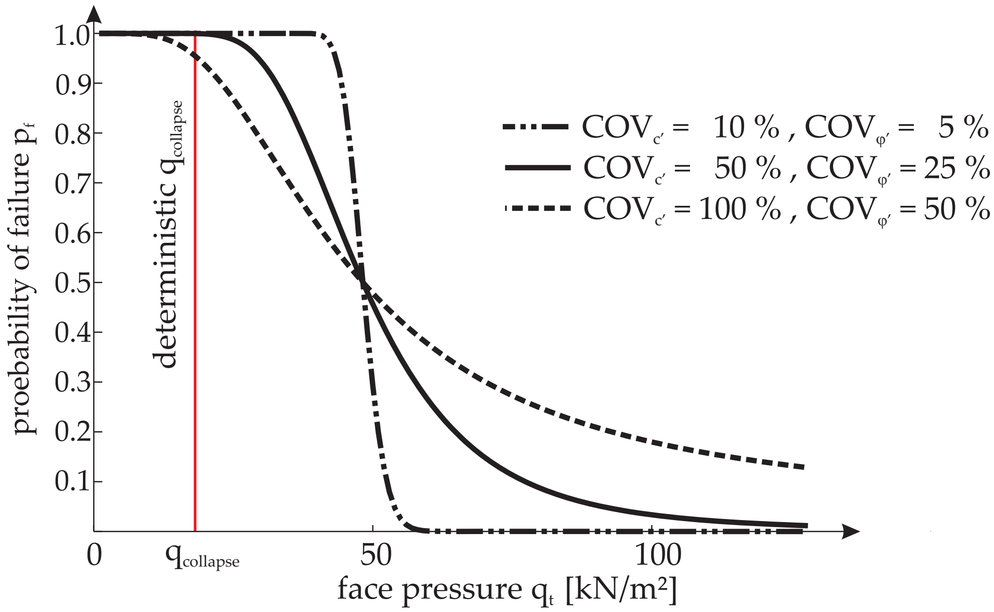

Figure 5.16: Influence of the COV of the cohesion c' and of the friction angle φ' on face pressure versus probability of failure using the Mohr-Coulomb criterion.

against the probability of failure p_f. It can be seen in figure 5.16 that p_f decreases with an increasing deterministic face pressure q_t and vice versa in the case of the reliability index. It can also be concluded that, the higher the variability of φ' and c', the higher is the probability of failure p_f. The deterministic value $q_{collapse}$ shown in figure 5.16 is based on the mean value of the cohesion and the friction angle.

The effects of positive and negative correlation between the cohesion c' and the friction angle φ' are shown in figure 5.17 (b). The ranges of $\rho_{c',\varphi'}$ are chosen according to the results of the literature study summarized in section 5.4.2. A positive correlation $\rho_{c',\varphi'}$ increases slightly the probability of failure. The influence of a negative correlation is more obvious. In this parametric study it is found to be conservative to neglect a negative correlation $\rho_{c',\varphi'}$, because the probability of failure is higher for $\rho_{c',\varphi'} = 0$.

Parametric study 2: In additional investigations, all parameters have been treated as random variables in order to investigate the consequences of variability of the soil properties (φ', c', γ'), of the geometry (represented by the tunnel diameter D) and of the construction process (represented by the face pressure q_t). The stochastic properties are defined in table 5.4 and have been used for a FORM analysis within the reliability assessment.

If all variables are treated as random, the probability of failure is much higher than in the case of parametric study 1. In that case, only the variability of the strength parameters was considered. Therefore, the probability of failure for a given face pressure of $q_t = 50\,\mathrm{kN/m^2}$ (figure 5.16) is much lower than in the previous parametric study. Additional calculations were carried out to get a more detailed insight into this problem.

For this purpose, the influence of the soil variability (c', φ') and of the tunnelling pro-

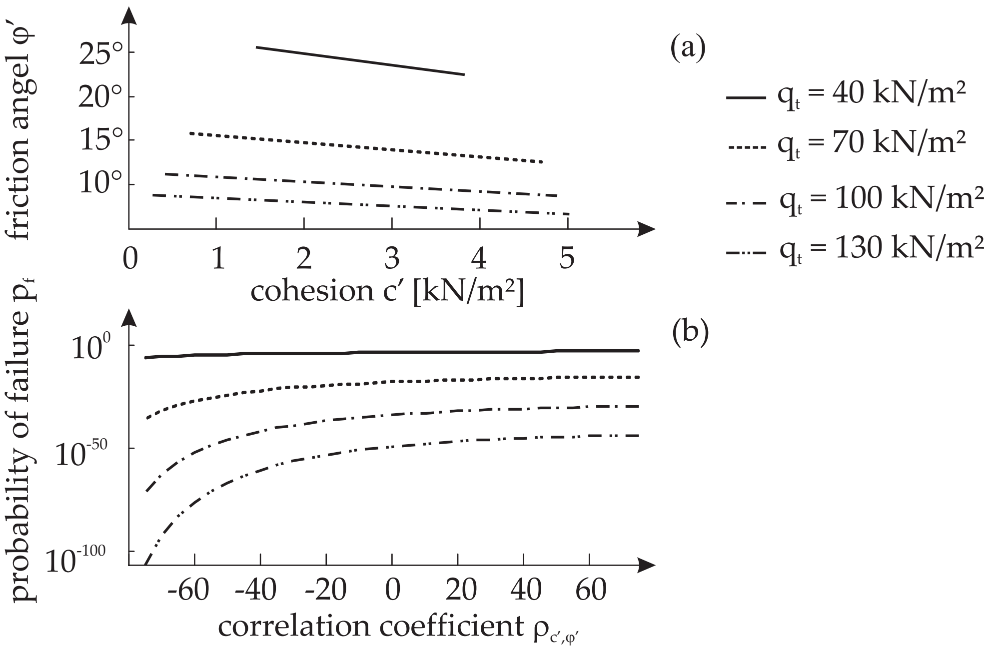

Figure 5.17: Limit state surfaces for different levels of the face pressure q_t in (a) and for probability of failure versus correlation coefficient between cohesion c' and friction angle φ' in (b) for the MC- criterion.

cess represented by the face pressure q_t is evaluated in additional calculations. The results of this study are shown in figure 5.18 (a). Herein, the soil variability is increased and compared to different levels of variability of the face pressure for a given face pressure $q_t = 50$ kN/m^2. Again, it can clearly be seen that a high level of variability of the variables causes a high probability of failure. Moreover it can be seen that the system behaviour of highly random properties (COV$_{c'} > 60\%$, COV$_{\varphi'} > 30\%$) are very similar.

The influence of different constitutive failure criteria is shown in figure 5.18 (b). Herein, the probabilities of failure differs significantly for MC, MN and LADE. Again, the MC-criterion offers conservative results in comparison to the more realisitic MN criterion, whereas the results of the LADE criterion are even lower.

Table 5.4: Properties of parametric study 2 on the tunnel heading using the Mohr-Coulomb failure criterion.

property	COV	distribution
$c' = 2.5$ kN/m ^{2}	20%	lognormal
$\varphi' = 35°$	10%	lognormal
$\gamma' = 18$ kN/m ^{3}	10%	lognormal
$D = 10$ m	10%	lognormal
$q_t = 50$ kN/m ^{2}	10%	lognormal

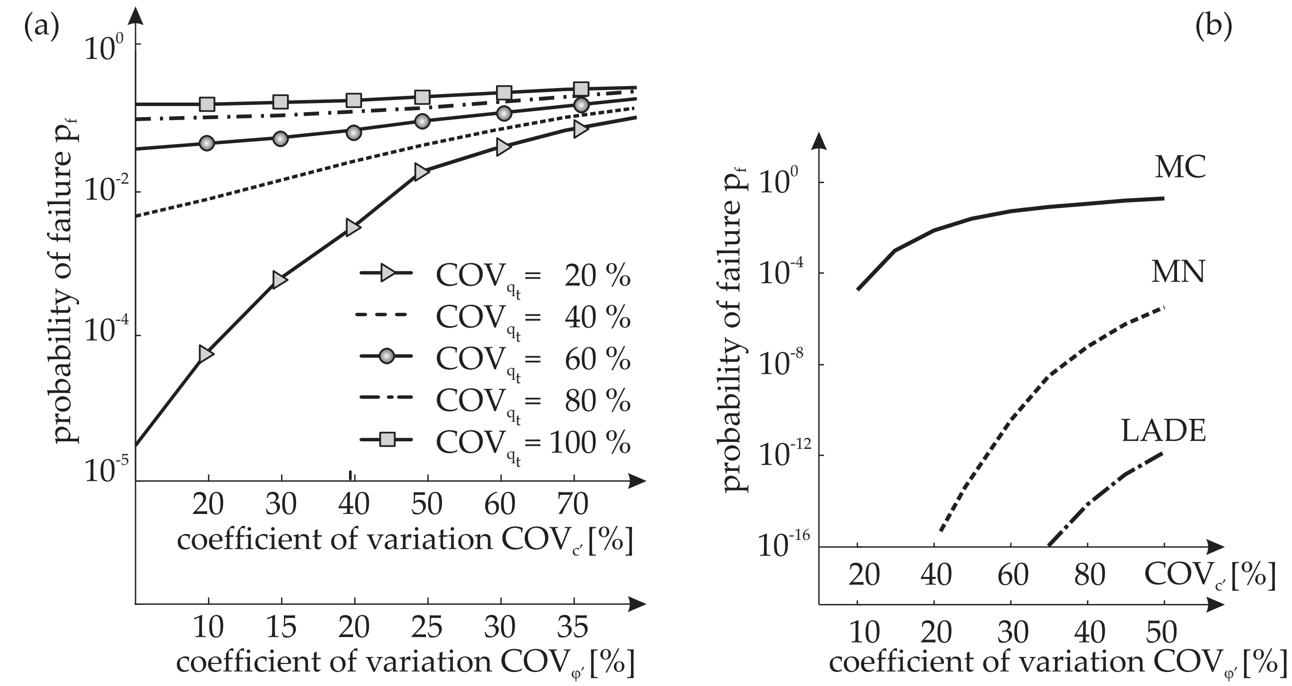

Figure 5.18: (a) Variation of the COVs for the cohesion c', the friction angle φ' and the tunnel face pressure q_t together with the corresponding probabilities of failure p_f.
(b) Variation of the coefficients of variation for the cohesion c' and the friction angle φ' for a given coefficient of variation $\text{COV}_{q_t} = 10\%$ the tunnel face pressure q_t, together with the corresponding probabilities of failure p_f.

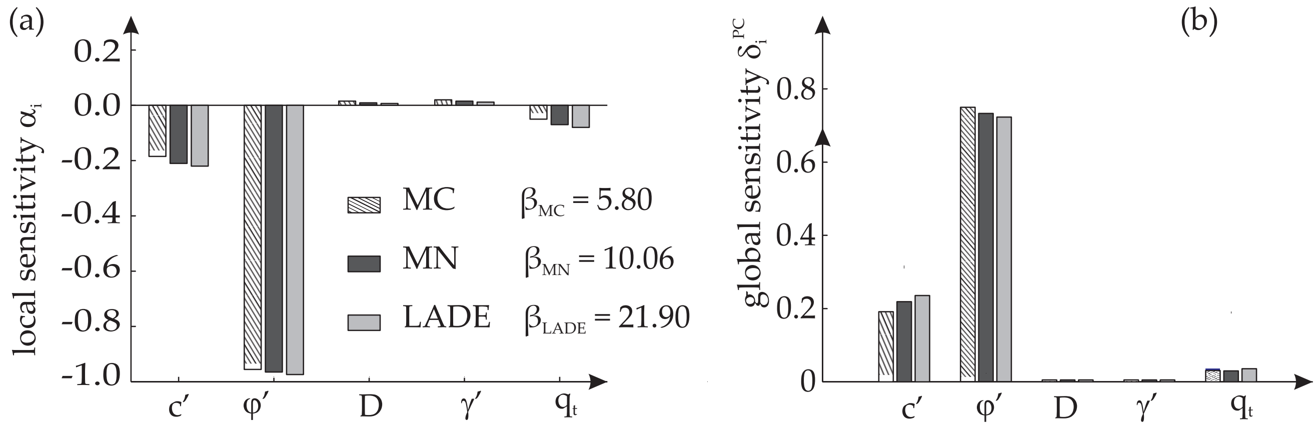

Figure 5.19: Reliability indices β_i and local sensitivity α_i (a) as well as the global sensitivity values δ_i^{PC} values (b) for parametric study 2 on the tunnel face stability using different constitutive failure criteria MC, MN, LADE.

5.4.4 Sensitivity analysis

The local and global sensitivity of each random variable are shown in figure 5.19. The load and resistance variables can be clearly identified from the local sensitivity measures in figure 5.19 (a). The diameter D and the soil weight γ' show a positive local sensitivity α_i. Therefore, they are load parameters of the limit state equation, whereas the cohesion c', the friction angle φ' and the face pressure q_t are resistance parameters. One can clearly derive from both local and global sensitivity analyses that the cohesion c' and the friction angle φ' have the largest influence on the reliability index, which is in agreement with comparable studies by Mollon et al. [255].

Comparing the different constitutive failure criteria MC, MN and LADE, one can see the same qualitative results of the sensitivity analyses. All three constitutive failure criteria have show a nearly the same local and global sensitivity measures. This implies that the contribution to the system behaviour is nearly the same for all investigated constitutive failure criteria.

5.4.5 Conclusions

Within two parametric studies, the influence of soil variability, geometry and construction process on the probability of failure is studied. The limit state equation is derived from 3D FEM studies using linear elastic, perfectly plastic constitutive models, which are using the Mohr-Coulomb, the Matsuoka-Nakai and the Lade-Duncan failure criteria. The assumption of uncorrelated shear strength parameters is found to be conservative (i.e. it gives a greater probability of failure) in comparison to that of negatively correlated parameters. The results of the parametric studies suggest that the strength parameters of the soil and the tunnel face pressure have the major influence on the probability of failure in comparison to the soil unit weight and tunnel diameter.

As a consequence of this, the influence of the different constitutive failure criteria is investigated. One can clearly see that the well known Mohr-Coulomb criterion offers very conservative results in relation to the more realistic Matsuoka-Nakai criterion and to optimistic Lade-Duncan criterion. As pointed out in the appendix F, there are differences in the definition of the failure surface, but the number of variables needed for these criteria are the same. Therefore one can say that the complexity of these models are similar.

It can be concluded from these results that the choice of the soil model and the constitutive constitutive failure criteria has significant influence on the reliability of the tunnel face. Additional investigation should focus on the model error and its considerations via e.g. partial safety factors in applied engineering.

5.5 Synopsis of the case studies

Three different case studies are quantifying the effects of soil variability on the performance of geotechnical structures in the ultimate limite state. Herein, the soil variability is considered via random variables following lognormal distributions.

This extends the state of the art given in EUROCODE 7 [119]: Soil variability is described via probability distribution within the framework of uncertainty quantification instead of constant safety factors.

Tunnel lining: The analytical solution of a continuum mechanical problem is used to describe the soil-structure interaction of a tunnel lining with soil. Herein, the behaviour of soil and concrete are approximated by purely elastic material models. The level of complexity is increased from 4 to 9 random variables within two parametric studies. It can be concluded from these results that only the driving parameters have to be considered as random properties. This is proven through the local and global sensitivity analyses. The identification of the key parameters of a mechanical system by means of sensitivity analysis is very important for practical issues because a low number of random variables implies less computation time.

Bearing capacity of vertically loaded strip footings: Within this case study on the ultimate limit state of a footing, the soil behaviour is modelled via linear elastic, perfectly plastic models, which follow different constitutive failure criteria; namely Mohr-Coulomb, Masuoka-Nakai and Lade-Duncan. These approaches are used within parametric 2D FEM studies, which are used to derive a semi-analytical limit state equations. Fragility curves are used as deterministic tools to quantify deterministically the stochastic system. Moreover, a local and global sensitivity analysis is conducted to investigate the contributions of soil strength parameters and other random input variables to the probability of failure.

Tunnel face stability: The ultimate limit state of the tunnel heading is investigated by using the Mohr-Coulomb, the Matsuoka-Nakai and the Lade-Duncan failure criteria, which are used within a parametric, 3D FEM study. A semi semi-analytical limit state equation is derived from these results, which is used in the subsequent reliability analysis. Similar to the results of the case study on the bearing capacity of strip footings, one can also identify the Mohr-Coulomb criterion as conservative approach for these two problems in comparison to the Masuoka-Nakai and the Lade-Duncan criteria.

Chapter 6

Selected case studies in uncertainty quantification including spatial variability

It is stated in the EUROCODE 7 [119] that "*characteristic values of soil and rock properties shall take account of the variabilities of the property values*". Controversially, although statistical methods are suggested as a possible way forward, there exists little guidance as to how this should be achieved. This suggests a need to take soil variability into account within a sound mathematical framework for geotechnical design.

The application of random fields, which represent the spatial variability of soil properties, is shown in different case studies in geotechnical engineering. The state-of-science in uncertainty quantification is applied in the the estimation of tunnelling induced settlements, slope stability and serviceability of footings. This chapter furthers the idea which are presented in the three case studies in the last chapter.

Moreover, these applications also extend the common approaches with respect to multiple scales of soil variability within the framework of uncertainty quantification. Finally, the uncertainty of geology represented by macro-scale variability is investigated by means of modern geostatistical simulation methods. This offers an insight into the effects of geological uncertainty.

6.1 Estimation of tunnelling induced settlements

This case study investigates the consequences of soil variability in connection with tunnelling induced surface settlements. These investigations are performed for a single layered and a two-layered soil involving different scales of spatial variability.

Soil variability can be simulated by the Random Finite Element Method, which is explained within this case study. The influencing factors on the probability of damage due to differential settlements are identified and compared to each other. The results of this contribution help to understand the influence of soil variability.

Schmidt [324] and Peck [274] were the first to show that the transverse settlement trough, taking place after construction of a tunnel, in many cases can be well described by the Gaussian function. Among others, Kolymbas [205] and Verruijt [393] derived the settlement curve analytically for the case of a homogeneous subsoil. This practical approach, as well as numerical methods such as the Finite Element Method (FEM) [253], are often based on the assumption of a homogeneous soil. O'Reilly & New [267] and Mair & Taylor [233] offered empirical formulae derived from case studies to take layered soils into account.

6.1.1 Mechanical description of the problem

Within this section, a 2D FEM mesh, shown in figure 6.1, is used to calculate the surface settlements. This Plaxis 2D [8] FEM model consists of 2,326 15-noded elements, which does not influence the stochastic soil properties due to the small grid size [174, 178]. Table 6.1 summarises the material parameters for the linear elastic, perfectly plastic soil model and the linear elastic material model for the concrete lining.

The conventional tunnelling excavation is simulated via the so-called STRESS REDUCTION METHOD [253]. In this 2D method the 3D excavation problem is captured through a stress relaxation factor. Using this, the stress relaxation of the ground due to the delayed installation of the shotcrete lining and the load sharing between soil and lining are nicely addressed. A full faced excavation with a stress relaxation of 35 % is chosen according to Möller [253]. The stiffness of the building is not taken into account in this evaluation of surface settlements. As described by several publications [205, 267, 274], the settlement trough follows a Gaussian function.

As pictured in figure 6.1, the limit state due to differential settlements is investigated. A limit state function g is defined to quantify the consequences of spatial variability. This function describes the difference between the rotation α, which is evaluated by the Random Finite Element Method (RFEM) and an ultimate rotation $\alpha_{ultimate}$, that is

$$g(\alpha) = \alpha_{ultimate} - \alpha \tag{6.1}$$

The ultimate rotation $\alpha_{ultimate} = 1/500$ due to differential settlements is taken from the DIN 4019 [102] to avoid cracks in masonry. This RFEM approach calculates the green-field settlements and does not consider soil structure interaction. Moreover, this procedure does not take into account the different convex and concave parts of the surface settlements as described by Netzel [263].

6.1.2 Stochastic variables

Within this section, the effects of spatial variability of the soil is investigated. Therefore, random fields are used to represent spatially variable stiffness of the soil. The RFEM is schematically pictured in figure 6.1 (a). The random fields are mapped onto the FEM mesh via the spatial averaging approach and used to evaluate the system response, which varies between the random fields.

Within RFEM, one has to pay attention to the generation of the random fields and to the coarseness of the random field mesh. It can be deduced from section 4.2.3 that the random field mesh has to be finer than the FEM mesh and one has to keep in mind that the coarseness of the random field is also dependent on the simulated correlation length.

The libraries of GSLIB [97] are used for this. The finer random fields have been mapped onto the coarser FEM mesh via the spatial averaging approach described in section 4.2.4. In this study the random field mesh is 10 times finer than the smallest element of the FEM mesh. This averaging over every single FEM element enables one to use non-structured FEM meshes.

Table 6.1: Material properties for the parametric study on tunnelling settlement in an single-layered subsoil.

Soil (linear-elastic, perfectly-plastic soil model using the MC criterion)	
soil unit weight	$\gamma_{soil}{}'$ = 20 kN/m^3
friction angle	φ' = 20 °
cohesion	c' = 40 kN/m ^{2}
Poisson's ratio	ν = 0.35
coefficient of horizontal earth pressure	K_0 = 0.34
modulus of elasticity	lognormally distributed
	μ_E = 60 MN/m^2
	$COV_E = 10 - 75$ %
	θ_h/D = 0.5-5
	$\theta_h / \theta_v = 1 - 50$
	exponential correlation function
Shotcrete (linear elastic material model)	
thickness of the lininig	d = 0.35 m
concrete unit weight	γ_c = 25 kN/m^3
modulus of elasticity	E = 7,500 MN/m^2
Poisson's ratio	ν = 0.20

In figure 6.1 the probability of damage is evaluated based on a modified Monte-Carlo approach. Although the Monte-Carlo approach is the most robust and accurate reliability method, it is very time consuming to reach good accuracy of the probability of failure, especially in the presence of small probabilities as mentioned in section 4.3.2. Therefore, the author fits a normal distribution to the system response of 300 random field realisations as proposed by Huber et al. [174] (see figure 6.1 b and c). This approach speeds up the evaluation of the influences of the variation of geometrical and stochastic properties relative to each other. Moreover, the convergence of this modified Monte-Carlo approach is checked by looking at the mean system behaviour after 300 RFEM calculations. It is found that that the mean value and standard deviation of the differential surface settlements do not change significantly after 300 random field realisations, [174]. The results are approximations, but nevertheless a basis for the investigations of influences of the above mentioned properties in comparison to each other. For this reason, this approach is used for the evaluation of the results in this chapter 6.1.

6.1.3 Parametric study on tunnelling settlement in a single-layered subsoil

Within this case study, different geometrical boundaries, such as the width of the building B, the location of the building relative to the tunnel axis and the overburden H of the tunnel are varied. On top of this also the effects of coefficient of variation of the stiffness $\mathrm{COV_E}$, the vertical correlation length θ_v, the horizontal correlation length θ_h and the ratio of horizontal and vertical correlation lengths θ_h/θ_v are investigated. All the presented results are symmetrical with respect to the tunnel axis. This is related to the symmetrical distribution of the principal stresses due to the simulation of the tunnel excavation.

Tunnelling creates a settlement trough that is centred directly above the tunnel. As mentioned in section 6.1.1, this settlement trough is following a Gaussian distribution function. As a consequence, the probability of damage is highest for a building above the steepest slope of this trough. In figure 6.1 the variable L stands for distance from midpoint of the building.

This is investigated in figure 6.2 (a). Different locations and different widths of a building are investigated. It can be concluded from this that larger buildings are less endangered than smaller ones, which is related to the geometry of the building in relation to the tunnel diameter D. However, one has to keep in mind that the building is assumed as a rigid block, otherwise the probability of damage for large buildings is expected to be significantly bigger.

In addition to the location and width of the building, the effects of the stochastic soil properties on the probability of damage p_{damage} are investigated in figure 6.2 (b,c,d). By comparing figures 6.2 (b) and (c) it can be clearly seen that the effects of the variability of the stiffness $\mathrm{COV_E}$ are larger than the effects of the spatial variability of the stiffness. This low influence of the spatial correlation structure can attributed to the construction process of the tunnelling. The changes of the stresses field due to the tunnelling excavation process are predominant in relation to the variations caused by the spatial correlation of the stiffness.

In contrast to this are the results in 6.2 (d). It is shown that the probability of damage p_{damage} is strongly influenced by introducing an anisotropy of the spatial correlation θ_h/θ_v. In the case of modelling the stiffness of the subsoil via isotropically random fields (θ_h/θ_v = 1), the probability of damage is far higher than in case of highly anisotropically random fields.

In addition to this, the influence of anisotropy θ_h/θ_v is shown in figure 6.3. The maximal probabilities of damage p_{damage} are plotted with the ratios of anisotropy θ_h/θ_v in figure 6.3. The isotropic correlation structure $\theta_h/\theta_v = 1.0$ causes the biggest probability of damage. The larger the horizontal correlation length θ_h becomes, the lower is the probability of damage.

By looking into geostatistic textbooks [79], one finds some hint to explain this: Large ratios of anisotropy θ_h/θ_v can be interpreted as soil layering. In this extreme case, the horizontal correlation length is θ_h is assumed to be endless whereas the vertical correlation length is shorter, which leads to a nearly one-dimensional distribution of soil properties. In figure 6.3 it is shown that this leads to a lower probability of damage than in the case

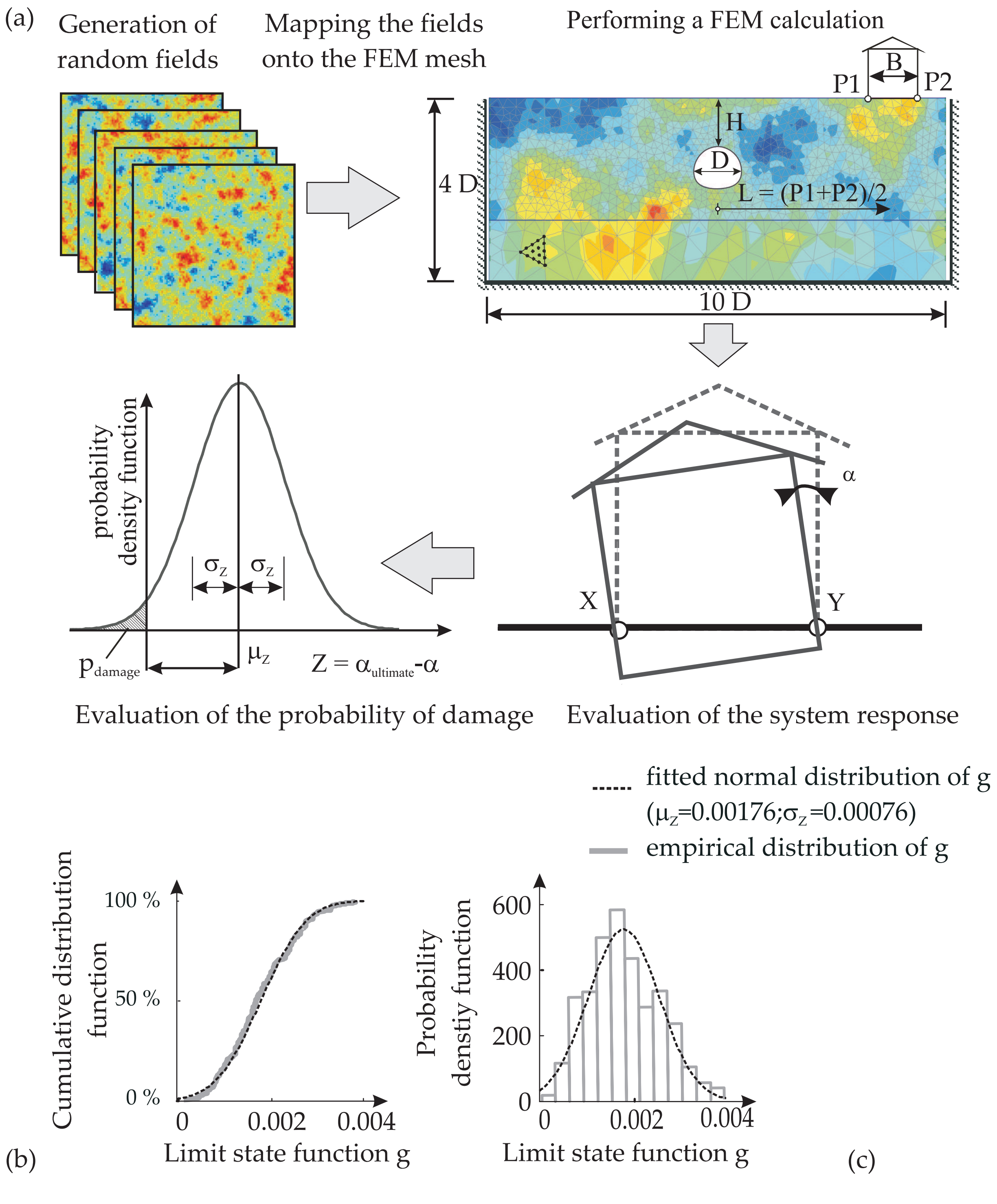

Figure 6.1: (a) Evaluation scheme of the probability of damage p_{damage} due to differential settlements,
(b) cumulative distribution function and
(c) histogram with fitted probability density function of the normally distributed limit state function g, based on an underlying random field ($B/D = 2$, $H/D = 1$, $\mu = 60$ MN/m^2, COV $= 50$ %, $\theta_h = \theta_v = 2D$).

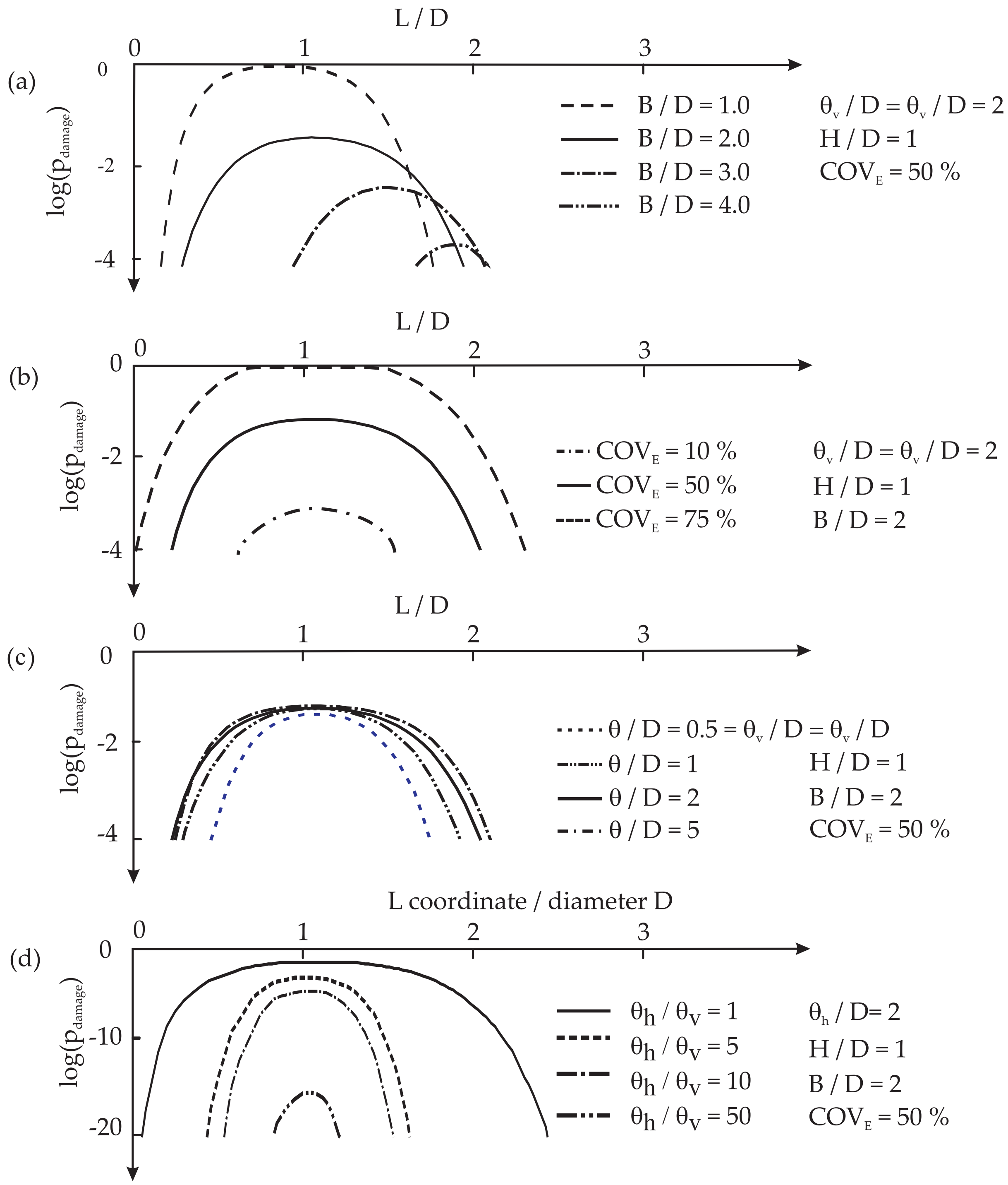

Figure 6.2: (a) Influence of the width B of the building,
(b) influence of the coefficient of variation,
(c) correlation lengths and
(d) influence of the anisotropy of the correlation structure on the surface settlements due to tunnel excavation.

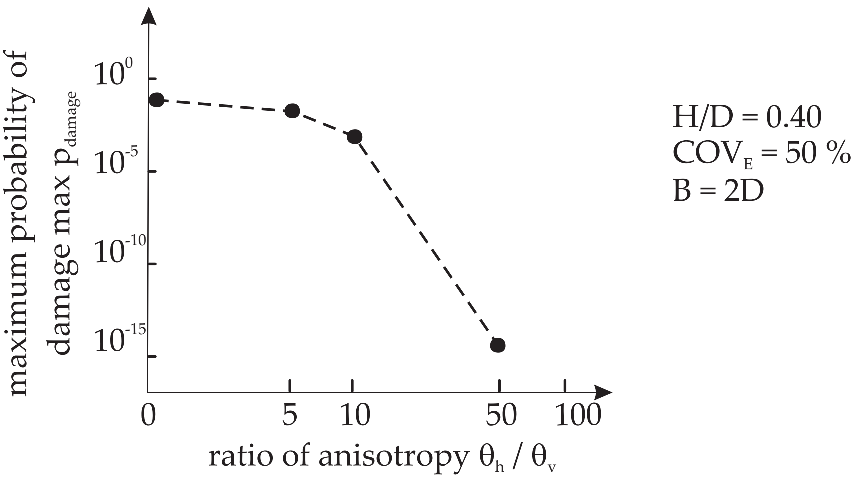

Figure 6.3: Effects of the ratio of anisotropy θ_h/θ_v on the maximum p_{damage}.

of an isotropically random field simulation.

6.1.4 Parametric study on tunnelling settlement in a two-layered soil

The results of the parametric study in a single-layered subsoil show clearly that the influence of spatial anisotropy is tremendously high in comparison to the the variation of geometrical conditions or (isotropic) stochastic properties. Therefore, the consequences of anisotropy are investigated in the sequel on a more generous basis. The extreme case of anisotropy is that the horizontal correlation length becomes nearly infinity. Then all points are practically correlated in the horizontal but not in the vertical direction. This macro-scale correlation can also be interpreted as soil layering.

Starting from this idea, a concept was set up to simulate soil layering or, geostatistically speaking: to simulate spatial variability at two scales: the meso-scale variability inside both soil layers is represented by two random fields following the properties indicated in table 6.2. The soil layers are separated by a one dimensional random field, which is conditioned to soil investigations. This one-dimensional random field is representing a macro-scale variability in this parametric study. The soil investigations are indicating the vertical location of the boundary between the upper and lower layer.

Figure 6.4 shows the tunnel and the location of three boreholes (B1, B2, B3). The ratio of overburden was chosen with H/D = 1 to skip the influences of shallow tunnels on the probability of damage.

At first, the influence of the number of boreholes is investigated. This can be interpreted as different levels of knowledge of the soil layering, as shown in figure 6.4. The results are shown in figure 6.5 (a). In case of one borehole B1, the reliability of the system is smaller than in case of 2 (B1+B2) or three (B1+B2+B3) soil investigations.

Apart from this, the effects of the soil layer boundaries are investigated. For this reason, the correlation length of the one dimensional random field $\theta_{boundary}$ is increased, while keeping the spatial variability of the upper and lower layers constant (table 6.2). The increase of the reliability of the system is shown in figure 6.5(b). Herein, a random

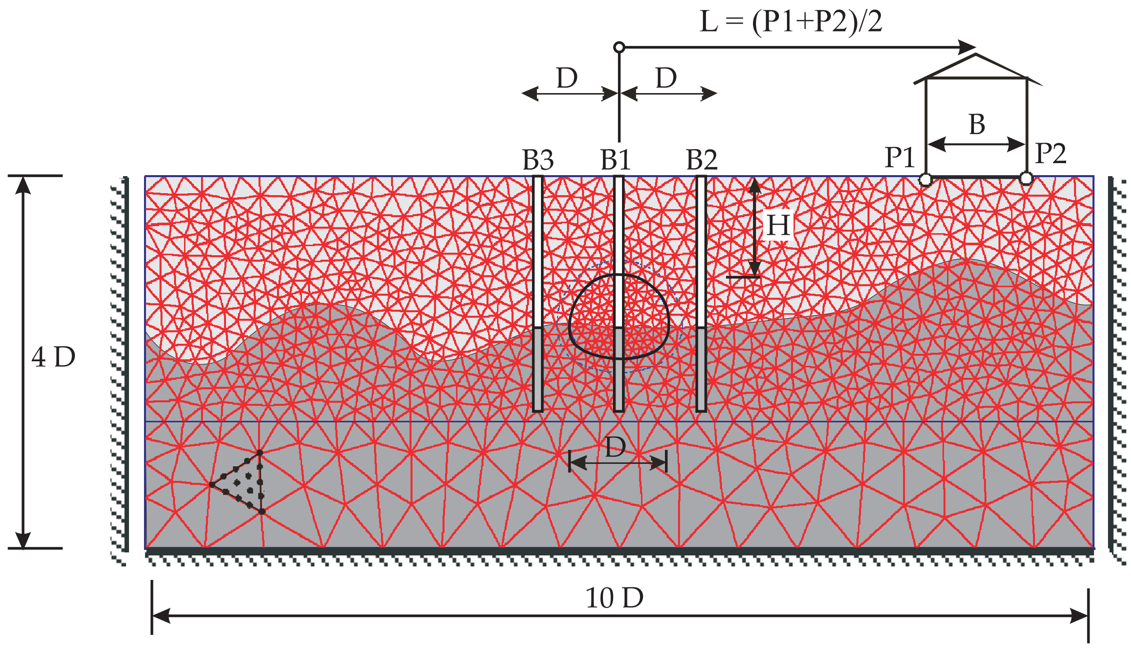

Figure 6.4: FEM mesh and location of the boreholes (B1,B2 B3).

Table 6.2: Material properties for the parametric study on tunnelling settlement in a layered soil.

Soil (linear-elastic, perfectly-plastic material model)				
upper layer			lower layer	
$\gamma' =$	$20\ \mathrm{kN/m^3}$		$21\ \mathrm{kN/m^2}$	
$\varphi' =$	$20\ ^\circ$		30°	
$c' =$	$30\ \mathrm{kN/m^2}$		$20\ \mathrm{kN/m^2}$	
$\nu =$	0.35		0.30	
$K_0 =$	0.34		0.34	
E-modulus	$\mu =$	$60\ \mathrm{MN/m^2}$	$\mu =$	$300\ \mathrm{MN/m^2}$
	COV =	50 %	COV =	50 %
	θ_h / D =	1	θ_h / D =	1
	θ_h / θ_v =	1-50	θ_h / θ_v =	1-50
			exponential correlation function	
Shotcrete (linear-elastic material model)				
d =	0.35 m			
$\gamma_{shotcrete} =$	$25\ \mathrm{kN/m^3}$			
E =	$7{,}500\ \mathrm{MN/m^2}$			
$\nu =$	0.20			

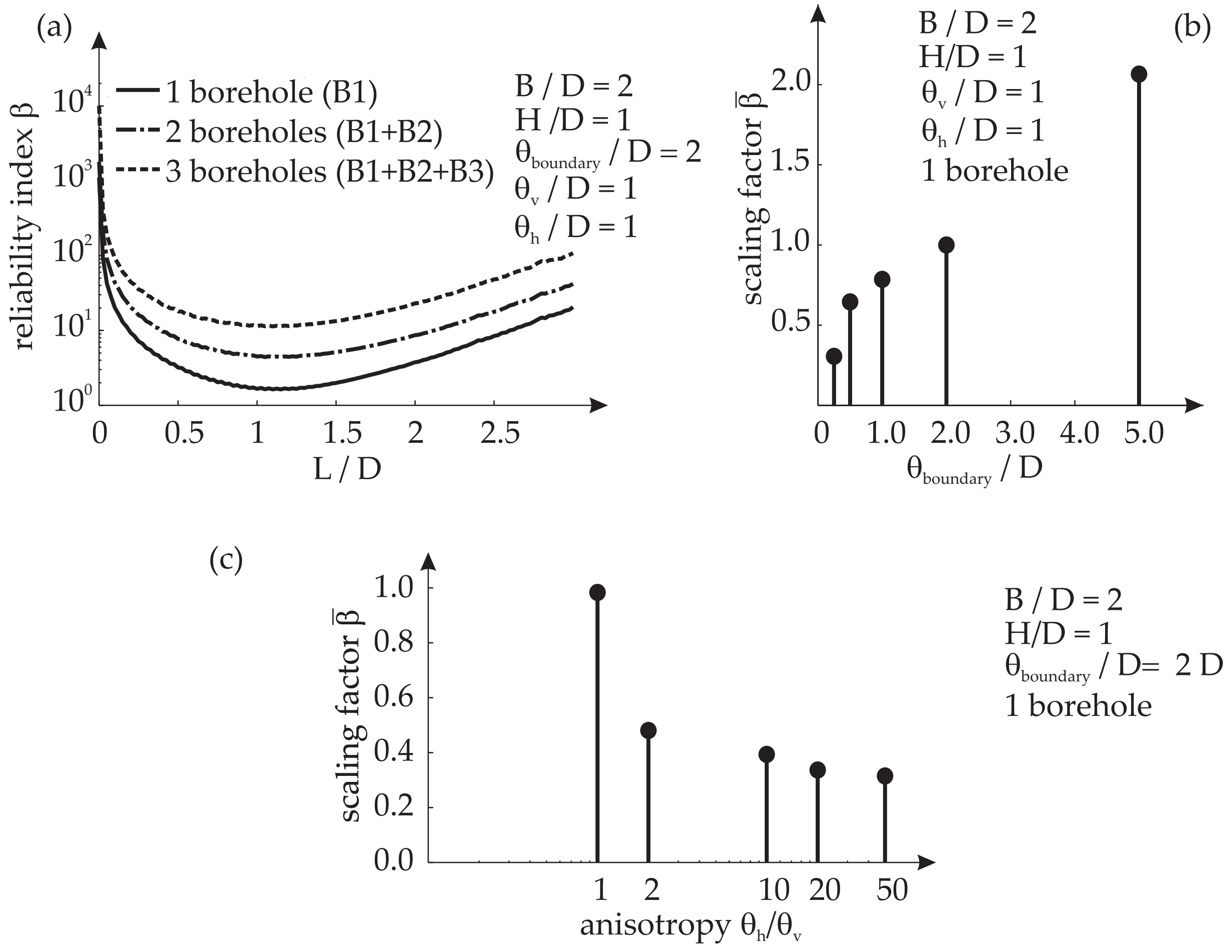

Figure 6.5: Results of parametric study on tunnelling in a layered soil.

process is conditioned to one borehole to simulate the boundary between the isotropic, homogeneous random fields of the upper and lower layers. Note that these random fields are unconditional and not conditioned to the borehole data. The effects of increasing values of $\theta_{boundary}$ are quantified via $\bar{\beta}$. This ratio $\bar{\beta}$ quantifies the effects of different values of $\theta_{boundary}$, which is normalized by the reliability index β with respect to $\theta_{boundary}/D = 2$ using one borehole for conditioning. It is clearly indicated in figure 6.5(b) that the boundary between both layers has a significant influence on the probability of damage, which is shown via the reliability index β. It can be concluded that a long correlation length of the stochastic boundary implies a larger reliability against damage of the building.

Another issue of interest is the effects of the anisotropy of the spatial correlations in the upper and lower layers. For this reason the spatial anisotropy θ_h/θ_v of the upper and lower layers are simultaneously stepwise increased. The boundary correlation length of $\theta_{boundary}/D = 2$ is kept constant. The results in figure 6.5 (c) show that, the larger the horizontal correlation lengths are, the bigger is the p_{damage} and the smaller is the reliability index β. Comparing the results of the figure 6.5 (b) and (c), one can see that the macro-scale variability of the boundary between the soil layers has more effect than the spatial anisotropy θ_h/θ_v within the layers.

6.1.5 Conclusions

This case study investigates the effects of spatial soil variability on a complex soil-structure interaction problem. The surface settlements are used for a simplified analysis of differential settlements of a rigid building, which are introduced by shallow tunnelling. These surface settlements are calculated on the basis of the linear elastic, perfectly plastic Mohr-Coulomb model and they are used to estimate the probability of damage of a building. Within this, the interaction between subsoil and the weightless and rigid building is investigated.

Although these assumptions simplify this complex soil-structure interaction problem, the effects of the spatial variability of the soil is quantified via the probability of damage by varying geometrical properties (location of the building L, width of the building B) and stochastic soil properties (coefficient of variation $\mathrm{COV_E}$, horizontal correlation length θ_h, vertical correlation length θ_v and the ration θ_h/θ_v). Within this, the single layered subsoil is assumed to have spatially correlated properties.

In addition to this, the effects of spatial variability of the stiffness at different scales are investigated. This is done in a simplified way: The medium-scale spatial variability of the stiffness is represented by random fields. The large scale spatial soil variability is considered by introducing two different layers. Herein, a stochastic process is separating the two layers, which are represented by random fields. At first, the stochastic process is conditioned to one borehole. It is found that additional boreholes for conditioning the stochastic process lower the probability of damage. Moreover, it is shown that a large correlation length of the stochastic process also lowers the probability of damage. Similar effects are observed for a large ratio of anisotropy θ_h/θ_v.

The presented case studies indicate the effects of spatial soil variability by using simplified approaches for estimating the probability of damage. Additional investigations on the soil-structure interaction should be carried out using advanced constitutive soil models. These studies would contribute quantitatively to the presented results.

Above all, it has to be pointed out that spatial soil variability is three dimensional and it cannot be fully described by two dimensional investigations. Therefore, only 3D RFEM studies can fully evaluate the impacts of the spatial variability of soil properties at different scales.

However, the uncertainty quantification, used in the case studies in chapter 5, is not fully performed. Although random fields are employed to represent the spatial soil variability and to evaluate the response of the mechanical model, the sensitivity analyses are not performed due to the absence of adequate methods presented in literature. This asks for the development of new approaches for sensitivity analyses in order to quantify the contribution of spatially correlated variables to the system response.

6.2 Slope stability

The slope stability problem is a very general geotechnical problem. Not only in urban, but also in rural areas slope stability problems can occur because slope stability is concerned with the stability of natural slopes, excavations, embankments, dams, road cuts, mining pits or landfills, [86].

The main objectives of slope stability analysis are finding endangered areas, investigation of potential failure mechanisms, determination of the slope sensitivity to different triggering mechanisms, designing of optimal slopes with regard to safety, reliability and economics, designing possible remedial measures, e.g. barriers and stabilization, [355].

Due to the importance of the slope stability problem, lots of scientists have been dealing with this issue from a deterministic as well from a probabilistic perspective. The probabilistic analysis of slope stability has been in the focus of science since more than 40 years e.g. [114, 371, 383, 407, 414] and is still a topic of ongoing research [157, 158, 254, 266, 355, 391]. These investigations are focusing on the effects of uncertain soil parameters including spatial variability as well as time dependent seepage forces.

This case study progresses this line of research. The influence of soil variability and spatial variability on a single-layered soil slope is investigated in two dimensional slope stability calculations. These calculations are compared to each other using different approaches including different correlation functions describing spatial variable soil properties and different random field generators. In addition to this, the effects of the anisotropy of spatial correlation on the slope reliability are investigated. Also a two-layered slope is investigated incorporating different scales of spatial variability. The sensitivity analysis of this problem helps to understand the contributions of the different sources of uncertainty and the different scales of variability to the failure probability of the systems.

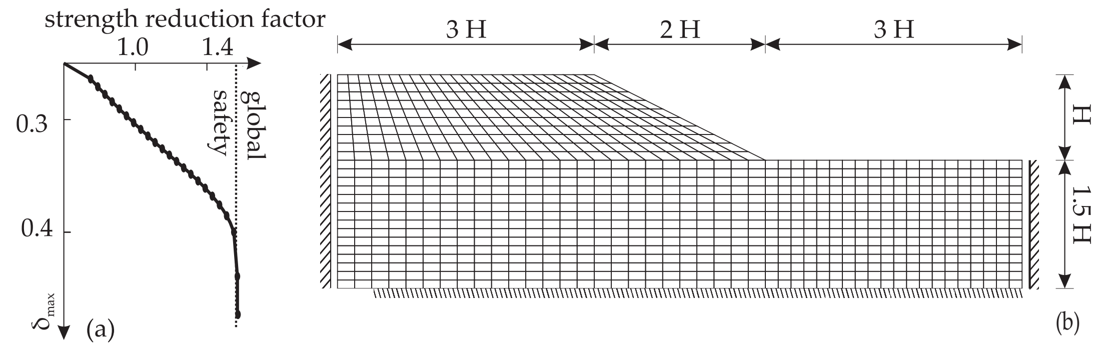

Figure 6.6: (a) Strength reduction factor versus maximum settlement of a 2D homogeneous slope ($c' = 50$ kN/m^2, $\varphi' = 0$) and
(b) FEM mesh of the investigated slopes with 8-noded, quadrilateral elements.

6.2.1 Mechanical description of the problem

Conventional slope stability analysis: Amongst others, Craig [86] reports that the stability of a slope is usually assessed using limit equilibrium methods. Stability analysis using the limit equilibrium approach involves solving the equilibrium problem by assuming force and/or moment equilibrium.

Over the years, many limit equilibrium methods for slope stability analysis have been developed and applied in practice, including the ordinary method of slices of Fellenius, Bishop's modified method, force equilibrium methods, Janbu's generalised procedure of slices, Morgenstern and Price's method and Spencer's method. These methods have been used for slope stability charts, which are useful for a preliminary analysis and a quick estimation of the stability of slopes [86]. However, in practice, detailed slope stability analysis is usually performed using a computer program and most of the available computer programs are based on the limit equilibrium approach.

In the conventional limit equilibrium approach, the stability of a slope is measured by the factor of safety (FOS), which is defined as the ratio between the shear strength of the soil to the shear stress required for limit equilibrium.

Finite Element Method for slope stability analysis: The finite element method (FEM) is a powerful technique for slope stability analysis. Herein, the strength parameters of the soil are reduced until the collapse of the system, which is called the strength-reduction method. The strength reduction method is illustrated by the strength reduction factor versus maximum settlement plot in figure 6.6 (a) for the FEM mesh shown in figure 6.6 (b). Although the FEM has been commonly used in the deformation analysis of embankments and other geotechnical problems, it is still not widely used for the stability analysis of slopes as compared with the conventional limit equilibrium methods [86, 147]. This can be deduced to the simplicity of the latter approach and to the available computer programs usually providing a quick and accurate estimation of the FOS of a slope.

In contrast, the FEM involves more complex theory and it usually requires more time for developing model parameters, performing the computer analyses and interpreting the results as described in detail in Smith & Griffiths [342].

Despite this, the FEM as in several advantages over the conventional limit equilibrium methods, as stated by Griffiths & Lane [147]:

- No assumption is required in advance with respect to the shape and location of the slip surface. Therefore, the failure finds its way through weak zones of the soil.
- There is no need to make assumptions about internal forces, which appear to be one of the major sources of inaccuracy for some limit equilibrium methods. The finite element method preserves global equilibrium until "failure" is reached.
- The FEM solution provides information about deformations at pre-failure stress levels if realistic soil stiffness parameters are used.

- The FEM is able to provide information on progressive failure up to and including overall shear failure.

Smith & Griffiths [342] state that the FOS computed by the FEM is in good agreement with that calculated by limit equilibrium methods, which is proven by various studies.

6.2.2 Parametric studies of single-layered soil slopes

Influence of soil variability on slope reliability: The aim of this section is to investigate and quantify the effects of the coefficient of variation and the spatial variability of soil properties on the estimated probability of failure p_f of a slope. For this reason, numerical studies are conducted using a modified version of the FEM programme of Smith & Griffiths [342] within the framework of MATLAB and of the FERUM libraries [49].

Within this section, the author does not follow methods like the First-Order-Second-Moment approach or Point-Estimate-Methods linked with limit equilibrium methods as published by [114, 265] amongst others, but the Monte Carlo approach with numerical methods as proposed by Fenton & Griffiths [127] and Hicks & Spencer [158] amongst others.

The First-Order-Reliability-Method (FORM) is used to evaluate the reliability of the slope shown in figure 6.6 (b). The cohesion c′ is considered as random variable as indicated in table 6.3 without taking spatial variability into account. The effects of the increase of soil variability on the probability of failure p_f and on the reliability index β is shown in figure 6.7. The probability of failure p_f is significantly higher for large $COV_{c'}$s than for low $COV_{c'}$s and vice versa in case of the reliability index β. This simple study does not take the spatially variability of the cohesion into account.

Influence of spatial variability on slope reliability: Therefore, the Random Finite Element Method (RFEM) approach [127] is used to quantify the effects of spatial variability. Within this RFEM study, random fields represent the spatial variability of a purely cohesive soil, which is represented by an idealised linear-elastic, perfectly-plastic soil model.

Table 6.3: Lognormal distributed input parameters of the parametric studies.

Soil properties			
soil unit weight	γ' = 21	kN/m^3	
friction angle	φ = 0°		
cohesion	c′	lognormal distribution	
		μ = 50 kN/m^2	
		$COV_{c'}$ = 10-100 %	exp. corr. function
		$\Theta = \theta/H$ = 1-10	
angel of dilatancy	ψ = 0°		
Poisson's ratio	ν = 0.3		
Geometry	height	H = 10 m	

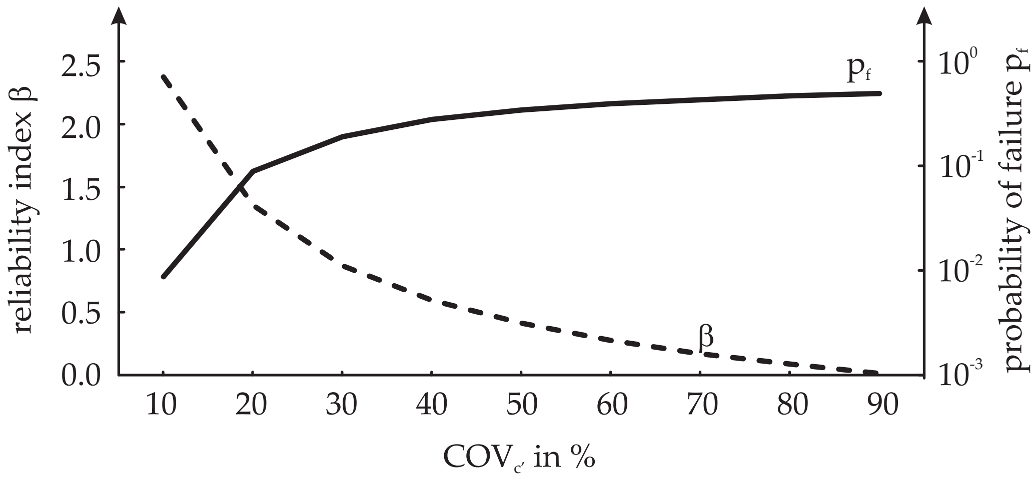

Figure 6.7: Effect of varying COV_c on the reliability index β and on the probability of failure p_f using lognormally distributed random variables for $\mu_c = 50$ kN/m^2.

On the basis of the Monte-Carlo approach in chapter 4.3.2, each random field realisation is represents a possible spatial distribution of higher and lower values, which influence the system response.

Following the concepts of Fenton & Griffiths [127], the COV and the correlation length of an isotropic random field of a cohesive slope are investigated using two different random field generators, namely Sequential Gaussian Simulation Method (SGSIM) and Sequential Indicator Simulation Method (SISIM). SGSIM and SISIM are basically similar in the way of random field generation, but differ in the representation of spatial correlation, as explained in appendix E. In the case of SISIM random fields, also the extreme high and low values have a spatial correlation in contrast to SGSIM random fields. This can be considered in the SISIM approach via different indicator correlation lengths. A more detailed explanation of the differences and similarities of these approaches can be found in Appendix E. The results of the case studies on the evaluation of the spatial variability of soil properties in chapter 3 clearly indicated that the investigated measurement data cannot be fully described by a mean value, a standard deviation and only one single spatial correlation function. Therefore, the SISIM approach is employed to investigate the effects of this.

The libraries of GSLIB [97] are used for the generation of random fields, which are used as input for the modified Monte-Carlo approach inside the RFEM framework, described in section 6.1.3. After checking the convergence of the mean and standard deviation of the REFM results, a normal distribution function is fitted to the simulation results via the best-fit criterion in order to estimate the p_f. Via this simplification it is possible to investigate also small failure probabilities within reasonable computation times.

In the figure 6.8 (b) the effect of the normalized isotropic correlation length $\Theta = \theta/H$ on reliability index β for $COV_c = 20\%$ can be seen. The reliability index of small normalized correlation lengths is significantly higher than for large correlation lengths. Similar results are reported Fenton & Griffiths [127].

Moreover, it is interesting to compare the outcomes of the different random field gen-

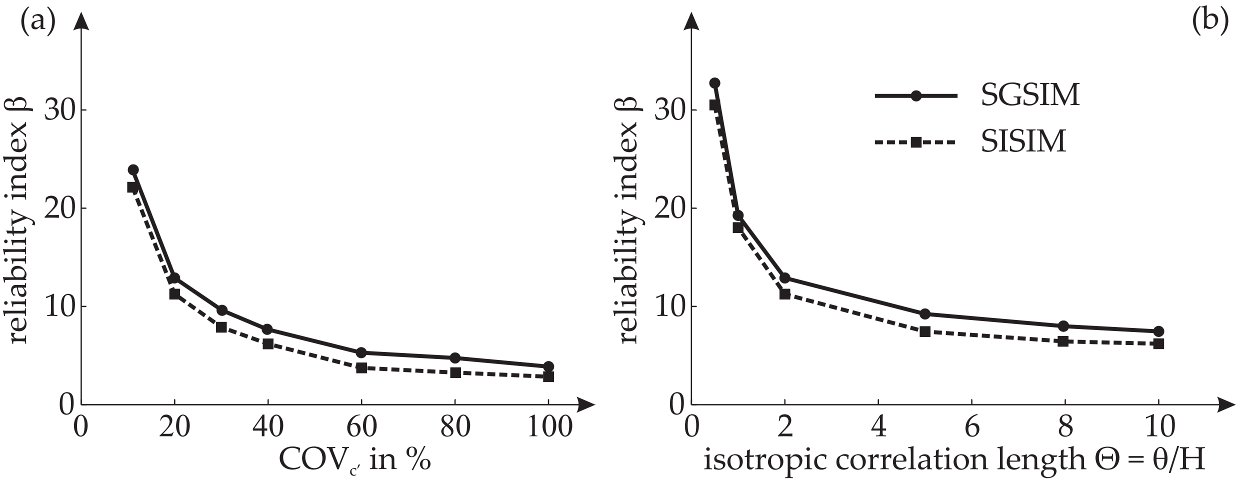

Figure 6.8: (a) Effects of varying COV$_c$ on the probability of failure using different random field generators with a $\Theta = \theta/H = 2$ and random variables for $\mu_c = 50$ kN/m^2 ;
(b) effects of varying $\Theta = \theta/H$ on the probability of failure for different random field generators in comparison to random variables with a COV$_{c'} = 20\%$.

erators SGSIM and SISIM. As pointed out before, the SGSIM and LAS approach are used in well known publications e.g. [127, 156, 158] due to their simplicity in describing a random field by the mean value, a standard deviation and one correlation function. Comparing the results in figure 6.8, one can deduce that the influence of the spatial correlation structure simulated via SGSIM and SISIM is offering comparable results. Although the differences between the two approaches are relatively small, the SISIM approach offers slightly lower reliability indices for the same spatial correlation lengths; the SGSIM random fields only differ in terms of the indicator correlation length, as described in detail in appendix E.4.

Additional conclusions can be drawn from figure 6.8 (a). Herein, the COV$_c$ has been increased while keeping the isotropic correlation length constant. This offers a clear insight into the effect of increasing COV$_c$, which is similiar to the presented uncertainty quantification of a single-layered soil slope using random variables instead of random fields, which represent soil variability. The bigger the COV$_c$ of the soil the more unreliable is the slope.

By comparing figures 6.7 and 6.8, one can deduce that the consideration of spatial variability results in a higher slope reliability. In the case of an infinite correlation length, all elements of a random field are fully correlated; therefore, the results of the RFEM and reliability methods are assumed to converge. If there is a very small spatial correlation of the cohesive soil, every single element of the random field is theoretically independent. As a consequence, there will be no variation of the system response between each realisation of a random field. In this case the slope stability problem is just influenced by the mean value and the reliability index is infinity.

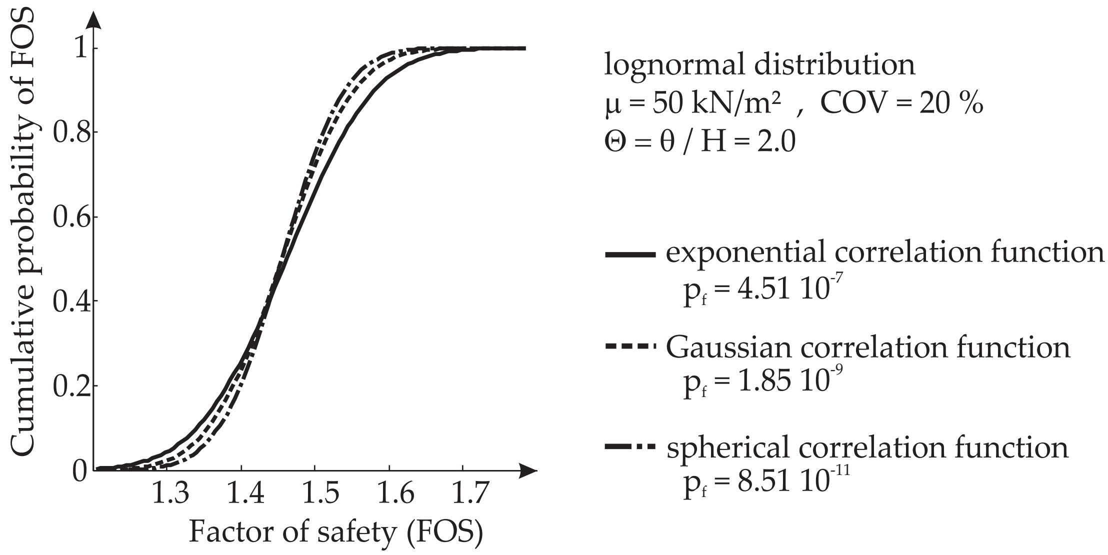

Figure 6.9: Influence of the spherical, exponential and Gaussian correlation function on the probability of failure of a slope.

Influence of the correlation function: An additional parametric study is carried out within the RFEM framework to focus on the influence of the spatial correlation function. For this reason, the spherical, exponential and Gaussian correlation functions are used within the Sequential Gaussian Method to generate 300 isotropic random field realisations as input for the modified Monte-Carlo approach. It can be seen in figure 6.9 that the resulting p_f values differ a lot and vary from $p_f = 4.51 \cdot 10^{-7}$ to $8.51 \cdot 10^{-11}$. The exponential correlation function shows the highest p_f in comparison to the other functions. Therefore, this exponential correlation function is used within this chapter for the generation of random fields.

Sensitivity analysis of the reliability of a single layered soil slope: Within this presented investigation, the influence of the stochastic properties is shown. One can clearly see the effect of an increasing or decreasing spatial correlation and $\text{COV}_{c'}$. The transfer of these findings to a practical situation is rather difficult, because at one site there will not be a wide range of correlation lengths or COVs as shown in figure 6.8. As shown in the results of previous chapter 3, one will get a probability density function (pdf) of the correlation length as a result of the Bayesian Model Averaging approach of measurement data, results presented in literature, correlation lengths derived from experiments in comparable soils and expert knowledge. Linking this with the results of the parametric studies shown in figure 6.8, it is possible to calculate the most probable system behaviour due to the probability density function of the correlation length. This idea offers the calculation of one single value of p_f of the single-layered soil slope. Also the surrogate model of polynomial-chaos-expansion (PCE) polynomial can be employed to approximate the system response, which offers as a by product the basis for the global sensitivity analysis.

Table 6.4: Lognormal distributed input parameters of the parametric study.

		mean value	COV
cohesion c'	mean value $\mu_{c'}$	50 kN/m^2	25 %
	coefficient of variation $COV_{c'}$	50 %	10 %
	horizontal correlation length $\Theta_{hor} = \theta_{hor}/H$	0.35	10 %
	vertical correlation length $\Theta_{ver} = \theta_{ver}/H$	7.00	10 %

For this reason, the PCE approach is used within the concept of the Random Finite Element Method (RFEM). This PCE mimics the system behaviour and represents the mechanical system in a mean way as shown in appendix G. As outlined in section 4.4.2, the global sensitivity indices can be calculated analytically by the presented formulae, which quantify the sensitivity of the input parameters on p_f.

Within this, the sensitivity of the uncertain variables for a 2D reliability analysis of the slope is shown in figure 6.16. The mean value, the coefficient of variation and the correlation lengths Θ_{hor} and Θ_{ver} are considered as stochastic variables as indicated in table 6.4. The system behaviour is approximated by a PCE at the different PCE evaluation points. 300 random field realisations are used for the computation of a mean system behaviour at each PCE evaluation point. The results are approximated by a normal distribution function, which allows one to extrapolate also small failure probabilities. Although this approach is speeding up the evaluation of the system response significantly, there is still a big computational effort for this study.

The fitting of the PCE to the system response is carried out with the approaches described in section 4.3.3 and shown in figure 6.10. It can be derived from figures 6.10 (a) and (b) that the expansion order M $= 3$ is enough to represent the system. By looking at the determination coefficient Q_2, one can see that the fitting of the PCE is accurate to almost 100 % for the expansion order M = 3. Besides this, it can be clearly derived from these results that the determination coefficient, the adjusted determination coefficient and the Q_2 determination coefficient quantify the fitting of the PCE-approximation clearer in comparison to the empirical error or PRESS. Therefore, the author recommends to used the determination coefficient and the Q_2 determination coefficient in this context.

One can clearly deduce form the global sensitivity measures in figure 6.15 (c) that the mean and COV of the cohesive soil are - as expected - the most influencing variables; the vertical correlation length is far less important than the horizontal one. From this, one can conclude that the vertical correlation length has a lower influence than the more dominating horizontal correlation length. As a consequence, more effort should be put into the investigation of the horizontal correlation length.

Effects of anisotropy of the spatial correlation on the probability of failure: As pointed out in chapter 2.4.1, the spatial variability of natural soils is anisotropic. Hicks & Spencer [158] point out that man-made deposits have a ratio of the horizontal and vertical correlation length of $5 < \theta_{hor}/\theta_{ver} < 25$, which is smaller than the ratio of natural soils with $\theta_{hor}/\theta_{ver} > 25$ as reported by Hicks & Samy[157].

Hicks & Spencer [158] identified in extensive three dimensional RFEM studies three

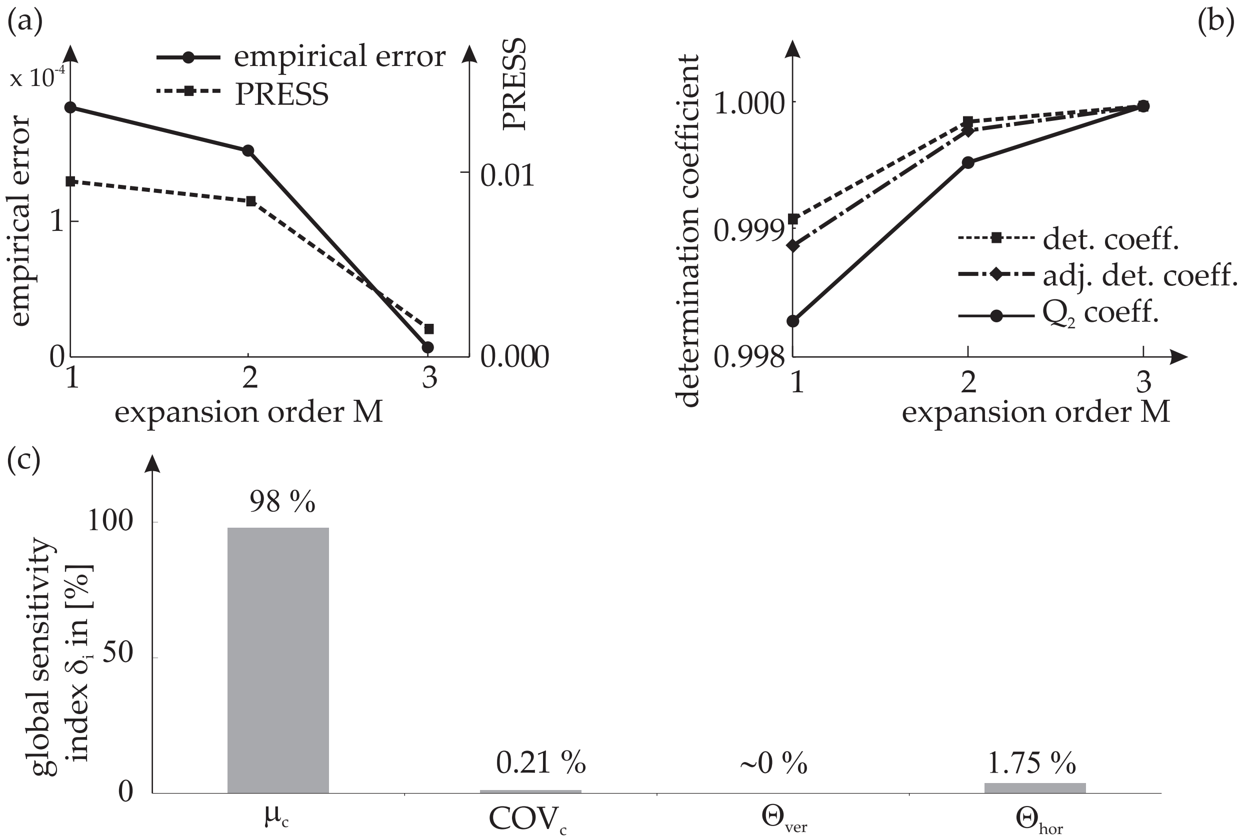

Figure 6.10: Different measures for the accuracy of the PCE to the system response of a 2D slope stability analysis (a,b) and (c) global sensitivity measures of the input variables.

different three failure modes, as illustrated by the typical deformed meshes and contours of horizontal (out-of-face) displacement shown in figure 6.11. These modes depend on the value of θ_{hor} relative to slope geometry, as defined by the slope height (H_S) and length (L), and are summarised as follows [158, 266]:

- Mode 1: For $\theta_{hor} < H_S$ there is little opportunity for failure to develop through semi-continuous weaker zones. Hence, failure goes through weak and strong zones alike, there is considerable averaging of property values over the failure surface, and the slope fails along its entire length. This case is analogous to a conventional 2D analysis based on the mean value, [266].

- Mode 2: For $H_S < \theta_{hor} < L/2$, there is a tendency for failure to propagate through semi-continuous weaker zones, leading to discrete 3D failures and a decrease in reliability as the slope length increases. Hicks & Spencer [158] showed how probabilistic theory could be used to predict the reliability of longer slopes based on the detailed 3D stochastic analysis of shorter slopes.

- Mode 3: For $\theta_{hor} > L/2$, the failure mechanism reverts to along the slope length. Although it is similar in appearance to Mode 1, it is a fundamentally different mecha-

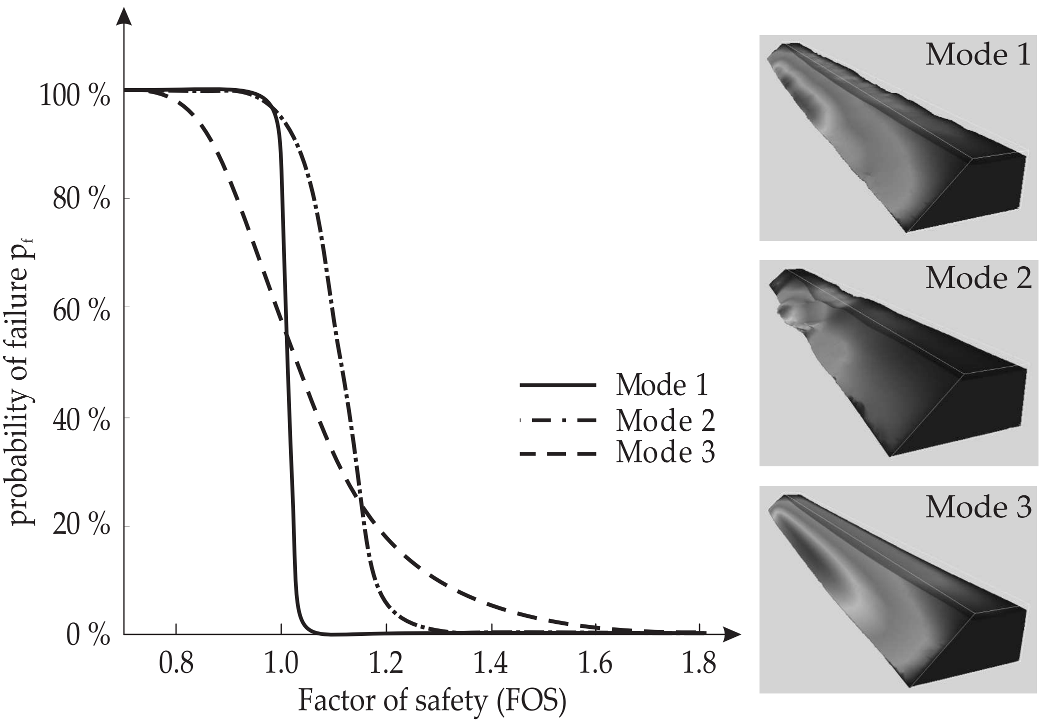

Figure 6.11: Different failure modes derived in Hicks & Spencer [158].

nism. In this case, failure propagates along weaker layers and there is a wide range of possible solutions that depend on the locations of these layers. The solution for this mode is analogous to a 2D stochastic analysis.

Effects of $c-\varphi$ correlation on the probability of failure: The results discussed so far are based on the assumption of purely cohesive material, which can be represented by a random variable or a random field. The next step is modelling the soil as a cohesive-frictional material, as mentioned by Chock [81]. Moreover, Chock [81] presents a study on the influence of the cross correlation $\rho_{c',\varphi'}$ between the effective cohesion and the effective friction angle on the probability of failure of slopes. The results of [81] indicate that, for all cases of COV and correlation lengths, negative correlation correlation $\rho_{c',\varphi'}$ leads to a lower estimate of the probability of failure, while a positive correlation $\rho_{c',\varphi'}$ leads to a higher estimate of the probability of failure.

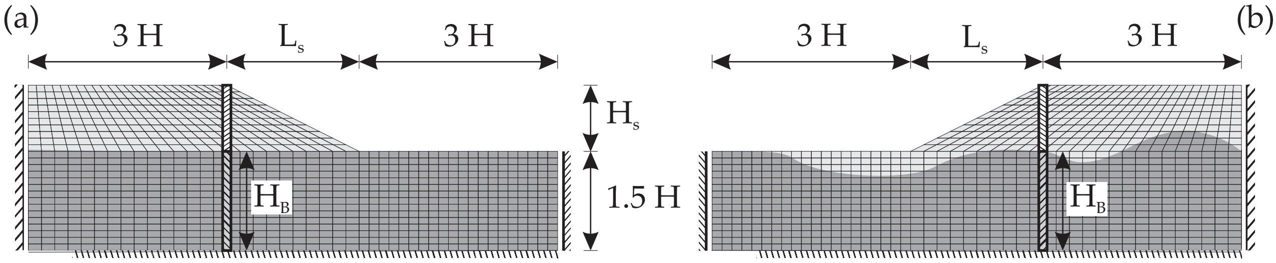

Figure 6.12: Geometry of the layered slope including one borehole using random variables (a) and random fields (b).

6.2.3 Parametric studies of two-layered soil slopes

In the previous section, the influence of soil variability on a single-layered soil slope is investigated. This concept is extended to a more general basis. In the following, the slope soil profiles consists of two soil layers with different properties.

The uncertainty of the layer boundary and geometry of the slope is investigated using a the framework of reliability based design (RBD).

Uncertainty quantification using random variables At first, the uncertainties of the strength properties are taken into account for the uncertainty quantification in case study I.A as indicated in table 6.5. In addition to this, the depth of the lower layer is considered as a lognormal distributed variable in case study I.B. Moreover, the boundary between the upper and lower layer is assumed to be a horizontal line in case study I.C, as shown in figure 6.12 (a).

In figure 6.13 the results of CASE STUDY A are shown. One can clearly see in figure 6.13 (a) the effects of taking different random variables into account. It is clear that the system in CASE STUDY I.A is more reliable than in CASE STUDY I.B, due to the uncertainty in the geometry (H_S, L_S). By considering H_B as an additional random variable in CASE STUDY I.C, the resulting reliability is even smaller. From these results it can be deduced that, the more uncertain variables that are introduced into a reliability analysis, the lower is the system reliability. However, it can also be possible that additional correlation between the random variables leads to different results. Furthermore, it is shown that an uncertain geometry of this slope problem introduces a significant uncertainty into the stability.

Uncertainty quantification including spatial variability of soil properties at different scales: But the consideration of the soil layer boundary as a simple horizontal line might not capture reality. The layering can be interpreted as large scale spatial variability, as indicated in section 2.4.1. Chiles & Delfiner [79] state that geological uncertainty can be considered via so called categorical variables. They [79] describe the spatial distribution of soil types via so called categorical variables, which can be described by multivariate distributions. These concepts can only be used in the presence of detailed soil

Table 6.5: Lognormal distributed input parameters of the CASE STUDIES I, II and III.

	upper layer		**lower layer**		**layer boundary**	
	μ	COV	μ	COV	σ/H	$\Theta_{boundary}$
CASE STUDY I.A						
cohesion c'	10 kN/m^2	10 %	11 kN/m^2	20 %	0	∞
friction angle φ'	25°	10 %	33°	20 %		
slope height H_S	20 m	deterministic				
slope length L_S	15 m	deterministic				
depth of the lower layer H_B	10 m	deterministic				
CASE STUDY I.B						
cohesion c'	10 kN/m^2	10 %	11 kN/m^2	20 %	0	∞
friction angle φ'	25°	10 %	33°	20 %		
slope height H_S	20 m	10 %				
slope length L_S	15 m	10 %				
depth of the lower layer H_B	10 m	deterministic				
CASE STUDY I.C						
cohesion c'	10 kN/m^2	10 %	11 kN/m^2	20 %	0	∞
friction angle φ'	25°	10 %	33°	20 %		
slope height H_S	20 m	10 %				
slope length L_S	15 m	10 %				
depth of the lower layer H_B	10 m	1 %				
CASE STUDY II						
cohesion c'	10 kN/m^2	10%	11 kN/m^2	20 %	0.5	0.10 to ∞
friction angle φ'	25°	10 %	33°	20 %		
$\Theta_{hor} = \theta_{hor}/H = \Theta_{ver}$	1.1		1.1			
slope height H_S	20 m	deterministic				
slope length L_S	15 m	deterministic				
depth of the lower layer H_B	10 m	deterministic				
CASE STUDY III						
cohesion c'	10 kN/m^2	10%	11 kN/m^2	20 %	0.1 to 1	
friction angle φ'	25°	10 %	33°	20 %		
$\Theta_{hor} = \Theta_{ver}$	1.0	10 %	2.0	20 %		
$\Theta_{boundary}$	10	10%				
slope height H_S	20 m	deterministic				
slope length L_S	15 m	deterministic				
depth of the lower layer H_B	10 m	deterministic				

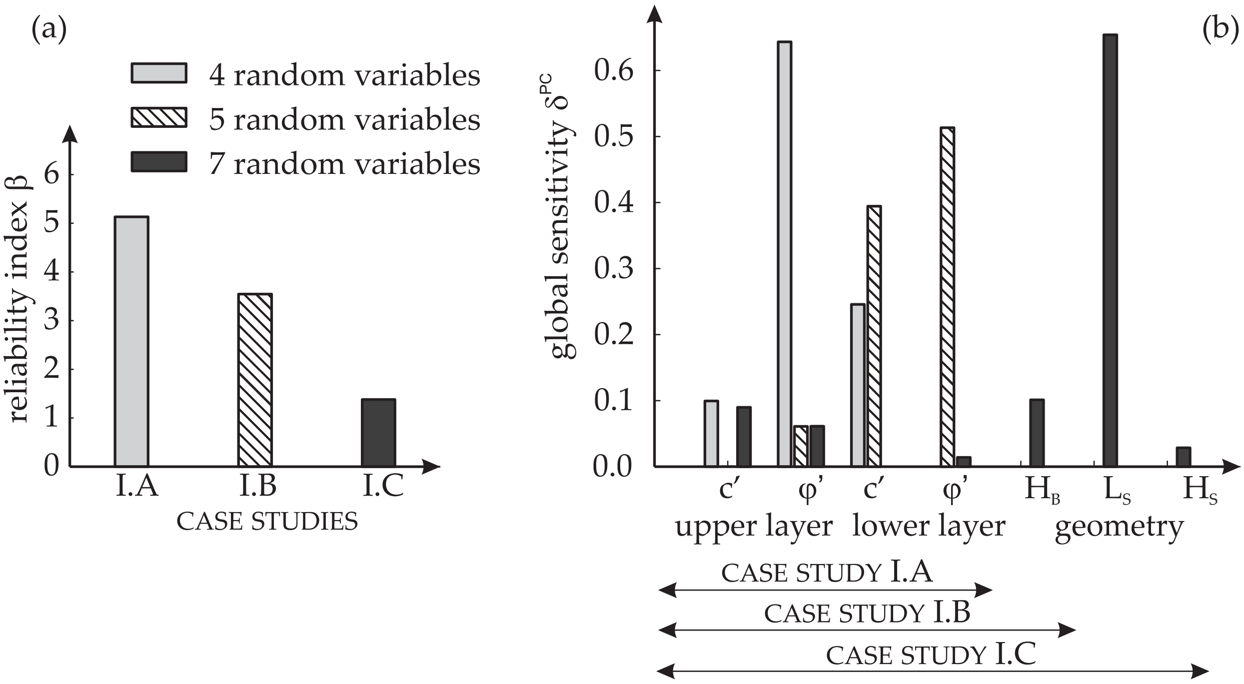

Figure 6.13: CASE STUDY I: Reliability evaluation of a two layered slope stability problem (a) and the corresponding global sensitivity measures (b).

investigations like in reservoir engineering, which are usually not present in geotechnical engineering.

Therefore, a simplified approach is set up. The combination of macro- and meso-scale variability of soil properties is captured via a two step procedure: at first, the borderline between the upper and lower layer is simulated via a one-dimensional random field, which is conditioned to the soil investigation as shown in figure 6.12 (b). The SGSIM-random fields of the strength properties of the upper and lower layer are generated and mapped on the FEM mesh via the local averaging approach. The stochastic properties are summarized table 6.5.

CASE STUDY II is conducted to simulate the soil layer boundary as a simple horizontal line and alternatively as a one dimensional random process, which is conditioned to a soil investigation at the head of the slope as indicated in figure 6.12 (b). The properties of both layers are shown in table 6.5. This illustrative example is showing the influence of spatial variability at two scales; Figure 6.14 shows the scaling factor $\bar{\beta}$ with respect to the correlation length $\Theta_{boundary} = \theta_{boundary}/H$ and the variance $\sigma^2_{boundary}$ of the stochastic process, which is representing the boundary between the lower and upper layer. The normalized reliability index $\bar{\beta}$ is scaled by the reliability index β of CASE STUDY I.A. One can clearly see that the reliability is decreasing with a bigger variance $\sigma^2_{boundary}$ and a longer correlation length $\Theta_{boundary}$. The influence of the stochastic process between both layers is vanishing in the case of an infinite correlation length $\Theta_{boundary}$. The probability of failure is significantly higher in the presence of spatial variability of both layers. It can be concluded that the consideration of spatial variability is an important step towards

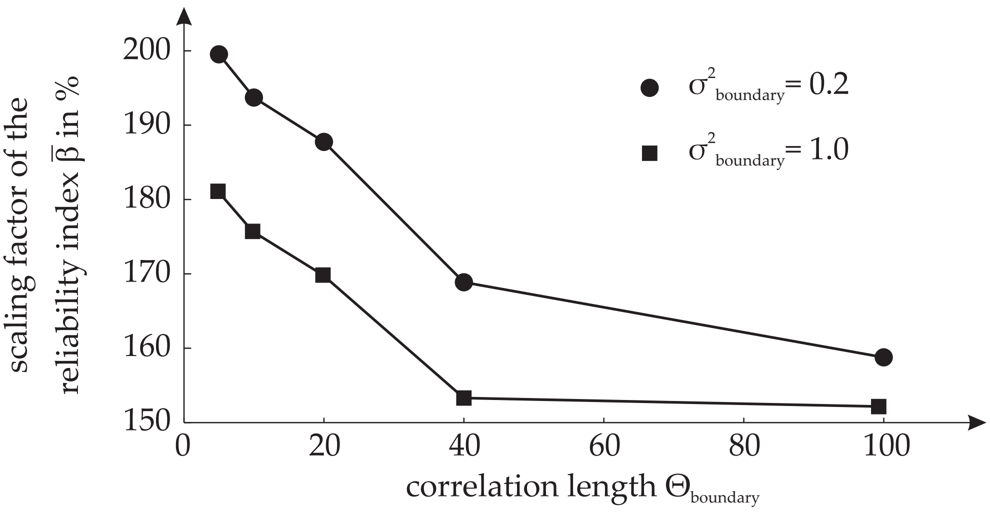

Figure 6.14: CASE STUDY II: Normalized reliability index of different RFEM approaches for a two layered slope with respect to a varying $\Theta_{boundary} = \theta_{boundary}/H$.

realistic modelling of the presented problem.

Sensitivity analysis of a layered soil slope: The global sensitivity is investigated by combining the RFEM approach with the PCE approximation of the system response. By employing the PCE-approach, it is possible to derive the global sensitivity measures δ_i^{PC} analytically. The results of CASE STUDY II are extended in the sense that also the uncertainty of the boundary correlation length $\Theta_{boundary}$ is taken into account. The stochastic soil strength parameters of both layers as well as the stochastic boundary between the layers are listed for CASE STUDY III in table 6.5.

The accuracy of PCE-approximation is estimated for different PCE expansion orders using different determination coefficients in figure 6.15. The calculated determination coefficients indicated are approximately 100 %, which implies that the PCE representation for M = 5 cannot be significantly improved by introducing a higher expansion order.

Therefore, the expansion order M = 5 is used for deriving the global sensitivity measures δ_i^{PC}. In figure 6.16 one can see that the sensitivity for the boundary correlation length $\Theta_{boundary}$ is more influential than the influence of the isotropic correlation length of the upper layer. Figure 6.16 shows also the sensitivities δ_{ij} between the investigated properties. However, the other investigate sensitivities are below 10 % and therefore one can neglect these sensitivity measures.

6.2.4 Conclusions

This case study investigates reliability of single- and a two-layered soil slopes. Herein, a linear elastic perfectly plastic constitutive model on basis of the Mohr-Coulomb criterion is used in a 2D FEM model.

At first, the effects of spatial soil variability are quantified for single layered soil slopes, which are compared to slopes with random and not spatially correlated soil properties.

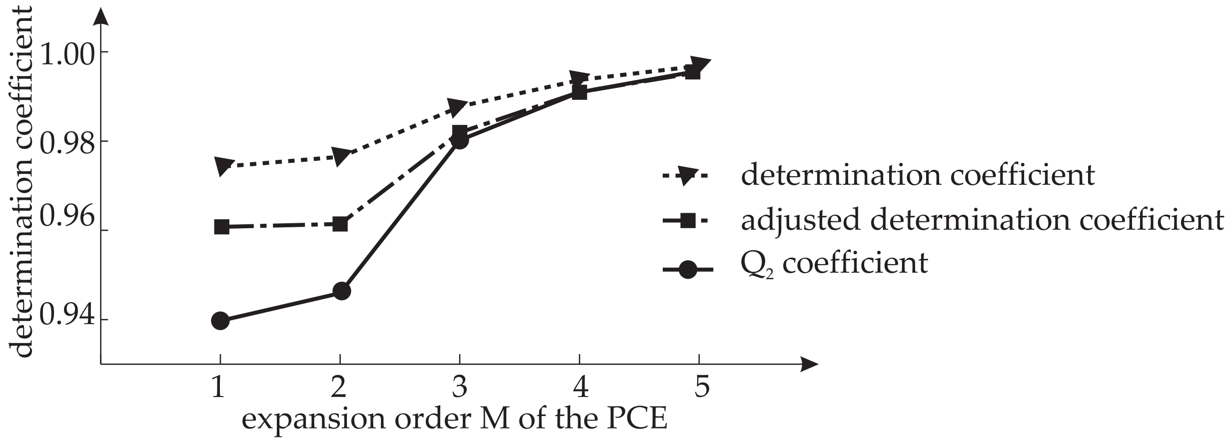

Figure 6.15: CASE STUDY III: Different determination coefficients for the PCE accuracy.

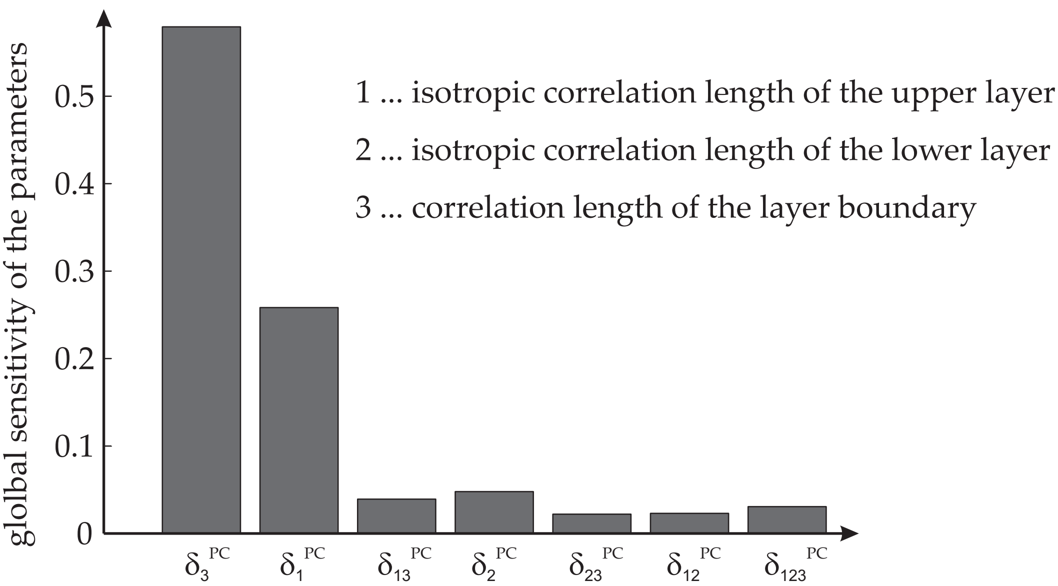

Figure 6.16: CASE STUDY III: Global sensitivity measures δ_i^{PC} for the isotropic correlation length of the upper layer (1) and the lower layer (2) as well as for the layer boundary (3) for the PCE expansion order M = 5.

Within the investigation of the effects of different correlation function on the reliability of single layered soil slopes, the exponential correlation function is identified as the most conservative one. Moreover, it is shown that different complex correlation structures of spatial variability, which are simulated by SGSIM and SISM algorithms, do not have a major effect on the calculated probability of failure.

The influences of mean value, coefficient of variation, correlation function and random field generators are investigated within the RFEM framework. Besides this, the effects of the mean value, the coefficient of variation and the anisotropy of the horizontal and vertical correlation length are quantified within a novel sensitivity analysis within the RFEM framework. It is shown that the mean valued, the coefficient of variation and the horizontal correlation length have the biggest influence on the probability of failure, whereas the contribution of the vertical correlation length is very small.

The effects of spatial variability at different scales is in the focus of additional parametric studies on two-layered soil slopes. Again the importance of spatial soil variability is highlighted by comparing the effects of random properties and spatially correlated random properties. Within this study the effects of an uncertain geometry are investigated. It is shown that the slope geometry and the soil layering have a bigger influence in comparison to the stochastic soil properties. The effects of spatial soil variability at different scales are quantified with respect to random soil properties. The spatial variability at the large scale and the spatial variability of the upper layer are contributing the most to the probability of failure of the investigated two layered soil slope.

The presented studies are fundamental investigations on the effects of soil variability. These studies can be enriched by additional investigations using 3D slope stability analyses, which would contribute to the quantification of the effects of spatial variability for slope analyses. In addition to this, the investigation of the uncertain slope geometry would offer additional insight into 3D slope stability analyses.

The presented findings can be further extended by additional 3D slope stability analyses, which would represent more exactly the spatial variability of the subsoil.

6.3 Risk based characterisation of an urban site

When planning new surface or underground infrastructures, it is vital to anticipate what geological conditions are likely to be encountered even before taking any specific survey or investigations works, as stated by Raspa et al [301]. An improved assessment of geometry and mechanical properties of underground layers would minimize project risks, from an economical point of view as well as from a technological point of view.

Faber & Stewart [122] define risk is a random event that may possibly occur and, if it did occur, would have a negative impact on the goals of the project. Thus, a risk is composed of three elements: the scenario, its probability of occurrence; and the size of its impact, if it did occur. Geological risk is defined by De Marsily et al. [88] as any geological conditions, which represents a potential threat to health, safety or welfare of people. Public administrations, civil protection agencies and research institutions are continuously involved in managing environmental hazards and planning future developments of urban areas, which both require in-depth knowledge of the subsoil as stated by Raspa et al. [301] amongst others [127, 149, 273].

The aim of this case study is to show a procedure of risk based site characterisation, which is employed to quantify the effects of macro-scale soil variability. Herein, the damage estimation of buildings is performed, which is triggered by the uncertainty of geology. This damage estimation of rigid buildings is performed by the calculation of differential settlements of buildings using an advanced constitutive model. The uncertainty of geology is simulated via the Pluri-Gaussian simulation approach, which is capturing the uncertainty of the domain boundaries of three spatially distributed soil types. Moreover, this approach considers soil investigations, stochastic soil properties and expert judgement within a sound mathematical framework of categorical random field simulation.

6.3.1 Site description

Geological description of the subsoil: The investigated site is located in the urban area of Rome. Additional information on the location of the site and its geological settings are given in the Appendix H. The model of the subsoil of Roma consists of the integration and analysis of the main available geological and geotechnical data: stratigraphy, lithology and texture, physical and mechanical properties, and hydrogeology. Information from more than 6,000 boreholes and measured stratigraphic logs, geological maps, and in-situ tests were homogenized, classified, and archived in a database thus far, as described in Raspa et al. [301]. Geological information retrieved from the database was interpreted and encoded to reconstruct the stratigraphic framework of the Tevere Valley. Attention was specifically focused on the upper Pleistocene–Holocene alluvial deposits.

The investigated site is a part of a complex geological system. This fluvio-deltaic area consists of complex channels and floodplain areas, which changed over time. Due to this, the complexity of the subsoil is almost impossible to describe via deterministic approaches properly. Therefore, geostatistical simulation approaches offer a proper way to model the subsoil-uncertainty.

Table 6.6: Mean values and standard deviations of the lognormally distributed measurement and literature data.

		c' in kN/m^2		φ' in degree		E in MN/m^2	
		μ	σ	μ	σ	μ	σ
measurements							
I	gravel, medium and coarse sand	0.0	0.0	39.4	3.2	42.7	11.7
II	silty fine sand, sandy silt	9.9	8.3	35.3	3.2	16.3	6.0
III	silty clay, clayey silt, organic clay	14.6	11.6	23.8	3.2	3.3	1.6
IV	bedrock	75.9	2.9	23.5	1.0	61.0	0.0
literature data							
I	gravel, medium and coarse sand	0.0	0.0	31.5	1.8	45.0	12.5
II	silty fine sand, sandy silt	2.5	1.3	36.0	2.0	27.5	6.3
III	silty clay, clayey silt, organic clay	10.0	2.5	25.0	2.5	7.5	1.8
IV	bedrock	76.0	3.8	24.0	1.2	610.0	30.5
data combinded via the Bayesian approach							
I	gravel, medium and coarse sand	0.01	0.0	33.3	1.5	43.9	8.4
II	silty fine sand, sandy silt	2.7	1.2	35.8	1.7	21.8	4.4
III	silty clay, clayey silt, organic clay	10.2	2.4	24.6	2.0	51.6	1.2
IV	bedrock	75.9	2.1	23.7	0.8	61.0	0.1

Information from more than 2,000 boreholes penetrating these deposits was used by Marconi [238] to model their lithological and textural associations in a conceptual geological model. This model has been used as the basis for the geostatistical simulations. For this case study, only geotechnical boreholes with geotechnical information penetrating these deposits were selected to derive geomechanical properties of the subsoil. This set includes 283 boreholes and 719 samples.

Five main soil types are derived from this large dataset and summarized in table 6.6, which have been used in the latter to simulate the soil behaviour. SOIL TYPE I consists of gravel, medium and coarse sand, SOIL TYPE II of silty fine sand, and sandy silt, SOIL TYPE III of silty clay, clayey silt and organic clay and SOIL TYPE IV of bedrock. Table 6.7 provides the number of measurement data for the strength and stiffness properties of the different soil types. The author combined the measurement data with literature [346] data using the Bayesian approach. Via this, the description of the variability of the subsoil is enriched by the combination of measurements and expert judgement.

Simulation of the geological uncertainty. The uncertainty of the geology is seen as uncertainty of different soil types, which includes the uncertainty of the domain boundaries of the spatially distributed soil types. This is done via the Pluri-Gaussian Simulation approach, which is simulating spatially distributed categorical variables. The principle of the Pluri-Gaussian Simulation is to simulate one or several continuous Gaussian fields and to truncate them in order to produce a categorical variable. Armstrong et al. [14] describe the concept of the Pluri-Gaussian simulation approach in depth and illustrate

Table 6.7: Number of measurements inside each soil type.

	soil types	c'	φ'	E
number of measurement samples				
I	gravel, medium and coarse sand	8	8	4
II	silty fine sand, sandy silt	40	40	3
III	silty clay, clayey silt, organic clay	86	86	92
IV	bedrock	2	2	1

the basic idea, as shown in figure 6.17: Two Gaussian random fields (figure 6.17 a,b) are used to describe the main characteristics of the soil, e.g. anisotropies. The different soil types are generated by truncating several Gaussian random fields (figure 6.17 a,b). This provides flexibility to handle complex transitions and anisotropy among the soil types. The truncation rule is called the lithotype rule (figure 6.17 c) because it synthesizes transitions between the soil types. One can easily deduce from this that the choice of a lithotype rule is a major step of the methodology. In this case study, the lithotype rule was derived from borehole logs providing a good basis, on which soil types can and cannot be in contact. These proportions are not constant over the domain, but vary vertically and laterally because of the existence of trends in the geological processes as shown in Appendix H. The mathematical theory of the Pluri-Gaussian [215, 241] methods is described in detail in by Marconi [238] amongst others [14, 118]. This includes the conditioning of the unconditional Pluri-Gaussian random field to borehole data via the Gibbs sampler.

In Appendix H, the details of the Pluri-Gaussian Simulations are listed, which have been provided by Marconi [238]: The plan view of the investigated area, the spatial statistics of the soil types, the lithotype rules and illustrative illustrations of one realisation of the Pluri-Gaussian Simulations are shown in Appendix H.

6.3.2 Calculation of fragility curves

As mentioned in section 5.3, fragility curves are useful tools to quantify the uncertainty of the soil: the deterministic load on a footing is stepwise increased, while the probability of damage is evaluated. The probability of damage p_{damage} is defined as the probability of exceeding a defined level of allowable settlements $\alpha_{ultimate}$. These fragility curves are used as the basis for the risk based site characterisation as described in the next section 6.3.3.

The area of this case study is shown in Appendix H in figure H.4 and is subdivided into 35 areas, which are used as input for the 2D RFEM calculations. The fragility curves are calculated form the RFEM results.

Mechanical description of the problem: Figure 6.19 shows the 2D FEM mesh of a rigid building (B/W = 30/15 m), which is used for the evaluation of the load - displacement curves. Within the stepwise construction of the rigid building (B=30 m) differential

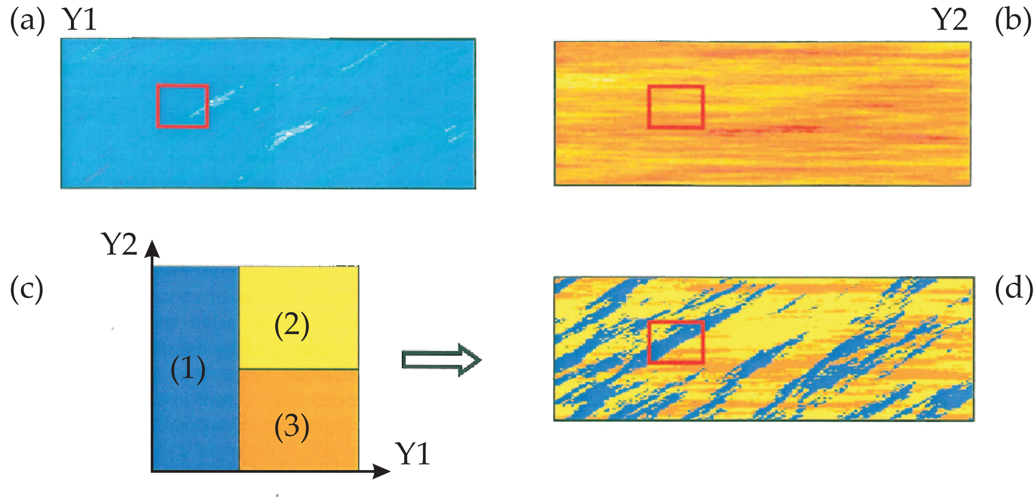

Figure 6.17: Principles of the Pluri-Gaussian Simulation approach, [14]:
Two uncorrelated Gaussian random fields Y1 (a) and Y2 (b) with different anisotropies are combined via the lithotype rule (c); the red square highlights the way the lithotype rule is used to construct the Pluri-Gaussian random field simulation (d).

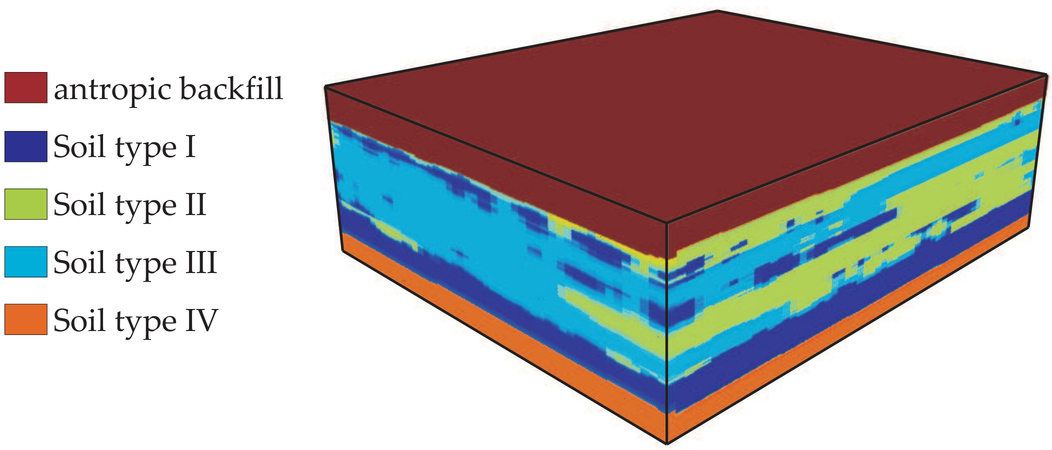

Figure 6.18: Part of the realisation of the Pluri-Gaussian random field (200/200/75m) including all soil types.

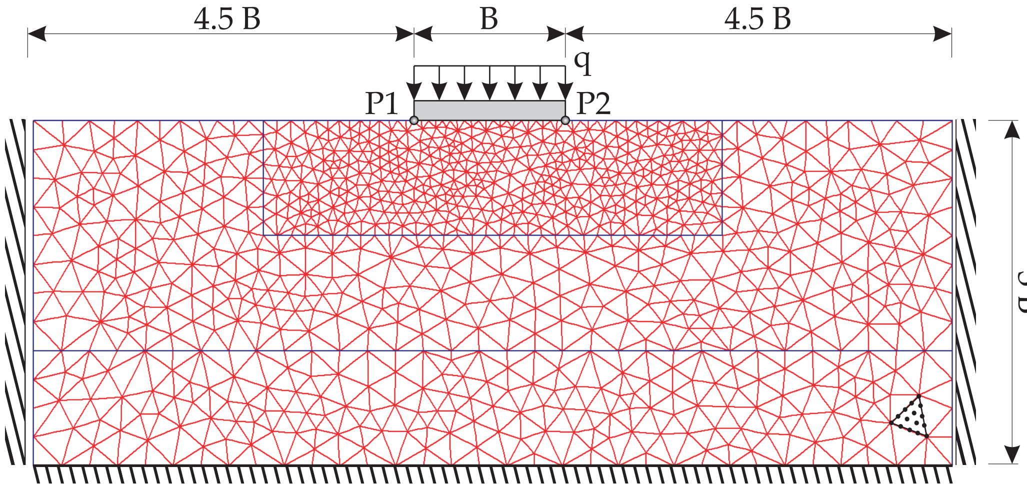

Figure 6.19: 2D FEM model used in this case study.

settlements between points P1 and P2 are observed, which are related to the spatial distribution of the 5 different soil types, as shown in table 6.6. Herein, the contact between the rigid building and the subsoil is assumed to be rigid with full bounding.

The soil behaviour is simulated by a small strain, double hardening model, which was developed by Benz [39]. This advanced, non-linear soil model is able to take the small strain behaviour as well as the non-linear stress-strain relationship of soil into account. The input variables of this soil model are given in the Appendix H in table H.1.

Stochastic soil properties: Although there is a large number of borehole data, it is quite difficult to estimate the strength and stiffness parameters of the different soil types: Most of these boreholes aimed for a geological description and only a relative small number of boreholes focused on geotechnical characterisation as indicated in table 6.7. Therefore, the measurement data are combined with expert knowledge from the Geotechnical Handbook [346] via the Bayesian approach as proposed by Ching et al. [80]. The results of this combination are given in table 6.6. One can clearly see that the combined values of the cohesion, friction angle and E-modulus show a smaller standard deviation. These lognormal distributed values are used for the random number generation of the strength and stiffness parameters of each soil type. These random variables, which are based on the mean values and standard deviations in table 6.6, are used in combination with the 300 Pluri-Gaussian random field realisations for the description of the geological heterogeneity. Each Pluri-Gaussian random field realisation has a length of 620 m, a width of 436 m and an overall-depth of 75 m with a horizontal discretisation of $\Delta_X = \Delta_Y = 5$ m and a vertical discretisation of $\Delta_Z = 0.05$ m. These Pluri-Gaussian random fields were generated by Marconi [238].

Due to the scarcity of data describing the mechanical behaviour of anthropic backfill material, this material is not considered in the subsequent investigations.

Random Finite Element approach & fragility curves: As mentioned above, the 3D Pluri-Gaussian random fields are used for the description of the geological uncertainty. A modified RFEM approach is used to quantify the effects of geological uncertainty.

Within the *preprocessing phase* of this case study, a simple mapping procedure has been used to map the 3D random field onto the 2D FEM mesh. The Pluri-Gaussian random field is divided into blocks ($5B \times 10B \times 75$ m). The transformation from 3D to 2D is carried out by averaging the soil properties in the third direction. Then the finer 2D random field is averaged over the coarser FEM mesh.

Within the *processing phase*, the differential settlements of the rigid building due to a load up to $q = 2,000$ kN/m^2 are evaluated by using the RFEM framework.

The boundaries of the mechanical model are chosen so as to minimize the influence on the settlement prediction as indicated in figure 6.19. This follows the recommendations for numerical modelling in geotechnical engineering in [291, 292].

As the first step within the *postprocessing phase*, the fragility curves are evaluated in the middle of the building, which is shifted over the entire field. The fragility curves describe the probability of exceeding the ultimate differential settlements due to a load, which is increased to $q = 2,000$ kN/m^2. As shown in literature e.g. [286, 289], this fragility curve can be approximated by a cumulative lognormal distribution function, which offers the possibility of a continuous definition of fragility due to differential settlements. For this purpose the probabilities of exceeding the ultimate differential settlement ($\alpha_{ultimate} = 1/300, 1/500, 1/600$ and $1/1,000$) for the different load levels are evaluated. Due to the fact that especially for small load levels the probability of exceeding $\alpha_{ultimate}$ is very small, the system response was approximated via a normal distribution function. Via this, it is possible to estimate the probability of exceeding $\alpha_{ultimate}$. One has to keep in mind that the absolute numbers of these probabilities are just approximations and offer a good basis to compare two different locations of the building.

6.3.3 Evaluation of the ultimate loads according to the state-of-the-art

The EUROCODE defines the probability of exceeding of the serviceability limit state (SLS) with $p_{exceeding} = 1.91 \cdot 10^{-3}$. This probability $p_{exceeding}$ is employed to estimate the ultimate load q_{SLS} by using the fragility curves. In figure 6.20 the fragility curve for ultimate differential settlements $\alpha_{ultimate} = 1/1,000$ is shown. The lognormal cumulative distribution function is fitted to the values via least square fitting, which have been derived from the RFEM calculations. This lognormal cumulative distribution function is used for the calculation of the load q_{SLS}, which does not exceed the probability of the SLS for differential settlements $\alpha_{ultimate} = 1/1,000$. One can extrapolate from this that for some regions, which have a very low probability of exceeding the ultimate differential settlements $\alpha_{ultimate}$ between the loads $q = 0$ kN/m^2 to $2,000$ kN/m^2, the load q_{SLS} might result in a higher value of the footing pressure than in the performed calculations. Therefore, these values are just valid for qualitative comparison of different positions and their susceptibility towards the probability of occurrence of differential settlements.

One has to keep this in mind while studying figure 6.21 and figure 6.22. These figures show the boreholes and the 35 locations of the midpoints of the building, which

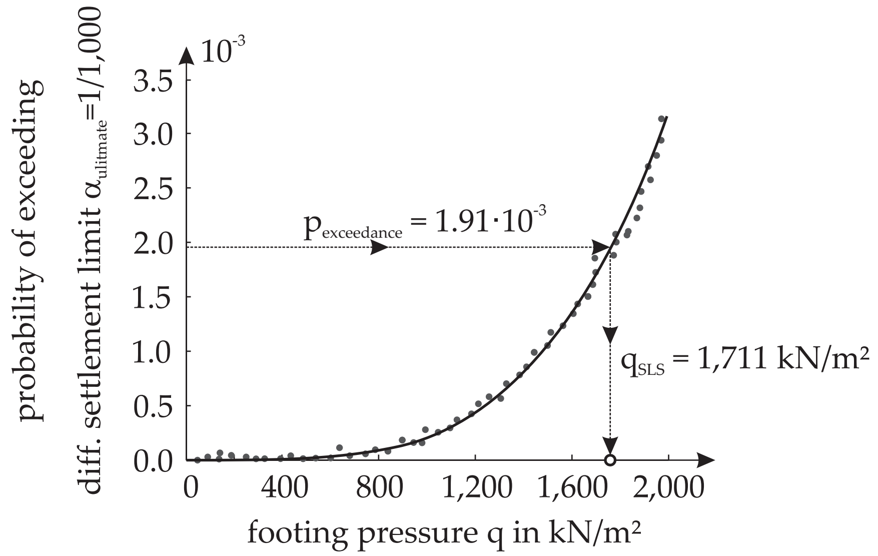

Figure 6.20: Sample fragility curve for ultimate differential settlements $\alpha_{ultimate} = 1/1,000$ and the fitted lognormal cumulative distribution function.

are indicated by black points. The orange squares indicate the location of the boreholes in the figures 6.21 and 6.22. The ultimate loads q_{SLS}, which are calculated for four differential settlement limits $\alpha_{ultimate} = 1/300, 1/500, 1/600, 1/1,000$. These ultimate loads q_{SLS} are plotted as grey-shaded regions in the background of figures 6.21 and 6.22. The grey-shaded regions between the points are interpolated using the Ordinary Kriging algorithm. By looking at the figures 6.21 and 6.22, one can clearly identify areas, which are less and more endangered to differential settlements under a specific load.

6.3.4 Conclusion

The presented case study presents a methodology for risk based site characterisation. This approach uses geostatistical simulation techniques and FEM modelling to derive the ultimate load over a site. Via the presented methodology, the geological uncertainty is combined with stochastic, geotechnical soil properties, which are based on measurement data and on expert judgement. The uncertainty of the complex geological conditions is quantified within a mathematical framework. By using RFEM in combination with fragility curves, these results are translated into into maps, which offer another insight into the effects of soil heterogeneity and the resulting risk, which is a novelty at the interface between engineering geology, geostatistics and geotechnical engineering. A by-product of this methodology of risk based site characterisation is the quantification of the effects of macro-scale soil variability.

By using the Pluri-Gaussian Simulation algorithm one has to be aware that modelling geological uncertainty by using different Gaussian random fields is a simplification. As pointed out in chapter 2, a Gaussian random field is a simple description of spatial variability using a mean value, a standard deviation and one single covariance function.

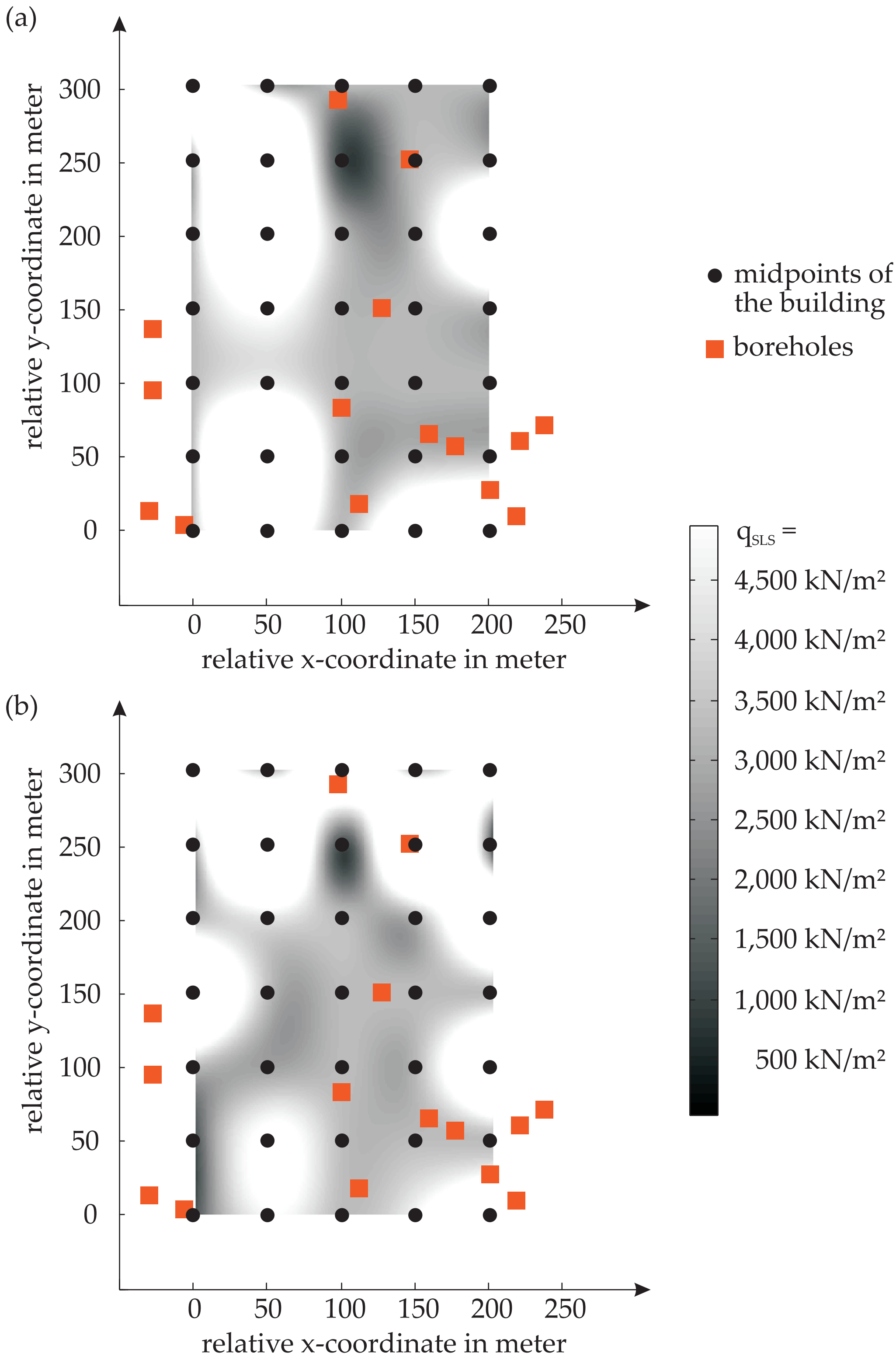

Figure 6.21: Map of allowable loads p_{SLS} on a footing with $\alpha_{ulitmate} = 1/300$ (a) and $\alpha_{ulitmate} = 1/500$ (b).

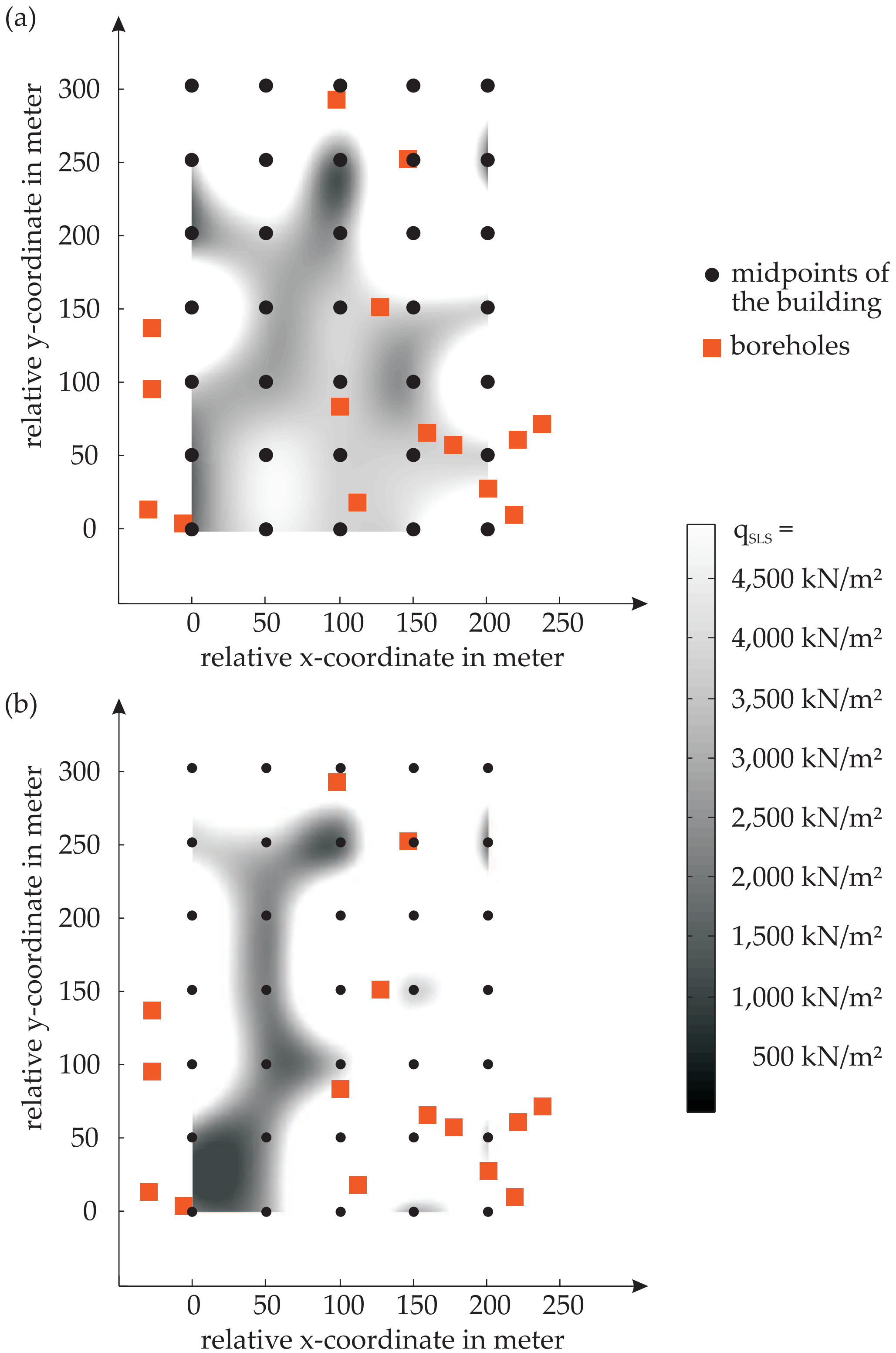

Figure 6.22: Map of allowable loads p_{SLS} on a footing with $\alpha_{ulitmate} = 1/600$ (a) and $\alpha_{ulitmate} = 1/1,000$ (b).

Moreover, one has to keep in mind that the lithotype is a subjective interpretation of geological conditions, although the lithotype rule is based on the analysis of a large set of boreholes.

However, the geological uncertainty can also be simulated by other simulation approaches in this context, which are able to simulate categorical variables described in literature [305].

Besides this, the Pluri-Gaussian simulation algorithm needs a large number of boreholes and laboratory tests to perform well. The stochastic properties of the Gaussian random fields and the definition of the lithotype rule needs a quite large database of boreholes. Otherwise, this simulation algorithm cannot be recommended for similar investigations in the case of a small dataset.

The presented case study on the risk based characterisation of an urban site extends the state of research presented in different contributions. Amongst others [24, 172, 312], Fenton [127] focused on the effects of meso-scale soil variability and neglected the macro-scale variability. On the basis of these results, Chen et al. [73] combine the micro- and the meso-scale variability via a multi-scale random field approach, which is applied to the ultimate limit state and to the serviceability limit state of strip footings.

However, the studied contributions [24, 127, 172, 312] do not take into account the available prior information like literature knowledge or soil investigations, a conceptual geological model or subjective engineering judgement. Therefore, the presented case study offers a promising scheme of evaluating the effects of geological, macro-scale uncertainty in the presence of a large borehole database. Moreover, the presented approach offers a realistic interpretation of spatially variable site conditions via the adopted fragility curve approach, which allows a realistic estimation of the risk of differential settlements. The results of this are transformed back to a limiting load, which is obeying the probability for SLS given in the EUROCODE 7. Via this, it is possible to identify endangered areas of a building site and this procedure quantifies the consequences of geological uncertainty.

6.4 Synopsis of the case studies

The presented case studies contribute to the description of uncertain performance of geotechnical structures in the ultimate and serviceability limit states. The effects of meso- and macro-scale variations of soil properties are investigated within three different case studies of geotechnical problems. These investigations show a possible way to combine two different scales of variability.

Tunnelling induced settlements: The RFEM approach is applied to the evaluation of tunnelling induced settlements. The effects of stochastic properties and the spatial variability of a single layered soil on the surface settlements is investigated. This approach is extended to a two layered system, which captures different scales of variability. The macro-scale variability is captured via a random process, which is conditioned to boreholes. The meso-scale variability inside the soil layers is simulated via random fields.

Slope stability: The reliability of single-layered soil slopes is investigated by means of RFEM. Within this, different random field generators are investigated and global sensitivity measures are used to quantify the influence of uncertain input parameters ($\mu_c, \mathrm{COV}_c, \Theta_{ver}, \Theta_{hor}$). The effects of multi-scale soil variability are considered via a simplified approach, similar to chapter 6.1. The effects of soil variability become clearer by comparing the results to a simplified approach using random variables and neglecting spatial variability. Within this, the uncertainty of the slope geometry is quantified in comparison to soil variability. Global sensitivity measures quantify the influence of the multi-scale spatial variability.

Risk based characterisation of an urban site: This case study investigates the effects of geological uncertainty. The different soil types are simulated as categorical variables by means of the Pluri-Gaussian simulation approach. This approach considers soil investigations and geostatistical subsoil characteristics as well as engineering judgement. These quantifications of macro-scale soil variability are used for the calculation of the footing serviceability. The footing serviceability is investigated by differential settlements and means of fragility curves. These fragility curves are the basis for risk maps, which visualize the effects of geological uncertainty and identifies endangered area. This study clearly quantifies the influence of macro scale soil variability and indicates clearly the need to consider this.

Chapter 7

Summary and conclusions

7.1 Potential and limitations of probabilistic methods

Geotechnical design is traditionally based on deterministic analysis using global or partial safety factors to take soil variability into account. These traditional approaches are mainly based on experience. Therefore, there is a need to evaluate the safety margins in the geotechnical design within a mathematical framework by using probabilistic methods to evaluate the probability of failure. Fluctuations of loads, variability of material properties, uncertainty in analysis models etc. all contribute to a failure probability [389]. The reliability, defined as the complement of the failure probability, is a rational measure of safety. Reliability methods deal with the uncertain nature of loads, resistance etc. and lead to assessment of the reliability. Reliability methods are based on established analysis models for the structure in conjunction with available information about loads and resistances and their associated uncertainties. The analysis models are usually imperfect, and the information about loads and resistances is usually incomplete. Therefore the reliability as assessed by reliability methods is generally not a purely physical property of the structure in its environment of loads. It is rather a nominal measure of the safety of the structure, given a certain analysis model and a certain amount and quality of information.

Correspondingly, also the estimated failure probability is dependent on the analysis model and the level of information, and it can therefore usually not be interpreted as the frequency of occurrence of failure for that particular type of structure [389].

Measuring the safety of a structure by its reliability makes the reliability a useful decision parameter. Fulfilment of a requirement to the reliability is then necessary in order to ensure a sufficient safety level in design. Such a requirement can either be derived by a utility optimisation in a decision analysis, or by requiring that the safety level as resulting from the design by a reliability analysis shall be the same as the safety level resulting from current deterministic design practice.

Probabilistic analyses are powerful and versatile tools for investigating the influence of uncertainties on a given geotechnical problem. However, one has always to keep in mind that the probabilistic analyses are done on the basis of the given input, but not from an inherent understanding of the statistics and physics of the problem. Thus, probabilistic analyses may be most beneficially used for enhancing the understanding of a physical problem that has already been identified. Preferably, the problem should even be largely understood aside of the probabilistic analysis itself.

The relative influence of the most important factors (e.g. variance or spatial correlation) may be studied via parametric studies, and this will bring confidence to the predicted behaviour in a given design situation. The way to conduct an uncertainty quantification in geotechnical engineering is shown in case studies onto tunnel lining, tunnel face stability, settlements introduced by tunnelling, slope stability, bearing capacity of vertically loaded strip footings and serviceability of footings. In these case studies semi-analytically defined and numerically simulated limit states are investigated with respect to their behaviour due to random variables and random fields. The contribution of the input variables is analysed by means of local and global sensitivity analyses. The presented case studies will show the potential of the framework of uncertainty quantification.

It is also very important to be aware of the limitations that lie in a probabilistic analysis. The presented approaches in chapter 2 allow to consider pre-knowledge from expert judgement, literature and/or available field tests, which can enrich a stochastic site characterisation. However, there is a need to conduct a bigger soil investigation campaign compared to the state-of-the-art because more input data are needed to derive statistical distributions and parameters describing spatial variability.

Besides this, another difficulty in using probabilistic concepts in applied engineering is the difficult statistical background, which is needed to understand the results of probabilistic analyses. Within chapter 3, a large number of field tests is analysed and contributes to the database on stochastic soil properties, which is assembled by the results of a large literature review in appendix A. The basics of safety and uncertainty are summarized in chapter 4 and shall help to develop an understanding of uncertainty quantification and to interpret results of probabilistic analyses presented in chapters 5 and 6. These case studies show the application of uncertainty quantification and shall guide the reader to a comprehensive understanding of the presented approaches. These different case studies in tunnelling and foundation engineering show the effects of soil variability and spatial variability at different scales. Moreover, sensitivity analyses are carried out to investigate the contribution of each random parameter to the probability of failure.

7.2 How well do we need to know soil variability?

Practitioners may ask how well do we have to know soil variability in order to make proper predictions. Generally spoken: The more we know about the subsoil, the better the predictions will be. The subjective engineering judgement shall be enriched by using the framework of uncertainty quantification to consider soil variability. The framework of uncertainty quantification offers a sound mathematical framework for a rigorous consideration of errors and uncertainties within a geotechnical design process. As shown in the case studies in the chapters 5 and 6, different limit state formulation ranging from semi-analytical to FEM defined can be incorporated depending on the level of accuracy. Moreover, also different uncertainties can be considered via (cross-correlated) random variables or random fields. But this framework needs statistical input parameters, which can be derived from soil samples of a site investigation. With a site investigation strategy, soil sampling strategies are a key-point in detecting soil variability within site characterisation. Different sampling concepts are offered in literature [257] e.g. simple random pattern, stratified random pattern or cluster sampling, and are used in groundwater ecology and geostatistics to guide the choice of additional soil samples. These concepts mainly focus on the properties of different homogeneous soil layers, which can be evaluated according to the statistical methods described in guidelines e.g. [195, 390]. It can be deduced from the case studies in chapter 6 that the spatial variability of soil properties has significant influence on the behaviour of geotechnical structures. Therefore, it is necessary to quantify theses effects in a rational manner. Not only literature data but also field investigations have to be conducted to investigate the the spatial correlation of soil properties. Consequently, the sampling schemes for detecting spatial variability at different scales have to be used from geostatistics [79, 248] or soil science [314] to evaluate the these properties in an economic and cost effective way.

7.3 What is the best way to evaluate the effects of soil variability?

The quantification of the effects of soil variability is probably one of the most important issues in geotechnical design. By using probabilistic methods, the recommendation for the most reliable way to calculate the probability of failure is an easy task. Focusing purely on the evaluation of the calculation of the probability of failure, it is the Monte-Carlo method. The Monte-Carlo method is a robust method for the evaluation of the probability of failure, although it is also the most time consuming one in comparison to e.g. FORM. As elaborated in section 4.3, different authors published various methods to evaluate the probability of failure apart from the Monte Carlo methods to overcome this drawback.

While reading the case studies in chapters 5 and 6, one can clearly see not only the effects of representing soil variability using random variables and random fields. Sensitivity analyses quantify the contribution of each uncertain variable and help the engineer to simulate effects of the important random variables, which helps to simplify the calculation. As a consequence, the evaluation of the probability of failure is speeded up by taking just the important variables into account.

Within this context, it has to be stressed that another important issue is the complexity of the limit state equation. The limit state equation is describing the system behaviour via a close form solution, an empirical equation, a numerical simulation model or a surrogate model. The best way to simulate the system response is the use of a numerical model in 3D together with an advanced constitutive model. But this cannot fulfil the requirements for a fast evaluation of the probability of failure. Therefore, the engineer has to make compromises to keep the mechanical simulation model as simple and as accurate as possible for a realistic description of the soil structure interaction as indicated by Potts et al. [291]. Within this, the approach of using surrogates or meta-models offers a promising way in this context.

There is no single answer to the question: which scales of variability do we have to consider in geotechnical design? Generally spoken, the very small scales of spatial variability do not play a major role. As shown in chapter 6, micro-scale variations (e.g. at the grain-size level) have minor effects on the overall failure probability of a structure, whereas large geological spatial variations (e.g. soil layers) can have significant effects as shown in the case studies. One can deduce from the presented case studies that the effects are significant for the combination of meso- and macro-scale spatial soil variability. The presented engineering approach is taking these two scales of spatial variability into account: The soil layer boundary is represented by a conditional, stochastic process, which is separating layers with spatial variable properties. By using the Polynomial-Chaos-Expansion (PCE) in connection with the Random Finite Element approach for the representation of the system response, it is possible to consider not only a single correlation length, but a lognormal distribution of correlation lengths. Moreover, the global sensitivity measures of the uncertain variables can be derived from the PCE analytically. This offers a possible way to quantify the effects of multi-scale spatial variability of soil properties.

7.4 Recommendations for research

The following recommendations for future research in science, education and applied engineering can be drawn from this research.

Science: Additional studies should be conducted to gain more knowledge and experience in the of stochastic quantification of soil properties. The presented literature study and the results of the case studies analysing a large set of CPT tests offer a good basis for this. This would form a good starting point for the formulation of a guideline for the evaluation of spatial variability and heterogeneity comparable to recommendations like [11, 17, 67, 95]. The need for cost effective sampling schemes is closely linked with this.

Apart from the presented Methods of Moments and Maximum Likelihood approaches in chapter 2, the author recommends inverse methods like in geostatistics or earthquake engineering to investigate the effects of soil variability. These methods are based on Bayesian approaches [164] or sequential approaches[171, 304] amongst others.

Moreover, the quality of the random field representation within the framework of uncertainty quantification and reliability based design is an important task. The forecast quality in meteorology [309] might be a staring point for further developments in this context .

Apart from this, the partial safety factors in the EC7, which are mainly based on experience, should be enriched and extended with the results from additional investigations. This would lead to a more precise separation between soil uncertainties and human related errors.

Another interesting part in the context of economic design is the optimization of a geotechnical structure including uncertainties. Reliability based design optimization includes different failure modes of complex structures incorporating the variability of loads and resistance forces in a proper way.

Education: In order to introduce probabilistic concepts in applied sciences, it is necessary to make engineers familiar with statistics and concepts of reliability. Therefore, it would be necessary to teach students in these fields and to teach them the linguistic aspects to be able to speak and exchange with experts from applied mathematics or physics. Mathematics and physics have a longer tradition in using the concepts of statistics in their fields.

Applied engineering: Guidelines and worked examples would be the best arguments to convince applied engineers to used reliability based design approaches. This has already been started by different groups like GeoSNET [360] or JCSS [399] amongst others [262, 280]. It has to be pointed out that user friendly software tools would support this, which would allow one to estimate the reliability of complex systems in a fast and efficient way by using robust and efficient algorithms.

Bibliography

[1] M. Aboufirassi and M.A. Marino. Cokriging of aquifer transmissivities from field measurements of transmissivity and specific capacity. *Mathematical Geology*, 16(1): 19–35, 1984.

[2] M. Abramovich and I.A. Stegun. *Handbook of Mathematical Functions, Graphs and Mathematical Tables*. National Bureau of Standards Applied Mathematics, Washington, 1964.

[3] M. Abramovich and I.A. Stegun. *Handbook of Mathematical Functions with Formulas, Graphs and Mathematical Tables*. Dover, 1974.

[4] A. AghaKouchak, A. Bárdossy, and E. Habib. Conditional simulation of remotely sensed rainfall data using a non-gaussian v-transformed copula. *Advances in Water Resources*, 33(6):624–634, 2010.

[5] H. Ahrens, E. Lindner, and K.H. Lux. Zur Dimensionierung von Tunnelausbauten nach den Empfehlungen zur Berechnung von Tunneln im Lockergestein (1980). *Die Bautechnik*, 8:260–311, 1982.

[6] H. Akaike. Information theory and an extension of the maximum likelihood principle. In *Proceedings of Second International Symposium on Information Theory*, volume 1, pages 267–281. Springer Verlag, 1973.

[7] H. Akaike. A Bayesian analysis of the minium AIC procedure. *Ann. Inst. Statist. Math.*, 30:9–14, 1978.

[8] R. Al-Khoury, K.J. Bakker, P.G. Bonnier, H.J. Burd, G. Soltys, and P.A. Vermeer. *PLAXIS 2D Version 9*. R.B.J. Brinkgreve and W. Broere and Waterman, 2008.

[9] D. Alber and W. Reitmeier. *Beschreibung der räumlichen Streuungen von Bodenkennwerten mit Hilfe der Zeitreihenanalyse*, volume 7. Technische Universität München, 1986.

[10] E.E. Alonso and R.J. Krizek. Stochastic formulation of soil properties. In *Proc. 2nd Int. Conf. on Applications of Statistics & Probability in Soil and Structural Engineering, Aachen*, volume 2, pages 9–32, 1975.

[11] American Society of Civil Engineers. *Standard Guideline for the Geostatistical Estimation and Block-averaging of Homogeneous and Isotropic Saturated Hydraulic Conductivity*. American Society of Civil Engineers, Environmental and Water Resources Institute, 2010.

[12] G. Anagnostou and K. Kovari. Face stability conditions with earth-pressure-balanced shields. *Tunnelling and Underground Space Technology*, 11(2):165–173, 1996.

[13] A.H.S. Ang and W.H. Tang. *Probability concepts in engineering planning and design, vol. 2: Decision, risk, and reliability.* JOHN WILEY & SONS, INC., 1984.

[14] M. Armstrong, A. Galli, H. Beucher, G. Loc'h, D. Renard, B. Doligez, R. Eschard, and F. Geffroy. *Plurigaussian simulations in geosciences*. Springer, 2011.

[15] A. Asaoka and D.A. Grivas. Spatial variability of the undrained strength of clays. *Journal of the geotechnical engineering division*, 108(5):743–756, 1982.

[16] D. Assimaki, A. Pecker, R. Popescu, and J. Prevost. Effects of spatial variability of soil properties on surface ground motion. *Journal of earthquake engineering*, 7:1–44, 2003.

[17] ASTM D 5549-94. Standard Guide for the Contents of Geostatistical Site Investigation Report, 2001.

[18] R. Azzouz and C. Bacconnet. Optimal approach to the planning of a network of in situ soil test. In *Proc. 6th Int. Conf. on Applications of Statistics and Probability in Soil and Structural Engineering*, pages pp. 654–659, Mexico City, 1991.

[19] R. Azzouz, C. Bacconnet, and J.-C. Faugeras. Analyse geostatistique dune campagne de reconnaissance au penetrometre statique. In *Proc. 5th Int. Conf. on Applications of Statistics and Probability in Soil and Structural Engineering*, pages 821– 828, Vancouver, 1987.

[20] G.L. Babu and S.M. Dasaka. The effect of spatial correlation of cone tip resistance on the bearing capacity of shallow foundations. *Geotechnical and Geological Engineering*, 26(1):37–46, 2008.

[21] G.B. Baecher. *Site Exploration: A probabilistic approach*. PhD thesis, Massachusetts Instiute of Technology, 1972.

[22] G.B. Baecher. Analyzing exploration strategies. In C.H. Dowding, editor, *Site Characterization and Exploration*, New York, 1978. American Society of Civil Engineers.

[23] G.B. Baecher and J.T. Christian. *Reliability and statistics in geotechnical engineering*. John Wiley & Sons Inc., 2003.

[24] G.B. Baecher and T.S. Ingra. Stochastic FEM in settlement predictions. *Journal of the Geotechnical Engineering Division*, 107(4):449–463, 1981.

[25] G.B. Baecher, M. Chan, T.S. Ingra, T. Lee, and L.R. Nucci. Geotechnical reliability of offshore gravity platforms. Technical Report Report MITSG 80-20, Sea Grant College Program, Mass. Inst, of Tech, 1980.

[26] G.B. Baecher, J.D. Ditmars, D.E. Edgar, and C.H. Dowding. Radioactive waste isolation in salt: A method for evaluating the effectiveness of site characterization measures. Technical report, Report ANL/EESTM-342, Argonne National Laboratory, Ill, 1988.

[27] S. Bakhtiari. *Stochstiac Finite Element Slope Stability Analysis*. PhD thesis, Manchester Centre for Civil and Construction Engineering, University of Manchester, England, 2011.

[28] A.A. Bakr, L.W. Gelhar, A.L. Gutjahr, and J.R. MacMillan. Stochastic analysis of spatial variability in subsurface flows. 1. comparison of one-and three-dimensional flows. *Water Resources Research*, 14(2):263–271, 1978.

[29] A. Bárdossy. Copula-based geostatistical models for groundwater quality parameters. *Water Resources Research*, 42(11):11416–11428, 2006.

[30] A. Bárdossy and Z.W. Kundzewicz. Geostatistical methods for detection of outliers in groundwater quality spatial fields. *Journal of Hydrology*, 115(1-4):343–359, 1990.

[31] A. Bárdossy, U. Haberlandt, and J. Grimm-Strele. Interpolation of groundwater quality parameters using additional information. In A. Soares, editor, *Proceedings of geoENV I-Geostatistics for Environmental Applications*. Kluver Academic Publishers, 1997.

[32] R. J. Barnes. Bounding the required sample size for geological site characterization. *Mathematical Geology*, 20(5):477–490, 1988.

[33] C. Bellehumeur and P. Legendre. Multiscale sources of variation in ecological variables: modeling spatial dispersion, elaborating sampling designs. *Landscape Ecology*, 13(1):15–25, 1998.

[34] J.S. Bendat and A.G. Piersol. *Random data analysis and measurement procedures*, volume 11. IOP Publishing, 2000.

[35] J.P. Benkendorfer, C.V. Deutsch, P.D. LaCroix, L.H. Landis, Y.A. Al-Askar, A.A. Al-AbdulKarim, and J. Cole. Integrated Reservoir Modelling of a Major Arabian Carbonate Reservoir. *Middle east oil show*, 298(96):1–26, 1995.

[36] R. J. Bennett. *Spatial Time Series*. Pion Ltd., London, 1979.

[37] C. Benson. Predicting excursions beyond regulatory thresholds of hydraulic conductivity using quality control measurements. In *Proceedings of the First Canadian Conference on Environmental Geotechnics*, pages 14–17, 1991.

[38] T. Benz. *Small-strain stiffness of soils and its numerical consequences*. PhD thesis, University of Stuttgart, Institute of Geotechnical Engineering, 2007.

[39] T. Benz. Small strain double hardening model. Technical report, NTNU, Trondheim, 2012.

[40] D. T. Bergado and K. T. How. A Probabilistic Spatial-Temporal Modelling of Embankment Settlement on Soft Bangkok Cly: A Case of Bangna-Bangpakong Highway, Thailand. In *Proc. of 6th Int. Conf. on Applications of Statistics and Probability in Soil and Structural Engineering*, pages pp. 808–815, 1991.

[41] D.T. Bergado and L.R. Anderson. Stochastic analysis of pore pressure uncertainty for the probabilistic assessment of the safety of earth slopes. *Soils and Foundations*, 25(2):87–105, 1985.

[42] J.O. Berger, V. De Oliveira, and B. Sansó. Objective Bayesian analysis of spatially correlated data. *Journal of the American Statistical Association*, 96(456):1361–1374, 2001.

[43] M. Berveiller, B. Sudret, and M. Lemaire. Presentation of two methods for computing the response coefficients in stochastic finite element analysis. In *Proceedings of 9th ASCE specialty Conference on Probabilistic Mechanics and Structural Reliability, Albuquerque, USA*, 2004.

[44] M. Berveiller, B. Sudret, and M. Lemaire. Stochastic finite element: a non-intrusive approach by regression. *Revue Européenne de Mécanique Numérique-Volume*, 15(1-2): 81–92, 2006.

[45] P. Biçer and P.T. Özener. Vertical variability of the undrained shear strength of golden horn clay. *Marine Georesources and Geotechnology*, 27(4):309–321, 2009.

[46] A. A. Binsariti. *Statistical analyses and stochastic modeling of the Cortaro aquifer in Southern Arizona*. PhD thesis, University of Arizona, 1980.

[47] G. Blatman and B. Sudret. An adaptive algorithm to build up sparse polynomial chaos expansions for stochastic finite element analysis. *Probabilistic Engineering Mechanics*, 25(2):183–197, 2010.

[48] R. Borja, editor. *Multiscale and multiphysics processes in geomechanics*. Springer, 2011.

[49] J.-M. Bourinet, C. Mattrand, and V. Dubourg. A review of recent features and improvements added to FERUM software. In *Proceedings of 10th International Conference on Structural Safety and Reliability (ICOSSAR'09)*, Osaka, Japan, 2009.

[50] D.S. Bowles and H.H. Ko, editors. *Probabilistic Characterization of Soil Properties: Bridge Between Theory and Practice*. ASCE, 1984.

[51] G.E.P. Box and G.M. Jenkins, editors. *Time Series Analysis: Forecasting and Control*. Holden-Day, San Fransisco, 1970.

[52] H. Bozdogan. Model selection and akaike's information criterium: The general tehory and its analytical extensions. *Psychometrika*, 52:345–370, 1987.

[53] K. Breitung. Asymptotic approximations for multi-normal integrals. *J. Engrg. Mech. Div., ASCE*, 110(3):357–366, 1984.

[54] D. Breysse, H. Niandou, S. Elachachi, and L. Houy. A generic approach to soil-structure interaction considering the effects of soil heterogeneity. *Geotechnique*, 55 (2):143–150, 2005.

[55] P.I. Brooker, J.P. Winchester, and A.C. Adams. A geostatistical study of soil data from an irrigated vineyard near Waikerie, South Australia. *Environment International*, 21(5):699–704, 1995.

[56] D.J. Brus and J.J. De Gruijter. Random sampling or geostatistical modelling? choosing between design-based and model-based sampling strategies for soil (with discussion). *Geoderma*, 80(1-2):1–44, 1997.

[57] C. Bucher. *Computational Analysis of Randomness in Structural Mechanics*. Taylor & Francis, 2009.

[58] C. Bucher and T. Most. A comparison of approximate response functions in structural reliability analysis. *Probabilistic Engineering Mechanics*, 23(2-3):154–163, 2008.

[59] P.A. Burrough. Multiscale sources of spatial variation in soil. I - The application of fractal concepts to nested levels of soil variation. *Journal of Soil Science*, 34(3): 577–597, 1983.

[60] P.A. Burrough. Multiscale sources of spatial variation in soil. III - The application of fractal concepts to nested levels of soil variation. *Journal of Soil Science*, 34(3): 578–599, 1983.

[61] P.A. Burrough. Multiscale sources of spatial variation in soil. II - A non-Brownian fractal model and its application in soil survey. *Journal of Soil Science*, 34(3):599–620, 1983.

[62] E. Byers and D.B. Stephens. Statistical and stochastic analyses of hydraulic conductivity and particle-size in a fluvial sand. *Soil Science Society of America Journal*, 47(6):1072, 1983.

[63] D.G. Cacuci, M. Ionescu-Bujor, and I.M. Navon. *Sensitivity and Uncertainty Analysis: Applications to large-scale systems*, volume 2. CRC, 2005.

[64] J. Caers. *Modeling Uncertainty in the Earth Sciences*. Wiley, 2011.

[65] F. Cafaro and C. Cherubini. Large sample spacing in evaluation of vertical strength variability of clayey soil. *Journal of geotechnical and geoenvironmental engineering*, 128:558, 2002.

[66] J.A. Calgaro. Safety philosophy of eurocodes. In *Proceedings of the 3rd International Symposium on Geotechnical Safety and Risk*, 2011.

[67] E.O.F. Calle, G.A.M Kruse, M.T. van der Meer, W.R. Halter, and B.M. Effing. Schematiseren Geotechnische Faalmechanismen bij Dijken - SBW Faalmechanismen TR Grondonderzoek, (in Dutch). Technical report, Deltares, 2009.

[68] R.G. Campanella, D.S. Wickremesinghe, and P.K. Robertson. Statistical treatment of cone penetration test data. In *Proceedings of the 5th International Conference on Reliability and Risk Analysis in Civil Engineering*, 1987.

[69] S.F. Carle and G.E. Fogg. Transition probability based indicator geostatistics. *Mathematical Geology*, 28(4):453–476, 1996.

[70] R. Caspeele. *Proabilistic evaluation of conformity control and the use of the Bayesian updating techniques in the framework of safety analyses of concerte structures*. PhD thesis, University Gent, 2009.

[71] CEN. Eurocode: Basis of structural design. European standard, EN 1990: 2002, 2002.

[72] R. Chaplow. The geology and hydrogeology of sellafield: an overview. *Quarterly Journal of Engineering Geology and Hydrogeology*, 29(Supplement 1):1–12, 1996.

[73] Q. Chen, A. Seifried, J.E. Andrade, and J.W. Baker. Characterization of random fields and their impact on the mechanics of geosystems at multiple scales. *International Journal for Numerical and Analytical Methods in Geomechanics*, 36(2):140–165, 2010.

[74] Q. Cheng. Multifractality and spatial statistics. *Computers & Geosciences*, 25:949–961, 1999.

[75] C. Cherubini. Data and considerations on the variability of geotechnical properties of soils. In *Proceedings of the international conference on safety and reliability, ESREL*, volume 97, pages 1583–1591, 1997.

[76] C. Cherubini. Reliability evaluation of shallow foundation bearing capacity on c'–φ' soils. *Canadian Geotechnical Journal*, 37(1):264–269, 2000.

[77] C. Cherubini, I. Giasi, and L. Rethati. The coeffcient of variation of some geotechnical parameters. In *Proceedings of Probabilistic Methods in Geotechnical Gengineering*, 1993.

[78] P. Chiasson and Y.J. Wang. Spatial variability of sensitive Champlain sea clay and an application of stochastic slope stability analysis of a cut. In *Proceedings of the 2nd International Workshop on Characterisation and Engineering Properties of Natural Soils. Singapore, November*, 2006.

[79] J.P. Chiles and P. Delfiner. *Geostatistics–modeling spatial uncertainty*. Wiley-Interscience, 1999.

[80] J. Ching, J.R. Chen, J.Y. Yeh, and K.K. Phoon. Updating uncertainties in friction angles of clean sands. *Journal of Geotechnical and Geoenvironmental Engineering*, 138 (2):217–229, 2011.

[81] Y.H. Chok. *Modelling the effects of soil variability and vegetation on the stability of natural slopes*. PhD thesis, University of Adelaide, School of Civil, Environmental and Mining Engineering, 2008.

[82] G. Christakos. *Random field models in earth sciences*. Academic Press, 1992.

[83] J. Chu, W. Hsču, H. Zhu, and A.G. Journel. The Amoco case study. Report 4, Stanford Center for Reservoir Forecasting, 1991.

[84] W.G. Cochran. *Sampling techniques*. Wiley, London, 3rd edition, 1977.

[85] P.D. Coddington. Random number generators for parallel computers. *The NHSE Review*, 2:1–26, 1997.

[86] R.F. Craig. *Soil mechanics*. Taylor & Francis, 2004.

[87] N. Cressie. Fitting variogram models by weighted least squares. *Mathematical Geology*, 17(5):563–586, 1985.

[88] G. De Marsily, F. Delay, J. Gonçalvès, P. Renard, V. Teles, and S. Violette. Dealing with spatial heterogeneity. *Hydrogeology Journal*, 13(1):161–183, 2005.

[89] E. De Rocquigny, N. Devictor, and S. Tarantola. *Uncertainty in industrial practice*. Wiley Online Library, 2008.

[90] D.J. DeGroot and G.B. Baecher. Estimating autocovariance of in-situ soil properties. *Journal of Geotechnical Engineering*, 119(1):147–166, 1993.

[91] J.P. Delhomme. Spatial variability and uncertainty in groundwater flow parameters: a geostatistical approach. *Water Resources Research*, 15(2):269–280, 1979.

[92] F.A. Delory, A.M. Crawford, and M.E.M. Gibson. Measurements on a tunnel lining in very dense till. *Canadian Geotechnical Journal*, 16(1):190–199, 1979.

[93] A. Der Kiureghian, H-Z. Lin, and S.-J. Hwang. Second-order reliability approximations. *J. Engrg. Mech. Div., ASCE*, 113(8):1208–1225, 1987.

[94] A.J. Desbarats and R. Dimitrakopoulos. Geostatistical simulation of regionalized pore-size distributions using min/max autocorrelation factors. *Mathematical Geology*, 32(8):919–942, 2000.

[95] C. Deutsch, M. Monteiro, S. Zanon, and O. Leuangthong. Procedures and guidelines for assessing and reporting uncertainty in geostatistical reservoir modeling. Technical report, Technical report, Centre for Computational Geostatistics, University of Alberta, Edmonton, AB, 2002.

[96] C.V. Deutsch. *Geostatistical Reservoir Modeling*. Oxford University Press, New York, USA, 2002.

[97] C.V. Deutsch and A.G. Journel. *GSLIB - Geostastical Software Library and Users's Guide*. Oxford University Press, 1998.

[98] J.L. Devary and P.G. Doctor. Pore velocity estimation uncertainties. *Water Resources Research*, 18(4):1157–1164, 1982.

[99] J. Diaz-Padilla and E.H. Vanmarcke. *Settlement of Structures on Shallow Foundations: A Probabilistic Analysis*. Dept. of Civil Engineering, Massachusetts Institute of Technology, 1974.

[100] C.R. Dietrich and M.R. Osborne. Estimation of covariance parameters in kriging via restricted maximum likelihood. *Mathematical Geology*, 23(1):119–135, 1991.

[101] DIN 4017. Baugrund-Berechnung des Grundbruchwiderstands von Flachgründungen, 2006.

[102] DIN 4019. Baugrund-Setzungsberechnungen, 2001.

[103] DIN 4094-1. Subsoil - field investigations - part 1: Cone penetration tests, 06 2002.

[104] DIN 4094-5. Geotechnical field investigations - part 5: Borehole deformation tests., 2001.

[105] O. Ditlevsen and H.O. Madsen. *Structural reliability methods*, volume 178. Wiley Chichester, 1996.

[106] D.N. Veritas. Recommended practice report dnv-rp-c207: Statistical representation of soil data. Technical report, D.N. Veritas, 1997.

[107] G.R. Dodagoudar and G. Venkatachalam. Reliability analysis of slopes using fuzzy sets theory. *Computers and Geotechnics*, 27(2):101–115, 2000.

[108] H. Duddeck. Empfehlungen zur Berechnung von Tunneln im Lockergestein. *Die Bautechnik*, 10:349–356, 1980.

[109] A.S. Dyminski, J. Howie, D. Shuttle, and A. Kormann. Soil variability study for embankment design of port of navegantes, brazil. In *Proceedings of GeoCongress 2006: Geotechnical Engineering in the Information Technology Age*, pages 1–6. ASCE, 2006.

[110] M.D. Ecker and A.E. Gelfand. Bayesian variogram modeling for an isotropic spatial process. *Journal of Agricultural, Biological, and Environmental Statistics*, 3:347–369, 1997.

[111] B. Efron. Bootstrap methods: another look at the jackknife. *The annals of Statistics*, 7(1):1–26, 1979.

[112] J. Eggleston and S. Rojstaczer. Identification of large-scale hydraulic conductivity trends and the influence of trends on contaminant transport. *Water Resources Research*, 34(9):2155–2168, 1998.

[113] M. El Gonnouni, Y. Riou, and PY Hicher. Geostatistical method for analysing soil displacement from underground urban construction. *Geotechnique*, 55:171–182, 2005.

[114] H. El-Ramly, N.R. Morgenstern, and D.M. Cruden. Probabilistic slope stability analysis for practice. *Canadian Geotechnical Journal*, 39(3):665–683, 2002.

[115] A.M.M. Elfeki. *Stochastic characterization of geological heterogeneity and its impact on groundwater contaminant transport*. PhD thesis, TU Delft, Delft University of Technolog, 1996.

[116] I. Elishakoff. Possible limitations of probabilistic methods in engineering. *Appl. Mech. Rev.*, 1(53):19–36, 2000.

[117] B.R. Ellingwood, O.C. Celik, and K. Kinali. Fragility assessment of building structural systems in mid-america. *Earthquake Engineering & Structural Dynamics*, 36 (13):1935–1952, 2007.

[118] X. Emery. Properties and limitations of sequential indicator simulation. *Stochastic Environmental Research and Risk Assessment*, 18(6):414–424, 2004.

[119] EN 1997-1:2004. Eurocode 7 - Geotechnical design–Part 1: General rules, 2004.

[120] J. Erdmann. *Vergleich ebener und Entwicklung räumlicher Berechnungsverfahren für Tunnel*. PhD thesis, Technische Universität Carolo-Wilhelmina zu Braunschweig, 1983.

[121] M. Faber and T. Vrouwenvelder. Probabilistic model code. Technical report, Joint Committee of Structural Safety, www.jcss.ethz.ch, May 2001. URL `www.jcss.ethz.ch`.

[122] M.H. Faber and M.G. Stewart. Risk assessment for civil engineering facilities: critical overview and discussion. *Reliability engineering & system safety*, 80(2):173–184, 2003.

[123] M. N. Fardis. Probabilistic liquefaction of sands during earthquakes. Technical Report R79-14, Dept. of Civil Engrg., MIT, 1979.

[124] M.A. Fardis and D. Veneziano. Estimation of SPT-N and relative density. *Journal of the Geotechnical Eengineering Division*, 107(10):1345–1359, 1981.

[125] G.A. Fenton. Random field modeling of CPT data. *Journal of Geotechnical and Geoenvironmental Engineering*, 125(6):486, 1999.

[126] G.A. Fenton. Estimation for stochastic soil models. *Journal of Geotechnical and Geoenvironmental Engineering*, 125(6):470, 1999.

[127] G.A. Fenton and D.V. Griffiths. *Risk assessment in geotechnical engineering*. John Wiley & Sons, 2008.

[128] S. Ferson. *Constructing probability boxes and Dempster-Shafer structures*. Sandia National Laboratories, 2002.

[129] Federal Highway Administration (FHWA). Federal highway administration's geotechnical research program, 06 2012. URL `http://www.fhwa.dot.gov/publications/publicroads/`.

[130] R.V. Field and M. Grigoriu. On the accuracy of the polynomial chaos approximation. *Probabilistic Engineering Mechanics*, 19(1):65–80, 2004.

[131] B. Fiessler, H.-J. Neumann, and R. Rackwitz. Quadratic limit states in structural reliability. *J. Engrg. Mech. Div., ASCE*, 105(4):661–676, 1979.

[132] G.E. Fogg, F.J. Lucia, and R.K. Senger. Stochastic simulation of interwell-scale heterogeneity for improved prediction of sweep efficiency in a carbonate reservoir. In *NIPER/DOE Second International Reservoir Characterization Technical Conference, Dallas, TX*, pages 355–381, 1989.

[133] S. Fuchs. Probabilities and uncertainties in natural hazard risk assessment. In D. Proske, M. Mehdianpour, and L. Gucma, editors, *Proceedings of 4th International Probabilistic Symposium*, pages 189–204, Berlin, 2006.

[134] C. Gascuel-Odoux and P. Boivin. Variability of variograms and spatial estimates due to soil sampling: a case study. *Geoderma*, 62(1-3):165–182, 1994.

[135] L.W. Gelhar, C. Welty, and K.R. Rehfeldt. A critical review of data on field-scale dispersion in aquifers. *Water Resources Research*, 28(7):1955–1974, 1992.

[136] A. Gelman, J.B. Carlin, H.S. Stern, and D.B. Rubin. *Bayesian data analysis*. CRC press, 2004.

[137] M.G. Genton. Highly robust variogram estimation. *Mathematical Geology*, 30(2): 213–221, 1998.

[138] R.G. Ghanem and P.D. Spanos. *Stochastic finite elements: a spectral approach*. Springer, 1991.

[139] A. Glockner, A. Igelbüscher, C. Moormann, H. Jud, K. Lindner, and H. Kunzmann. Bau eines neuen Stahlwerks auf weichen Sedimentböden naha Rio D Janeiro geotechnische Herausforderungen in ungewöhnlichen Dimensionen. In *Vorträge der Baugrundtagung 2008*, pages 199–206, 2007.

[140] D.I. Goggin. Patterns of Permeability in Eolian Deposits: Page Sandstone (Jurassic), Northeastern Arizona, SPE, U. of Texas ll. A. Chandler, U. of Texas. *SPE reprint series*, 2(27):46, 1988.

[141] D.J. Goggin, M.A. Chandler, G. Kocurek, and L. Lake. Permeability transects of eolian sands and their use in generating random permeability fields. *SPE Formation Evaluation*, 7(1):7–16, 1992.

[142] J. Goldsworthy. *Reducing the Risk of Foundation Failures by Improving the Effectiveness of Geotechnical Investigations*. PhD thesis, School of Civili and environmental Engineering, University of Adelaide, 2006.

[143] J.J. Gómez-Hernández and X.H. Wen. Multigaussian models: The danger of parsimony. *Statistical Methods & Applications*, 4(2):167–181, 1995.

[144] J.J. Gómez-Hernández and X.H. Wen. To be or not to be multi-Gaussian? A reflection on stochastic hydrogeology. *Advances in Water Resources*, 21(1):47–61, 1998.

[145] P. Goovaerts. *Geostatistics for natural resources evaluation*. Oxford University Press, USA, 1997.

[146] P.A. Graniero and V.B. Robinson. A real–time adaptive sampling method for field mapping in patchy, heterogeneous environments. *Transactions in GIS*, 7(1):31–53, 2003.

[147] D.V. Griffiths and P.A. Lane. Slope stability analysis by finite elements. *Geotechnique*, 49(3):387–403, 1999.

[148] G. Gudehus. Sicherheitsnachweise für Grundbauwerke. *Geotechnik*, 10(1):4–34, 1987.

[149] R. Hack, B. Orlic, S. Ozmutlu, S. Zhu, and N. Rengers. Three and more dimensional modelling in geo-engineering. *Bulletin of Engineering Geology and the Environment*, 65(2):143–153, 2006.

[150] I.S. Halim and W.H. Tang. Bayesian method for characterization of geological anomaly. In *Proceedings of Uncertainty Modeling and Analysis*, pages 585–590. IEEE, 1990.

[151] C.P. Haslauer, J. Li, and A. Bárdossy. Application of copulas in geostatistics. In *Proceedings of geoENV VII–Geostatistics for Environmental Applications*, pages 395–404. Springer, 2010.

[152] A.M. Hasofer and N.C. Lind. Exact and invariant second-moment code format. *Journal of the Engineering Mechanics Division*, 100(1):111–121, 1974.

[153] T. Haukaas and A. Der Kiureghian. Strategies for finding the design point in non-linear finite element reliability analysis. *Probabilistic Engineering Mechanics*, 21(2): 133 – 147, 2006. ISSN 0266-8920.

[154] Y.A. Hegazy, P.W. Mayne, and S. Rouhani. Geostatistical assessement of spatial variability in piezocone tests. In *Proceedings of Uncertainty in the geological environment: from theory to practice*, New York, 1996. ASCE.

[155] K.M. Hess. Use of a borehole flowmeter to determine spatial heterogeneity of hydraulic conductivity and macrodispersion in a sand and gravel aquifer, cape cod, massachusetts. In *Proceedings of New Field Techniques for Quantizing the Physical*

and Chemical Properties of Heterogeneous Aquifers, National Water Well Association, Dublin, OH, pages 497–508, 1989.

[156] M.A. Hicks and C. Onisiphorou. Stochastic evaluation of static liquefaction in a predominantly dilative sand fill. *Geotechnique*, 55:123–133, 2005.

[157] M.A. Hicks and K. Samy. Influence of anisotropic spatial variability on slope reliability. In *Proceedings of the 8th International Symposium on Numerical Models in Geomechanics, Rome, Italy*, pages 535–9, 2002.

[158] M.A. Hicks and W.A. Spencer. Influence of heterogeneity on the reliability and failure of a long 3D slope. *Computers and Geotechnics*, 37(7):948–955, 2010.

[159] C. Hilldale. A probabilistic approach to estimating differential settlement of footings on sand. Master's thesis, Massachusetts Institute of Technology, 1971.

[160] K. Hoeg and W.H. Tang. Probabilistic considerations in the foundation engineering for offshore structures. In *Proceedings of 2nd International Conference on Structural Safety and Reliability, ICOSSAR, Munich*, pages 267–269, 1977.

[161] R.J. Hoeksema and P.K. Kitanidis. Analysis of the spatial structure of properties of selected aquifers. *Water Resources Research*, 21(4):563–572, 1985.

[162] J.A. Hoeting, D. Madigan, A.E. Raftery, and C. T. Volinsky. Bayesian Model Averaging: a tutorial. *Statistical Science*, 14(14):382–417, 1999.

[163] W. Hof. Zum Begriff Sicherheit. *Beton- und Stahlbetonbau*, 86(12):286–289, 1991.

[164] A. Hommels, M. Huber, F. Molenkamp, and P.A.: Vermeer. Inverse modelling including spatial variability applied to the construction of a road embankment. In T. Benz, editor, *Proceedings of the 7th European Conference on Numerical Methods in Geotechnical Engineering, Trondheim, 2010 (NUMGE)*, pages 369–374, 2010.

[165] Y. Honjo. A new identification method for autocorrelation function of geotechnical data: the exteded bayesian metho. In R. Poettler, H. Klapperich, and H.F. Schweiger, editors, *Proceedings of International Conference on Probabilistic in Geotechnics: Technical and Economic Risk Estimation*, pages 71–78, 2002.

[166] Y. Honjo. Challenges in geotechnical reliability based design. In N. Vogt, B. Schuppener, D. Straub, and G. Bräu, editors, *Proceedings of ISGSR: Geotechnical Safety and Risk*, pages 11–28, 2011.

[167] Y. Honjo and K. Kuroda. A new look at fluctuating geotechnical data for reliability design. *Soils and Foundations*, 31(1):110–120, 1991.

[168] Y. Honjo, T. Hara, M. Suzuki, M. Shirato, T.C. Le Kieu, and Y. Kikuchi. Code calibration in reliability based design level i verification format for geotechnical structures. In *Proceedings of 2nd International Symposium on Geotechnical Safety and Risk*, pages 435–452, 2009.

[169] N. Horn. Horizontaler Erddruck auf senkrechte Abschlussflächen von Tunnelröhren. In *Proceedings of Landeskonferenz der ungarischen Tiefbauindustrie (German translation by STUVA Düsseldorf)*, pages 7–16, 1961.

[170] L. Houy, D. Breysse, and A. Dents. Influence of soil heterogeneity on load redistribution and settlement of a hyperstatic three-support frame. *Geotechnique*, 55(2): 163–170, 2005.

[171] L.Y. Hu, G. Blanc, and B. Noetinger. Gradual deformation and iterative calibration of sequential stochastic simulations. *Mathematical Geology*, 33(4):475–489, 2001.

[172] M. Huber, A. Möllmann, A. Bárdossy, and P.A. Vermeer. Contributions to probabilistic soil modelling. In H. Vrijling P.H.A.J.M. van Gelder, D. Proske, editor, *7th International Probabilistic Symposium*, pages 519–530, 2009.

[173] M. Huber, P.A. Vermeer, and A. Bardossy. Untersuchungen zur Variabilität des Untergrundes. In H. Schad and C. Vogt, editors, *Proceedings of Bauen in Boden und Fels*, 2009.

[174] M. Huber, M.A. Hicks, P.A. Vermeer, and C. Moormann. Probabilistic calculation of differential settlement due to tunnelling. In L. Gucma, P. van Gelder, and D. Proske, editors, *Proceedings of 8th International Probabilistic Symposium*, 2010.

[175] M. Huber, A. Möllmann, and P.A. Vermeer. PC-River–reliability analysis of embankment stability. *Georisk*, 5(2):132–142, 2011.

[176] M. Huber, M.R.S. Sadaghiani, C. Moormann, and K.J. Witt. Beitrag zur räumlichen Beschreibung der Heterogenität des Untergrundes. In J. Tiedemann, editor, *Proceedings of 18. Tagung für Ingenieurgeologie*, 2011.

[177] M. Huber, P.A. Vermeer, M.A. Hicks, and C. Moormann. Reliability based design in tunnelling. In Ch. Brenguer, editor, *Proceedings of the European Safety and Reliability Conference: Advances in Safety, Reliability and Risk Management, Troyes, France*, pages 308–317, 2011.

[178] M. Huber, P.A. Vermeer, and C. Moormann. Evaluation and implications of soil variability in tunneling. In M.H. Faber, editor, *Proceedings of Applications of Statistics and Probability in Civil Engineering, Proceedings of the 11th International Conference on Applications of Statistics and Probability in Civil Engineering (ICASP11), Zürich, Switzerland*, pages 2785–2791, 2011.

[179] P. Hufschmied. Estimation of three-dimensional statistically anisotropic hydraulic conductivity field by means of single well pumping tests combined with flowmeter measurements. *Hydrogeologie*, 2:163–174, 1986.

[180] J. Iqbal, J.A. Thomasson, J.N. Jenkins, P.R. Owens, and F.D. Whisler. Spatial variability analysis of soil physical properties of alluvial soils. *Soil Science Society of America Journal*, 69:1338–1350, 2005.

[181] E.H. Isaaks. Indicator simulation: application to the simulation of a high grade uranium mineralization. In *Geostatistics for Natural resources characterization; P II. D. Reidel, Dordrecht*, pages 1057–1069, 1984.

[182] E.H. Isaaks and R.M. Srivastava. *Applied geostatistics*, volume 2. Oxford University Press New York, 1989.

[183] ISO 2394. General principles on the reliability of structures, 1998.

[184] M. B. Jacksa. *The influence of spatial variability on the geotechnical design properties of a stiff, overconsolidated clay*. PhD thesis, The University of Adelaide, 1995.

[185] M.B. Jaksa, P.I. Brooker, and W.S. Kaggwa. Modelling the spatial variability of the undrained shear strength of clay soils using geostatistics. In *Proceedings of 5th International Geostatistics Congress*, pages 1284–1295, 1997.

[186] M.B. Jaksa, W.S. Kaggwa, and P.I. Brooker. Experimental evaluation of the scale of fluctuation of a stiff clay. In *Proceedings of 8th International Confernece on the Application of Statistics and Probability*, volume 1, pages 415–422. Sydney, AA Balkema, Rotterdam, 1999.

[187] M.B. Jaksa, W.S. Kaggwa, G.A. Fenton, and H.G. Poulos. A framework for quantifying the reliability of geotechnical investigations. In *Proceedings of 9th International Conference on the Application of Statistics and Probability in Civil Engineering*, pages 1285–1291, 2003.

[188] A.G. Journel. Resampling from stochastic simulations. *Environmental and Ecological Statistics*, 1(1):63–91, 1994.

[189] A.G. Journel and F. Alabert. Non-gaussian data expansion in the earth sciences. *Terra Nova*, 1(2):123–134, 1989.

[190] A.G. Journel and C.J. Huijbregts. *Mining geostatics*. Academic Press, London, 1978.

[191] H. Karadeniz and T. Vrouwenvelder. SAFERELNET : Task 5.1: Overview reliability methods. Technical report, TU Delft, The Netherlands, October 2003.

[192] J.M. Keaveny, F. Nadim, and S. Lacasse. Autocorrelation functions for offshore geotechnical data. In *Proceedings of the 5th International Conference on Structural Safety and Reliability (ICOSSAR)*, pages 263–270, 1994.

[193] R. Kerry and M. A. Oliver. Determining the effect of asymmetric data on the variogram II - Outliers. *Computers & Geosciences*, 33(10):1233–1260, 2007.

[194] R. Kerry and M.A. Oliver. Determining the effect of asymmetric data on the variogram I - Underlying asymmetry. *Computers & Geosciences*, 33(10):1212–1232, 2007.

[195] L. Kirkup and R.B. Frenkel. *An Introduction to Uncertainty in Measurement: Using the GUM (Guide to the Expression of Uncertainty in Measurement)*. Cambridge University Press, 2006.

[196] A. Kirsch. *On the face stability of shallow tunnels in sand*. PhD thesis, Universtität Innsbruck, 2009.

[197] P.K. Kitanidis. Statistical estimation of polynomial generalized covariance functions and hydrologic applications. *Water Resources Research*, 19(4):909–921, 1983.

[198] P.K. Kitanidis. Parameter uncertainty in estimation of spatial functions: Bayesian analysis. *Water Resources Research WRERAO Vol. 22*, 22(4):499–507, 1986.

[199] P.K. Kitanidis. Parametric estimation of covariances of regionalized variables. *Journal of the American Water Resources Association*, 23(4):557–567, 1987.

[200] P.K. Kitanidis and R.W. Lane. Maximum likelihood parameter estimation of hydrologic spatial processes by the Gauss-Newton method. *Journal of hydrology*, 79 (1-2):53–71, 1985.

[201] M. Kittridge, L. Lake, F. Lucia, and G. Fogg. Outcrop/subsurface comparisons of heterogeneity in the San Andres Formation. *SPE Formation Evaluation*, 5(3):233–240, 1990.

[202] H. Klammler, M. McVay, D. Horhota, and P. Lai. Influence of spatially variable side friction on single drilled shaft resistance and lrfd resistance factors. *Journal of Geotechnical and Geoenvironmental Engineering*, 136:1114, 2010.

[203] M. Kleiber and T.D. Hien. *The Stochastic Finite Element Method*. John Wiley & Sons Inc, 1992.

[204] C.E. Koltermann and S.M. Gorelick. Heterogeneity in sedimentary deposits: A review of structure-imitating, process-imitating and descriptive approaches. *Water Resources Research*, 32(9):2617–2658, 1996.

[205] D. Kolymbas. *Tunnelling and tunnel mechanics: a rational approach to tunnelling*. Springer Verlag, 2005.

[206] A.S.D.A.C.M. Kormann and J.H.D. Shuttle. Variability Analysis of SPT and CPT data for a Reliability-based Embankment Design of a Southern Brazilian Port Site. In *Proceedings of XIII Brazilian Conference on Soil Mechanics and Geotechnical Engineering*. Curitiba, Brazil, 2006.

[207] H. Kreuter. *Ingenieurgeologische Aspekte geostatistischer Methoden*. PhD thesis, Technische Universität Karlsruhe,Institute of Geotechnicla Engineering, 1996.

[208] P. Kulatilake and A. Ghosh. An investigation into accuracy of spatial variation estimation using static cone penetrometer data. In *Proceedings of the 1st International Conference on Penetration Testing, Orlando, Fla*, pages 815–821, 1988.

[209] P.H.S.W. Kulatilake and J.G. Um. Spatial variation of cone tip resistance for the clay site at texas university. *Geotechnical and Geological Engineering*, 21(2):149–165, 2003.

[210] H. Kupfersberger and C.V. Deutsch. Methodology for integrating analog geologic data in 3-d variogram modeling. *AAPG bulletin*, 83(8):1262–1278, 1999.

[211] S. Lacasse and J.Y. de Lamballerie. Statistical treatment of CPT data. In *Proceedings of the International Symposium on Cone Penetration Testing*, pages 4–5, 1995.

[212] S.M. Lacasse, C.C. Ladd, and A.K. Barsvary. Undrained behavior of embankments on new liskeard varved clay. *Canadian Geotechnical Journal*, 14(3):367–388, 1977.

[213] P.V. Lade and J.M. Duncan. Elastoplastic stress-strain theory for cohesionless soil. *Journal of the Geotechnical Engineering Division*, 101(10):1037–1053, 1975.

[214] R.M. Lark. Estimating variograms of soil properties by the method-of-moments and maximum likelihood. *European Journal of Soil Science*, 51(4):717–728, 2000.

[215] G. Le Loc'h, H. Beucher, A. Galli, B. Doligez, HERESIM Group, et al. Improvement in the truncated gaussian method: Combining several gaussian functions. In *ECMOR IV, Proceedings of the 4th European Conference on the Mathematics of Oil Recovery, R oslash ros, Norway*, 1994.

[216] E. Leca and L. Dormieux. Upper and lower bound solutions for the face stability of shallow circular tunnels in frictional material. *Geotechnique*, 40(4):581–606, 1990.

[217] M. Lemaire, A. Chateauneuf, and J.C. Mitteau. *Structural reliability*. Wiley Online Library, 2009.

[218] A. Lentz. *Acceptability of civil engineering decisions involving human consequences*. PhD thesis, Technischen Universität München, München, 2007.

[219] C.C. Li and A. der Kiureghian. Optimal discretization of random fields. *Journal of Engineering Mechanics*, 119:1136, 1993.

[220] J. Li, A. Bárdossy, L. Guenni, and M. Liu. A copula based observation network design approach. *Environmental Modelling & Software*, 26(11):1349–1357, 2011.

[221] K.S. Li and I.K. Lee. The assessment of geotechnical safety. In *Selected Topics in Geotechnical Engineering-Lumb Volume*, 1991.

[222] C. N. Liu and C.-H. Chen. Spatial correlation structures of CPT data in a liquefaction site. *Engineering Geology*, 111(1-4):43 – 50, 2010.

[223] C.N. Liu and C.H. Chen. Estimating spatial correlation structures based on CPT data. *Georisk: Assessment and Management of Risk for Engineered Systems and Geohazards*, 4(2):99–108, 2010.

[224] K. Loague and G.A. Gander. R-5 revisited: Spatial variability of infiltration on a small rangeland catchment. *Water Resources Research*, 26(5):957–971, 1990.

[225] N. Luhmann. Die Moral des Risikos und das Risiko der Moral. In *Proceedings of Risiko und Gesellschaft*, pages 327–338. Westdeutscher Verlag, Opladen, 1997.

[226] P. Lumb. Safety factors and the probability distribution of soil strength. *Canadian Geotechnical Journal*, 7(3):225–242, 1970.

[227] P. Lumb. Application of statistics in soil mechanics. In *Soil Mechanics: New Horizons*, pages 44–112, 1974.

[228] P. Lumb. Spatial variability of soil properties. In *Proceedings of the 2nd International Conference on Application of Statistics and Probability to Soil and Structural Engineering, Aachen*, volume 2, pages 397–421, 1975.

[229] P. Lumb and J.K. Holt. The undrained shear strength of a soft marine clay from Hong Kong. *Geotechnique*, 18(1):25–36, 1968.

[230] H.J. Lund, H. Ates, E. Kasap, and R.W. Tillman. Comparison of Single and Multi-Facies Variograms of Newcastle Sandstone: Measures for the Distribution of Barriers to Flow. In *Low Permeability Reservoirs Symposium*, pages 507–522, 1995.

[231] R.J. Luxmoore, B.P. Spalding, and I.M. Munro. Areal variation and chemical modification of weathered shale infiltration characteristics. *Soil Science Society of America Journal*, 45(4):687, 1981.

[232] A.V. Lyamin, R. Salgado, S.W. Sloan, and M. Prezzi. Two-and three-dimensional bearing capacity of footings in sand. *Géotechnique*, 57(8):647–662, 2007.

[233] R.J. Mair and R.N. Taylor. Theme lecture: Bored tunneling in the urban environment. In *Proceedings of the 14th International Conference on Soil Mechanics and Foundation Engineering*, pages 2353–2385, 1997.

[234] H.B. Mann. Nonparametric tests against trend. *Econometrica: Journal of the Econometric Society*, 2:245–259, 1945.

[235] A. Marache, J. Dubost, D. Breysse, A. Denis, and S. Dominique. Understanding subsurface geological and geotechnical complexity at various scales in urban soils using a 3D model. *Georisk: Assessment and Management of Risk for Engineered Systems and Geohazards*, 1(1):1–14, 2009.

[236] B.P. Marchant and R.M. Lark. Estimating variogram uncertainty. *Mathematical Geology*, 36(8):867–898, 2004.

[237] B.P. Marchant and R.M. Lark. Adaptive sampling and reconnaissance surveys for geostatistical mapping of the soil. *European Journal of Soil Science*, 57(6):831–845, 2006.

[238] F. Marconi. *Ricostruzione con metodi geostatistici di corpi alluvionali sepolti per la valutazione delle pericolosita geologiche in aree urbane*. PhD thesis, Universita degli studi di Roma "Sapienza", Facolta di Ingegneria, Dipartimento Ingegneria Chimica Materiali Ambiente, 2013.

[239] G. Matheron. *The theory of regionalized variables and its applications*, volume 5. École national supérieure des mines, 1971.

[240] G. Matheron and F. Blondel. *Traité de géostatistique appliquée*. Editions Technip, 1962.

[241] G. Matheron, H. Beucher, A. Galli, D. Guerillot, and C. Ravenne. Conditional simulation of the geometry of fluvio-deltaic reservoirs. In *SPE Annual Technical Conference and Exhibition*, 1987.

[242] M. Matsuo. Reliability in embankment design. Technical Report R76-33., Department of Civil Engineering, Massachusetts Institute of Technology, Cambridge, Res. Rept. R, 1976.

[243] H. Matsuoka and T. Nakai. Relationship among Tresca, Mises, Mohr-Coulomb and Matsuoka-Nakai failure criteria. *Soils and Foundations*, 25(4):123–128, 1985.

[244] H.G. Matthies and A. Keese. Galerkin methods for linear and nonlinear elliptic stochastic partial differential equations. *Computer Methods in Applied Mechanics and Engineering*, 194(12):1295–1331, 2005.

[245] H.G. Matthies, C. Brenner, C. Bucher, and C. Guedes Soares. Uncertainties in probabilistic numerical analysis of structurs and solids – stochastic finite elements. *Structural Safety*, 19(3):283–335, 1997.

[246] B. Matti. *Geological heterogeneity in landslides: characterization and flow modelling*. PhD thesis, Ecole Polytechnique Federale de Lausanne, 2008.

[247] A.B. McBratney and R. Webster. Choosing functions for semi-variograms of soil properties and fitting them to sampling estimates. *European Journal of Soil Science*, 37(4):617–639, 1986.

[248] A.B. McBratney, R. Webster, and T.M. Burgess. The design of optimal sampling schemes for local estimation and mapping of of regionalized variables: Theory and method. *Computers & Geosciences*, 7(4):331–334, 1981.

[249] M.D. McKay. Evaluating prediction uncertainty. Technical report, Office of Nuclear Regulatory Research. Division of Systems Technology and Los Alamos National Laboratory, 1995.

[250] S.A. McKenna. Probabilistic Approach to Site Characterization: MIU Site, Tono Region, Japan. Technical report, Sandia National Labs., Albuquerque, NM (US); Sandia National Labs., Livermore, CA (US), 2001.

[251] G. G. Meyerhof. Development of geotechnical limit state design. *Canadian Geotechnical Journal*, 32(1):128–136, 1995.

[252] B. Möller, M. Beer, W. Graf, A. Hoffmann, and J.-U. Sickert. Modellierung von Unschärfe im Ingenieurbau. *Bauinformatik Journal*, 3(11):697–708, 2000.

[253] S.C. Möller. *Tunnel induced settlements and structural forces in linings*. PhD thesis, Institute of Geotechnical Engineering, University of Stuttgart, 2006.

[254] A.F.D. Möllmann. *Probabilistische Untersuchung von Hochwasserschutzdeichen mit analytischen Verfahren und der Finite-Elemente-Methode*. PhD thesis, University of Stuttgart, Institute of Geotechnical Engineering, 2009.

[255] G. Mollon, D. Dias, and A.H. Soubra. Probabilistic analysis of circular tunnels in homogeneous soil using response surface methodology. *Journal of Geotechnical and Geoenvironmental Engineering*, 135:1314–1325, 2009.

[256] G. Mollon, D. Dias, and A.H. Soubra. Face stability analysis of circular tunnels driven by a pressurized shield. *Journal of Geotechnical and Geoenvironmental Engineering*, 136:215–229, 2010.

[257] Monitor Environmental Consultants Ltd. Secondary model procedure for the development of appropriate soil sampling strategies for land contamination, 2012. URL `www.environment-agency.gov.uk`.

[258] R.L. Muhanna, H. Zhang, and R.L. Mullen. Interval finite elements as a basis for generalized models of uncertainty in engineering mechanics. *Reliable Computing*, 13(2):173–194, 2007.

[259] D.J. Mulla. Estimating spatial patterns in water content, matric suction, and hydraulic conductivity. *Soil Sciences Society of America Journal*, 52(6):1547–1553, 1988.

[260] D.S. Murty and G.L.S. Babu. Effect of spatial correlation structure and transformation model on the design of shallow strip footing. *Geomechanics and Geoengineering*, 5(2):91–97, 2010.

[261] J. Murzewski. *Sicherheit der Baukonstruktionen*. VEB Verlag für Bauwesen, Berlin, 1974.

[262] A. Nasekhian. *Application of non-probabilistic and probabilistic concepts in finite element analysis fo tunneling*. PhD thesis, TU Graz, Institute of Soil Mechanics, 2011.

[263] H.D. Netzel. *Building response due to ground movements*. PhD thesis, Delft University of Technology, 2011.

[264] I.T. Ng and C.Y. Zhou. Uncertainty-based optimization of site characterization using cpt. In *Proceedings of 2nd International Symposium on Cone Penetration Testing*, Huntington Beach, CA, USA, May 2010 2010.

[265] V.U. Nguyen and R.N. Chowdhury. Simulation for risk analysis with correlated variables. *Geotechnique*, 35(1):47–58, 1985.

[266] J.D. Nuttall. *Parallel Implementation and Application of the Random Finite Element Method*. PhD thesis, The University of Manchester, Manchester, UK, 2011.

[267] M. P. O'Reilly and B. M. New. Settlements above tunnels in the UK-their magnitude and prediction. In *Proceedings of Tunnelling, 82*, pages 173–181, 1982.

[268] J. Ortiz and C.V. Deutsch. Calculation of uncertainty in the variogram. *Mathematical Geology*, 34(2):169–183, 2002.

[269] J. Ouellet, D.E. Gill, and M. Soulié. Geostatistical approach to the study of induced damage around underground rock excavations. *Canadian Geotechnical Journal*, 24 (3):384–391, 1987.

[270] E. Pardo-Iguzquiza. Maximum likelihood estimation of spatial covariance parameters. *Mathematical Geology*, 30(1):95–108, 1998.

[271] E. Pardo-Igúzquiza. Varfit: a fortran-77 program for fitting variogram models by weighted least squares. *Computers & Geosciences*, 25(3):251–261, 1999.

[272] E. Pardo-Iguzquiza and P. Dowd. Variance–covariance matrix of the experimental variogram: Assessing variogram uncertainty. *Mathematical Geology*, 33(4):397–419, 2001.

[273] R.L. Parsons and J.D. Frost. Evaluating site investigation quality using GIS and geostatistics. *Journal of Geotechnical and Geoenvironmental Engineering*, 128(6):451–461, 2002.

[274] R.B. Peck. Deep excavations and tunnelling in soft ground. In *7th Int. Conf. on Soil Mech. and Found. Engrg., Mexico*, pages 225–290. Sociedad Mexican de Mecanica de Suelos, 1969.

[275] Pacific Earthquake Engineering Research Center (PEER). Strong motion database, 06 2012. URL `http://peer.berkeley.edu`.

[276] B. Peintinger and R. Rackwitz. Berichte zur Zuverlaessigkeitstheorie der Bauwerke: Numerical uncertainty analysis of slopes. Technical report, Technische Universität München, 1980.

[277] E.W. Perau. *Ein systematischer Ansatz zur Berechnung des Grundbruchwiderstands von Fundamenten*. PhD thesis, Universität Gesamthochschule Essen, 1995.

[278] G. Peschl and H. Schweiger. Reliability analysis in geotechnics with finite elements-comparison of probabilistic, stochastic and fuzzy set methods. In *Proceedings of Symposium on Imprecise Probabilities and their Applications ISIPTA'03*, 2003.

[279] G.M. Peschl. *Reliability Analysis in Geotechnics with the Random Set Element Method*. PhD thesis, TU Graz, Institute of Soil Mechanics, 2004.

[280] G.M. Peschl. *Reliability analyses in geotechnics with the random set finite element method*. PhD thesis, TU Graz, Institute of Soil Mechanics, 2011.

[281] A.N. Pettitt and A.B. McBratney. Sampling designs for estimating spatial variance components. *Journal of the Royal Statistical Society. Series C (Applied Statistics)*, 42(1): 185–209, 1993.

[282] K.-K. Phoon and F.H. Kulhawy. Evaluation of geotechnical property variabaility. *Canadian Geotechnical Journal*, 36:625–639, 1999.

[283] K.-K. Phoon and F.H. Kulhawy. Characterization of geotechnical variability. *Canadian Geotechnical Journal*, 36:612–624, 1999.

[284] K.-K Phoon, S.-T. Quek, and P. An. Identification of statistically homogeneous oil layers using modified Bartlett stastistics. *Journal of Geotechnical and Geoenvironmental Engieneering*, 120(7):649–659, 2003.

[285] K.K. Phoon. *Reliability-based design of foundations for transmission line structures*. PhD thesis, Cornell University, 1995.

[286] K.K. Phoon. *Reliability-Based Design in Geotechnical Engineering - Computations and Applications*. Taylor & Francis, 2008.

[287] J.S. Piersol. Random data analysis and measurement procedures. *Measurement Science and Technology*, 11:1825, 2000.

[288] R. Popescu. *Stochastic variability of soil properties: data analysis, digital simulation, effects on system behavior*. PhD thesis, Princeton University, 1995.

[289] R. Popescu, G. Deodatis, and A. Nobahar. Effects of random heterogeneity of soil properties on bearing capacity. *Probabilistic Engineering Mechanics*, 20(4):324 – 341, 2005.

[290] R. Pöttler and H.F. Schweiger. Anwendung der Random-Set-Methode (RSM) für Standsicherheitsuntersuchungen im Tunnelbau. *Bautechnik*, 83(11):754–759, 2006.

[291] D. Potts, K. Axelsson, L. Grande, H.F. Schweiger, and M. Long. *Guidelines for the use of advanced numerical analysis*. Thomas Telford Services Limited, 2002.

[292] D.M. Potts and L. Zdravković. *Finite element analysis in geotechnical engineering: application*, volume 2. Thomas Telford Services Limited, 2001.

[293] L. Prandtl. Über die Härte plastischer Körper. *Göttingen Nachr. Math. Phys. Kl*, 12: 74–85, 1920.

[294] W.H. Press, S.A. Teukolsky, W.T. Vettrling, and B.P. Flannery. *Numerical Recipes in FORTRAN - The Art of Scientific Computing*, volume second edition. Cambridge University Press, second edition edition, 1992.

[295] D. Proske. *Catalogue of Risks - Natural, Technical, Social and Health Risks*. Springer-Verlag Berlin, 2008.

[296] D. Proske. Debris flow impact uncertainty modeling with Grey Numbers. In L. Gucma, P. van Gelder, and D. Proske, editors, *Proceedings of 8th International Probabilistic Symposium*, pages 285–294, 2010.

[297] D. Proske, P. Lieberwirth, and P. van Gelder. *Sicherheitsbeurteilung historischer Steinbogenbrücken*. Dirk Proske Verlag, Wien Dresden, 2006.

[298] Z.P. Qiu and I. Elishakoff. Antioptimization of structures with large uncertain-but-non-random parameters via interval analysis. *Computer methods in Applied Mechanics and Engineering*, 152(3):361–372, 1998.

[299] R. Rackwitz. Optimization and risk acceptability based on the life quality index. *Structural Safety*, 24(2-4):297–331, 2002.

[300] A. Raftery, F. Balabdaoui, T. Gneiting, and M. Polakowski. Using Bayesian Model Averaging to calibrate froecast ensembles. Technical Report 440, Department of statistics, Unviersity of Washington, December 2004.

[301] G. Raspa, M. Moscatelli, F. Stigliano, A. Patera, F. Marconi, D. Folle, R. Vallone, M. Mancini, G.P. Cavinato, S. Milli, et al. Geotechnical characterization of the upper Pleistocene-Holocene alluvial deposits of Roma (Italy) by means of multivariate geostatistics: Cross-validation results. *Engineering Geology*, 101(3-4):251–268, 2008.

[302] K.R. Rehfeldt. *Prediction of macrodispersivity in heterogeneous aquifers*. PhD thesis, Massachusetts Institute of Technology, Dept. of Civil Engineering, 1988.

[303] K.R. Rehfeldt, J.M. Boggs, and L.W. Gelhar. Field study of dispersion in a heterogeneous aquifer 3. geostatistical analysis of hydraulic conductivity. *Water Resources Research*, 28(12):3309–3324, 1992.

[304] N. Remy, A. Boucher, and J. Wu. *Applied geostatistics with SGeMS: A user's guide*. Cambridge University Press, 2008.

[305] N. Remy, Alexandre. Boucher, and Jianbing. Wu. *Applied geostatistics with SGeMS*. Cambridge University Press, 2009.

[306] O. Renn. Concepts of risk: a classification. In S. Krimsky and D. Golding, editors, *Proceedings of Social Theories of Risk*, pages 53–79. Praeger, London, 1992.

[307] M. Riva, L. Guadagnini, A. Guadagnini, T. Ptak, and E. Martac. Probabilistic study of well capture zones distribution at the Lauswiesen field site. *Journal of Contaminant Hydrology*, 88(1-2):92–118, 2006.

[308] P.K. Robertson. Soil classification using the cone penetration test. *Canadian Geotechnical Journal*, 27(1):151–158, 1990.

[309] P.J. Roebber. Visualizing multiple measures of forecast quality. *Weather and Forecasting*, 24(2):601–608, 2009.

[310] K.O. Ronold and P. Bjerager. Model uncertainty representation in geotechnical reliability analyses. *Journal of Geotechnical Engineering*, 118:363, 1992.

[311] N.M. Ruse. *Räumliche Betrachtung der Standsicherheit der Ortsbrust beim Tunnelvortrieb*. PhD thesis, Institute of Geotechnical Engineering, University of Stuttgart, 2004.

[312] C. Russelli. *Probabilistic methods applied to the bearing capacity problem*. PhD thesis, Institute of Geotechnical Engineering, University of Stuttgart, 2008.

[313] D. Russo. A geostatistical approach to solute transport in heterogeneous fields and its applications to salinity management. *Water Resources Research*, 20(9):1260–1270, 1984.

[314] D. Russo. Design of an optimal sampling network for estimating the variogram. *Soil Science Society of America Journal*, 48(4):708–716, 1984.

[315] D. Russo and E. Bresler. Soil hydraulic properties as stochastic processes: I. an analysis of field spatial variability. *Soil Science Society of America Journal*, 45(4):682, 1981.

[316] L. Sachs. *Angewandte Statistik*. Springer, 2002.

[317] A. Saltelli. *Sensitivity analysis in practice: a guide to assessing scientific models*. John Wiley & Sons Inc, 2004.

[318] A. Saltelli and I.M. Sobol. About the use of rank transformation in sensitivity analysis of model output. *Reliability Engineering & System Safety*, 50(3):225–239, 1995.

[319] A. Saltelli, S. Tarantola, and K.P.S. Chan. A quantitative model-independent method for global sensitivity analysis of model output. *Technometrics*, 41:39–56, 1999.

[320] P. Samui and T.G. Sitharam. Site characterization model using artificial neural network and kriging. *International Journal of Geomechanics*, 10:171–180, 2010.

[321] H. Schad. *Zeit-und geschwindigkeitsabhängiges Materialverhalten in der Geotechnik: Experimentelle Erfassung und numerische Analyse*. PhD thesis, Institute of Geotechnical Engineering, University of Stuttgart, 1992.

[322] H. Schad and G. Teutsch. Geostatistical analysis of hydraulic conductivity related data based on core samples from a heterogeneous fluvial aquifer. *Statistical Methods and Applications*, 4(1):125–140, 1995.

[323] M.T. Schafmeister and A. Pekdeger. Spatial structure of hydraulic conductivity in various porous media-problems and experiences. *Geostatistics Tróia'92*, 1:733–743, 1993.

[324] B. Schmidt. *Settlements and ground movements associated with tunneling in soil*. PhD thesis, University of Illinois., 1969.

[325] J. Schneider. *Sicherheit und Zuverlässigkeit im Bauwesen: Grundwissen für Ingenieure*. VDF, Hochschul-Verl. an der ETH, 1996.

[326] G.I. Schueller. A state-of-the-art report on computational stochastic mechanics. *Probabilistic Engineering Mechanics*, 12(4):197–321, 1997.

[327] G.I. Schueller, H.J. Pradlwarter, and P.S. Koutsourelakis. A comparative study of reliability estimation procedures for high dimensions. In *Proceedings of 16th ASCE Engineering Mechanics Conference*, pages 233 – –243, 2003.

[328] M.T. Schultz, B.P. Gouldby, J.D. Simm, and J.L. Wibowo. Beyond the factor of safety: developing fragility curves to characterize system reliability. Technical report, DTIC Document, 2010.

[329] B. Schuppener. Eurocode 7 geotechnical design. part 1: General rules and its latest developments. *Georisk*, 4(1):32–42, 2010.

[330] B. Schuppener. Nachweiskonzepte und Sicherheit in der Geotechnik. In C. Boley, editor, *Handbuch Geotechnik*, pages 225–258. Vieweg+Teubner Verlag, 2012. ISBN 978-3-8348-8272-1.

[331] T. Schweckendiek and E.O.F. Calle. A factor of safety for geotechnical characterization. In *Proceedings of Seventeenth Southeast Asian Geotechnical Conference (17SEAGC)–Geo-Engineering for Natural Hazard Mitigation and Sustainable Development*, volume 2, pages 227–230, 2010.

[332] H.F. Schweiger and G.M. Peschl. Reliability analysis in geotechnics with the random set finite element method. *Computers and Geotechnics*, 32(6):422–435, 2005.

[333] H.F. Schweiger, R. Thurner, and R. Pöttler. Reliability analysis in geotechnics with deterministic finite elements. *International Journal of Geomechanics*, 1(4):389–413, 2001.

[334] H.F. Schweiger, G.M. Peschl, and R. Pöttler. Application of the random set finite element method for analysing tunnel excavation. *Georisk*, 1(1):43–56, 2007.

[335] R.K. Senger, F.J. Lucia, C. Kerans, M. Ferris, and C. E. Fogg. Geostatistical/Geological Permeability Characterization of Carbonate Ramp Deposits in Sand Andres Outcrop, Algerita Escarpment, New Mexico . In *Permian Basin Oil and Gas Recovery Conference, Midland, Texas*, pages 287–301. Society of Petroleum Engineers, 1992.

[336] K. Sett, B. Jeremić, and M.L. Kavvas. Probabilistic elasto-plasticity: solution and verification in 1D. *Acta Geotechnica*, 2(3):211–220, 2007.

[337] M.A. Shahin, M.B. Jaksa, and H.R. Maier. Artificial neural network applications in geotechnical engineering. *Australian Geomechanics*, 36(1):49–62, 2001.

[338] J.E. Shigley and C.R. Mischke. *Mechanical Engineering Design*. McGraw Hill, New York, 2001.

[339] T.W. Simpson, T.M. Mauery, J.J. Korte, and F. Mistree. Kriging models for global approximation in simulation-based multidisciplinary design optimization. *AIAA journal*, 39(12):2233–2241, 2001.

[340] J.B. Sisson and P.J. Wierenga. Spatial variability of steady-state infiltration rates as a stochastic process. *Soil Science Society of America Journal*, 45(4):699, 1981.

[341] T.G. Sitharam, P. Samui, and P. Anbazhagan. Spatial variability of rock depth in bangalore using geostatistical, neural network and support vector machine models. *Geotechnical and Geological Engineering*, 26(5):503–517, 2008.

[342] I.M. Smith and D.V. Griffiths. *Programming the finite element method*. John Wiley & Sons, Inc., 1998.

[343] J.L. Smith and R.A. Freeze. *A stochastic analysis of steady-state groundwater flow in a bounded domain*. 1978., 1978.

[344] L. Smith. Spatial variability of flow parameters in a stratified sand. *Mathematical Geology*, 13(1):1–21, 1981.

[345] H.U. Smoltczyk. *Ermittlung eingeschränkt plastischer Verformungen im Sand unter Flachfundamenten*. W. Ernst, 1960.

[346] U. Smoltczyk. *Geotechnical Engineering Handbook - Volumen I: Fundamentals*. Wiley-VCH, 2003.

[347] I.M. Sobol. Global sensitivity indices for nonlinear mathematical models and their monte carlo estimates. *Mathematics and computers in simulation*, 55(1-3):271–280, 2001.

[348] V.V. Sokolovski and J.K. Kushner. Statics of granular media. *Journal of Applied Mechanics*, 33:239, 1966.

[349] P. Soos. Die Rolle des Baugrundes bei der Anwendung der neuen Sicherheitstheorie im Grundbau. *Geotechnik*, 19:82–91, 1990.

[350] A.H. Soubra. Kinematical approach to the face stability analysis of shallow circular tunnels. In *Proceedings of 8th International Symposium on Plasticity*, pages 443–445, 2000.

[351] A.H. Soubra, D.S. Youssef Abdel Massih, and K. Kalfa. Bearing capacity of foundations resting on a spatially random soil. In *Geocongress008*, 2008.

[352] M. Soulié. Geostatistical applications in geotechnics. *Geostatistics for natural resources characterization, Pt*, 2:703–730, 1984.

[353] M. Soulié, P. Montes, and V. Silvestri. Modelling spatial variability of soil parameters. *Canadian Geotechnical Journal*, 27(5):617–630, 1990.

[354] M.G. Speedie. Selection of design value from shear test results. In *Proceedings of the 2nd Australia-New Zealand Conference on Soil Mechanics and Foundation Engineering*, pages 107–109, Wellington, 1965.

[355] W.A. Spencer. *Parallel stochastic and finite element modelling of clay slope stability in 3D*. PhD thesis, University of Manchester, UK, 2007.

[356] M.J. Spry, F.H. Kulhawy, and M.D. Grigoriu. Reliability-based foundation design for transmission line structures: Geotechnical site characterization strategy. Technical Report EL-5507, Electric power research institute, Palo Alto, California, 1988.

[357] F.I. Stalkup. Permeability variation in a sandstone barrier island-tidal channel-tidal delta complex, ferron sandstone (lower cretaceous), central utah. In *Proceedings of SPE Annual Technical Conference and Exhibition*, 1986.

[358] G. Stefanou. The stochastic finite element method: Past, present and future. *Computer Methods in Applied Mechanics and Engineering*, 198:1031 – 1051, 2009. ISSN 0045-7825.

[359] A. Stein and J.W. van Groenigen. Constrained optimization of spatial sampling using continuous simulated annealing. *Journal of Environmental Quality*, 27(5):1078–1086, 1998.

[360] D. Straub. Reliability benchmarks in geotechnical engineering, May 2012. URL `http://geosnet.geoengineer.org/`.

[361] D. Straub, A. Lentz, I. Papaioannou, and R. Rackwitz. Life quality index for assessing risk acceptance in geotechnical engineering. In *Proceedings of the 3rd International Symposium on Geotechnical Safety and Risk*, pages 37–46, 2011.

[362] R. Suchomel and D. Mašín. Spatial variability of soil parameters in an analysis of a strip footing using hypoplastic model. In *Proceedings of 7th European conference on numerical methods in geomechanics, Trondheim, Norway, Taylor & Francis Group, London*, pages 383–388, 2010.

[363] E.A. Sudicky. A natural gradient experiment on solute transport in a sand aquifer: Spatial variability of hydraulic conductivity and its role in the dispersion process. *Water Resources Research*, 22(13):2069–2082, 1986.

[364] B. Sudret. *Uncertainty propagation and sensitivity analysis in mechanical models–Contributions to structural reliability and stochastic spectral methods*. Habilitation a diriger des recherches, Université Blaise Pascal, Clermont-Ferrand, France, 2007.

[365] B. Sudret. Global sensitivity analysis using polynomial chaos expansions. *Reliability Engineering & System Safety*, 93(7):964–979, 2008.

[366] B. Sudret and A. Der Kiureghian. Stochastic finite element methods and reliability: A state-of-the-art report. Technical report, Department of Civil & Cnvironmental Cngineering, University of California, Berkeley, 2000.

[367] B. Sudret and A. Der Kiureghian. Comparison of finite element reliability methods. *Probabilistic Engineering Mechanics*, 17(4):337–348, 2002.

[368] W.H. Tang. Probabilistic evaluation of penetration resistances. *Journal of the Geotechnical Engineering Division*, 105(10):1173–1191, 1979.

[369] W.H. Tang. Principles of probabilistic characterizations of soil properties. In *Probabilistic Characterization of Soil Properties - Bridge Between Theory and Practice*, pages 74–89. ASCE, 1984.

[370] W.H. Tang. Updating anomaly statistics-single anomaly case. *Structural safety*, 4 (2):151–163, 1986.

[371] J.M. Tantalla, J.H. Prevost, and G. Deodatis. Spatial variability of soil properties in slope stability analysis: fragility curve generation. In *Proceedings of ICOSSAR*, volume 1, pages 17–21, 2001.

[372] D.W. Taylor. Fundamentals of soil mechanics. *Soil Science*, 66(2):161, 1948.

[373] K. Terzaghi and R.B. Peck. *Soil mechanics in engineering practice*. Wiley, 1948.

[374] R. Thurner. *Probabilistische Untersuchungen in der Geotechnik mittels deterministischer Finite Elemente-Methode*. PhD thesis, TU Graz, Institute of Soil Mechanics, 2001.

[375] A. Tillmann, A. Englert, Z. Nyari, I. Fejes, J. Vanderborght, and H. Vereecken. Characterization of subsoil heterogeneity, estimation of grain size distribution and hydraulic conductivity at the krauthausen test site using cone penetration test. *Journal of Contaminant Hydrology*, 95(1-2):57–75, 2008.

[376] L. Tvedt. Distribution of quadratic forms in normal space– approximation to structural reliability. *Journal of Engineering Mechanics Division, ASCE*, 116(6):1183–1197, 1990.

[377] K. Tyler, A. Henriquez, and T. Svanes. Modeling heterogeneities in fluvial domains: A review of the influence on production profiles. *Stochastic Modeling and Geostatistics, AAPG Comput. Appl. Geol*, 3:77–89, 1994.

[378] Brussels Universite Catholique de Louvain. Ofda/cred international disaster database, 2012. URL `www.emdat.be`.

[379] K. Unlu, D.R. Nielsen, and W. Biggar. Stochastic analysis of state unsaturated flow. one dimensional monte carlo simulations and comparisons with spectral perturbation analysis and field observations. *Water Resources Research*, 26(1):2207–2218, 1990.

[380] U.S. Geological Survey (USGS). Earthquake hazards program, 06 2012. URL `http://earthquake.usgs.gov/`.

[381] M. Uzielli, G. Vannucchi, and K.K. Phoon. Random field characterisation of stress-normalised cone penetration testing parameters. *Geotechnique*, 55(1):3–20, 2005.

[382] P.H.A.J.M. van Gelder. *Stasticial methods fro the risk-based design of civil structures*. PhD thesis, Delft University of Technology, 2000.

[383] E.H. Vanmarcke. Reliability of earth slopes. *Journal of Geotechnical Engineering*, 103: 1247–1265, 1977.

[384] E.H. Vanmarcke. Probabilistic characterization of soil profiles. In *Site Characterization & Exploration*, pages 199–219. ASCE, 1978.

[385] E.H. Vanmarcke. *Random fields: analysis and synthesis*. MIT Press, 1984.

[386] E.H. Vanmarcke and N.F. Fuleihan. Probabilistic prediction of levee settlements. In *Proceedings of the 2nd International Conference on Applications of Statistics and Probability in Soil and Structural Engineering, Aachen*, volume 2, pages 175–190, 1975.

[387] E.H. Vanmarcke and M. Grigoriu. Stochastic finite element analysis of simple beams. *Journal of Engineering Mechanics*, 109:1203, 1983.

[388] V.N. Vapnik. *The nature of statistical learning theory*. Springer-Verlag New York Inc., 2000.

[389] Det Norske Veritas. *Structural reliability analysis of marine structures*. D.N.V., 1992.

[390] Det Norske Veritas. Statistical representation of soil data. Technical report, D.N.V., 1997.

[391] P. A. Vermeer, B. Westrich, A. Möllmann, U. Merkel, and M. Huber. PC-River - Zuverlässigkeitsanalys und Risikoabschätzung für den Hochwasserschutz unter integrierter Berücksichtigung geotechnischer, hydrologischer und hydraulischer Einflussgrössen. Technical report, University of Stuttgart, Institute of Geotechnical Engineering, 2011.

[392] P.A. Vermeer, N. Ruse, and T. Marcher. Tunnel heading stability in drained ground. *Felsbau*, 20(6):8–18, 2002.

[393] A. Verruijt and J.R. Booker. Surface settlements due to deformation of a tunnel in an elastic half plane. *Geotechnique*, 46(4):753–756, 1996.

[394] A. Verruijt and S. van Baars. *Soil mechanics*. VSSD, 2007.

[395] M.F. Versteeg. External safety policy in the netherlands: an approach to risk management. *Journal of hazardous materials*, 17(2):215–222, 1988.

[396] G. Vessia, C. Cherubini, J. Pieczyńska, and W. Puła. Application of random finite element method to bearing capacity design of strip footing. *Journal of Geoengineering*, 4(3):103–112, 2009.

[397] J.P. Visodic. *Design Stress Factors*, volume 55. ASME International, New York, 1948.

[398] U.H. Vollenweider. *Beitrag zur Behandlung bodenmechanischer Grenzwertprobleme nach der Plastizitätstheorie*. PhD thesis, Institut für Baustatik der ETH Zürich, 1969.

[399] T. Vrouwenvelder. The JCSS probabilistic model code. *Structural Safety*, 19(3):245–251, 1997.

[400] T. Vrouwenvelder and E.O.F. Calle. Measuring spatial correlation of soil properties. *HERON*, 48(4):2003, 2003.

[401] H. Wackernagel. *Multivariate geostatistics: an introduction with applications*. Springer Verlag, 2003.

[402] R. Webster and M.A. Oliver. Sample adequately to estimate variograms of soil properties. *Journal of soil science*, 43(1):177–192, 1992.

[403] R. Webster and M.A. Oliver. *Geostatistics for environmental scientists*. John Wiley & Sons Inc., 2007.

[404] D. Wickremesinghe and R.G. Campanella. Scale of fluctuation as a descriptor of soil variability. In *Proceedings of Conference on Probabilistic Methods in Geotech. Engrg*, pages 233–239, 1993.

[405] D.S. Wickremesinghe. *Stasticial characterisation of soil profile using in situ tests*. PhD thesis, University of British Columbia, 1989.

[406] T. Wolff. *Ein methodischer Bemessungsansatz zur Abschätzung des Tragverhaltens von Pfahlgründungen in weichem kalkigem Sedimentgestein*. PhD thesis, Bauhaus-Universität Weimar, 2009.

[407] T.F. Wolff. *Analysis and design of embankment dam slopes: a probabilistic approach*. PhD thesis, Purdue University, Lafayette, Ind., 1985.

[408] S.Y. Wong. *Stochastic Characterization and Reliability of Saturated Soils*. PhD thesis, Ph. D. Thesis, Manchester Centre for Civil and Construction Engineering, University of Manchester, England, 2004.

[409] A.D. Woodbury and EA Sudicky. The geostatistical characteristics of the Borden aquifer. *Water Resources Research*, 27(4):533–546, 1991.

[410] WS Atkins Consultants Ltd . Risk implications in site characterisation and analysis for offshore engineering and design. Technical report, Health and Safety Executive, 2004.

[411] T.H. Wu. Uncertainty, safety, and decision in soil engineering. *Journal of the Geotechnical Engineering Division*, 100(3):329–348, 1974.

[412] T.H. Wu and A. El-Jandali. Use of time series in geotechnical data analysis. *Geotech. Test. J*, 8(4):151–158, 1985.

[413] J. R. Ximenez de Embun and M. R. Romana. The formulation of soil model from penetrometer probabilistic information - application to differential settlement prediction. In *Proc. 4th Int. Conf. on Applications of Statistics and Probability in Soil and Structural Engineering*, pages 1601–1613, Pitagora Editrice, 1983.

[414] M.S. Yucemen, W.H. Tang, and A.H.S. Ang. A probabilistic study of safety and design of earth slopes. Technical report, Engineering Experiment Station, College of Engineering, University of Illinois at Urbana-Champaign, 1973.

[415] H. Zhang, R.L. Mullen, and R.L. Muhanna. Interval Monte Carlo methods for structural reliability. *Structural Safety*, 32(3):183–190, 2010.

[416] J. Zhang, L.M. Zhang, and W.H. Tang. Bayesian framework for characterizing geotechnical model uncertainty. *Journal of geotechnical and geoenvironmental engineering*, 135:932, 2009.

[417] Z.J. Zhang and M.T. Tumay. Statistical to fuzzy approach toward CPT soil classification. *Journal of Geotechnical and Geoenvironmental Engieneering*, 125(3):179–186, 1999.

Appendix A

Database on stochastic soil properties

A.1 Database on the variability of rock

Table A.1: Database on the variability of rock

property	soil type	θ_{ver} [m]	θ_{hor} [m]	applied spatial model	reference
permeability	outcrop of grainstone and dolomit	0.1	0.8		[201]
permeability	sand and gravel aquifer	0.5	20		[179]
permeability	sandstone aquifer	1			[28]
permeability	subsurface of dolomitized packstone and sandstone	2.6	2.7		[201]
permeability	eolian sandstone outcrop	3	8		[140]
permeability	limestone aquifer		3,500		[91]
permeability	limestone aquifer		6,300		[91]
permeability	chalk		7,500		[91]
permeability	sandstone aquifer		17,000		[91]
permeability	sandstone aquifer		45,000		[161]
SPT	soft rock, hard soils	4		spherical	[202]
SPT	soft rock, hard soils	5		spherical	[202]

A.2 Database on the variability of frictional soil

Table A.2: Database on the variability of frictional soils.

property	**soil type**	θ_{ver} [m]	θ_{hor} [m]	applied spatial model	reference
φ' + c'	sand	5.1	242		[362]
buldk density	medium gravel	0.2		exponential	[375]
buldk density	coarse sand, fine gravel	0.3		exponential	[375]
buldk density	medium gravel	0.4		exponential	[375]
CPT	sand	0 ~ 2		exponential	[10]
CPT	alluvial deposits	0.1 ~ 2.6		exponential	[413]
CPT	sand	0.1 ~ 2		exponential	[222]
CPT	sand	0.3 ~ 1.2	3.5 ~ 15	Campanella	[408]
CPT	sand	0.3		LAS	[405]
CPT	sand	0.4 ~ 2.4		LAS	[27]
CPT	sand	0.5	5.4	LAS	[288]
CPT	sand	1	12.1	LAS	[288]
CPT	clean sand	1			[208]
CPT	soft glacial clay, North sea	1			[412]
CPT	soft glacial clay, North sea	1			[412]
CPT	sand and gravel	1.2			[352]
CPT	fine silty sand, North sea	1.4			[412]
CPT	clean sand	1.6			[208]
CPT	sand	2	20	exponential	[353]
CPT	sand	2.6	16	Gaussian	[16]
CPT	sandy gravel	5	95	Gaussian	[207]
CPT	coastal sand	5			[25]
CPT	sand	28		LAS	[405]
CPT	sand	32.4		LAS	[405]
CPT	prairie soil		8		[224]
CPT	dense sand		9.6		[211]
d_{10} to d_{90}	sand	6.1		exponential	[123]

Continued on next page

Table A.2 – continued from previous page

property	soil type	θ_{ver} [m]		θ_{hor} [m]		applied spatial model	reference
d_{10} to d_{90}	sand			49		exponential	[123]
d_{50}	Pleistocene Quadra sand	1					[344]
d_{50}	Pleistocene Quadra sand	6.5					[344]
d_{50}	sand			3.3			[344]
density	sand	3					[269]
index property	sand	0.2	~ 2				[148]
index property	sandy clay	0.4	~ 1.1	1.2	~ 2.5		[349]
index property	poorly sorted gravel	0.7		15			[307]
index property	sand	0.9				exponential	[109]
index property	sand	1	~ 3	5	~ 15		[276]
permeability	sand	3		25		exponential	[303]
permeability	fluvial sand	0.1		3			[62]
permeability	braided river environment	0.3		10			[322]
permeability	medium gravel	0.3	~ 0.9	2	~ 11.4	exponential	[375]
permeability	medium gravel	0.4		1.8		exponential	[375]
permeability	medium gravel	0.4		0.3		exponential	[375]
permeability	sand aquifer	0.5		21.5			[409]
permeability	sandy gravel	0.6		1.2			[377]
permeability	coarse sand, fine gravel	0.6		5		exponential	[375]
permeability	sandy soil	0.9		9			[335]
permeability	fluvial sand	1.5		13			[302]
permeability	sand	1.7					[344]
permeability	sand	3.7				exponential	[123]
permeability	sand	3.7				exponential	[124]
permeability	strongly weathered rock	3.8		600			[132]
permeability	sandstone	4.5		1.6			[141]
permeability	heterogeneous alluvial aquifer	4.8		38.4			[303]
permeability	sand	6		900			[94]

Continued on next page

Table A.2 – continued from previous page

property	soil type	θ_{ver} [m]	θ_{hor} [m]	applied spatial model	reference
permeability	sand	7.2	5.4		[357]
permeability	sand	12 $\sim$ 16	40		[379]
permeability	sand	12	1,200		[83]
permeability	limestone	42	6,300		[35]
permeability	sand	» 40			[123]
permeability	compacted clay		0.5 $\sim$ 2		[37]
permeability	weathered shale subsoil		2		[231]
permeability	Pleistocene Quadra sand		3.3		[344]
permeability	sand		6	exponential	[92]
permeability	strony layer, medium gravel		9.5	exponential	[375]
permeability	sand and gravel aquifer		12.5		[112]
permeability	mediterranean soil		20		[315]
permeability	sand		40 $\sim$ 280		[159]
permeability	and		67	exponential	[123]
permeability	sand		67	exponential	[124]
permeability	salt dome		1,500		[26]
permeability	chalk		10,000		[88]
porosity	gravelly sand	0 $\sim$ 2.2	8.5 $\sim$ 12	exponential	[10]
sand fraction	poorly sorted gravel	0.7	15		[307]
sand fraction	sandy silt		50 $\sim$ 60	exponential, spherical	[113]
sand fraction	sandy gravel		100 $\sim$ 120	exponential, spherical	[113]
SPT	clean sand	0 $\sim$ 4		exponential	[10]
SPT	sand fill	0.3		exponential	[228]
SPT	dune sand		20		[25]
water content	coarse sand, fine gravel	0.2		exponential	[375]
water content	medium gravel	0.2		exponential	[375]
water content	medium gravel	0.4		exponential	[375]

A.3 Database on the variability of cohesive soil

Table A.3: Database on the variability of cohesive soils.

property	**soil type**	θ_{ver} [m]	θ_{hor} [m]	applied spatial model	reference
CPT	organic, soft clay	0.1			[206]
CPT	organic clay	0.1		exp	[109]
CPT	clay	0.1 $\sim$ 0.7		exp + cos	[68]
CPT	clay, silty sand	0.1 $\sim$ 0.6		exp	[381]
CPT	deltatic soils	0.1 $\sim$ 0.4			[404]
CPT	clay	0.2 $\sim$ 0.3		exp	[209]
CPT	organic, soft clay	0.2			[206]
CPT	organic clay	0.2		exp	[109]
CPT	clay, silty sand	0.2		exp	[381]
CPT	clay	0.2 $\sim$ 0.7		exp	[396]
CPT	clay	0.2 $\sim$ 0.4	0.2 $\sim$ 0.7		[65]
CPT	clay	0.2 $\sim$ 1.7	0.5 $\sim$ 3		[9]
CPT	silty clay	0.2		exp	[221]
CPT	clay, silty sand	0.2 $\sim$ 0.5		exp	[381]
CPT	deltatic soils	0.2 $\sim$ 0.3			[404]
CPT	silt to silty clay	0.3 $\sim$ 1		exp	[381]
CPT	organic, soft clay	0.3			[206]
CPT	organic clay	0.3 $\sim$ 0.4		exp	[109]
CPT	sandy silt	0.4		exp	[381]
CPT	deltatic soils	0.4			[404]
CPT	clay	0.4			[156]
CPT	clay, silty sand	0.4 $\sim$ 1		exp	[381]
CPT	clay	0.5 $\sim$ 5	20 $\sim$ 200		[125]
CPT	silty sand,clay	0.6 $\sim$ 0.8		exp	[381]
CPT	sandy clay	0.6			[19]
CPT	clay	0.7			[156]
CPT	silty clay	0.7		exp	[356]

Continued on next page

Table A.3 – continued from previous page

property	soil type	θ_{ver} [m]	θ_{hor} [m]	applied spatial model	reference
CPT	clay	0.7			[156]
CPT	clay mixed with silt	0.8		exp	[381]
CPT	clean sand, silty sand	1 $\sim$ 1.1		exp	[381]
CPT	silty clay	1	5 $\sim$ 12		[211]
CPT	silty clays	1 $\sim$ 4		exp	[40]
CPT	varved clay	1			[90]
CPT	clay	1.2 $\sim$ 5.6		exp	[45]
CPT	marine clay	1.5		exp	[242]
CPT	clay	2	5	exp	[20]
CPT	sea clay	2	40		[78]
CPT	soft clay	2	40		[167]
CPT	sensitive clay	2			[78]
CPT	sensitive clay	2			[78]
CPT	sensitive clay	2			[78]
CPT	sensitive clay	2			[78]
CPT	sandy clay	2.5 $\sim$ 4.5	20 $\sim$ 30	exp	[207]
CPT	clay	4	24	exp	[16]
CPT	varved clay	5		exp	[383]
CPT	alluvial clay	6.5			[167]
CPT	clay	8.6 8.6			[411]
CPT	varved clay	46		exp	[212]
CPT	marine clay	55	35 $\sim$ 60	exp	[15]
CPT	marine clay	6		exp	[227]
CPT	clay		0.2		[260]
CPT	silty clay		0.2 $\sim$ 1.9	exp	[223]
CPT	sandy clay		25		[18]
CPT	seabed deposits		30 $\sim$ 60		[160]
CPT	seabed deposits		53	exp	[368]

Continued on next page

Table A.3 – continued from previous page

property	soil type	θ_{ver} [m]	θ_{hor} [m]	applied spatial model	reference
CPT	alluvial clay		200		[167]
CPT	silty clay		212 $\sim$ 245	exp	[264]
CPT	clay		278 $\sim$ 286	exp	[264]
CPT	clay	0.6 $\sim$ 1.8		exp	[186]
CPT	silty clay	1			[211]
CPT	sensitive clay	2			[78]
CPT	clay	2		exp	[310]
CPT	clay	10	289	exp	[185]
CPT	deep glacial sands	20 $\sim$ 35		exp	[400]
CPT	clay		9.6		[211]
CPT	North sea soil		13.9		[192]
CPT	marine clay		400	exp	[229]
CPT	North sea clay		30		[368]
CPT	North sea soil		37.5		[192]
CPT (friction ratio)	clay	0 $\sim$ 0.6		exp	[10]
CPT (friction ratio)	clay to silty clay	0.1 $\sim$ 0.5		exp	[381]
CPT (friction ratio)	clay, silty sand	0.1 $\sim$ 0.5		exp	[381]
CPT (friction ratio)	clean sand, silty sand	0.2 $\sim$ 0.6		exp	[381]
CPT (friction ratio)	clay, silty sand	0.2 $\sim$ 0.3		exp	[381]
CPT (friction ratio)	claen sand, silty sand	0.3 $\sim$ 0.6		exp	[381]
CPT (friction ratio)	clay, silty sand	0.4		exp	[381]
CPT (friction ratio)	silty sand to sandy silt	0.4		exp	[381]
CPT (friction ratio)	claen sand,silty sand	0.5 $\sim$ 0.6		exp	[381]
CPT (friction ratio)	silty sand to sandy silt	0.6		exp	[381]
CU (triaxial)	offshore soil	1			[192]
CU (triaxial)	offshore soil	3			[192]
density	compacted clay	5			[25]
density	compacted clay		4 $\sim$ 5		[25]

Continued on next page

Table A.3 – continued from previous page

property	**soil type**	θ_{ver} [m]	θ_{hor} [m]	applied spatial model	reference
density	clay		10 $\sim$ 15		[9]
Index Properties	marine clay	1.6		exp	[227]
liquid limit	soft silty loam	0 $\sim$ 3.6	18 $\sim$ 22	exp	[10]
liquid limit	clay		» 0		[227]
liquid limit	clay		» 0		[228]
modulus of elasticity	clay	2 $\sim$ 5			[186]
modulus of elasticity	clay	6	298.5	spherical	[185]
modulus of elasticity	clay		400		[235]
permeability	glacial Lacustirne sand	0.1	3		[363]
permeability	glacial outwash sand	0.3	5		[155]
permeability	clay	0.4	5		[343]
permeability	fine sands	1.5	14		[323]
permeability	clay, fine sands	5.4	3		[230]
permeability	silty clay		0.1		[340]
permeability	fluvial soil		7.6		[135]
permeability	alluvial soil		15		[180]
permeability	alluvial aquifer		150		[91]
permeability	gravelly loamy sand		500		[313]
permeability	alluvial clay		800		[46]
permeability	alluvial aquifer		820		[98]
permeability	alluvial aquifer		1,800		[91]
permeability	clay		4,000		[1]
φ'	clay		800		[301]
preconsolidation pressure	soft, silty clay	0.6		exp	[99]
preconsolidation pressure	soft, silty clay		180	exp	[99]
sand fraction	soft silty loam	0 $\sim$ 5.4	19.6 $\sim$ 23	exp + cos	[10]
sand fraction	clay, silty sand	0.3		exp	[381]
sand fraction	silty sand,clay	0.6		exp	[381]

Continued on next page

Table A.3 – continued from previous page

property	**soil type**	θ_{ver} [m]	θ_{hor} [m]	applied spatial model	reference
sand fraction	clay, silty sand	1		exp	[381]
silt fraction	soft silty loam	0 $\sim$ 5.4	19.5 $\sim$ 23	exp + cos	[10]
silt fraction	soft silty loam		0 $\sim$ 3.8	exp	[10]
UCS	Mexico City clay		0 $\sim$ 0.9	exp	[10]
unit weight	soft silty loam	0 $\sim$ 3	17 $\sim$ 22	exp + cos	[10]
unit weight	soft clay	1.2			[386]
void ratio	soft silty loam	0 $\sim$ 4.5	16.8 $\sim$ 22	exp + cos	[10]
Void ratio	soft, silty clay	3		exp	[99]
VST	very soft clay	1	22		[41]
VST	soft clay	1.2			[15]
VST	sensitive clay	2			[78]
VST	soft clay	2.4		exp	[15]
VST	sensitive clay	3	30		[353]
VST	marine clay	3			[353]
VST	organic soft clay	3.1			[352]
VST	soft clay	6.2		exp	[15]
VST	soft clay		0 $\sim$ 0.5	exp + cos	[10]
VST	marine clay		30		[353]
water content	sandy clay	40 $\sim$ 70		spherical	[259]
water content	soft organic silty clay	3		exp	[99]
water content	clay		0 $\sim$ 2.5	exp	[10]
water content	mexican clay		0 $\sim$ 1.6	exp	[10]
water content	soft, silty loam		0 $\sim$ 5	exp + cos	[10]
water content	clay		5 $\sim$ 10		[9]
water content	sandy clay		400		[55]

Figure A.2 shows the frequency of the used correlation functions and techniques used in the different entries of the database entries. One can clearly deduce from figure A.2 that nearly 50% of the literature sources in the database only offered the experimental variogram or engineering judgement, but not a theoretical covariance function. Many of the studied publications fitted an exponential correlation function to the experimental values.

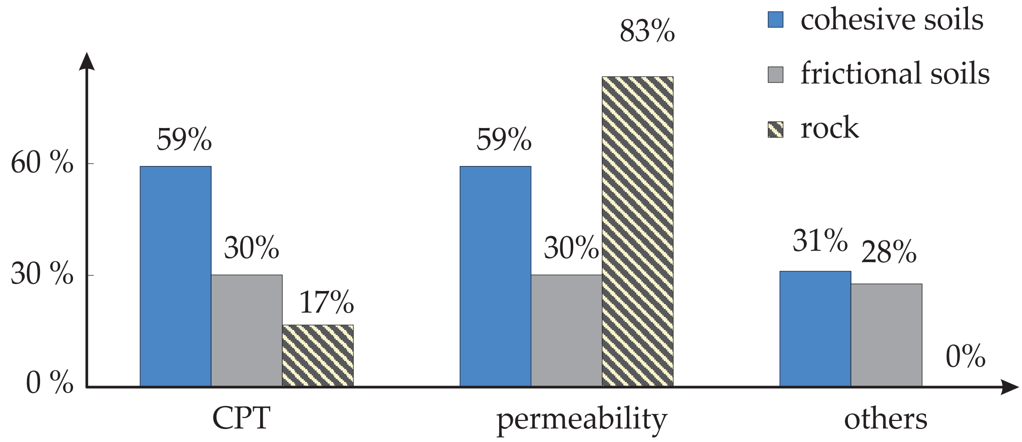

Figure A.1: Statistics of the available properties in the literature database.

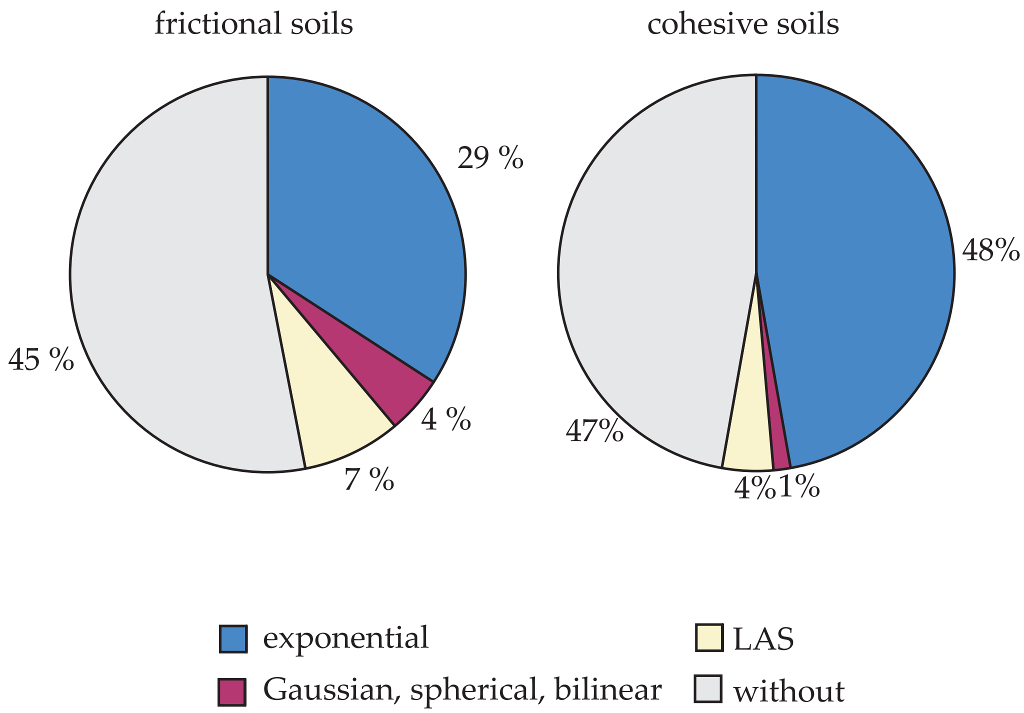

Figure A.2: Frequency of the correlation functions in the database for frictonal and cohesive soils.

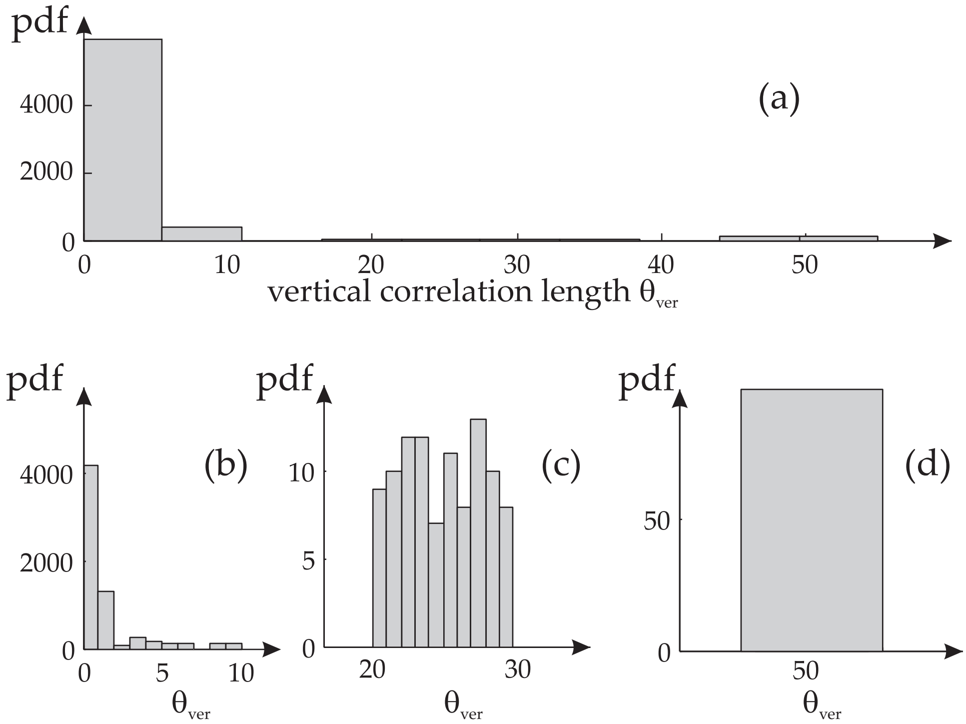

Figure A.3: Histogram of vertical correlation lengths in cohesive soils for all scales (a), for small(b), medium (c) and large scales (d).

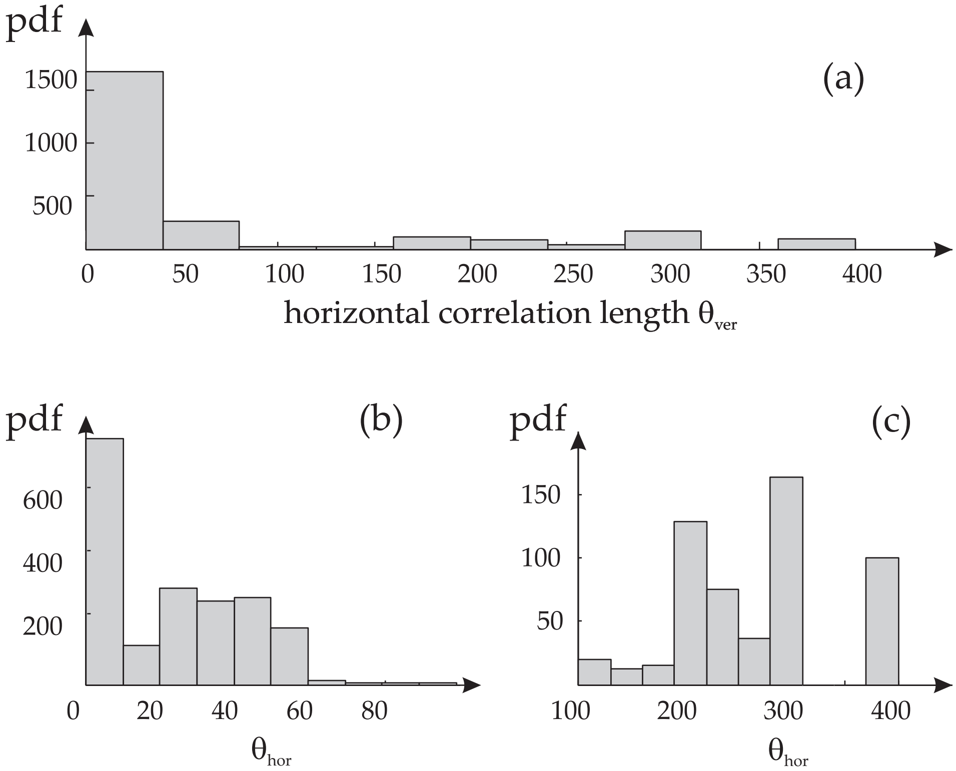

Figure A.4: Histogram of horizontal correlation lengths in cohesive soils for all scales (a), medium (b) and large scales (c).

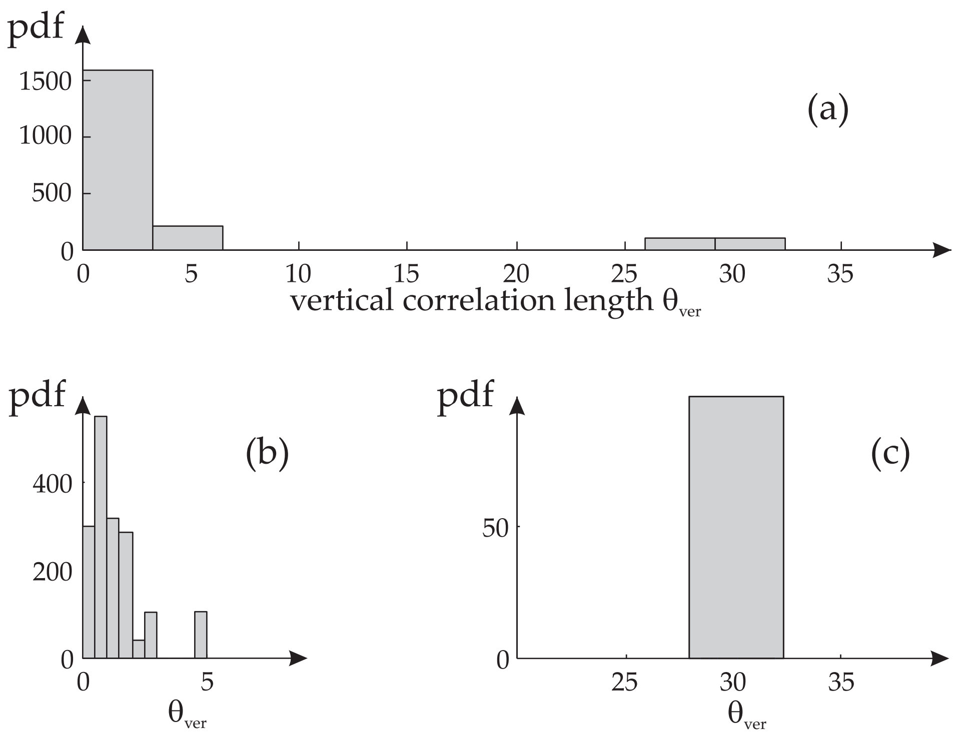

Figure A.5: Histogram of vertical correlation lengths in frictional soils for all scales (a), medium (b) and large scales (c).

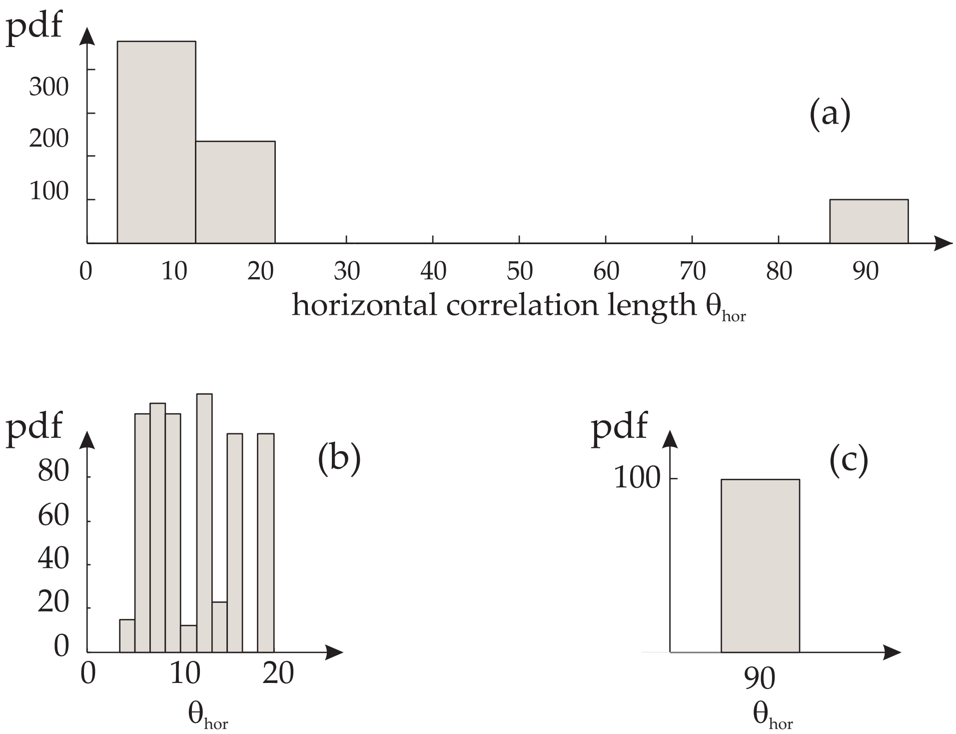

Figure A.6: Histogram of horizontal correlation lengths in frictional soils for all scales (a), medium (b) and large scales (c).

Appendix B

Measurement data of CPT - databases

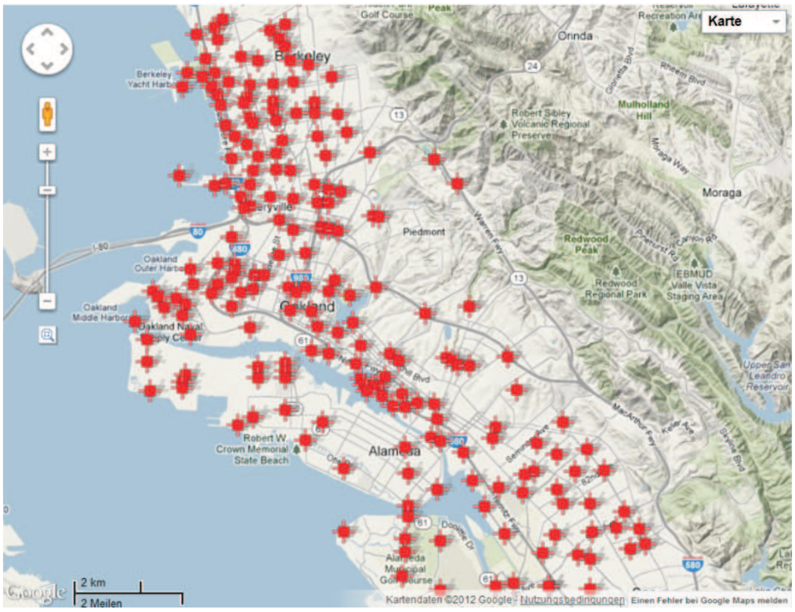

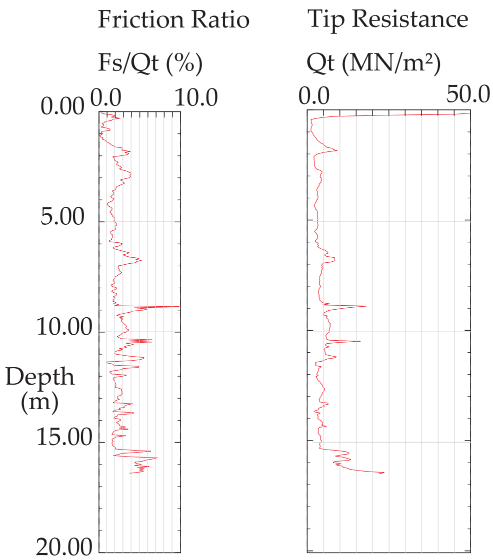

Figure B.1: Plan view and typical CPT profile of NGES site ALAMEDA.

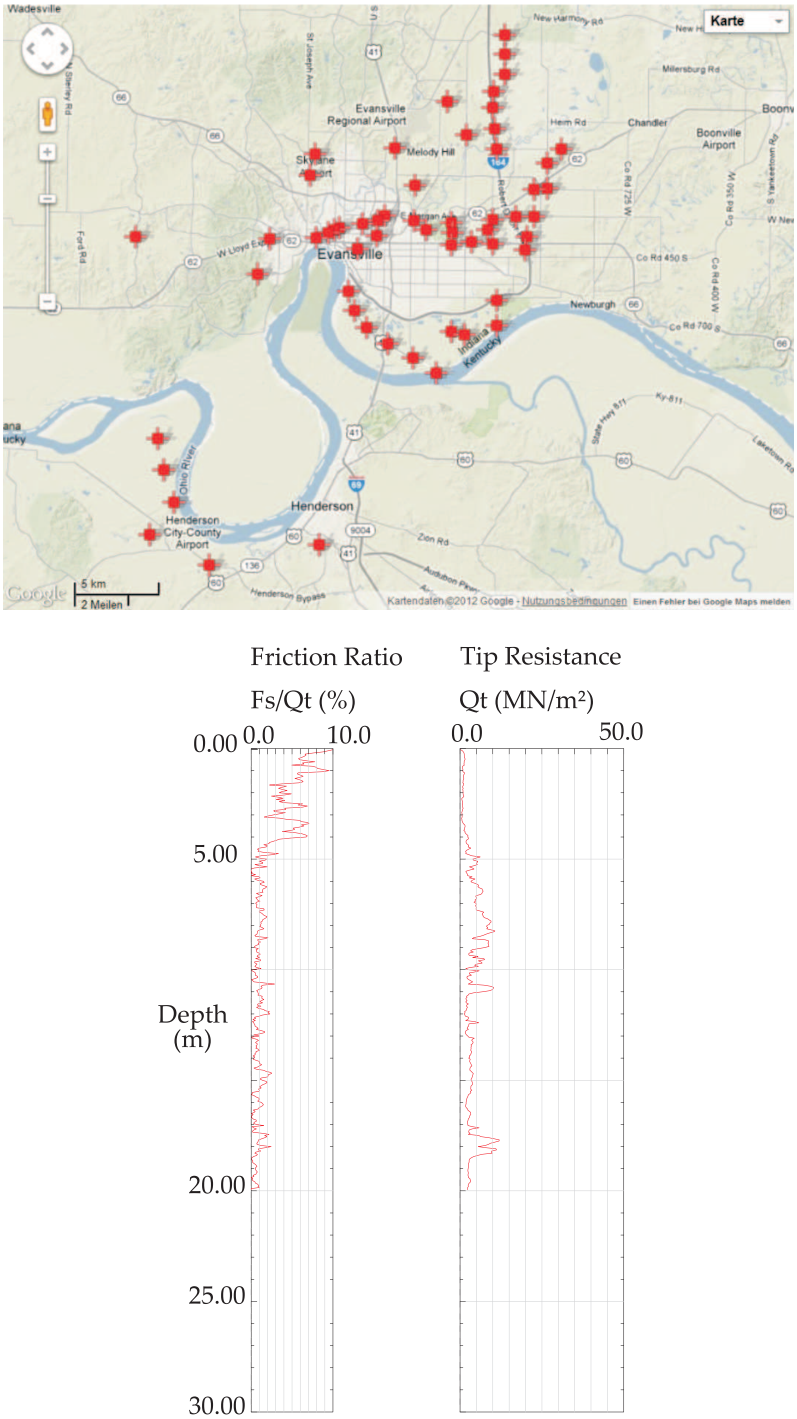

Figure B.2: Plan view and typical CPT profile of NGES site EVANSVILLE AREA.

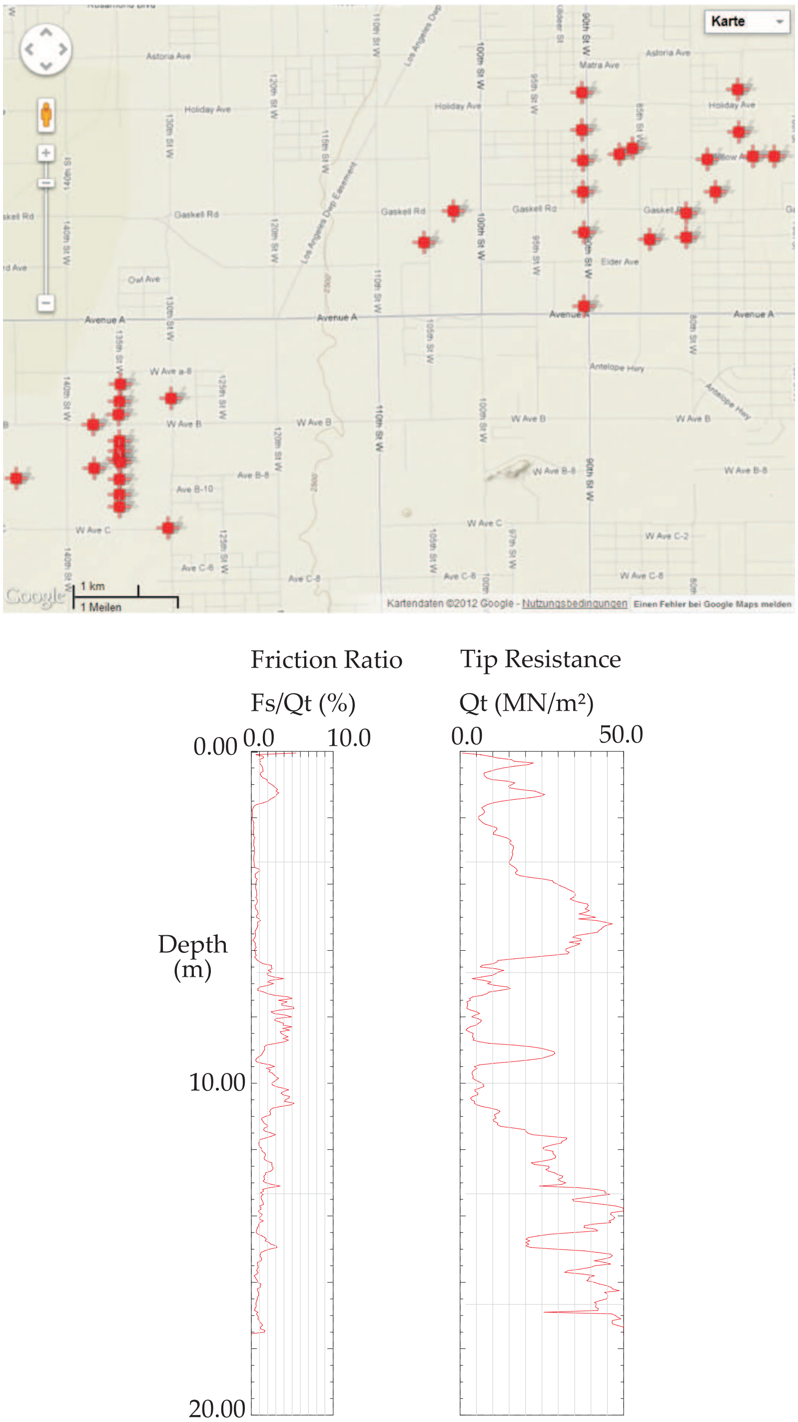

Figure B.3: Plan view and typical CPT profile of NGES site LANCESTER.

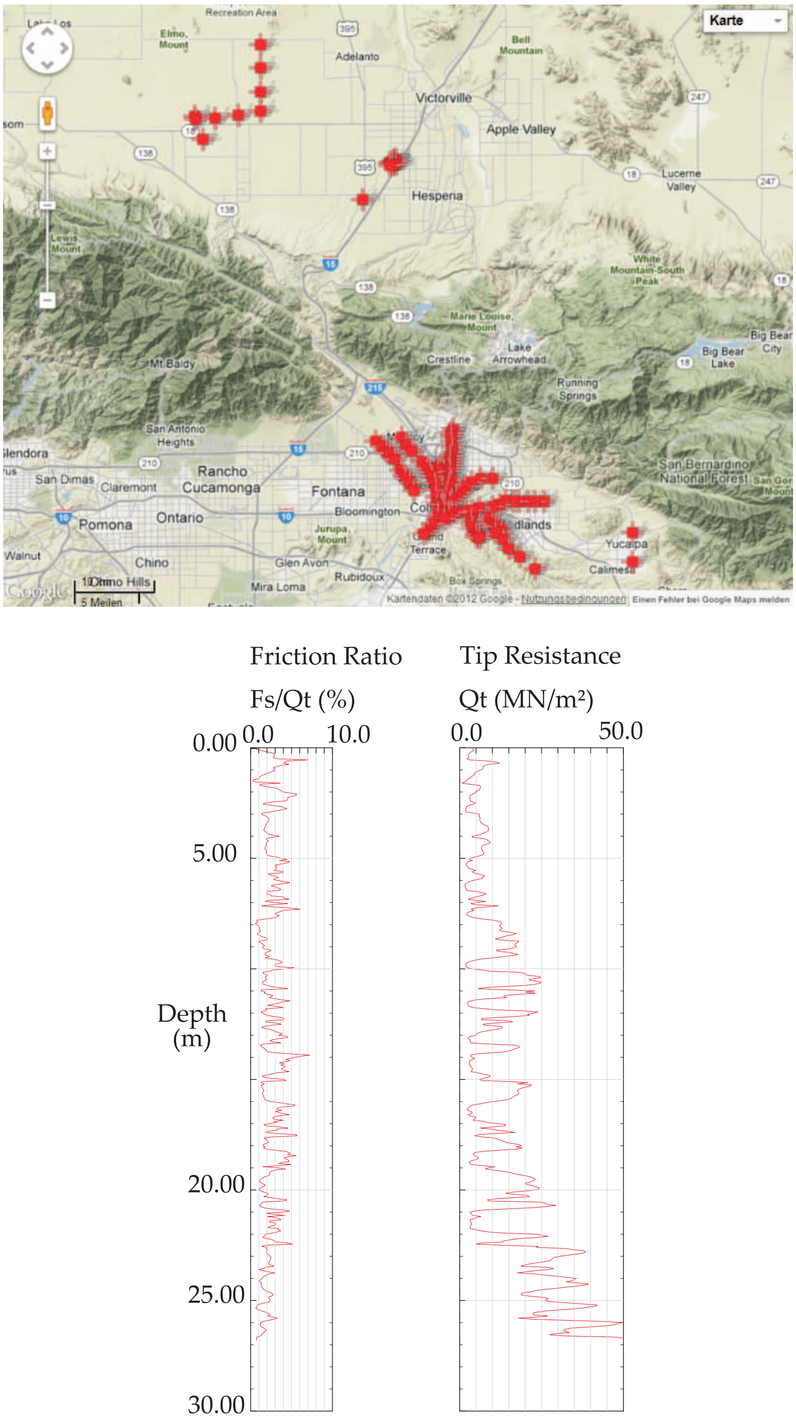

Figure B.4: Plan view and typical CPT profile of NGES site SAN BERNADINO COUNTY.

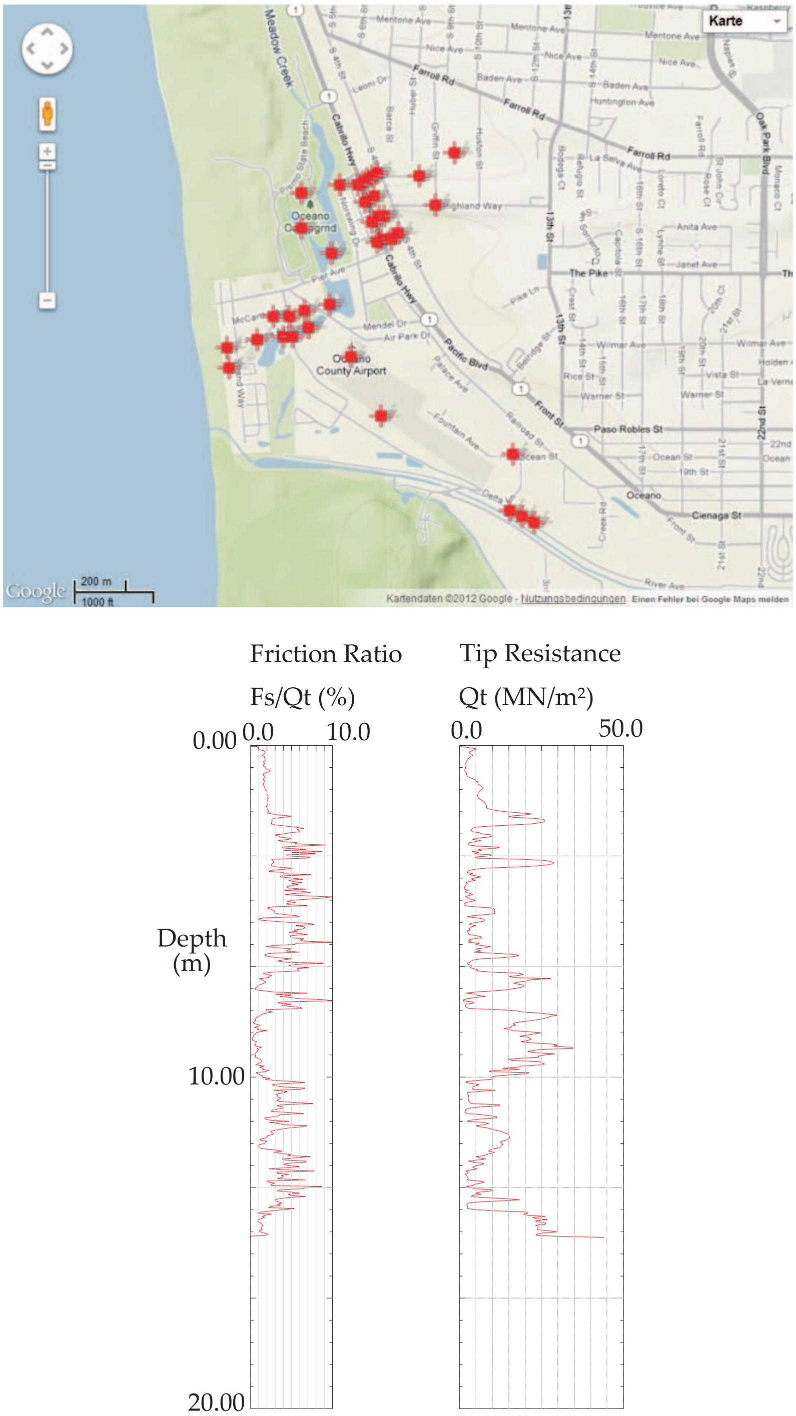

Figure B.5: Plan view and typical CPT profile of NGES site SAN LUIS OBISPO COUNTY.

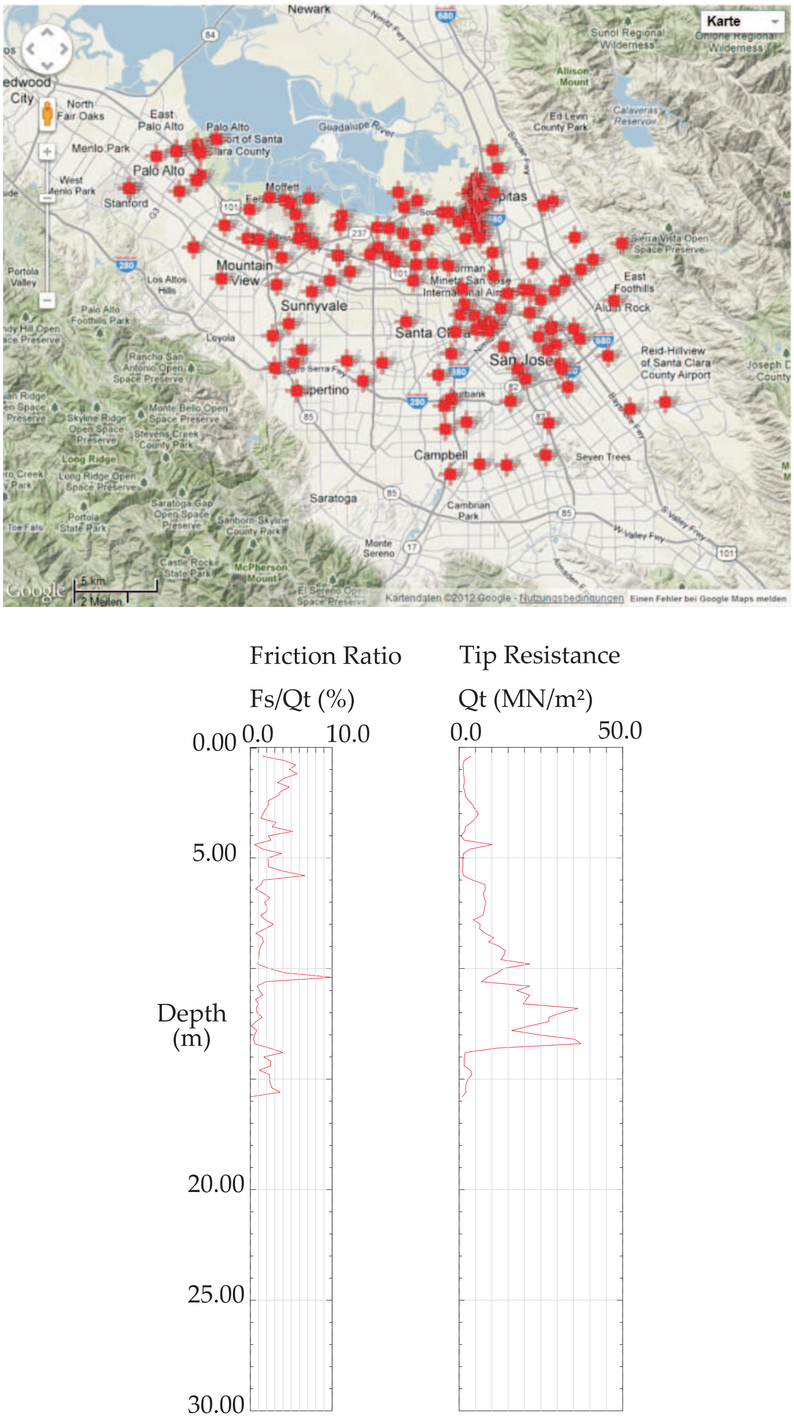

Figure B.6: Plan view and typical CPT profile of NGES site SANTA CLARA COUNTY.

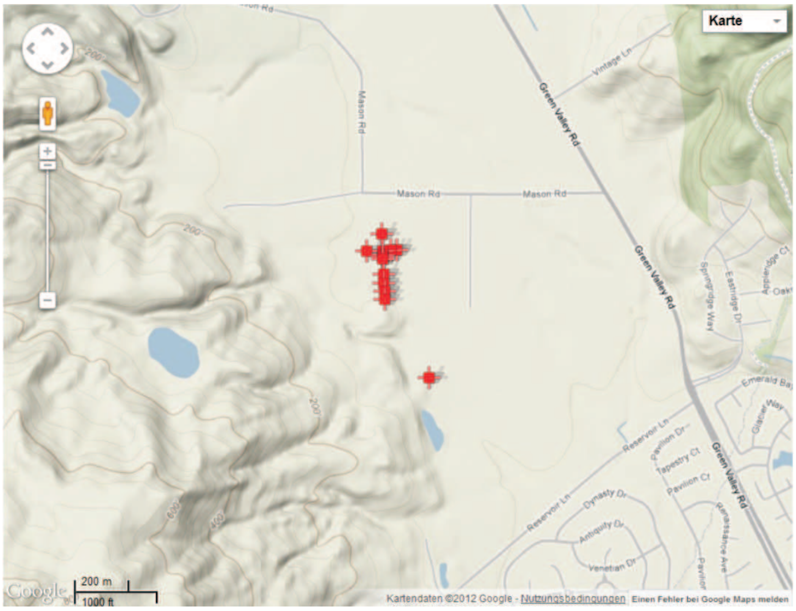

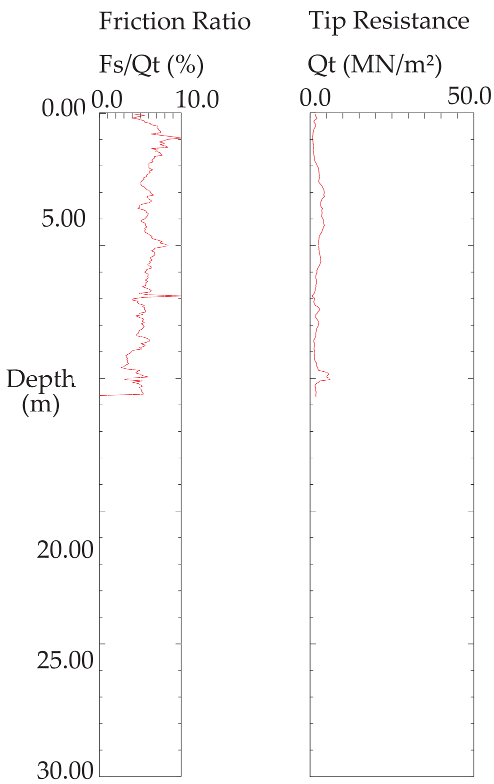

Figure B.7: Plan view and typical CPT profile of NGES site SOLANO COUNTY.

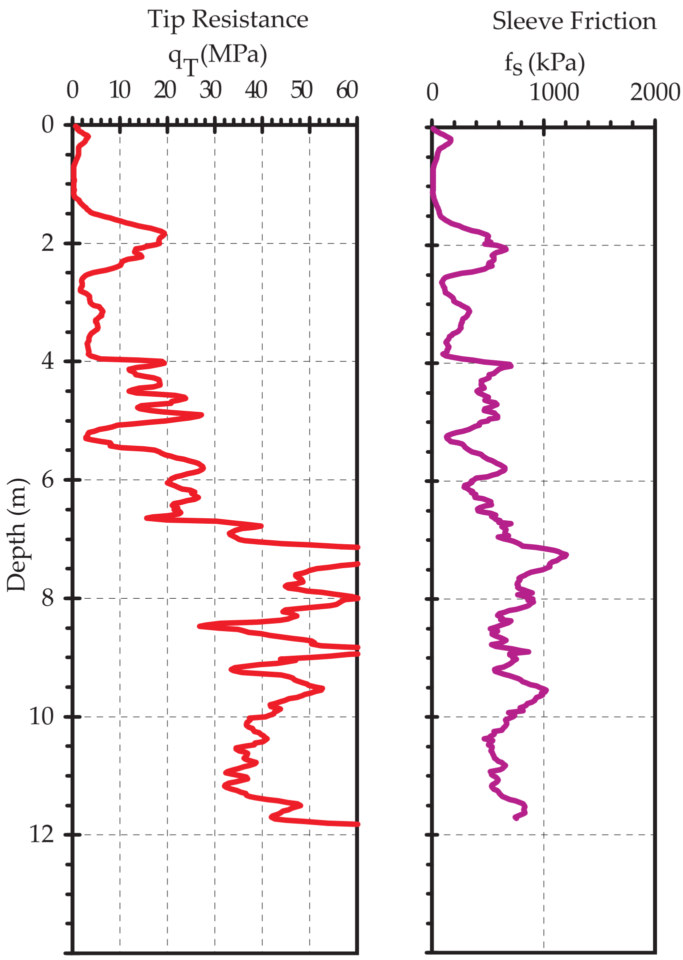

Figure B.8: Plan view and typical CPT profile of PEER site ANSSALL.

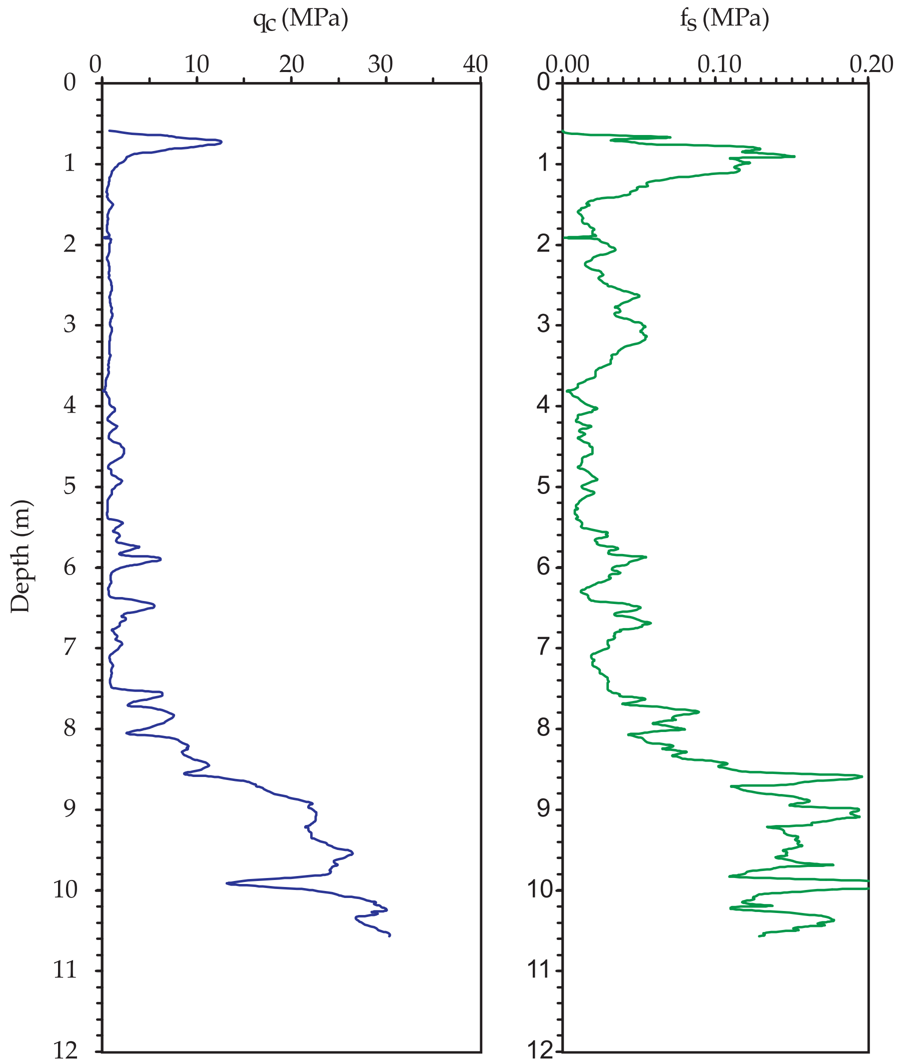

Figure B.9: Plan view and typical CPT profile of PEER site BERKELEY.

Appendix C

Basic definitions & statistical background

C.1 Moments of a distribution function

Every distribution function can be characterized by different moments listed below.

- First moment of distribution & mean value

$$\mu = \int_{-\infty}^{\infty} x\, f(x)\, dx = E[X] \tag{C.1}$$

- Second moment of distribution & variance

$$\sigma^2 = \int_{-\infty}^{\infty} (x-\mu)^2\, f(x)\, dx = E\left[(X-\mu)^2\right] \tag{C.2}$$

  Coefficient of variation

$$COV = \frac{\sigma}{\mu} \tag{C.3}$$

- Third moment of distribution & skewness

$$\gamma_1 = \frac{1}{\sigma^3}\int_{-\infty}^{\infty} (x-\mu)^3\, f(x)\, dx = \frac{\mu^3}{\sigma^3} = \frac{E\left[(X-\mu)^3\right]}{\sigma^3} \tag{C.4}$$

- Fourth moment of distribution & excess kurtosis

$$\gamma_{2,excess} = \frac{1}{\sigma^4}\int_{-\infty}^{\infty} (x-\mu)^4\, f(x)\, dx - 3 = \frac{\mu^4}{\sigma^4} - 3 = \frac{E\left[(X-\mu)^4\right]}{\sigma^4} - 3 \tag{C.5}$$

C.2 Distribution functions

Looking into statistical textbooks like Sachs [316] or Abramovich & Stegun [2], one can find a vast number of different probability distribution function. According to Remy et al. [304], a distribution function should account for all information available; it provides all that is needed to quantify the uncertainty about the actual outcome of the variable x. For example,

- probability intervals can be derived as

$$\text{Prob}\left\{Z \in (a, b)\right\} = \text{F}(b) - \text{F}(a) = \int_a^b f(z)\, dz. \tag{C.6}$$

- quantile values can be derived such as the 0.10 quantile or the 1st decile:

$$q_{0.10} = F^{-1}(0.10) = z - \text{outcome value such that Prob}(Z \leq q_{0.10}) = 0.10 \tag{C.7}$$

Phoon [286] as well as Baecher & Christian [23] point out the normal and the lognormal distribution function as widespread probability distribution functions in geotechnical engineering, which are explained in detail afterwards.

C.2.1 Normal distribution function

The normal distribution is a continuous probability distribution that has a bell-shaped probability density function, also known as the Gaussian function.

$$f(x; \mu, \sigma^2) = \frac{1}{\sigma\,\sqrt{2\,\pi}}\ \exp\left(-\frac{(x-\mu)^2}{2\,\sigma^2}\right) = \frac{1}{\sigma}\ \Phi\left(\frac{x-\mu}{\sigma}\right) \tag{C.8}$$

The location of the distribution function is controlled by the mean value μ; the shape is defined by the variance σ^2. A normal distribution with $\mathcal{N}(\mu = 0, \sigma^2 = 1)$ is called the standard normal. Function f(x) is unimodal and symmetric around the point $x = \mu$, which is at the same time the mode (peak value of the distribution function that occurs most frequently), the median (middle value and location parameter separating the the lower and upper half of the distribution) and the mean of the distribution. The inflection points of the curve occur one standard deviation away from the mean (i.e. at $x = \mu - \sigma$ and $x = \mu + \sigma$). The n-th derivative is given by $\Phi^{(n)}(x) = (-1)^n\ H_n(x)\ \Phi(x)$, where H_n is the Hermite polynomial of order n.

The cumulative distribution function (CDF) describes probability of a random variable falling in the interval $(-\infty, x]$. The CDF of the standard normal distribution Φ can be computed as an integral of the probability density function:

$$\Phi(x) = \frac{1}{\sqrt{2\,\pi}}\ \int_{-\infty}^{x} f(x; \mu, \sigma^2) = \frac{1}{\sigma\,\sqrt{2\,\pi}}\ \exp\left(-\frac{(x-\mu)^2}{2\,\sigma^2}\right) = \frac{1}{\sigma}\ \Phi\left(\frac{x-\mu}{\sigma}\right) \tag{C.9}$$

$$F(x; \mu, \sigma) = \Phi\left(\frac{x-\mu}{\sigma}\right) \tag{C.10}$$

Table C.1: Summary of the normal distribution

support	$x \in \mathbf{R}$
mean	μ
median	μ
mode	μ
variance	σ^2
skewness	0
excess kurtosis	0

C.2.2 Lognormal distribution function

In probability theory, a log-normal distribution is a continuous probability distribution of a random variable whose logarithm is normally distributed. If X is a random variable with a normal distribution, then $Y = \exp(X)$ has a lognormal distribution; likewise, if Y is log-normally distributed, then $X = \log(Y)$ is normally distributed.

A variable might be modelled as log-normal if it can be thought of as the multiplicative product of many independent random variables each of which is positive. In a lognormal distribution X, the parameters denoted μ and σ, are the mean and standard deviation, respectively, of the variable' s natural logarithm (by definition, the variable' s logarithm is normally distributed), which means using Z as a standard normal variable.

$$X = e^{\mu+\sigma\ Z} \tag{C.11}$$

On a non-logarithmised scale, μ and σ can be called the location parameter and the scale parameter respectively. The probability density function of a lognormal distribution is as shown in the following equation.

$$f_X(x;\mu,\sigma) = \frac{1}{x\ \sigma\ \sqrt{2\ \pi}}\ \exp\left(\frac{(\ln x - \mu)^2}{2\ \sigma^2}\right) \quad x > 0 \tag{C.12}$$

The cumulative distribution function of a lognormal distribution is

$$F_X(x;\mu,\sigma) = \Phi\left(\frac{\ln x - \mu}{\sigma}\right) \tag{C.13}$$

Table C.2: Summary of the lognormal distribution

support	$x \in (0, +\infty)$
mean	$e^{\,\mu+\sigma^2/2}$
median	$e^{\,\mu}$
mode	$e^{\,\mu-\sigma^2}$
variance	$e^{\,\sigma^2} - 1\; e^{\,2\mu+\sigma^2}$
skewness	$e^{\,\sigma^2} + 2\,\sqrt{e^{\,\sigma^2} - 1}$
excess kurtosis	$e^{\,4\sigma^2} + 2\,e^{\,3\sigma^2} + 3\,e^{\,2\sigma^2} - 6$

Table C.3: Summary of the multivariate normal distribution

support	$x \in \mu + \text{span}(\mathbf{\Sigma}) \subseteq \mathbf{R^k})$
mean	μ
median	μ
mode	μ
variance	$\mathbf{\Sigma}$

C.2.3 Multivariate normal distribution

The multivariate normal distribution of a k-dimensional random vector $\mathbf{z} = [Z_1, Z_2, ..., Z_k]$ of the random variables Z can be written in the following notation:

$$\mathbf{z} = \mathcal{N}_\mathbf{k}(\mu, \mathbf{COV_{ZZ}}) \tag{C.14}$$

with a k - dimensional mean vector

$$\mu = [\text{E}[Z_1], \text{E}[Z_2], ..., \text{E}[Z_k]] \tag{C.15}$$

and a $k \times k$ covariance matrix

$$\mathbf{COV_{ZZ}} = [\ \mathbf{COV}\,[\mathbf{Z_i}, \mathbf{Z_j}]\ ]\,, \mathbf{i} = \mathbf{1}, \mathbf{2}, ..., \mathbf{k}; \mathbf{j} = \mathbf{1}, \mathbf{2}, ..., \mathbf{k} \tag{C.16}$$

The main diagonal gives the variance and the off-diagonals are symmetrical covariances. The covariance matrix is not singular and definite. In case of a singular covariance matrix, the corresponding distribution has no density.

The probability density function $f(\mathbf{z})$ can be written in the following form.

$$f(\mathbf{z}) = (\mathbf{2}\,\pi)^{\mathbf{k}\ \mathbf{2}}\,|\mathbf{COV_{ZZ}}|^{-\mathbf{1/2}}\,\exp[-\mathbf{1/2}\,(\mathbf{z} - \mu)^\mathbf{T}\ \mathbf{COV_{ZZ}}\,(\mathbf{z} - \mu)] \tag{C.17}$$

According to Sachs [316], no analytical expression exists for den cumulative density function.

C.2.4 Estimation methods for probability distribution functions

In civil engineering practice many parameter estimation methods for probability distribution functions are in circulation. According to van Gelder [382], well known methods are for example:

- the method of moments,
- the method of maximum likelihood,
- the method of least squares,
- the method of Bayesian estimation,
- the method of probability weighted moments,
- the method of L-moments and
- the method of maximum entropy.

In Gelder [382] a comparison of the different methods together with applications of these approaches are presented.

Appendix D

Polynomial Chaos Expansion

D.1 Hermite polynomials

The Hermite polynomials $\mathrm{He}_n(\xi)$ are solution of the following differential equation:

$$y'' - x\,y' + n\,y = 0 \quad n \in \mathbb{N} \tag{D.1}$$

The Hermite polynomials $\mathrm{He}_n(x)$ are defined in the following formula as stated in Abramovic & Stegun [2].

$$\begin{aligned} \mathrm{He}_0(x) &= 1 \\ \mathrm{He}_{n+1}(x) &= x\,\mathrm{He}_n(x) - n\,\mathrm{He}_{n-1}(x) \end{aligned} \tag{D.2}$$

They are orthogonal with respect to the Gaussian probability measure:

$$\int_{-\infty}^{\infty} \mathrm{He}_m(x)\,\mathrm{He}_n(x)\,\varphi(x)\,\mathrm{d}x = n!\,\delta_{mn} \tag{D.3}$$

where $\varphi(x) = 1/\sqrt{2\pi}\,\exp(-x^2/2)$ is the standard normal PDF. If ξ is a standard normal random variable, the following relationship holds:

$$\mathrm{E}[\mathrm{He}_m(\xi)\,\mathrm{He}_n(\xi)] = n!\,\delta_{mn} \tag{D.4}$$

The first three Hermite polynomials are

$$\begin{aligned} \mathrm{He}_1(x) &= x \\ \mathrm{He}_2(x) &= x^2 - 1 \\ \mathrm{He}_3(x) &= x^3 - 3\,x \end{aligned} \tag{D.5}$$

D.2 Computation of the expectation of products of bivariate Hermite polynomials

A multivariate Hermite polynomial is defined as the product of several univariate Hermite polynomials of different variables. For n variables, its expression is given by

$$\Gamma_{i1,i2,\ldots in}(\xi_1, \xi_2, \ldots, \xi_n) = \mathrm{He}_{i1}(\xi_1) \cdot \mathrm{He}_{i2}(\xi_2) \cdot \ldots \cdot \mathrm{He}_{in}(\xi_n) \tag{D.6}$$

In case of two variables, the expression of the bivariate Hermite polynomials is:

$$\Gamma_{i,j}(\xi_1, \xi_2) = \mathrm{He}_{i1}(\xi_1) \cdot \mathrm{He}_{i2}(\xi_2) \tag{D.7}$$

For a simple use in mathematical formulas, the multivariate Hermite polynomials are often renamed and sorted by using only one numerical index, for example:

$$\Gamma_{i,j}(\xi_1, \xi_2) = \psi_i \tag{D.8}$$

Each polynomial ψ_i of the basis of the PCE of two variables ξ_1 and ξ_2 can be entirely defined by two indexes $i1$ and $i2$ such that

$$\psi_i = \Gamma_{i,j}(\xi_1, \xi_2) = \mathrm{He}_i(\xi_1) \cdot \mathrm{He}_i(\xi_2) \tag{D.9}$$

With this notation, the following equations have been derived by Sudret & Kiureghian [366].

$$\begin{aligned} \mathrm{E}(\psi_i^2) &= i_1! \cdot i_2! \\ \mathrm{E}(\psi_i \cdot \psi_j \cdot \psi_k) &= \mathrm{D}_{i1,j1,k1} \cdot \mathrm{D}_{i2,j2,k2} \\ \mathrm{E}(\psi_i \cdot \psi_j \cdot \psi_k \cdot \psi_l) &= \mathrm{D}_{i1,j1,k1,l2} \cdot \mathrm{D}_{i2,j2,k2,l2} \end{aligned} \tag{D.10}$$

In these expressions, the D terms are obtained by:

$$\mathrm{C}_{i,j,k} = \begin{cases} \frac{i!\ j!}{((i+j-k)/2)!\ ((j+k-i)/2)!\ ((k+i-j)/2)!} & \begin{cases} (i+j+k)\text{even} \\ k \in [|i-j|\ ,\ i+j] \end{cases} \\ 0 & \text{otherwise} \end{cases} \tag{D.11}$$

$$\mathrm{D}_{i,j,k} = \mathrm{C}_{i,j,k} \cdot k! \tag{D.12}$$

$$\mathrm{D}_{i,j,k,l} = \sum_{q \geq 0} \mathrm{D}_{i,j,q} \cdot \mathrm{C}_{k,l,q} \tag{D.13}$$

D.3 Two variables PCEs used for different values of the PCE order

M = expansion order of the PCE
PCE_{num} = number of the unknown PCE coefficients
m = number of the available collocation points

M	Roots of the univariate Hermite polynomials order M+1	Expression PCEs for different orders	PCE_{num}	m
2	$\left\{0; \pm\sqrt{3}\right\}$	$U_2 = a_{0,0} \cdot \Gamma_{0,0} + a_{1,0} \cdot \Gamma_{1,0}(\xi_1) + a_{0,1} \cdot \Gamma_{0,1}(\xi_2) + a_{2,0} \cdot \Gamma_{2,0}(\xi_1) + a_{1,1} \cdot \Gamma_{1,1}(\xi_1, \xi_2) + a_{0,2} \cdot \Gamma_{0,2}(\xi_2)$	6	9
3	$\left\{\pm\sqrt{3 \pm \sqrt{6}}\right\}$	$U_3 = a_{0,0} \cdot \Gamma_{0,0} + a_{1,0} \cdot \Gamma_{1,0}(\xi_1) + a_{0,1} \cdot \Gamma_{0,1}(\xi_2) + a_{2,0} \cdot \Gamma_{2,0}(\xi_1) + a_{1,1} \cdot_{1,1} (\xi_1, \xi_2) + a_{0,2} \cdot \Gamma_{0,2}(\xi_2) + a_{3,0} \cdot \Gamma_{3,0}(\xi_1) + a_{2,1} \cdot_{2,1} (\xi_1, \xi_2) + a_{1,2} \cdot \Gamma_{1,2}(\xi_1, \xi_2) + a_{0,3} \cdot \Gamma_{0,3}(\xi_2)$	10	16+1
4	$\left\{0; \pm\sqrt{5 \pm \sqrt{10}}\right\}$	$U_4 = a_{0,0} \cdot \Gamma_{0,0} + a_{1,0} \cdot \Gamma_{1,0}(\xi_1) + a_{0,1} \cdot \Gamma_{0,1}(\xi_2) + a_{2,0} \cdot \Gamma_{2,0}(\xi_1) + a_{1,1} \cdot \Gamma_{1,1}(\xi_1, \xi_2) + a_{0,2} \cdot \Gamma_{0,2}(\xi_2) + a_{3,0} \cdot \Gamma_{3,0}(\xi_1) + a_{2,1} \cdot \Gamma_{2,1}(\xi_1, \xi_2) + a_{1,2} \cdot \Gamma_{1,2}(\xi_1, \xi_2) + a_{0,3} \cdot \Gamma_{0,3}(\xi_2) + a_{4,0} \cdot \Gamma_{4,0}(\xi_1) + a_{3,1} \cdot \Gamma_{3,1}(\xi_1, \xi_2) + a_{2,2} \cdot \Gamma_{2,2}(\xi_1, \xi_2) + a_{1,3} \cdot \Gamma_{1,3}(\xi_1, \xi_2) + a_{0,4} \cdot \Gamma_{0,4}(\xi_2)$	15	25
5	$\left\{\begin{array}{l} \pm 3.324257\,; \\ \pm 3.889176\,; \\ \pm 0.616707 \end{array}\right\}$	$U_5 = a_{0,0} \cdot \Gamma_{0,0} + a_{1,0} \cdot \Gamma_{1,0}(\xi_1) + a_{0,1} \cdot \Gamma_{0,1}(\xi_2) + a_{2,0} \cdot \Gamma_{2,0}(\xi_1) + a_{1,1} \cdot \Gamma_{1,1}(\xi_1, \xi_2) + a_{0,2} \cdot \Gamma_{0,2}(\xi_2) + a_{3,0} \cdot \Gamma_{3,0}(\xi_1) + a_{2,1} \cdot \Gamma_{2,1}(\xi_1, \xi_2) + a_{1,2} \cdot \Gamma_{1,2}(\xi_1, \xi_2) + a_{0,3} \cdot \Gamma_{0,3}(\xi_2) + a_{4,0} \cdot \Gamma_{4,0}(\xi_1) + a_{3,1} \cdot \Gamma_{3,1}(\xi_1, \xi_2) + a_{2,2} \cdot \Gamma_{2,2}(\xi_1, \xi_2) + a_{1,3} \cdot \Gamma_{1,3}(\xi_1, \xi_2) + a_{0,4} \cdot \Gamma_{0,4}(\xi_2) + a_{5,0} \cdot \Gamma_{5,0}(\xi_1) + a_{4,1} \cdot \Gamma_{4,1}(\xi_1, \xi_2) + a_{3,2} \cdot \Gamma_{3,2}(\xi_1, \xi_2) + a_{2,3} \cdot \Gamma_{2,3}(\xi_1, \xi_2) + a_{1,4} \cdot \Gamma_{1,4}(\xi_1, \xi_2) + a_{0,5} \cdot \Gamma_{0,5}(\xi_2)$	21	36+1

Appendix E

Sequential simulation algorithms

The aim of sequential simulation, as it was originally constructed, is to reproduce desirable multivariate properties through the sequential use of conditional distributions [79, 97]. Consider a set $\{Z(\mathbf{u}_j), j = 1, \ldots N\}$ of N random variables defined at N locations $\mathbf{u}_j$. The objective is to generate several joint realizations $\left\{z^l(\mathbf{u}_j), j = 1, \ldots, N\right\}$, $l = 1, \ldots, L$ conditional to the available data and to some structural model such as the variogram. It can be shown that the N- point multivariate distribution can be decomposed into a set of N one-point conditional cumulative distribution function's as

$$\begin{aligned} F\left(\mathbf{u}_1, \ldots, \mathbf{u}_n; z_1 \ldots, z_N \right| (n)) &= F\left(\mathbf{u}_N; z_N \right| (n + N - 1)) \cdot \\ &\cdot F\left(\mathbf{u}_{N-1}; z_{N-1} \right| (n + N - 2)) \cdot \\ &\cdot F\left(\mathbf{u}_2; z_2 \right| (n + 1)) \cdot F\left(\mathbf{u}_1; z_1 \right| (n)) \end{aligned} \tag{E.1}$$

where $F\left(\mathbf{u}_N; z_N \right| (n + N - 1))$ is the conditional CDF of $Z(\mathbf{u}_N)$ given the set of n original data values and the previous $(N - 1)$ realizations $z^{(l)}\left(\mathbf{u}_j\right), j = 1, \ldots, N - 1$ [145]. This decomposition allows us to generate an image by sequentially visiting each node. Sequential simulation, under a given multivariate distribution, amounts to read the decomposition E.2 from left to right, i.e. the purpose of sequential simulation is to reproduce the properties of the given multivariate distribution. The simulation algorithm proceeds as follows according to Goovaerts [145]:

- Perform a transformation if necessitated by the theory
- Define a random path visiting all nodes
- For each node $\mathbf{u}_i, i = 1, \ldots, N$ do
  - model the conditional distribution $F\left(\mathbf{u}_i; z \right| (n + i - 1))$ of $Z\left(\mathbf{u}_i\right)$, given the n original data values and all $i - 1$ previously drawn values $z^{(l)}\left(\mathbf{u}_j\right), \mathbf{u}_i, j = 1, \ldots, i - 1$
  - draw the simulated value $z^{(l)}\left(\mathbf{u}_j\right)$ from $F\left(\mathbf{u}_i; z | (n + i - 1)\right)$
- end loop
- Perform a back-transform to identify the target histogram

The sequential simulation principle is independent of the algorithm or model to establish the equation $E.2$ [97].

Within the Sequential Gaussian Simulation algorithm, all conditional cumulative distribution $F(\cdot)$ are assumed Gaussian and their means and variances are given b a series fo N simple kriging systems; in terms of the Sequential Indicator Simulation algorithm, the conditional cumulative distribution are obtained directly by indicator kriging, as shown below.

E.1 Sequential Gaussian Simulation algorithm

The most straight forward algorithm for generating realizations of a multivariate Gaussian field is provided by the sequential principle. As described by various authors [97, 403], each value is simulated sequentially according to its normal conditional cumulative distribution (nccd) function, which must be determined at each location to be simulated. The conditioning data comprise all the original data and all previously simulated values within the neighbourhood of the point being simulated. Sequential Gaussian simulation (SGSIM) starts with the assumption that the kriging error is normally distributed with mean 0 and variance $\sigma_K^2(\mathbf{x}_0)$, i.e. $\mathcal{N}(0, \sigma_K^2(\mathbf{x}_0))$. In these circumstances the probability distribution for the true values is $\mathcal{N}(\widehat{Z}(\mathbf{x}_0), \sigma_K^2(\mathbf{x}_0))$; it is simply shifted by $\widehat{Z}(\mathbf{x}_0)$.

Deutsch & Journel [97] as well Webster & Oliver [403] list the following steps of SGSIM algorithm:

1. Ensure that the data are approximately normal; transform to a standard normal distribution if necessary.

2. Compute and model the variogram.

3. Specify the coordinates of the points at which you want to simulate. These will usually be on a grid.

4. Determine the sequence in which the points, $\mathbf{x}_j; j = 1, 2, \ldots$ will be visited for the simulation. Choosing the points at random will maximize the diversity of different realizations.

5. Simulate at each of these points as follows:
   (a) Use simple kriging with the variogram model to obtain $\widehat{Z}(\mathbf{x}_i)$ and $\sigma_K^2(\mathbf{x}_i$.
   (b) Draw a value at random from a normal distribution $\mathcal{N}(\widehat{Z}(\mathbf{x}_i), \sigma_K^2(\mathbf{x}_i))$.
   (c) Insert this value into the grid at $\mathbf{x}_i$, and add it to the data.
   (d) Proceed to the next node and simulate the value at this point in the grid.
   (e) Repeat steps (a) to (c) until all of the nodes have been simulated.

6. Back-transform the simulated values if there is a need to.

The SGSIM algorithm is very fast and straightforward because the modelling of the ccdf at each location $\mathbf{u}$ requires the solution of only a sling kriging system at that location. The implicit assumption is that the spatial variability of the attribute values can be fully characterized by sa single covariance function. In particular, this precludes modelling patterns of spatial continuity specific to difference classes of values. Possibly more critical, the maximum entropy property of the multi-Gaussian random field model does not allow for any significant correlation of extreme values [96, 97, 143, 144, 189] and for a given covariance maximizes their scattering in space, which is called destructuration effect by Goovaerts [145] .

E.2 Kriging algorithm

As reported by Remy et al. [304], Kriging has been historically at the source of acceptance of geostatistics and remains a major data integration tool and is used in most geostatistical estimation and simulation algorithms. Kriging is a generic name adopted by geostatisticians for a family of generalized least squares regression algorithms, [145]. All kriging estimators are but variants of the basis linear regression estimator $Z^*(\mathbf{u})$ as defined as

$$Z^*(\mathbf{u}) - m(\mathbf{u}) = \sum_{\alpha=1}^{n(\mathbf{u})} \lambda_\alpha(\mathbf{u}) \ [Z(\mathbf{u}_\alpha) - m(\mathbf{u}_\alpha)] \tag{E.2}$$

where λ_α is the weight assigned to the location $z(\mathbf{u}_\alpha)$ interpreted as a realization of the random variable $Z(\mathbf{u})$. The quantities $m(\mathbf{u})$ and $m(\mathbf{u}_\alpha)$ are the expected values of the random variables $Z(\mathbf{u})$ and $Z(\mathbf{u}_\alpha)$. The number of data involved in the estimation as well as their weights may change form on location to another. Goovaerts [145] reports amongst others [79, 97], that in practice, only the $n(\mathbf{u})$ closest to the location $\mathbf{u}$ being estimated are retained, the data within a given neighbourhood or window $W(\mathbf{u})$ centered on $\mathbf{u}$.

The interpretation of the unknown value $z(\mathbf{u})$ and data values $z(\mathbf{u}_\alpha)$ as realizations of the random variables $Z(\mathbf{u})$ and $Z(\mathbf{u}_\alpha)$ allows on to define the estimation error as a random variable $Z^*(\mathbf{u}) - Z(\mathbf{u})$. All flavours of kriging share the same objective of minimizing the estimation or error variance $\sigma_E^2(\mathbf{u})$ under the constraint of unbiasedness of the estimator that is,

$$\sigma_E^2(\mathbf{u}) = \mathrm{Var}\left[Z^*(\mathbf{u}) - Z(\mathbf{u})\right] \tag{E.3}$$

is minimized unter the constraint that.

$$\mathrm{E}\left[Z^*(\mathbf{u}) - Z(\mathbf{u})\right] = 0 \tag{E.4}$$

Goovaerts [145] distinguishes three kriging variants according to the model considered for the rend $m(\mathbf{u})$.

1. Simple kriging considers the mean $m(\mathbf{u})$ to be known and constant through the study area A

$$m(\mathbf{u}) = m \ \ , \ \ \text{known} \quad \forall\, \mathbf{u} \in A \tag{E.5}$$

2. Ordinary kriging accounts for local fluctuations of the mean by limiting the domain of stationarity of the mean to the local neighbourhood $W(\mathbf{u})$

$$m(\mathbf{u}') = \text{constant but known} \quad \forall\, \mathbf{u}' \in W(\mathbf{u}) \tag{E.6}$$

3. Kriging with a trend model considers that the unknown local mean $m(\mathbf{u}')$ smoothly varies with each local neighbourhood $W(\mathbf{u})$, hence over the entire study area A. The trend component is modelled as a linear combination of functions $f_k(\mathbf{u})$ of the coordinates:

$$m(\mathbf{u}') = \sum_{k=0}^{K} a_k(\mathbf{u}')\, f_k(\mathbf{u}') \tag{E.7}$$

$$\text{with} a_k(\mathbf{u}) \approx a_k \text{constant but unknown} \quad \forall\ \mathbf{u}' \in W(\mathbf{u})$$

The coefficients $m(\mathbf{u}')$ are unknown and deemed constant with each local neighbourhood $W(\mathbf{u})$. By convention, $\mathbf{f}_0(\mathbf{u}') = 1$, hence the case $K = 0$ is equivalent to ordinary kriging (constant but unknown mean a_0).

$$\mathrm{E}\left[Z^*(\mathbf{u}) - Z(\mathbf{u})\right] = 0 \tag{E.8}$$

E.3 Sequential Indicator Simulation algorithm

In earth sciences, connected strings of large or small values are common and are critical for many applications, as shown by various publications e.g. [97, 143, 144, 189]. Amongst others, Goovaerts [145] states that the multi-Gaussian random field model is inappropriate, whenever the structural analysis or qualitative information indicates that extreme values could be better correlated in space than medium values. Even in absence of of information about connectivity of extreme values, the user must be aware that the analytical simplicity of SGSIM is balancey by the risk of understanding the potential for critical features, such as strings of small or large values.

The Sequential Indicator Simulation (SGSIM) algorithm is the most widely used non-multi-Gaussian simulation technique. The indicator formalism introduced in section 2.4.2 is used to model the sequence of conditional cdfs from which simulated values are drawn. Unlike SGSIM, the indicator approach allows one to account for class specific patterns of spatial continuity through different indicator semivariogram models [145].

Consider first the simulation of a single continuous attribute z at N grid nodes $\mathbf{u}_j'$ conditional only to the z- data $\{z\left(\mathbf{u}_\alpha\right), \alpha = 1, \ldots, n\}$. Sequential indicator simulation proceeds as follows [145]:

- Discretize the range of variation of z into $(K+1)$ classes using K threshold values z_k. Then, transform each datum $z(\mathbf{u}_\alpha)$ into a vector of hard indicator data, defined as

$$i\left(\mathbf{u}_\alpha; z_k\right) = \begin{cases} 1 & \text{if } z(\mathbf{u}_\alpha) \leq z_k \qquad k = 1, \ldots, K \\ 0 & \text{otherwise} \end{cases}$$

- Define a random path visiting each node of the grid only once.

- At each node $\mathbf{u}'$:

1. Determine the K ccdf values $F(\mathbf{u}_\alpha; z_k|(n))$ using an indicator kriging algorithm e.g. simple indicator kriging. The conditioning information consists of indicator transform of neighbouring original z-data and previously simulated z-values.
2. Correct for any order relation deviations resulting from negative kriging weights [145]. Then build a complete ccdf model $(\mathbf{u}'; z|(n)), \forall z$.
3. Draw a simulated valued $z^{(l)}(\mathbf{u}')$ form that conditional cumulative distribution function.
4. Add the simulated value to the conditioning data set.
5. Proceed to the next node along the random path, and repeat steps 1 to 4.

Goovaerts [145] explains to repeat the entire procedure with a different random path to generate another realization $\left\{z^{(l')}(\mathbf{u}'_j, j = 1, \ldots, N\right\}, l' \neq l$. Additional information on the SGSIM algorithm can be found in various publications [79, 96, 97, 143–145, 189, 304].

E.4 Comparison of SGSIM and SISIM algorithms

Two different random field realisations are shown in figure E.1. Both random fields follow the same isotropic correlation length, but they look different. One can deduce from the description of these two algorithms the similarities and the differences. It is shown in figure E.2 (a) that the variogram and in figure figure E.2 (b) the cumulative distribution function are nearly the same. But in terms of the indicator correlation lengths both algorithms offer a different insight into their spatial correlation structure . As shown in figure E.3, the indicator correlation lengths are different for the extreme values, whereas for the median values they are similar. One can derive from this that the influence of different algorithms for the simulation of spatial correlation results in two completely different visualisations of spatial variability.

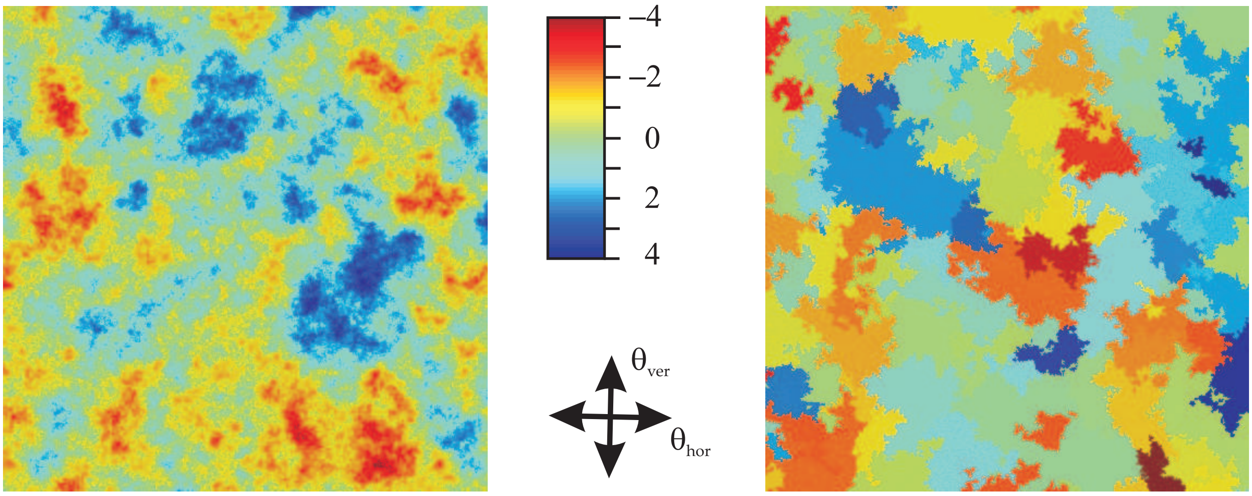

Figure E.1: Random field realisations of the SGSIM (a) and the SISIM (b) algorithm with an isotropic, spatial correlation ($\theta_{ver} = \theta_{hor}$).

For the sake of completeness, figures E.4 and E.5 summarize different methods for the simulation of random fields, which are taken from Chiles & Delfiner [79]

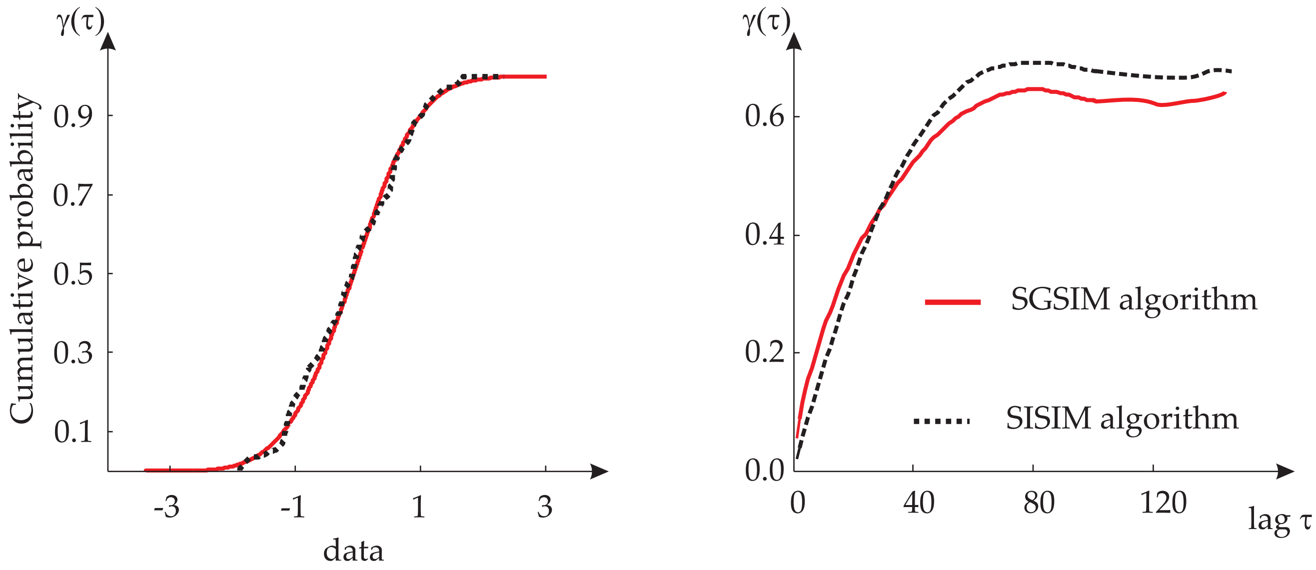

Figure E.2: Cumulative probability distribution (a) and variograms (b) of the SGSIM and SISIM random field in figure E.1.

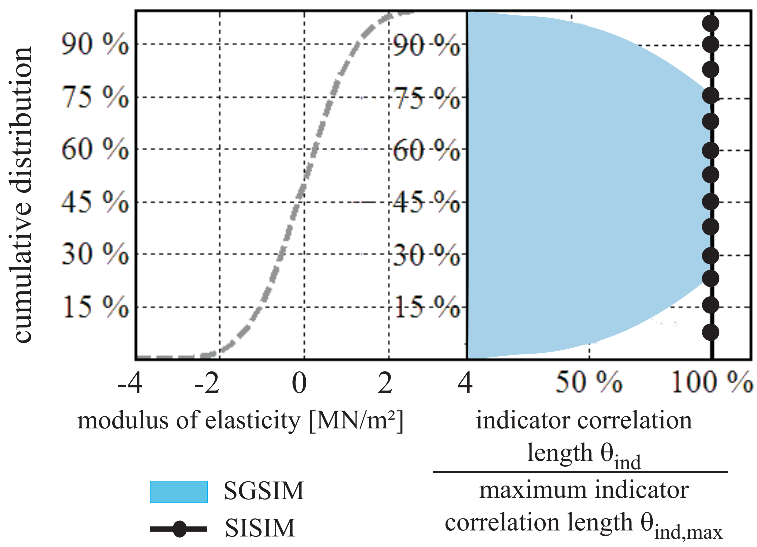

Figure E.3: Indicator correlation lengths for each threshold of the SGSIM and SISIM algorithm.

Method	Covariance	$\mathbb{R}^n$	Model Type	Ergodic	Conditioning	Systematic Grid Required	N_S	Exact Covariance
Sequential Gaussian	All C	All n	Gaussian	Yes	Direct	No	$< 10^3$	Yes
							$> 10^3$	No
Matrix decomposition	All C	All n	Gaussian	Yes	Direct	No	$< 10^3$	Yes
Turning bands	All C, γ, K	$n > 1$	*	No, if single direction	Kriging	No	All N_S	*
Autoregressive	Damped exponential and sinusoidal	$n = 1,2$	Gaussian	Yes	Kriging	Yes	All N_S	Yes
Moving average	Most C with short range	$n = 1,2$	Gaussian	Yes	Direct	Yes	All N_S	Yes
		$n > 2$			Kriging			
Dilution	Most C, γ	All n	Jump	Yes	Kriging	No	All N_S	Yes
Continuous spectral	All C, γ	All n	Gaussian (Periodic)	No	Kriging	No	All N_S	Yes
Discrete spectral	Most $C, \gamma = \|h\|^\alpha$, polynomial K	$n = 1$	Gaussian	Yes	Kriging	Yes	All N_S	Yes
	All C finite range	$n > 1$						

Note: C, γ and K indicate the possibility of simulating covariances, variograms and generalized covariances; n: dimension of the space; N_S: number of points simulated; for methods that are coupled with another method, * indicates a property that depends on the associated method, — means not applicable or unknown. Many variants exist, notably as regards the model type.

Figure E.4: Main characteristics of various random field simulation methods from Chiles & Delfiner [79].

Method	Covariance	$\mathbb{R}^n$	Model Type	Ergodic	Conditioning	Systematic Grid Required	N_S	Exact Covariance
Poisson hyperplanes	Linear	All n	Jump	No	Kriging	No	All N_S	Yes
Integration	Polynomial or spline K	$n = 1$	Apparent drift	—	Kriging	No	All N_S	*
Sequential indicators	All valid C	All n	Discrete	Yes	Direct	No	All N_S	*
Truncated Gaussian	C of a particular family	All n	Discrete	*	Iterative	*	*	*
Voronoi	Specific C	All n	Mosaic	Yes	Not known	No	All N_S.	Yes
Poisson polyhedra	Exponential	All n	Mosaic	Yes	Not known	No	All N_S	Yes
Substitution	Particular C	All n	—	*	Kriging	*	*	*
Boolean	Specific C	All n	Binary	Yes	Iterative	No	All N_S	Yes
Simulated annealing	—	All n	Not known	Yes	Iterative	Yes	All N_S	No

Note: C, γ and K indicate the possibility of simulating covariances, variograms and generalized covariances; n: dimension of the space; N_S: number of points simulated; for methods that are coupled with another method, * indicates a property that depends on the associated method, — means not applicable or unknown. Many variants exist, notably as regards the model type.

Figure E.5: Main characteristics of various random field simulation methods from Chiles & Delfiner [79].

Appendix F

Failure criteria in constitutive modelling of soil

Benz [38] states, that the Mohr-Coulomb failure criterion for soils is one of the earliest and most trusted failure criteria.

It is experimentally verified in triaxial compression and extension and is of striking simplicity. However, the Mohr-Coulomb (MC) criterion is very conservative for intermediate principal stress states between triaxial compression and extension. The Mohr-Coulomb failure criterion in principal stress space is defined as:

$$\begin{aligned} f_1 &= |\sigma_1 - \sigma_2| - (\sigma_1 + \sigma_2)\sin\varphi - 2\,c\cos\varphi \\ f_2 &= |\sigma_2 - \sigma_3| - (\sigma_2 + \sigma_3)\sin\varphi - 2\,c\cos\varphi \\ f_3 &= |\sigma_3 - \sigma_1| - (\sigma_3 + \sigma_1)\sin\varphi - 2\,c\cos\varphi \end{aligned} \tag{F.1}$$

Matsuoka & Nakai [243] (MN) proposed a failure criterion that is in better agreement with the experimental data, which is shown in figure 5.7 with the MC and the Lade - Duncan criteria [213] (LADE). Matsuoka & Nakai [243] propose the concept of a Spatial Mobilized Plane (SMP), which defines the plane of maximum spatial, averaged particle mobilization in principal stress space. The SMP is geometrically constructed by deriving the mobilized (Mohr-Coulomb) friction angles for each principal stress pair separately (figure F.1, left) and sketching the respective mobilized planes in principal stress space (figure F.1, right). Matsuoka & Nakai derive their failure criterion by limiting the averaged ratio of spatial normal stress to averaged spatial shear stress on this plane. Their failure stress ratio can be expressed as a simple function of the first, second, and third stress invariant, I_1, I_2, and I_3 as shown in equation F.3 and F.3. With the SMP concept, the Matsuoka-Nakai criterion automatically retains the well established material strength of the Mohr-Coulomb criterion in triaxial compression and extension. The likewise well-known failure criterion by Lade & Duncan appears compared to the Mohr-Coulomb criterion and the Matsuoka-Nakai criterion rather optimistic in plane strain conditions and triaxial extension. Benz [38] points out that using bifurcation analysis, progressive failures would most likely "correct" for the Lade criterion's overly optimistic, ultimate material strength estimate.

Both failure criteria, Matsuoka-Nakai and Lade, are functions of the first, second, and third stress invariants, I_1, I_2, and I_3 respectively:

$$f_{\mathrm{MN}} = \frac{I_1\,I_2}{I_3} - c_1 = 0 \quad \text{with} \quad c_1 = \frac{9 - \sin^2\varphi}{-1 + \sin^2\varphi} \tag{F.2}$$

$$f_{\mathrm{Lade}} = \frac{I_1^3}{I_3} - c_2 = 0 \quad \text{with} \quad c_2 = \frac{(-3 + \sin\varphi)^3}{(-1 + \sin\varphi)\;(-1 + \sin\varphi)^2} \tag{F.3}$$

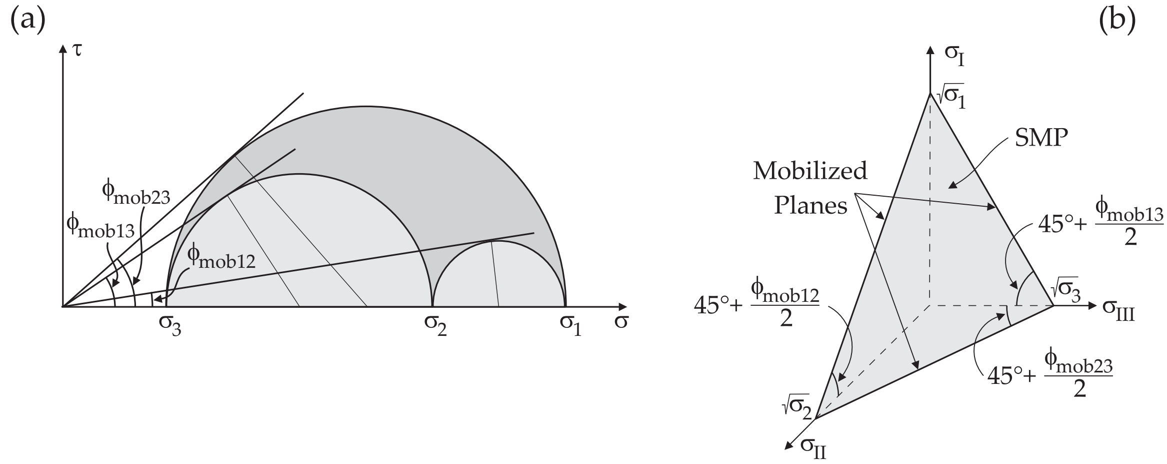

Figure F.1: The SMP concept of Matsuoka & Nakai.
(a) Three mobilized planes where the maximum shear stress to normal stress ratio is reached for the respective principal stresses.
(b) SMP in principal stress space from Benz [38].

where

$$
\begin{aligned}
I_1 &= \sigma_{ij} \\
I_2 &= \frac{1}{2}\left(\sigma_{ij}\,\sigma_{ij} - \sigma_{ii}\,\sigma_{jj}\right) \\
I_3 &= \frac{1}{6}\left(\sigma_{ii}\,\sigma_{jj}\,\sigma_{kk} \;+\; 2\,\sigma_{ij}\,\sigma_{jk}\,\sigma_{ki} - 3\,\sigma_{ij}\,\sigma_{ji}\,\sigma_{kk}\right)
\end{aligned}
\tag{F.4}
$$

In principal stress, the stress invariants simplify to:

$$
\begin{aligned}
I_1 &= \sigma_1 + \sigma_2 + \sigma_3 \\
I_2 &= -\sigma_1\,\sigma_2 - \sigma_2\,\sigma_3 - \sigma_3\,\sigma_1 \\
I_3 &= \sigma_1\,\sigma_2\,\sigma_3
\end{aligned}
\tag{F.5}
$$

The constants c_1 and c_2 in equation F.3 and F.3 are defined so that both failure criteria are identical to the Mohr-Coulomb criterion in triaxial compression.

Appendix G

Application of non-intrusive SFEM to a reliability problems

The non-intrusive Stochastic Finite Element Method (SFEM) is applied to a simple example in order to visualize the steps described in section 4.3.3. The limit state eqution 5.11 is used for the comparison of the probability of failure between non-intrusive SFEM and FORM, the statistical moments of the response and for the calculation of the Sobol indices. Within this example the soil properties of the parametric study 1 in section 5.4 and table 5.3 and a $COV_{\varphi'} = 20\%$ and $COV_{c'} = 10\%$ are used.

The deterministic results of the system response as a function of the random input variables in the shown in figure G.1.

The probabilistic results of a parametric study are shown in the figure G.2. Generally speaking, it can be deduced that the higher the face pressure, the higher the reliability of the system.

FORM and non-intrusive SFEM represent this qualitatively in the same way. The influence of the cohesion c' and of the friction angle φ' remains constant while varying the face pressure q_t.

To enlighten the concept of non-intrusive SFEM, the collocation points for different PCE orders are plotted in the Gaussian as well in the physical space (figure G.4). The dependency of the statistical moments to the PCE order is shown in figure G.3. Together with the results of figure G.5 and figure G.6, the reader can see the convergence of the non-intrusive SFEM approximation. The mean value, the variance, the skewness and also the kurtosis show only minor changes at the PCE order M = 5. This can also be deduced from Figure G.5 : The PCE order M = 5 is acceptable for the probability of failure p_f. This is strengthened the graphs of the empirical error and the coefficient of determination in figure G.3.

The difference of both approaches can be clearly seen in Figure 4. The lower the probability of failure, the bigger is the difference of FORM and CSRSM. This is due to the approximation of the system response via a PCE within CSRSM, which becomes more inaccurate with deceasing probability of failure. The dependency of the Sobol indices to the PCE order M is rather low, which is enlightened in Figure G.7.

It can be concluded from the presented study that the non-intrusive SFEM cannot be accurately applied to evaluate the small probability of failures, which was also reported in literature e.g. Phoon [286]. This can be deduced to the concept approximation of the stochastic system response using a high order polynomial, which does not represent the small tails of the distribution of system response. But the concept of non-intrusive SFEM is can be efficiently applied to evaluate the first and second statistical moments of the system response as well as for the analytical evaluation of global sensitivities. These benefits can be applied to any sort of uncertain input variable ranging from soil strength properties, correlation lengths,... etc.

If this approach is applied to the system response assuming uncertain correlation lengths, on as to keep in mind that the evaluation points are mean values and the fitted PCE model will just approximate the real response surface; therefore, the sensitivity factors derived from the PCE are not global factors but help to understand the importance between the input variables between each other.

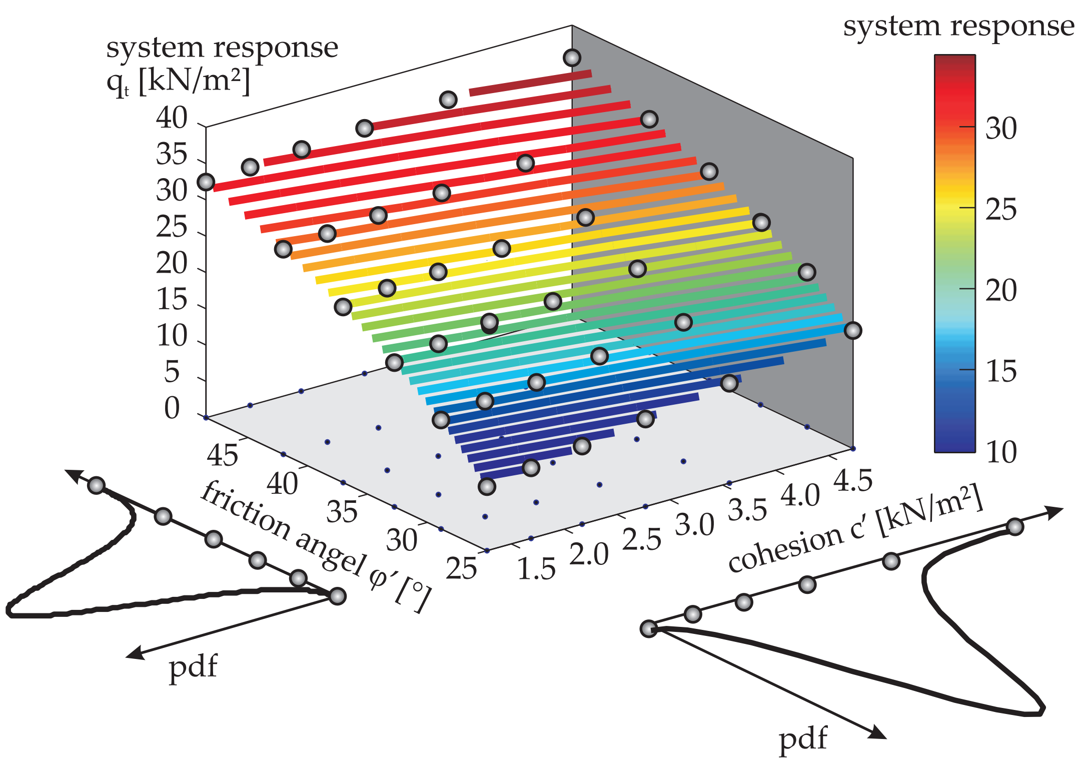

Figure G.1: Input variables and system response of an PCE with order $M = 5$ and a face pressure of q_t = 40 kN/m^2.

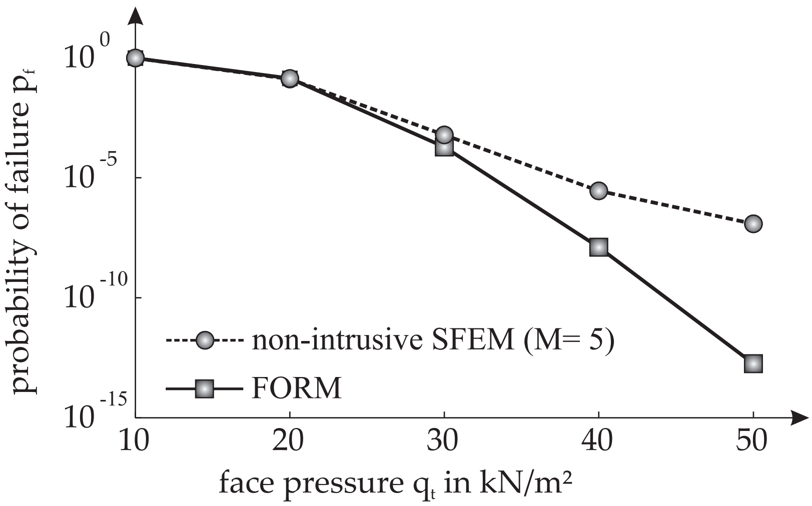

Figure G.2: Comparison of non-intrusive SFEM and FORM in terms of the probability of failure for a $\mathrm{COV}_{\varphi'} = 5$ % and $\mathrm{COV}_{\varphi'} = 10$ % .

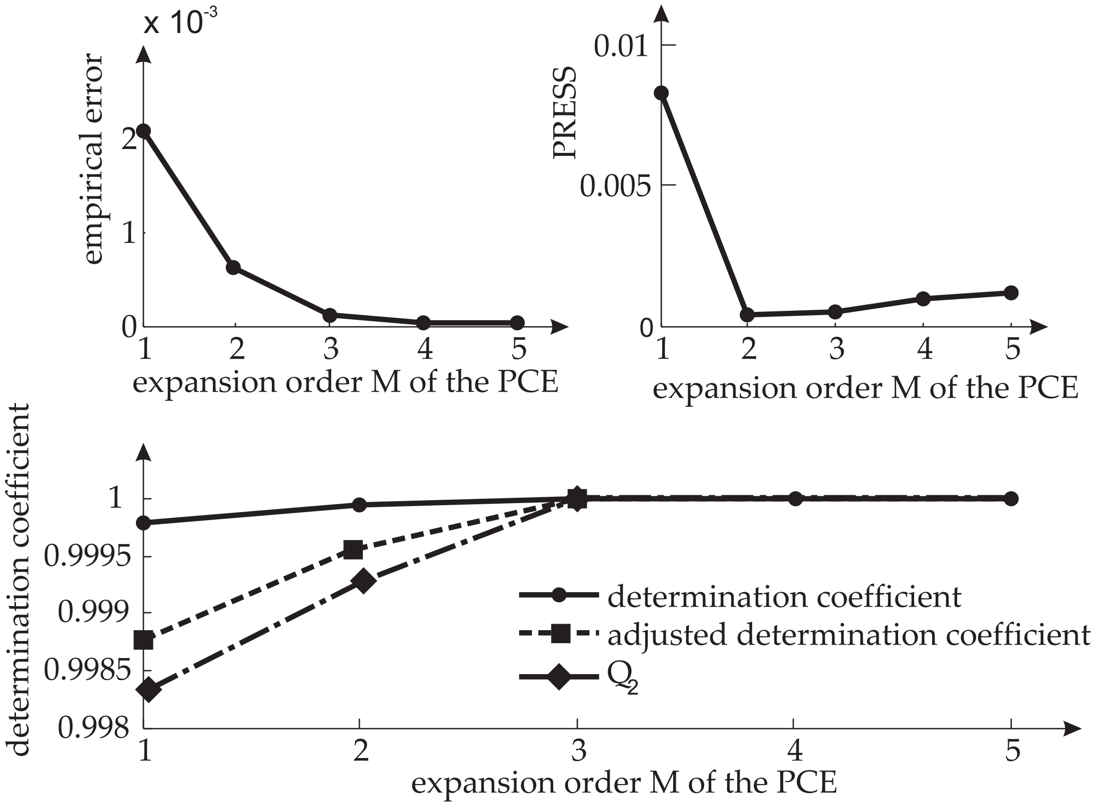

Figure G.3: Acccuracy of the PCE fitting for a face pressure $q_t = 40$ kN/m^2.

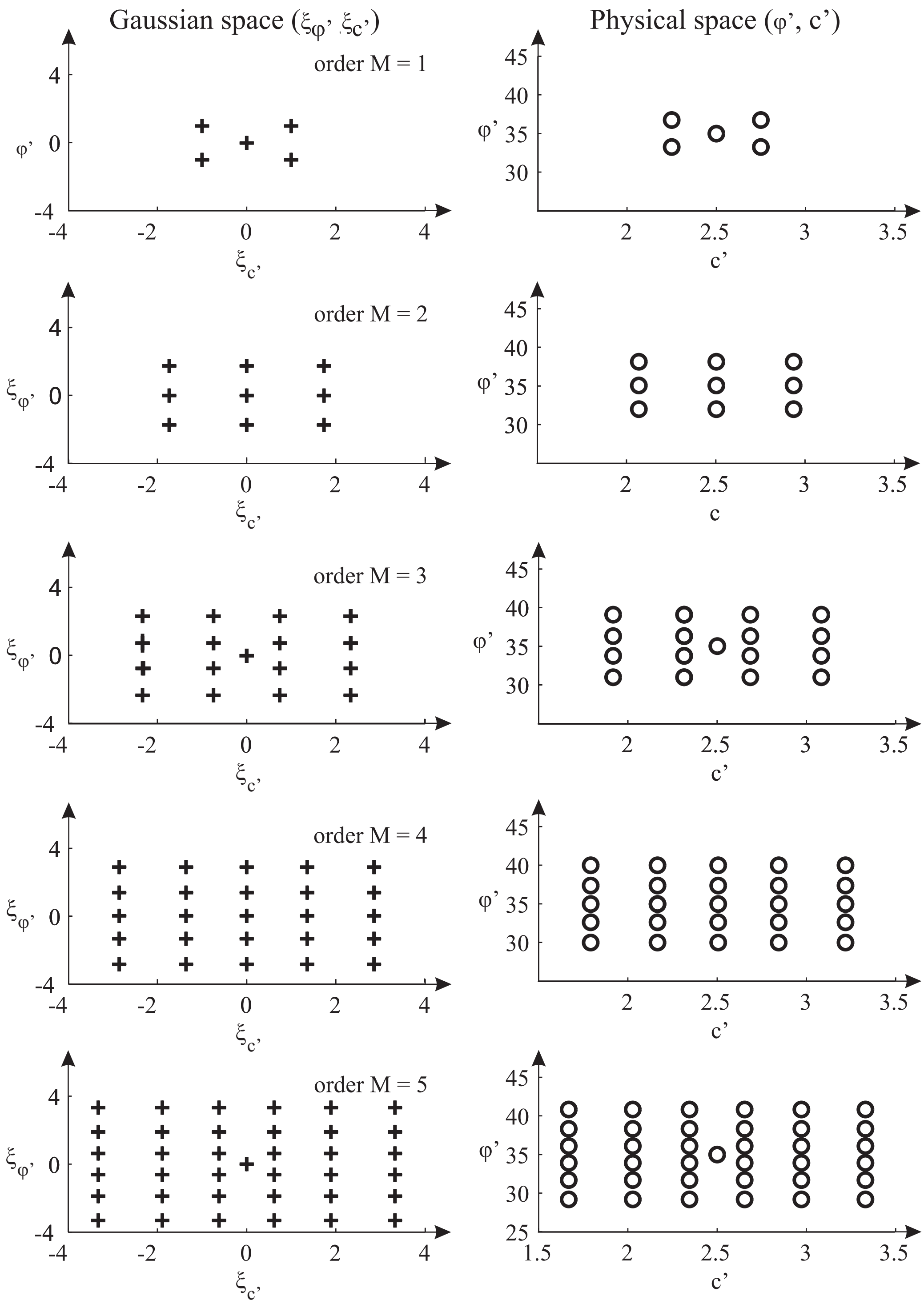

Figure G.4: Collocation points in Gaussian space and physical space for several PCE expansion orders M.

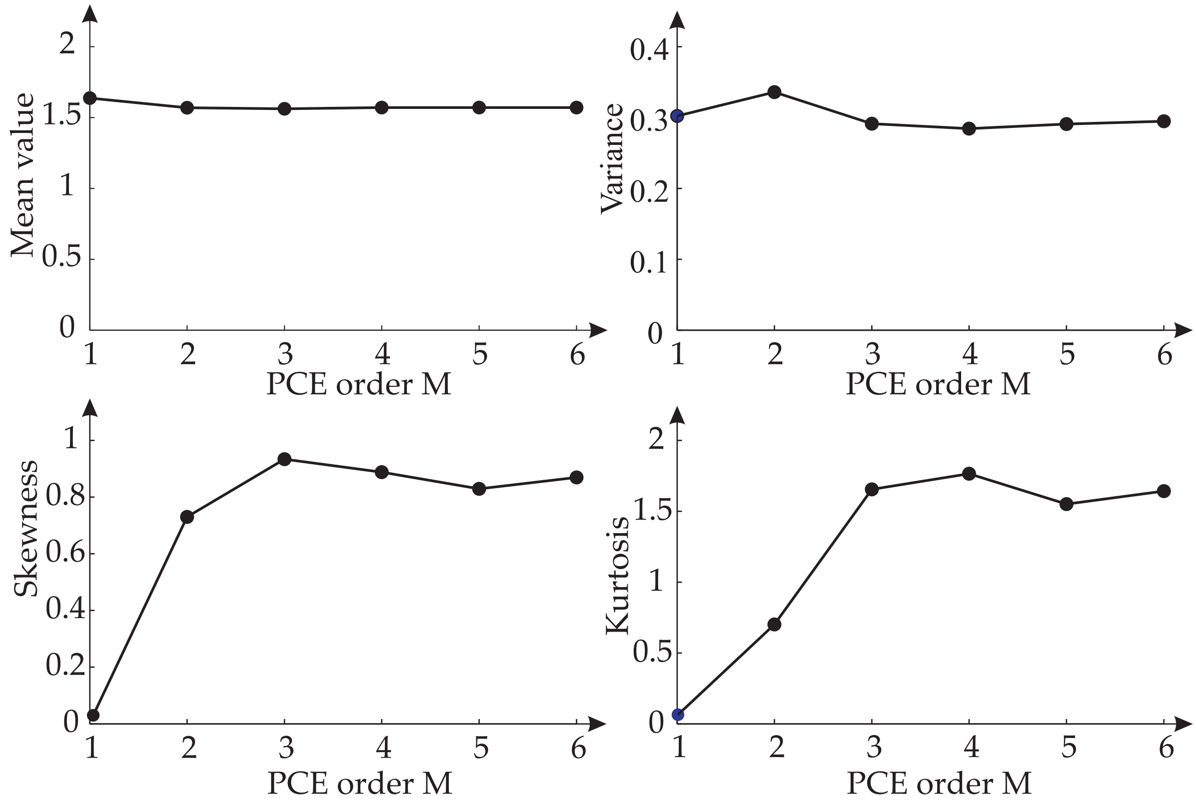

Figure G.5: Statistical moments of the approximated system response for a face pressure $q_t = 40\ \mathrm{kN/m^2}$.

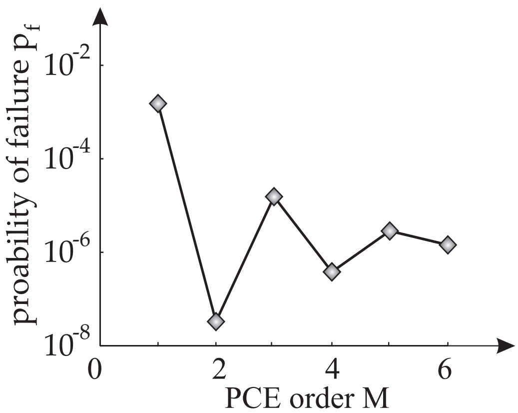

Figure G.6: Probability of failure as a function of the PCE expansion order.

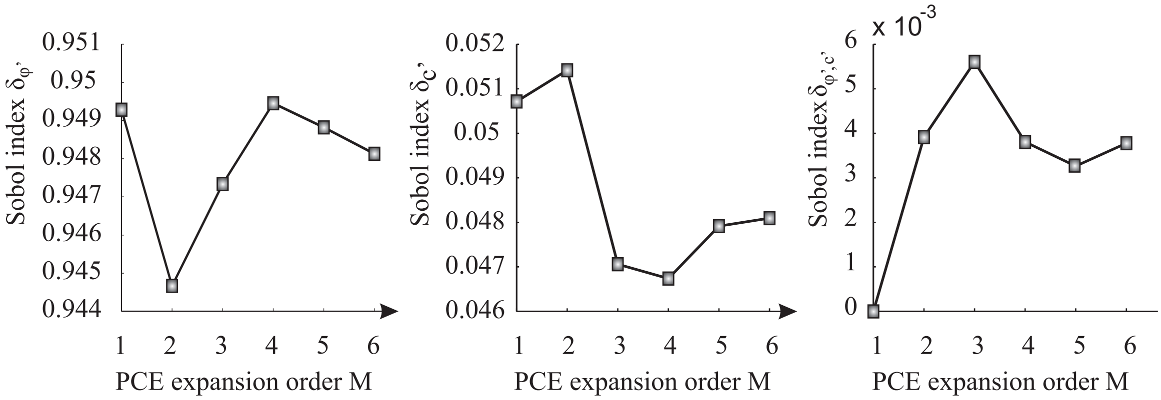

Figure G.7: Sobol indices for several PCE expansion orders for the face pressure $q_t = 40$ kN/m ^{2}.

Appendix H

Pluri-Gaussian Simulation Method

H.1 Introduction

Soil properties vary naturally through space as a result of the complex geological processes through which soil evolve, [204]. Physical and chemical processes, including structural deformation, deposition and diagenesis control the geometry and texture of sedimentary deposits and create soil variability at different scales.

This multi-scale spatial variability of soil properties can be captured by geostatistical simulation approaches. Koltermann & Gorelick [204] group the simulation approaches in three main categroies: structure imitating, process imitating and descriptive. Structure-imitating methods rely on spatial statistics, probabilistic rules and deterministic constraints to depict geometric relations within aquifers and reservoirs. Process-imitating methods solve governing equations to represent either the processes through which soil form or the physics of subsurface fluid-flow and transport. Descriptive methods divide subsoil into zones by synthesizing measured soil properties and geologic observations into a conceptual depositional model.

Structure-imitating methods are further subdivided into Gaussian and Non-Gaussian methods. *Gaussian-related methods* produce images of a continuous variable with the same mean, variance, covariance function and a Gaussian univariate distribution of values. The continuous distribution can be truncated or grouped into categories, [204]. *Non-Gaussian algorithms* include indicator-based methods, simulated annealing, Boolean methods, and Markov chains. Boolean methods do not reproduce a covariance function but create a geologic image by random1y generating in space simple shapes commonly observed in sedimentary deposits. In contrast, indicator-based methods are based on variogram models, simulated annealing solves an optimization formulation derived from the problem of solidification of a solid from a hot liquid upon cooling, and Markov chains are based on transition probabilities, [204]. Geologic information can be considered through training images that contain geologic features deemed important to the investigated problem.

Geologic information can be considered through training images that contain geologic features deemed important to subsurface fluid flow and transport. Kupfersberger & Deutsch [210] report that training images can be geologic maps, cross sections, well logs data, fence diagrams, outcrop maps, conditioning data grouped into zones or images from quantitative depositional models. The form and parameters of a model of spatial correlation must reflect the features observed in the training image, [79].

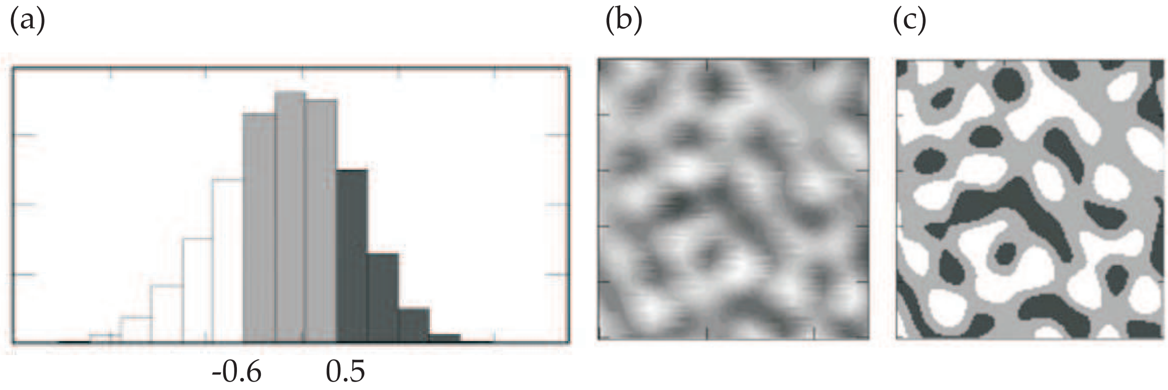

Figure H.1: (a) Histogram of a standard normal distribution (i.e. $\mathcal{N}(\mu = 0, \sigma = 1)$) showing the two thresholds -0.6 and 0.5,
(b) simulated greytone image with $\mathcal{N}(\mu = 0, \sigma = 1)$ and
(c) same image after being truncated at the thresholds -0.6 an 0.5.
Values below -0.6 have been shaded dark grey, those between -0.6 and 0.5 are coloured light grey while values above 0.5 are shown in white, [14].

H.2 Pluri-Gaussian simulation approach

The principle of truncated Gaussian simulation (TGS) was established almost 20 years ago Chiles & Delfiner [79] and by Isaaks [181] and then developed further developed as an efficient method for simulating spatial categorical variables that can be represented by indicators.

The underlying idea in both truncated Gaussian and pluri-Gaussian simulations is to set up one or more simulations of standard normal random functions in the area of interest and to attribute the soil type depending on the simulated values at each point. This is done by truncating. When only one Gaussian random field is used, the truncation is effectively defined by the values of thresholds as shown in figure H.1. When two or more Gaussian random fields are used, the situation is more complex. It is represented graphically via the lithotype rule.

H.2.1 Geological constraints

The complex geological setting is pictured in figure H.2. The simplified geological sketch map of the study area from Raspa et al.[301] shows togeather with the conceptual geological model the complex subsoil of the study area. This is even more emphasised by figure H.3 (a). The boreholes are shown in figure H.3 (b) in a 3D plot and in plan view in figure H.4. Moreover, the area of the case study is indicated in figure H.4.

Figure H.5 shows the the results of variogram analysis of the categorical variable soil type, which includes the values 1,2,3 for the corresponding soil type. The variograms are calculated for all directions on the horizontal plane with a mutual lag distance of 100 m and tolerance of 50 m. It allows to analyse the spatial continuity of the variable in all directions as well as investigating the anisotropy. From the map in figure H.5 one can identify two directions (N50 and N150) with a very high anisotropy.

Experimental variograms in the horizontal plane coordinate system of three indicator variables considered, calculated with a pitch of 100 m, 50 m tolerance step angular tolerance of $45°$. The variograms are calculated in both directions N60 and N150 (direction of maximum anisotropy) and exhibit a variability of the spatial distribution of soil types, especially medium-large, non-stationarity of the phenomenon, made more apparent by the study of proportions in figure H.8 (b), is partly masked by the fact of having areas with mixed distributions very different.

In figure H.8 (a) the vertical proportion curves of an area 500 m x 500 m and map of the vertical proportion curves of the soil types 1, 2 and 3 H.8 (b).

These proportion curves in figure H.8 are analysed to derive the lithotypes, which are used in the pluri-Gaussian simulations shown in figure H.9.

(a)

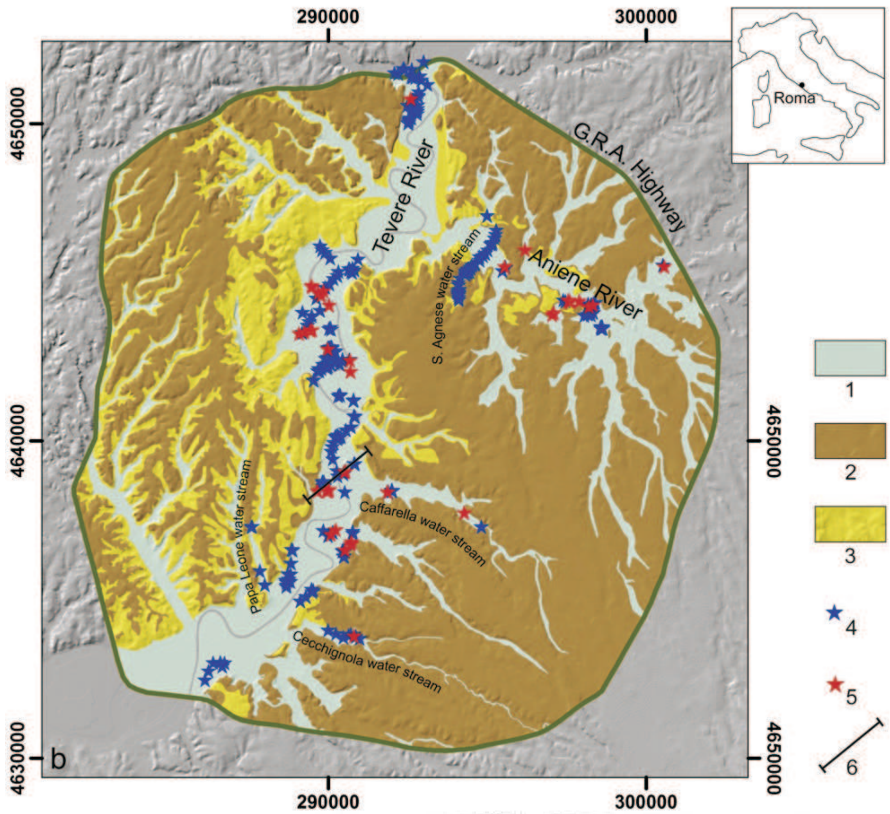

(b)

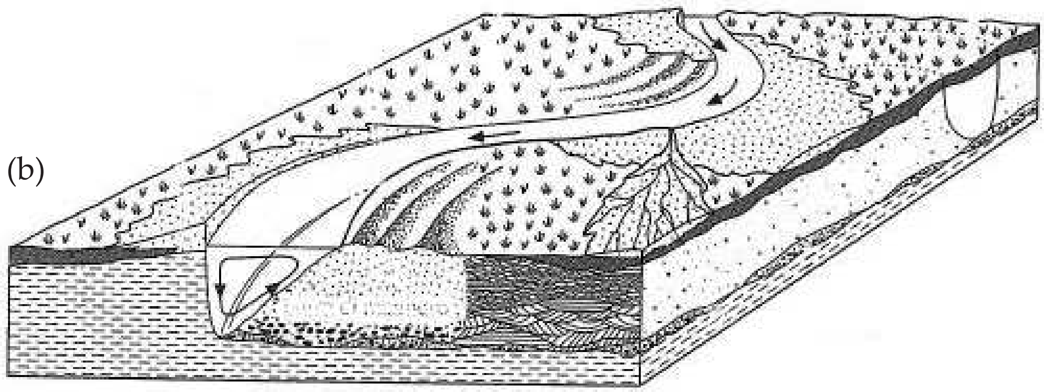

Figure H.2: (a) Simplified geological sketch map of the study area from Raspa et al.[301].
Legend:
(1) upper Pleistocene - Holocene alluvial deposits,
(2) middle-upper Pleistocene volcanic bedrock,
(3) Plio-Pleistocene sedimentary bedrock,
(4) boreholes with geotechnical samples,
(5) boreholes with samples endowed with the full set of geotechnical information and
(6) track of the geological cross section in figure H.3 (a).

(b) conceptual geological model of the Tevere valley by [238].

(a)

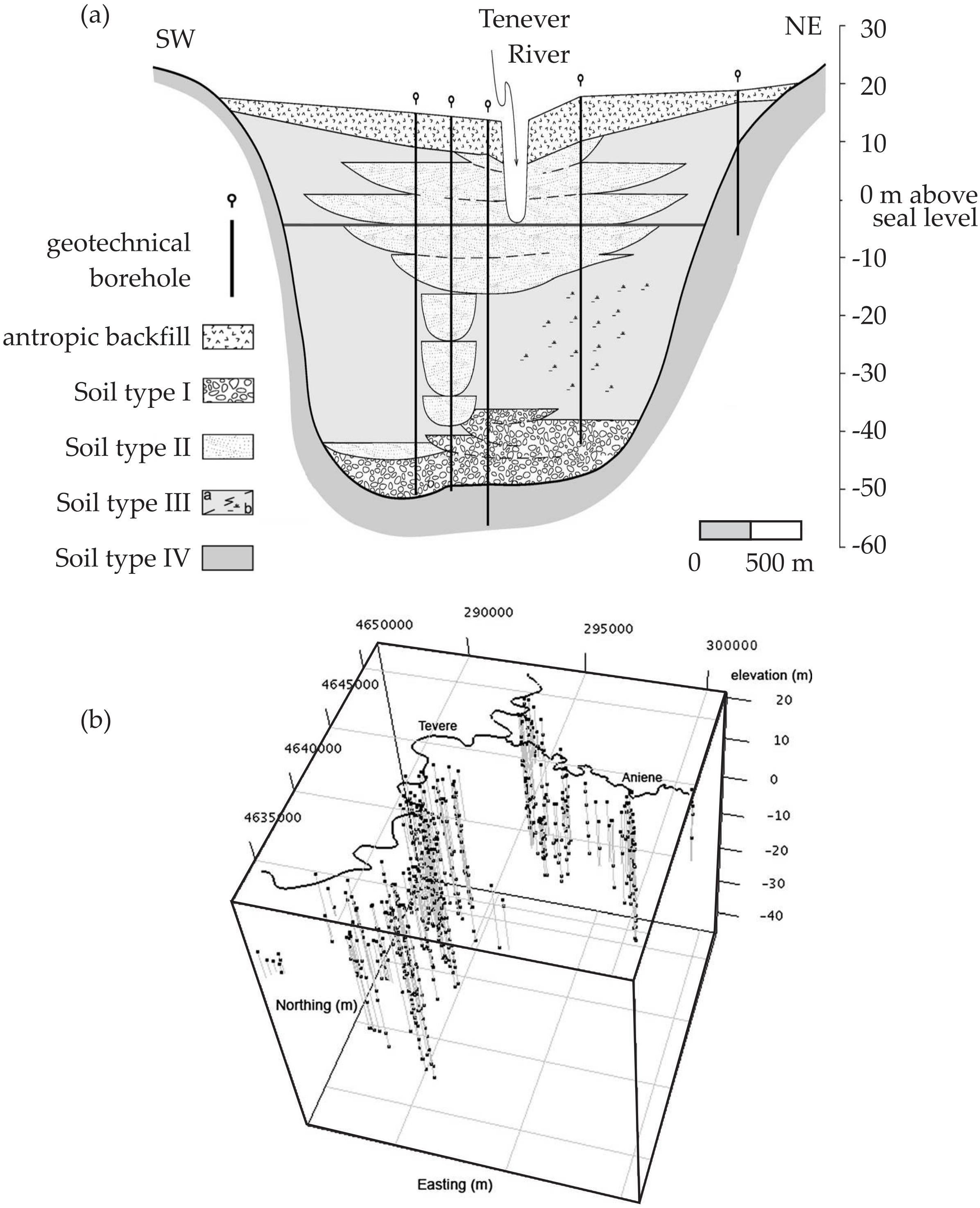

(b)

Figure H.3: (a) Geological cross section of the recent alluvial deposits filling the Tevere valley from [301].
(b) 3D plot of the selected boreholes with location of the geotechnical samples (black points) for location of the boreholes in figure H.2 from [301].

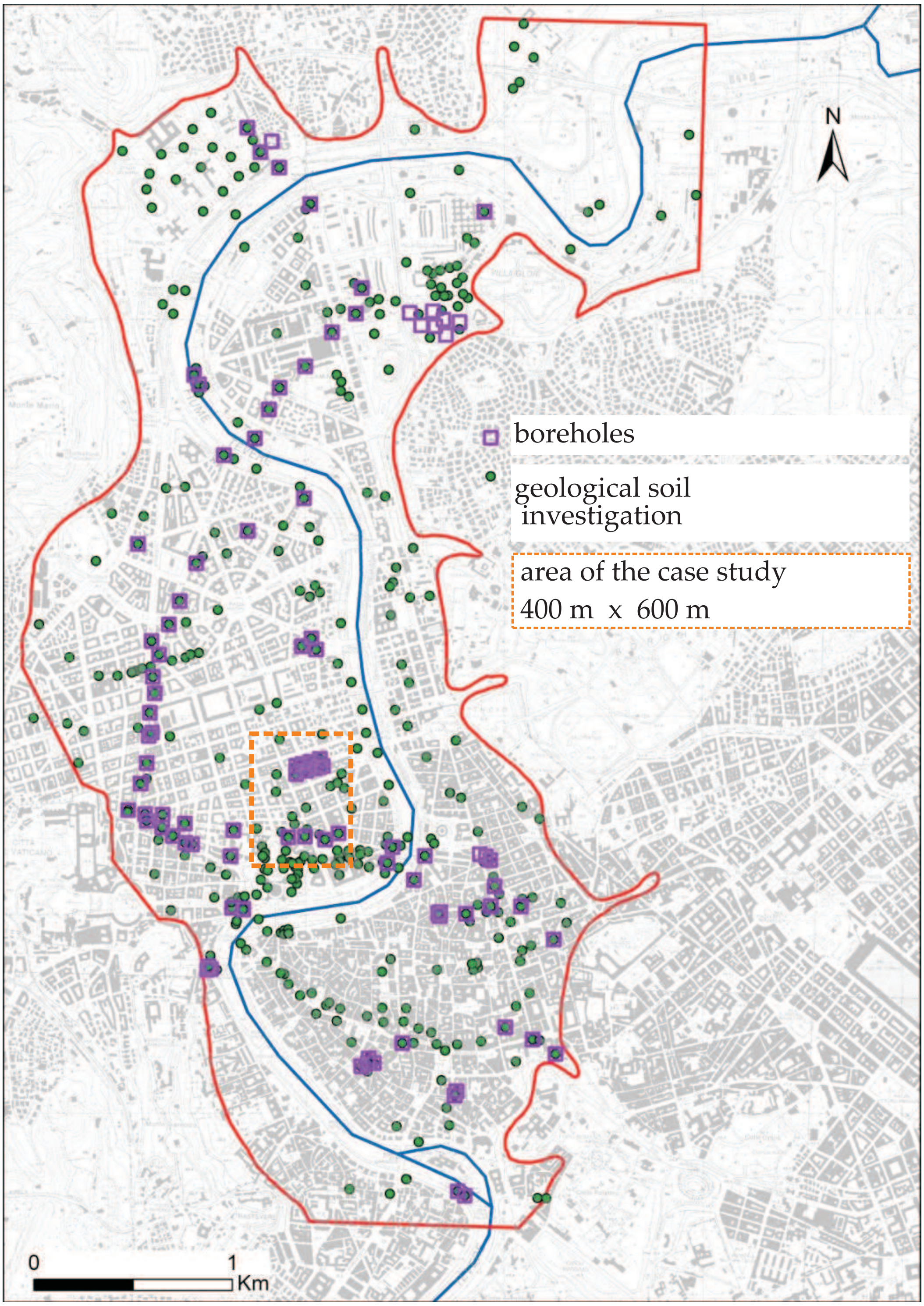

Figure H.4: Plan view investigated area and area of the case study (400 m x 600 m) in the city of Rome with locations of the boreholes and soil investigations from [238].

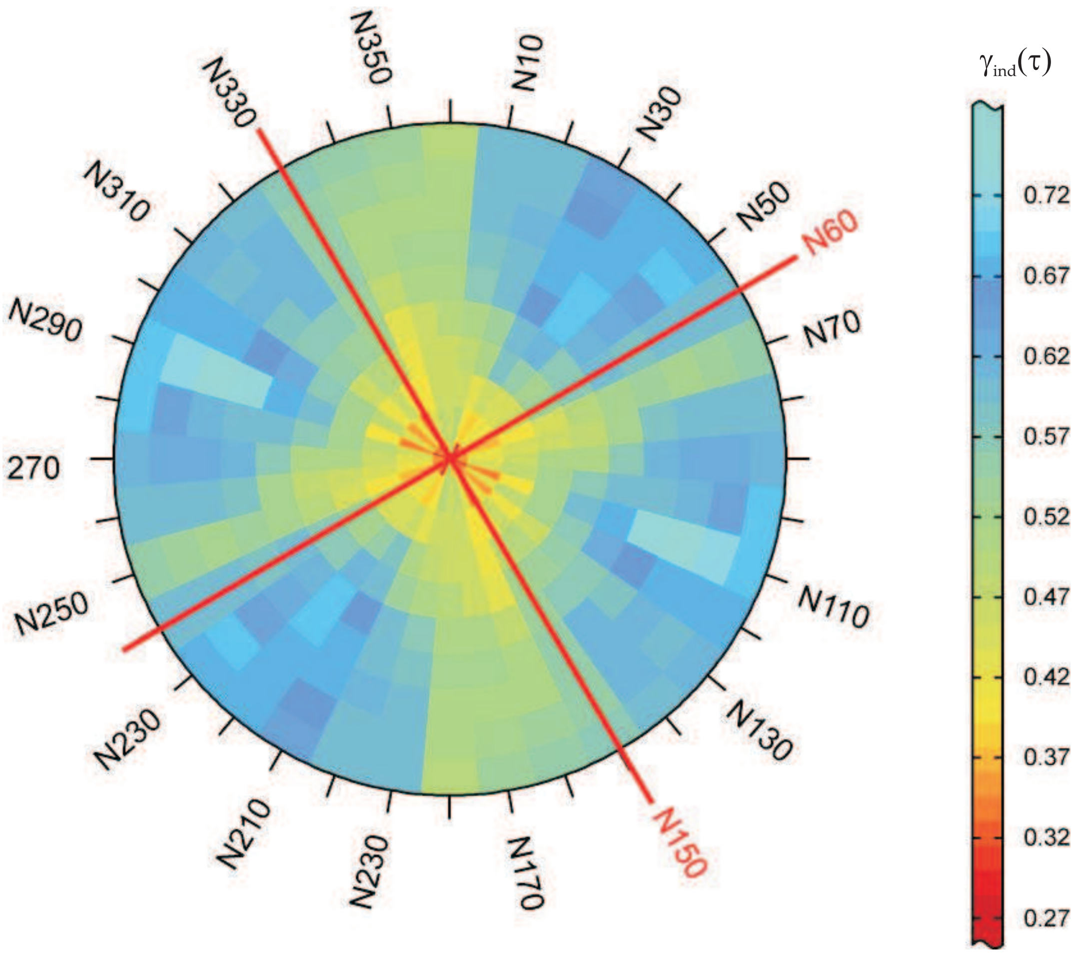

Figure H.5: Variogram map from Marconi [238].

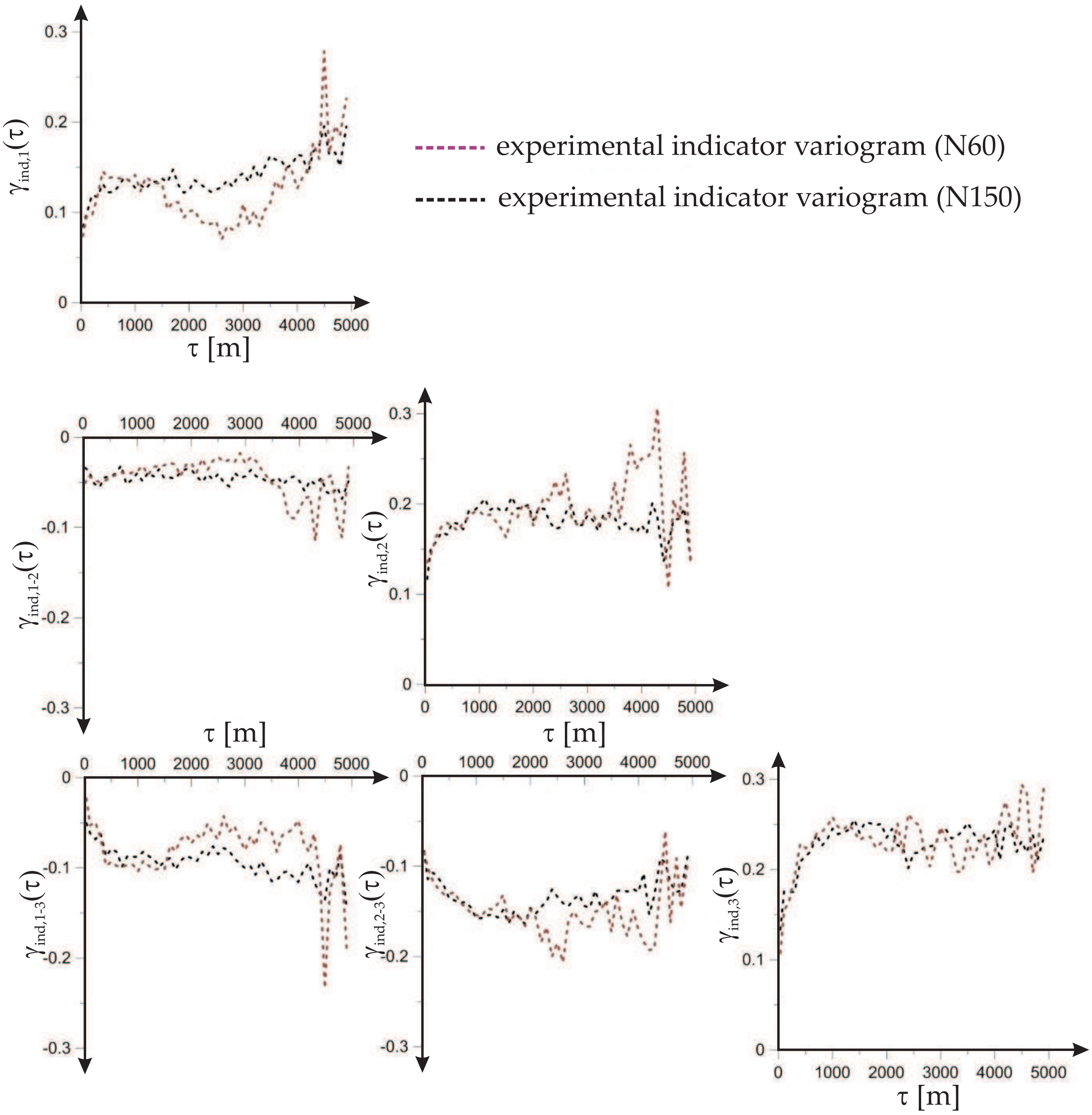

Figure H.6: Horizontal indicator variograms of the three different soil types from [238].

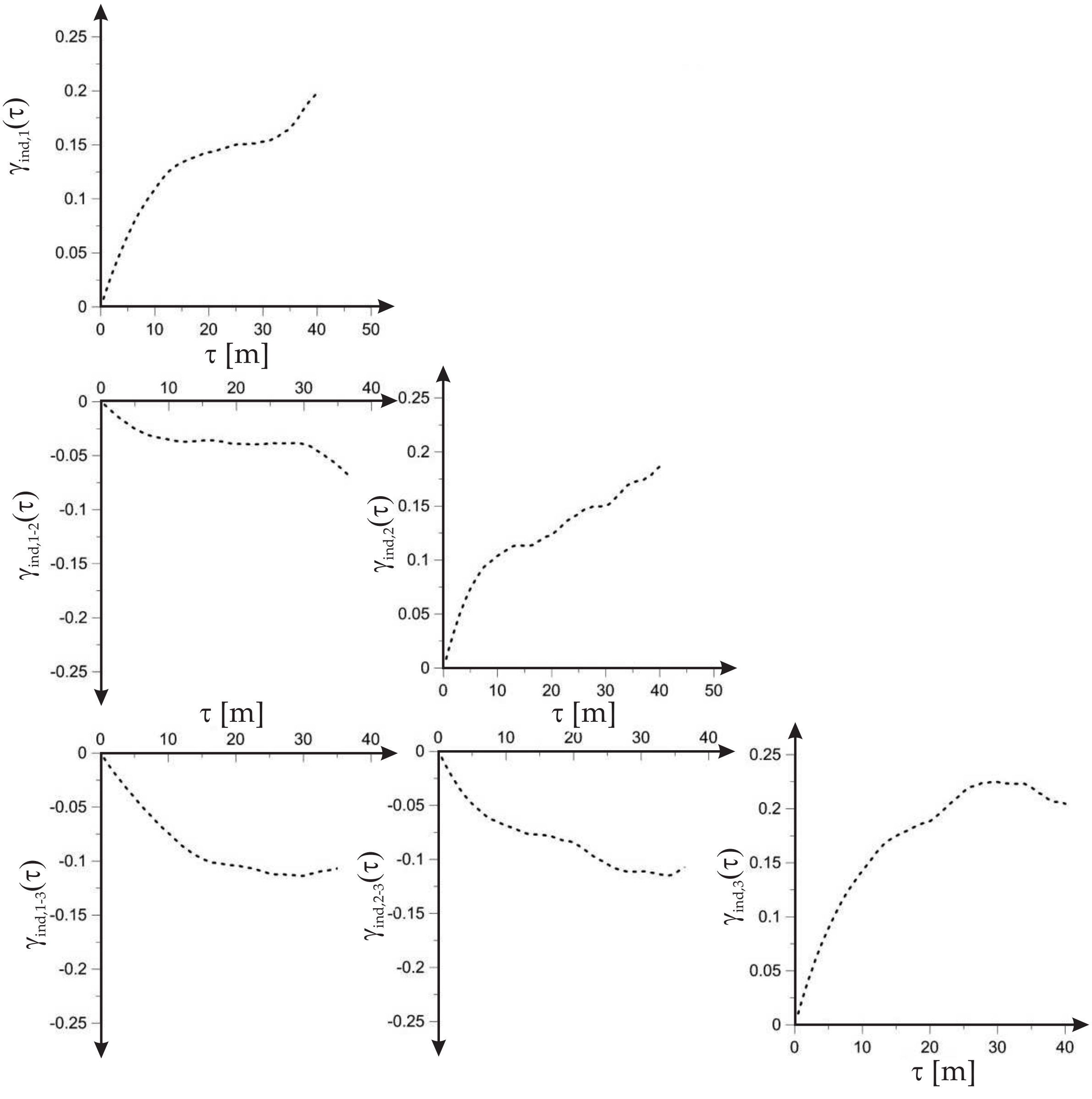

Figure H.7: Vertical indicator variograms of the three different soil types from [238].

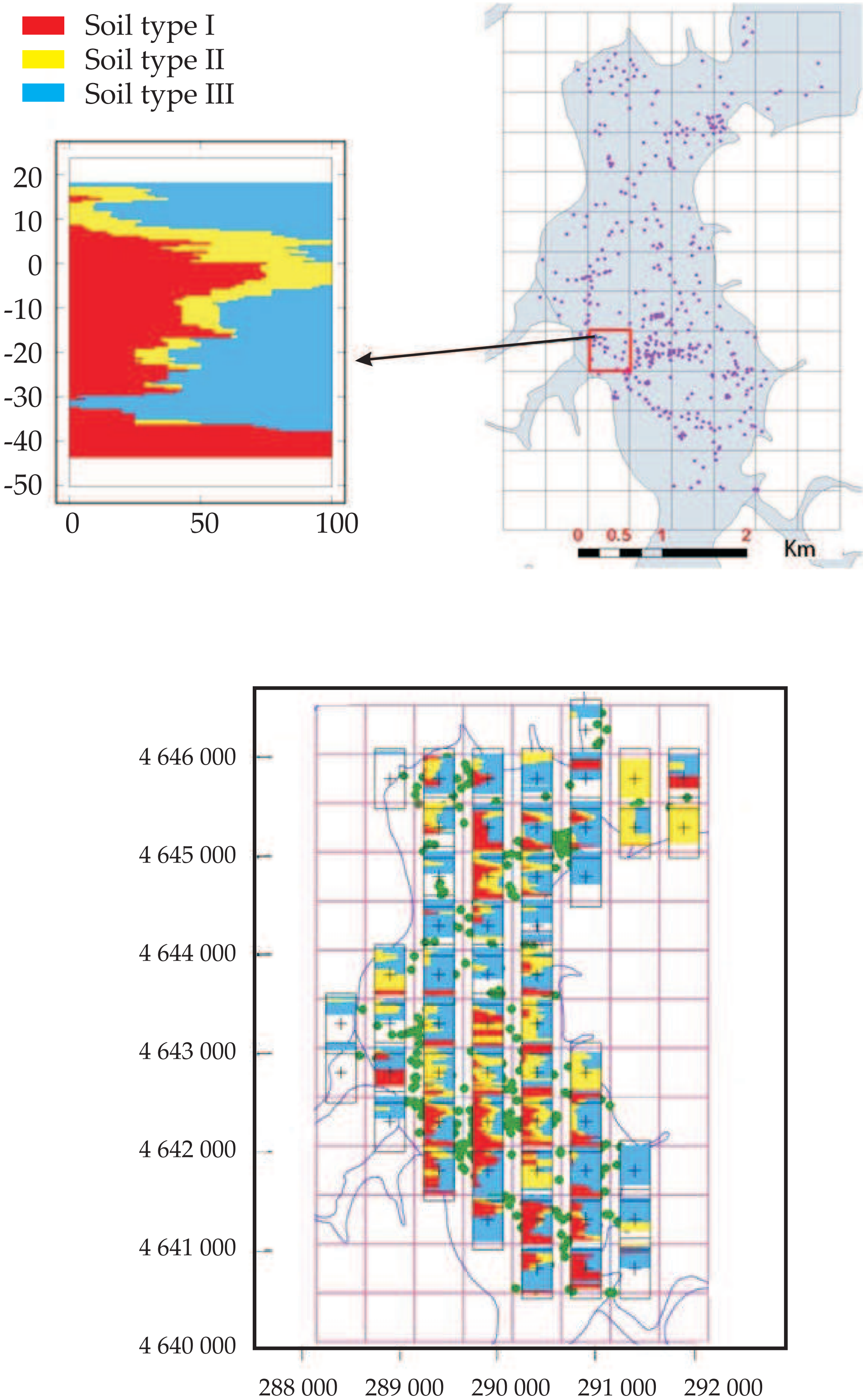

Figure H.8: Vertical proportion curve of an area 500 m x 500 m (a) and map of the vertical proportion curves of the soil types 1, 2 and 3, [238].

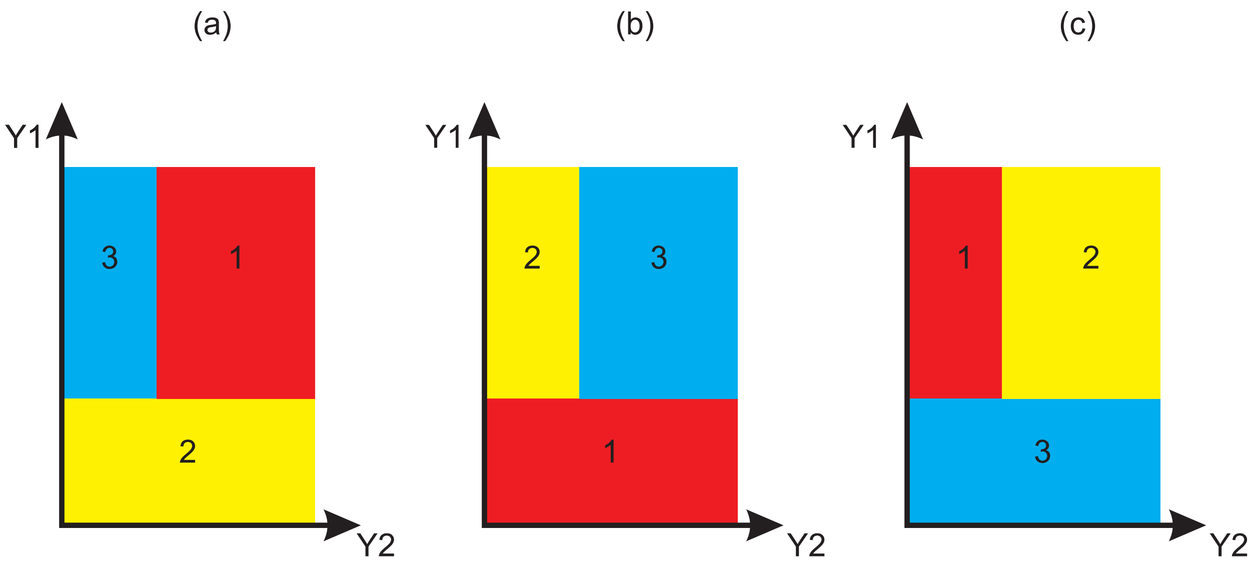

Figure H.9: Used lithotypes for the Pluri-Gaussian Simulation [238].

H.2.2 Pluri-Gaussian simulations

The Pluri-Gaussian simulation algorithm of [238] was used to simulate 300 random fields using the mesh shown in figure H.10. A part of one realisation is shown in figure H.11 and H.12.

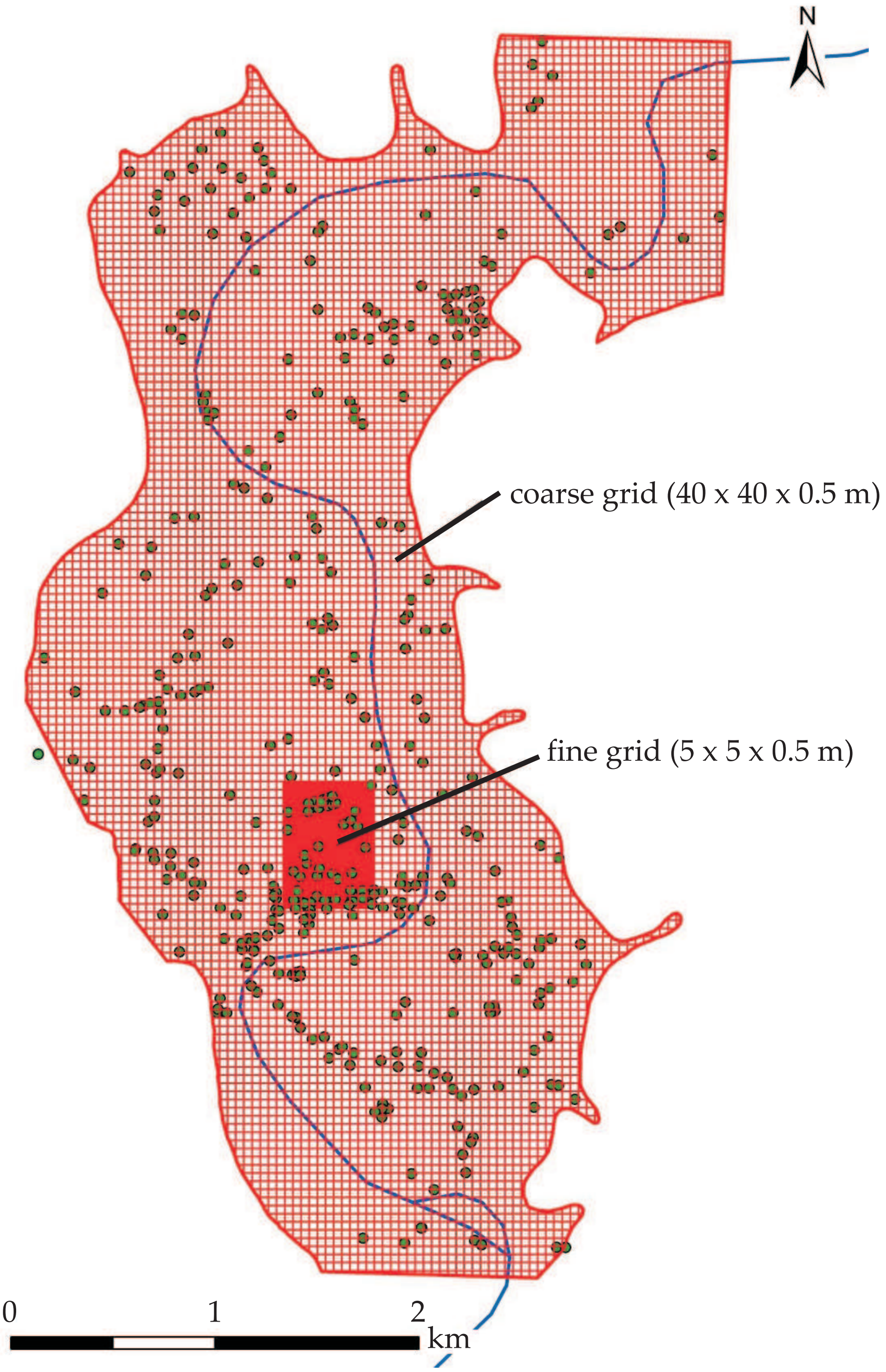

Figure H.10: Plan view of the Pluri-Gaussian mesh from Marconi [238].

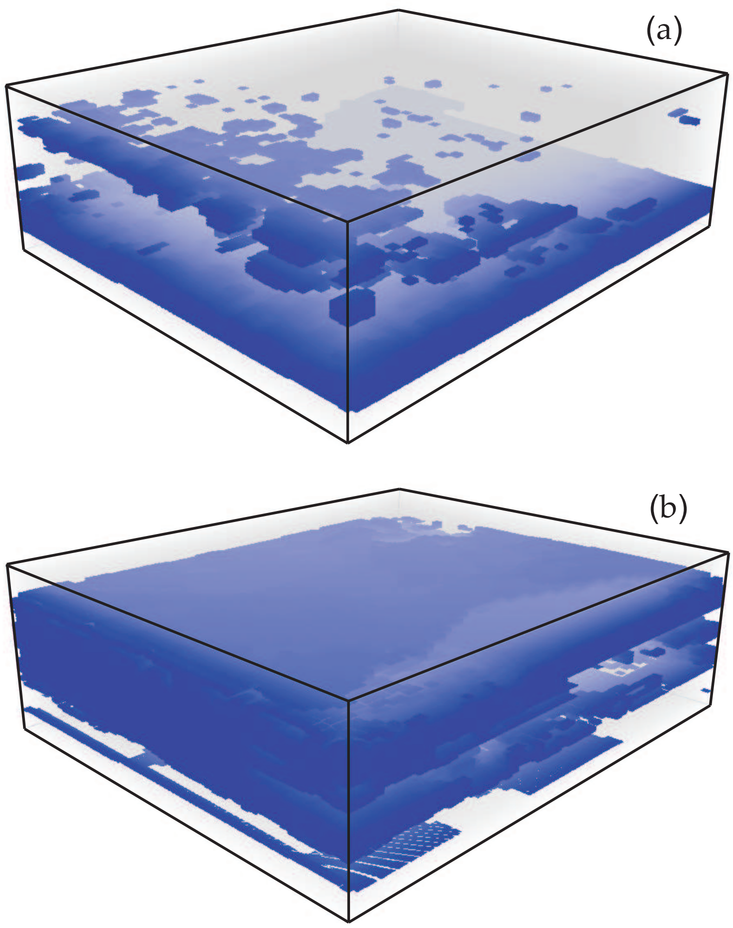

Figure H.11: Part of the realisation of the pluri-Gaussian random field for soil type 1 (a), soil type 2 (b).

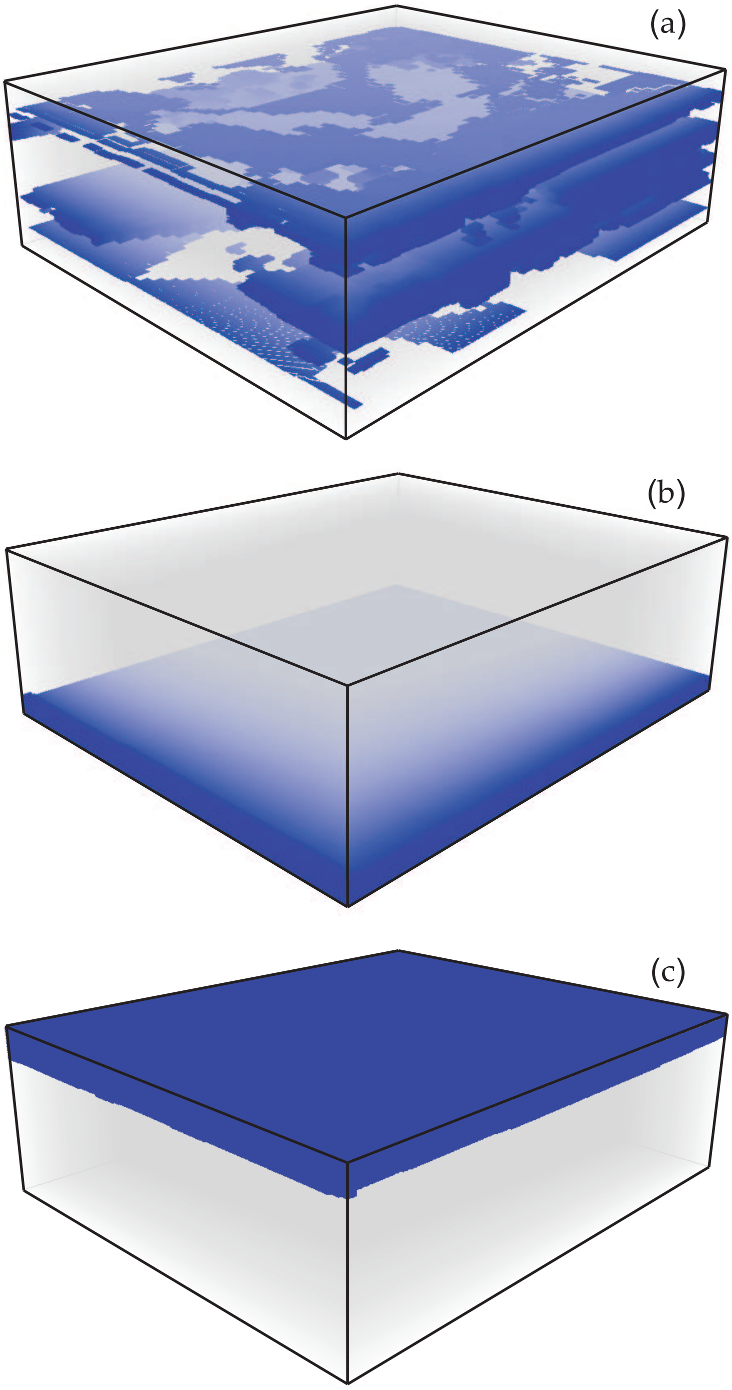

Figure H.12: Part of the realisation of the pluriGaussian random field including soil type 3 (a), soil type 4 (b), antropogenetic top soil layer (c).

Table H.1: Input parameters of the soil model.

	Soil type I	Soil type II	Soil type III	Soil type IV
friction angel φ' [°]	stochastic	stochastic	stochastic	stochastic
cohesion c' [kN/m^2]	stochastic	stochastic	stochastic	stochastic
tension cut-off s_t [kN/m^2]	0	0	0	0
dilatancy angel ψ [°]	0	0	0	0
power m [-]	0.5000	0.80	0.89	0.40
reference pressure p_{ref} [kN/m^2]	100	100	100	100
failure ratio R_f [-]	0.9	0.9	0.9	0.9
Poisson's ratio ν [-]	0.33	0.37	0.37	0.37
reference Young's modulus E_{50} [kN/m^2]	stochastic	stochastic	stochastic	stochastic
reference Young's modulus for unloading-reloading E_{ur} [kN/m^2]	$105,000$	$12,000$	$8,000$	$300,000$
ratio of shear moduli G_0 / G_{ur} [-]	2.0	2.0	2.0	2.0
threshold shear strain $\gamma_{0.7}$ [-]	10^{-4}	10^{-4}	10^{-4}	10^{-4}

Lebenslauf

30.09.1979 Geboren in Linz (Österreich)

1999-2004 Technische Universität Graz (Österreich)
Studium des Bauingenieurwesens (Dipl.-Ing.)

1999-2005 Technische Universität Graz (Österreich)
Studium des Wirtschaftsingenieurwesen-Bauwesen (Dipl.-Ing.)

2005 Technische Universität Graz, Institut für Wasserbau & Wasserwirtschaft
Forschungsstipendiat

2005-2007 FHCE - Floegl Hydro Consulting Engineering
Projektingenieur in den Bereichen Wasserbau, Geotechnik und Ingenieurbau

2007-2013 Universität Stuttgart, Institut für Geotechnik
akademischer Mitarbeiter

Mitteilungen des Instituts für Geotechnik der Universität Stuttgart

Mitteilungen des Baugrundinstitutes Stuttgart
(Institut für Grundbau und Bodenmechanik)
der Universität Stuttgart
Hrsg.: Prof. Dr.-Ing. Dr. h.c. U. Smoltczyk

Nr. 01	Thamm, B. R.	(1974)	Anfangssetzungen und Anfangsporenwasserüberdrücke eines normalverdichteten wasser-gesättigten Tones
Nr. 02	Gußmann, P.	(1975)	Einheitliche Berechnung von Grundbruch und Böschungsbruch
Nr. 03	Feeser, V.	(1975)	Die Bedeutung des Kalziumkarbonats für die bodenphysikalischen Eigenschaften vom Löß
Nr. 04	Du Thin, K.	(1976)	Standsicherheit von Böschungen: Programm-Dokumentation
Nr. 05	Smoltczyk, U. Pertschi, O. Hilmer, K.	(1976)	Messungen an Schleusen in der UDSSR. Schleusennorm der UDSSR (SN 30365)

Nr. 06	Hilmer, K.	(1976)	Erddruck auf Schleusenkammerwände
Nr. 07	Laumans, Q.	(1977)	Verhalten einer ebenen, in Sand eingespannten Wand bei nicht-linearen Stoffeigenschaften des Bodens
Nr. 08	Lächler, W.	(1977)	Beitrag zum Problem der Teil-flächenpressung bei Beton am Bei-spiel der Pfahlkopfanschlüsse
Nr. 09	Spotka, H.	(1977)	Einfluß der Bodenverdichtung mittels Oberflächenrüttelgeräten auf den Erd-druck einer Stützwand bei Sand
Nr. 10	Schad, H.	(1979)	Nichtlineare Stoffgleichungen für Böden und ihre Verwendung bei der numerischen Analyse von Grundbau-aufgaben
Nr. 11	Ulrich, G.	(1980)	Verschiebungs- und kraftgesteuerte Platten-druckversuche auf konsolidierenden Böden
	Gußmann, P.		Zum Modellgesetz der Konsolidation
Nr. 12	Salden, D.	(1980)	Der Einfluß der Sohlenform auf die Traglast von Fundamenten

Nr. 13	Seeger, H.	(1980)	Beitrag zur Ermittlung des horizontalen Bettungsmoduls von Böden durch Seitendruckversuche im Bohrloch
Nr. 14	Schmidt, H.H.	(1981)	Beitrag zur Ermittlung des Erddrucks auf Stützwände bei nachgiebigem Baugrund
Nr. 15	Smoltczyk, U. Schweikert, O.	(1981)	Vorstudie über bauliche Alternativen für Durchgangsstraßen in Siedlungen
Nr. 16	Malcharek, K. Smoltczyk, U.	(1981)	Vergleich nationaler Richtlinien für die Berechnung von Fundamenten
Nr. 17	Gruhle, H.D.	(1981)	Das Verhalten des Baugrundes unter Einwirkung vertikal gezogener Ankerplatten als räumliches Problem des Erdwiderstandes
Nr. 18	Kobler, W.	(1982)	Untersuchungen über Böschungs- und Grundbruch bei begrenzten Lastflächen
Nr. 19	Lutz, W.	(1983)	Tragfähigkeit des geschlitzten Baugrunds neben Linienlasten

Nr. 20	Smoltczyk, U.	(1983)	Studienunterlagen "Bodenmechanik und Grundbau"; überarbeitete Ausgabe 1993
Nr. 21	Schweikert, O.	(1984)	Der Einfluß des Böschungswinkels auf die Berechnung des aktiven Erddrucks
Nr. 22	Vogt, N.	(1984)	Erdwiderstandsermittlung bei monotonen und wiederholten Wand-bewegungen in Sand
Nr. 23	Buchmaier, R.	(1985)	Zur Berechnung von Konsolidationsproblemen bei nichtlinearem Stoffverhalten
Nr. 24	Schad, H. Smoltczyk, U.	(1985)	Möglichkeiten der Böschungssicherung bei kleinen Baugruben
	Schad, H. Zoller, P.		Sonderkonstruktionen der Böschungssicherung
Nr. 25	Gußmann, P.	(1986)	Die Methode der Kinematischen Elemente
Nr. 26	Steinmann, B.	(1985)	Zum Verhalten bindiger Böden bei monotoner einaxialer Beanspruchung
Nr. 27	Lee, S.D.	(1987)	Untersuchungen zur Standsicherheit von Schlitzen im Sand neben Einzelfundamenten

Mitteilungen des
Instituts für Geotechnik der Universität Stuttgart
Hrsg.: Prof. Dr.-Ing. Dr. h.c. U. Smoltczyk

Nr. 28	Kolb, H.	(1988)	Ermittlung der Sohlreibung von Gründungskörpern unter horizontalem kinematischen Zwang
Nr. 29	Ochmann, H.	(1988)	Ebene Grenzzustände von Erdböschungen im stochastischen Sicherheitskonzept
Nr. 30	Breinlinger, F.	(1989)	Bodenmechanische Stoffgleichungen bei großen Deformationen sowie Be- und Entlastungsvorgängen
Nr. 31	Smoltczyk, U. Breilinger, F. Schad, H. Wittlinger, M.	(1989)	Beitrag zur Bemessung von Tunneln in offener Bauweise
Nr. 32	Gußmann, P. Schanz, T. Smoltczyk, U. Willand, E.	(1990)	Beiträge zur Anwendung der KEM (Erddruck, Grundbuch, Standsicher-heit von Böschungen)
Nr. 33	Gruhle, H.D.	(1990)	Der räumliche Erdwiderstand vor überwiegend horizontal belasteten Ankerplatten

Nr. 34	Henne, J.	(1995)	Zur Bewehrung von verformten Bodenschichten durch Einsatz zugfester Geokunststoffe
Nr. 35	Wittlinger, M.	(1994)	Ebene Verformungsuntersuchungen zur We-ckung des Erdwiderstandes bindiger Böden
Nr. 36	Schad, H.	(1992)	Zeit- und geschwindigkeits-abhängiges Materialverhalten in der Geotechnik – Experimentelle Erfassung und numerische Analyse
Nr. 37	Belz, I.	(1992)	Zur Ermittlung dynamischer Boden-kennwerte in situ aus der Systemantwort des Erregers
Nr. 38	Ma, J.	(1994)	Untersuchungen zur Standsicherheit der durch Stützscheiben stabilisierten Böschungen
Nr. 39	Smoltczyk, U.	(1994)	Sonderheft: 25 Jahre Lehre und Forschung in der Geotechnik
Nr. 40	Rilling, B.	(1994)	Untersuchungen zur Grenztragfähigkeit bindiger Schüttstoffe am Beispiel von Lößlehm

Mitteilungen des
Instituts für Geotechnik der Universität Stuttgart
Hrsg.: Prof. Dr.-Ing. P.A. Vermeer

Nr. 41	Vermeer, P.A.	(1996)	Deponiebau und Geotechnik
Nr. 42	Vermeer, P.A.	(1997)	Baugruben in Locker- und Festgestein
Nr. 43	Brinkmann, C.	(1998)	Untersuchungen zum Verhalten von Dichtungsübergängen im Staudammbau
Nr. 44	Fiechter-Scharr, I.	(1998)	Beeinflussung von Erdbaustoffen durch Beimischen eines organophilen Bentonits
Nr. 45	Schanz, T.	(1998)	Zur Modellierung des mechanischen Verhaltens von Reibungsmaterialien
Nr. 46	Akinrogunde, A.E.	(1999)	Propagation of Cement Grout in Rock Discontinuities Under Injection Conditions
Nr. 47	Vogt-Breyer, C.	(1999)	Experimentelle und numerische Untersuchungen zum Tragverhalten und zur Bemessung horizontaler Schraubanker
Nr. 48	Vermeer, P.A.	(1999)	Neue Entwicklungen in der Geotechnik

Nr. 49	Marcher, T.	(2002)	Resultate eines Versuchsprogramms an Beaucaire Mergel
Nr. 50	Marcher, T.	(2003)	Nichtlokale Modellierung der Entfestigung dichter Sande und steifer Tone
Nr. 51	Ruse, N.M.	(2004)	Räumliche Betrachtung der Stand-sicherheit der Ortsbrust beim Tunnelvortrieb
Nr. 52	Beutinger, P.H.	(2005)	Ein geotechnischer Beitrag zur Standsicherheit mobiler Bau-maschinen
Nr. 53	Wehnert, M.	(2006)	Ein Beitrag zur drainierten und undrainierten Analyse in der Geotechnik
Nr. 54	Möller, S. C.	(2006)	Tunnel induced settlements and forces in linings
Nr. 55	Benz, T.	(2007)	Small-Strain Stiffness of Soils and its Numerical Consequences
Nr. 56	Abed, A.	(2008)	Numerical Modeling of Expansive Soil Behavior

Nr. 57	Hintner, J.	(2008)	Analyse der Fundamentverschiebungen infolge vertikaler und geneigter Belastung
Nr. 58	Russelli, C.	(2008)	Probabilistic Methods applied to the Bearing Capacity Problem
Nr. 59	Peña Olarte, A.A.	(2008)	Influence of Particle Shape on the Global Mechanical Response of Granular Packings: Micromechanical Investigation of the Critical State in Soil Mechanics
Nr. 60	Neher, H. P.	(2008)	Zeitabhängiges Materialverhalten und Anisotropie von weichen Böden – Theorie und Anwendung
Nr. 61	Vermeer, P.A.	(2008)	Von der Forschung zur Praxis: Symposium zum 80. Geburtstag von Prof. U. Smoltczyk
Nr. 62	Satibi, S.	(2009)	Numerical Analysis and Design Criteria of Embankments on Floating Piles
Nr. 63	Lächler, A.	(2009)	Bedeutung herstellungsbedingter Einflüsse auf das Trag- und Verformungsverhalten von Schlitzwänden

Nr. 64	Möllmann, A.	(2009)	Probabilistische Untersuchung von Hochwasserschutzdeichen mit analytischen Verfahren und der Finite-Elemente-Methode

Mitteilungen des
Instituts für Geotechnik der Universität Stuttgart
Hrsg.: Prof. Dr.-Ing. habil. Ch. Moormann

Nr. 65	Moormann, Ch.	(2011)	7. Stuttgarter Geotechnik-Symposium
Nr. 66	Beuth, L.	(2012)	Formulation an Application of a Quasi-Static Material Point Method
Nr. 67	Moormann, Ch., Huber, M., Proske, D.	(2012)	Proceedings of the 10th International Probabilistic Workshop
Nr. 68	Schneider, M.	(2013)	Zur energetischen Nutzung von Tunnelbauwerken – Messungen und numerische Berechnungen am Beispiel Fasanenhoftunnel
Nr. 69	Huber, M.	(2013)	Soil variability and its consequences in geotechnical engineering